Global buckling of eccentrically loaded cellular members

Melissa Kerkhove

Supervisors: Dr. ir. Delphine Sonck, Prof. dr. ir.-arch. Jan Belis

Master's dissertation submitted in order to obtain the academic degree of
Master of Science in Civil Engineering

Department of Structural Engineering
Chairman: Prof. dr. ir. Luc Taerwe
Faculty of Engineering and Architecture
Academic year 2014-2015

UNIVERSITEIT
GENT

Global buckling of eccentrically loaded cellular members

Melissa Kerkhove

Supervisors: Dr. ir. Delphine Sonck, Prof. dr. ir.-arch. Jan Belis

Master's dissertation submitted in order to obtain the academic degree of
Master of Science in Civil Engineering

Department of Structural Engineering
Chairman: Prof. dr. ir. Luc Taerwe
Faculty of Engineering and Architecture
Academic year 2014-2015

UNIVERSITEIT
GENT

The author gives permission to make this master dissertation available for consultation and to copy parts of this master dissertation for personal use. In the case of any other use, the copyright terms have to be respected, in particular with regard to the obligation to state expressly the source when quoting results from this master dissertation.

Melissa Kerkhove
May 2015, Ghent

Acknowledgements

Almost at the end of this master thesis, I would like to express my gratitude towards all people who contributed in some way to this final work.

First of all, I would like to thank my supervisors Delphine Sonck and Jan Belis for offering me the opportunity to undertake this numerical research concerning the interesting subject of cellular members. Special thanks go to Delphine Sonck for her guidance during the complete year and for transferring parts of her Abaqus knowledge to me. Without her encouragement, insightful comments and her patience on learning me the do's and don'ts of programming, this thesis would never have been written nor completed.

I feel also very grateful towards everyone of the thesis committee for their constructive comments that undoubtedly led to additional insight and improved the quality of this work. Furthermore, I would like to show my appreciation to everyone who inspired me during the past years and in this way kept me on track during my study of Civil Engineering.

Last but not least, I would like to thank my parents and friends for supporting me during the last five and many more years. Thank to my fellow students for the sleepless nights of working together before deadlines, the stimulating discussions and the joy during and outside lectures.

Melissa Kerkhove
May 2015, Ghent

Global buckling of eccentrically loaded cellular members

Author: Melissa Kerkhove
Supervisors: Dr. ir. Delphine Sonck, Prof. dr. ir.-arch. Jan Belis

Master's dissertation submitted in order to obtain the academic degree of
Master of Science in Civil Engineering

Department of Structural Engineering
Chairman: Prof. dr. ir. Luc Taerwe
Faculty of Engineering and Architecture
Academic year 2014-2015

Summary

In this master thesis, numerical research is performed on the global buckling of eccentrically loaded cellular members, i.e. members with openings introduced in the web subjected to a strong-axis bending moment and axial compressive force. The application of cellular members is especially favourable for longer spans due to the higher moment-of-inertia-to-weight ratio of cellular members compared to plain-webbed members. Different design rules are applicable to describe the global buckling of eccentrically loaded plain-webbed members: the design rules proposed by the ECCS and the formulations currently adopted in Eurocode 3.
This work will serve as an extended research of the numerical study performed in (Gevaert, 2010) on plain-webbed members, where design rules ECCS-Vandepitte, ECCS-Van Impe were compared with Method 1 adopted in Eurocode 3. However, since ECCS-Van Impe has been adapted afterwards based on the research of D. Gevaert and to clarify the assumptions made in Gevaert's work, part of his study was repeated, but extended with Method 2 of Eurocode 3. Afterwards, a parametric study was performed on cellular members with the finite element program Abaqus. The numerical results were compared with the four mentioned design rules, adapted to take into account the openings in the web. Similar findings as for plain-webbed members were possible, showing that application of the design rules of Eurocode 3 and ECCS-Van Impe is generally safe, except for short length members. For longer lengths, the analytically obtained results are very conservative compared to the numerical values. Design rule ECCS-Vandepitte is in general unsafe, but similarly as for the other methods, the safety of this design rule is increasing with increasing length. Consequently, application of ECCS-Vandepitte is safe for longer lengths and can be an alternative to the conservative approach of other methods.

Keywords: Eccentrically loaded compression members, Flexural buckling, Lateral Torsional Buckling, Web openings, Finite Element Analysis, Abaqus

Global buckling of eccentrically loaded cellular members

Melissa Kerkhove

Supervisor(s): dr. ir. Delphine Sonck, prof. dr. ir.-arch. Jan Belis

Abstract— **A numerical investigation was performed on global buckling of eccentrically loaded cellular members as an extension of the study on plain-webbed members by D. Gevaert. Four available design rules for members subjected to combined bending and compression were compared: the formulations of the ECCS (ECCS-Vandepitte and ECCS-Van Impe) and the design rules currently adopted in Eurocode 3 (Method 1 and Method 2). The four design rules are applicable to plain-webbed members, but were adapted to take into account the web openings. The analytical results were further compared with the results of numerical simulations executed with the finite element program Abaqus. In this way, general conclusions can be drawn about the safety and applicability of the four different design rules.**

Keywords— **Eccentrically loaded compression members, Flexural buckling, Lateral Torsional Buckling, Web openings, Finite Element Analysis, Abaqus**

I. INTRODUCTION

To restrict the wide topic of eccentrically loaded members, only simply supported doubly symmetric members subjected to a strong axis-bending moment and axial load were considered. The rotation around the x-axis as well as the displacement in y- and z-direction are obstructed.

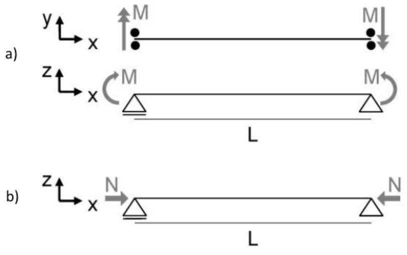

Fig. 1. Members subjected to bending moment (a) and axial load (b).

Although numerical research on plain-webbed members was already performed in [1], it was necessary to clarify the assumptions made in Gevaert's work regarding among others the cross-section classification and the exact formulation of the ECCS-Van Impe design rule. The Van Impe design rule was namely adapted during the years to better correspond to the design rules adopted in Eurocode 3. Therefore, it was uncertain based on which formulation the conclusions regarding the safety of this design rule were drawn. Eventually, it was decided to repeat part of the study of Gevaert, extended with the six additional profiles that were used as parent sections of the cellular members to extend the limited research on plain-webbed members. Additionally, comparison was also made with the analytical expressions of Method 2, which were not considered by Gevaert. Finally, the results of this extended study on plain-webbed members could be compared with the results of the parametric study on cellular members.

II. STUDIED CASES

Three different moment distributions were considered (Fig. 2) determined by the parameter ψ, expressing the ratio between the moments at both end sections. The relation between the applied bending moment and axial load is determined by the parameter μ (Eq. 1), for which seven different values were considered (Fig. 3).

$$\mu = \frac{\frac{M_{Ed,left}}{M_{cr}}}{\frac{N_{Ed}}{N_{cr,z}}} \tag{1}$$

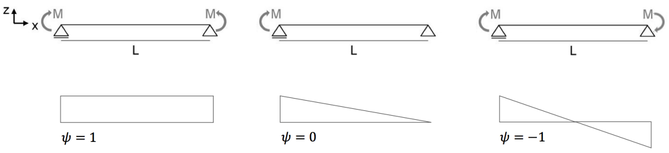

Fig. 2. Considered values of ψ.

μ						
0	0.1	0.5	1	5	10	∞

Fig. 3. Considered values of μ.

III. DESIGN RULES

In total, four different design rules are compared: ECCS-Vandepitte, ECCS-Van Impe, EC3-Method 1 and EC3-Method 2. Design rule ECCS-Van Impe was based on ECCS-Vandepitte, but adapted to obtain a better correspondence with the Eurocode formulations. In Method 1 of Eurocode 3, individual factors are introduced to reflect the influence of different physical phenomena with a high level of accuracy. In contrast to the transparency of Method 1, simplicity is enhanced with Method 2 by using one compact interaction factor. It should be noted that the lateral-torsional buckling resistance was determined based on the Modified General method, in which a modification factor f is introduced to take into account non-uniform bending moments. Due to this modification factor, an increase in lateral-torsional buckling resistance of 25% can be obtained for members under double curved bending ($\psi = -1$) and for an optimal value of the non-dimensionless slenderness $\overline{\lambda}_{LT}$ of 0.8.

Based on the value of ψ and μ, the initial axial load and bending moment were determined according to Eqs.2-3. For M_{start}, a value of 1 kNm was considered. Both analytically and numerically (GMNIA analysis) the load proportionality factor can be determined, i.e. the factor by which the starting values of M and N should be multiplied to obtain the failure load.

$$M = \lambda_{start} M_{start} \tag{2}$$

$$N = \lambda_{start} N_{start} \tag{3}$$

IV. NUMERICAL SIMULATIONS

As geometric imperfection, a half-sine wave with amplitude L/1000 was considered as out-of-plane imperfection for both the plain-webbed and cellular members. Preference was given to quadratic shell elements S8R5 with reduced integration to obtain accurate results at a reasonable cost. A mesh size of six elements per flange with was chosen based on a preliminary refinement study. The cross-sectional properties were calculated based on a wire model (c=h-t_f-2r) to obtain a better correspondence with the numerical model, in which fillets are omitted. However, the cross-section classification itself is performed according to EC3 (c=h-2t_f-2r).

A. Plain-webbed members

For the plain-webbed members, 840 GMNIA simulations were executed on the ten profiles considered by Gevaert and 504 on the six profiles that will be used as parent sections for the plain-webbed members. The residual stress pattern as proposed in [2] was introduced in the model using a user subroutine (Fig. 4).

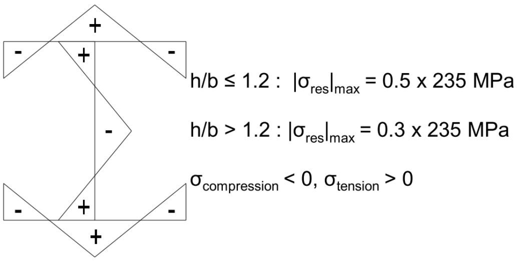
+
-
+
-
-
+
-
+
-
+
h/b ≤ 1.2 : |σ$_{res}$|$_{max}$ = 0.5 x 235 MPa
h/b > 1.2 : |σ$_{res}$|$_{max}$ = 0.3 x 235 MPa
σ$_{compression}$ < 0, σ$_{tension}$ > 0

Fig. 4. Residual stress pattern plain-webbed members [2].

B. Cellular members

Due to the additional cutting and welding procedure for cellular members, an increase of the compressive residual stress in the flanges can be noticed, resulting in a modified residual stress pattern. Therefore, the residual stresses in cellular members have a more detrimental effect on the global buckling resistance compared to residual stresses in plain-webbed members. A preliminary proposal for this adapted residual stress pattern was made in [3] (Fig. 5).

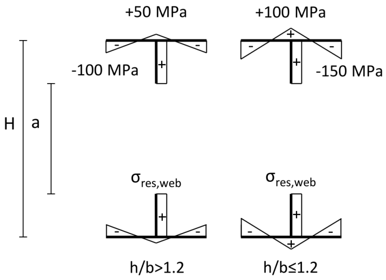

Fig. 5. Proposed residual stress pattern cellular members [3].

For the cellular members, in total 2520 GMNIA (420 per section) and 420 LBA analyses were performed. The examined parent sections are given in Fig. 6.

Parent sections					
IPE300	IPE600	HE320A	HE320M	HE650A	HE650M

Fig. 6. Examined parent sections.

V. CONCLUSION

Similar findings were possible for plain-webbed members as well as for cellular members. It can be concluded that design-rules ECCS-Van Impe, EC3-Method 1 and EC3-Method 2 are safe, except for shorter lengths. In general, safety is increasing with increasing length. Therefore, application of design rule ECCS-Vandepitte would be a good alternative to the other design rules, showing a large safety for longer lengths. Design rule ECCS-Vandepitte is however not applicable for short and intermediate lengths.

This is illustrated in Fig. 7 by means of normalized probability density functions, from which the insecurity of applying this method can be noticed. The largest variability in the results was obtained for members subjected to a non-uniform bending moment ($\psi = -1$).

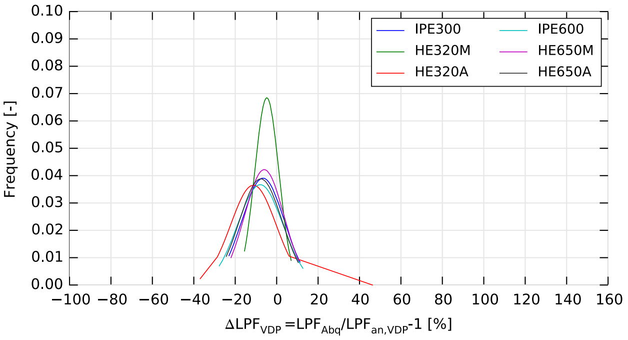

Fig. 7. Normal probability density functions of deviations ΔLPF according to method ECCS-Vandepitte.

The difference between the four different design rules is illustrated for cellular members in Figs. 8-10, but similar findings are possible for plain-webbed members. For members subjected to a constant bending moment ($\psi = 1$), largest deviations are clearly observed for method ECCS-Vandepitte, as mentioned previously. Similar deviations in load proportionality factor are obtained for the other methods.

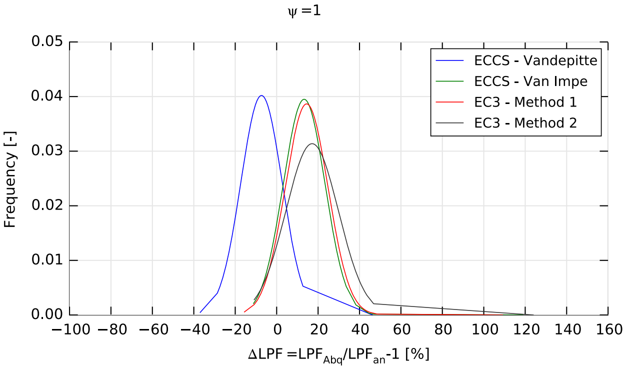

Fig. 8. Normal PDF of ΔLPF according to four different methods ($\psi = 1$).

Compared to $\psi = 1$, a much larger standard deviation can be observed for $\psi = 0$ (Fig. 9) for all methods. It should be noted that application of design rule ECCS-Vandepitte is still unsafe, whereas design rules ECCS-Van Impe and EC3-Method 2 are becoming conservative for longer lengths. Therefore, application of EC3- Method 1 for $\psi = 0$ can be a could alternative. For $\psi = -1$, the standard deviation of all distribution functions is even larger and very conservative results are obtained by application of methods ECCS-Van Impe and EC3-Method 2. Application of EC3-Method 1 is therefore a good alternative, but for $\psi = -1$ even ECCS-Vandepitte can be preferred. Except for short length members, application of the latter is safe and less conservative than the other methods.

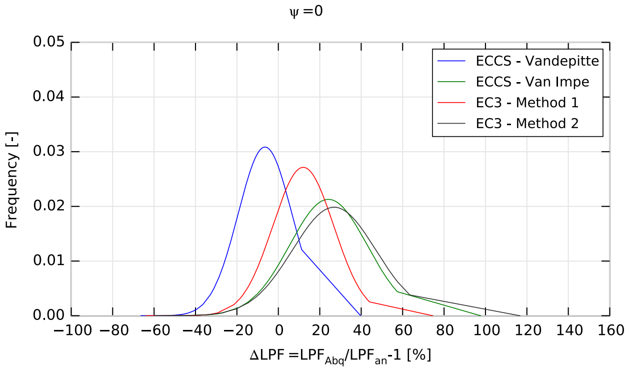

Fig. 9. Normal PDF of ΔLPF according to four different methods ($\psi = 0$).

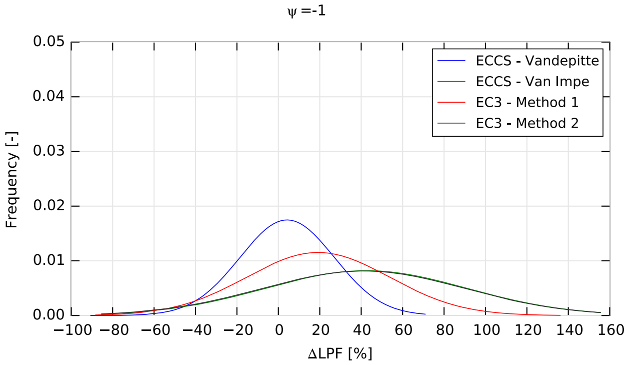

Fig. 10. Normal PDF of ΔLPF according to four different methods ($\psi = -1$).

REFERENCES

[1] Gevaert, D. *De sterkte van excentrisch samengedrukte staven*, 2010.

[2] ECCS, *Ultimate Limit State Calculation of Sway Frames with Rigid Joints*, ECCS General Secretariat, 1984.

[3] Sonck, D. *Global Buckling of Castellated and Cellular Steel Beams and Columns*, 2014.

Contents

I Introduction and state of the art 1

1 Introduction 3
- 1.1 Advantages/disadvantages 3
- 1.2 Application as beam-columns 3
- 1.3 Production method cellular members 4
- 1.4 Residual stresses 4
  - 1.4.1 Parent sections 5
  - 1.4.2 Cellular and castellated members 6
- 1.5 Failure modes of cellular members 7
  - 1.5.1 Vierendeel mechanism 7
  - 1.5.2 Web post buckling 7
  - 1.5.3 Shear resistance 8
- 1.6 Previous and recent research 8
- 1.7 Overview thesis research 9
- 1.8 Organisation of the thesis 10

2 Stability design rules 13
- 2.1 Member behaviour 13
- 2.2 General 14
- 2.3 Column buckling 15
  - 2.3.1 Buckling resistance ECCS 15
  - 2.3.2 Buckling resistance EC3 17
  - 2.3.3 The Ayrton-Perry-Robertson approach 18
  - 2.3.4 Critical buckling load 19
- 2.4 Lateral-torsional buckling of beams 20
  - 2.4.1 Critical buckling moment 20
  - 2.4.2 Non-uniform bending moments 21
  - 2.4.3 Buckling resistance 23
    - 2.4.3.1 EC3 - General method 23
    - 2.4.3.2 EC3 - Specific method 24
    - 2.4.3.3 EC3 - Modified Specific method 25
    - 2.4.3.4 Taras Approach 26
  - 2.4.4 Lateral distortional buckling 27
- 2.5 Beam-columns 27
  - 2.5.1 Cross-section resistance 28
  - 2.5.2 Plastic resistance 28
    - 2.5.2.1 Reduced plastic moment resistance $M_{N,Rd}$ 29
    - 2.5.2.2 Influence of shear force 30
    - 2.5.2.3 ECCS - Vandepitte 30

2.5.2.4 General formula plastic resistance . . . 30
2.5.3 Elastic resistance . . . 31
2.5.3.1 Combined shear and bending . . . 31
2.5.4 ECCS - Vandepitte . . . 31
2.5.4.1 Design formula . . . 31
2.5.4.2 Ideal shape imperfections . . . 32
2.5.4.3 Adaptations design formula . . . 33
2.5.4.4 Equivalent moment factor β . . . 33
2.5.4.5 Members susceptible to lateral torsional buckling . . . 34
2.5.5 ECCS - Van Impe . . . 35
2.5.5.1 General strength conditions . . . 35
2.5.5.2 Strong-axis bending . . . 36
2.5.5.3 Weak-axis bending . . . 37
2.5.6 Eurocode . . . 37
2.5.7 Method 1 . . . 37
2.5.7.1 Derivation of general formulae . . . 37
2.5.7.2 Beam-column under biaxial bending and axial force . . . 38
2.5.7.3 Members susceptible to lateral-torsional buckling . . . 39
2.5.7.4 Continuity to cross-sectional resistance . . . 41
2.5.7.5 Equivalent uniform moment factor C_m . . . 41
2.5.8 Method 2 . . . 42
2.5.8.1 Characteristics buckling rules Method 2 . . . 43
2.5.8.2 Members not susceptible to lateral torsional buckling . . . 44
2.5.8.3 Members susceptible to lateral torsional buckling . . . 45
2.5.8.4 Members of class 3 or 4 . . . 47
2.6 Application to cellular members . . . 48
2.6.1 Design approach for cellular members . . . 48
2.6.1.1 2T Approach . . . 48
2.6.1.2 1T Approach . . . 48
2.6.2 Buckling curves . . . 49
2.6.2.1 Buckling curves for FB . . . 49
2.6.2.2 Buckling curves for LTB . . . 49

II Numerical research 51

3 Eccentrically loaded plain-webbed members 53
3.1 Scope of Chapter 3 . . . 53
3.2 Analytical determination of load proportionality factor . . . 54
3.3 Levels of numerical analysis . . . 55
3.4 Numerical determination of load proportionality factor . . . 56
3.5 Element type . . . 57
3.6 Mesh size . . . 58
3.7 Boundary conditions and load application . . . 58
3.8 Geometric imperfection . . . 60
3.9 Residual stress pattern for plain-webbed members . . . 61
3.10 Profiles . . . 61
3.10.1 Classification cross-section . . . 61
3.11 Differences with D. Gevaert . . . 65

3.11.1 Length 65
3.12 Critical load N_{cr} 67
3.13 Deviation of $M_{cr,0}$ 68
3.14 Determination critical LTB moment 69
3.14.1 Numerical determination 69
3.14.2 Analytical determination 69
3.14.3 Comparison different methods 71
3.15 Influence numerical or analytical determination $M_{cr,0}$ on LPF 72
3.16 Parametric study: results and discussion 74
3.16.1 ECCS - Vandepitte 74
3.16.2 ECCS - Van Impe 78
3.16.3 EC3 - Method 1 80
3.16.4 Influence of the considered μ value 83
3.16.5 Comparison different approaches Method 1 83
3.16.6 EC3 - Method 2 85
3.17 Conclusion applicability of the design rules 88

4 Extended parametric study on plain-webbed members 89
4.1 Deviation of $M_{cr,0}$ 89
4.2 Classification cross-section 90
4.3 Alternative representation of the results 92

5 Parametric study on cellular members 95
5.1 Parent sections 95
5.1.1 Parameters cellular openings 95
5.1.2 Profile length 97
5.1.3 Cross-section classification cellular members 98
5.1.4 Types of analyses 100
5.1.5 Critical bending moment M_{cr} 100
5.2 Comparison numerical results with buckling curves for limit cases 101
5.2.1 Flexural buckling 101
5.2.2 Lateral-torsional buckling 103
5.2.3 Members subjected to bending and axial load 105
5.3 Deviation of LPF for different lengths 107
5.4 Deviation of LPF for different slendernesses 107
5.5 Influence of the considered μ value 110
5.6 Influence of the cross-section classification 110
5.7 Influence of the choice of parent section 110
5.7.1 Members subjected to a constant bending moment ($\psi = 1$) 111
5.7.2 Members subjected to a non-uniform bending moment ($\psi = 0$ or $\psi = -1$) . . . 113
5.8 Influence of the dimensions of the web openings and web post width 116
5.9 Comparison of the different methods 118

6 General conclusions and further research 121

III Appendices 123

A Sectional properties 125
A.1 Plain-webbed members 125

A.2 Cross-section classification plain-webbed members according to (CEN, 2005) 126
A.3 FB curve selection according to (CEN, 2005) 126
A.4 Cellular members 126
A.5 Geometrical constraints 127

B Design rules eccentrically loaded members **131**
B.1 Overview stability design rules simply supported members 131
B.1.1 ECCS - Vandepitte 131
B.1.2 ECCS - Van Impe 132
B.1.3 EC3 - Method 1 134
B.1.4 EC3 - Method 2 134
B.2 Safety of the design rules 135
B.3 Deviation between $M_{cr,Abq}$ and $M_{cr,2T,avg}$ for cellular members. 136
B.4 Flexural buckling: additional results for N_{Rd} 137
B.5 Lateral-torsional buckling: additional results for $M_{b,Rd}$ 140
B.6 Members subjected to bending and compression 145
B.7 Deviation LPF according to four different methods 151

C Method 2 **153**
C.1 Members not susceptible to lateral torsional buckling 153
C.1.1 Buckling under N + M_y 153
C.1.2 In plane buckling under N + M_z 154
C.1.3 Buckling under biaxial bending and axial compression 154
C.1.4 Class 3 cross-sections 155
C.2 Members susceptible to lateral torsional buckling 155
C.2.1 Buckling under $N + M_y$ 155

D Additional results parametric study cellular members **159**
D.1 Deviation factor ΔM_{Abq} 159
D.2 Deviation of N_{cr} 161
D.3 Yield and buckling phenomena in GMNIA and LBA analysis 162

List of Figures

1.1 Cellular, castellated and Angelina^{TM} beams. Extracted from (ArcelorMittal, 2008b). 3
1.2 Manufacturing process of cellular members according to method 3. Extracted from (Westok, 2013). 5
1.3 Residual stress distribution for hot-rolled members proposed in (ECCS, 1984). 5
  a a) Variation of original stress pattern in plain-webbed members h/b>1.2 (ECCS). 6
  b b) Cellular and castellated members (Sonck, 2014). 6
1.4 Proposed residual stress patterns. 6
1.5 Vierendeel mechanism with formation of plastic hinge. Extracted from (Durif et al., 2013). 8
  a a) Inclined compression line over web post's height. Extracted from (Durif et al., 2013). 8
  b b) Compressive and tensile forces across the web post. Extracted from (Durif et al., 2013) and (Tsavdaridis & D'Mello, 2011). 8
1.6 Web-post buckling cellular member. 8
1.7 Overview prior research master thesis. 9
1.8 Overview thesis research. 10

2.1 General structural behaviour of steel member. Extracted from (Trahair et al., 2007). . 13
2.2 Axis conventions, extreme load cases and boundary conditions. Extracted from (Sonck, 2014). 14
2.3 Compressive axial load in longitudinal direction with eccentricity e_z. 15
2.4 Limit behaviour of beam-columns: lateral-torsional buckling and flexural buckling. . . 15
2.5 Deviation of buckling curves ECCS with analytical approximation. 16
2.6 Buckling curves according to EC3-1-1. Extracted from (Taras, 2010). 18
2.7 Ayrton-Perry derivation for simply supported member. 18
2.8 Possible buckling modes at N_{cr}: (a) weak-axis flexural buckling, (b) strong-axis flexural buckling, (c) torsional buckling. Extracted from (Sonck, 2014). 20
2.9 Lateral-torsional buckling of beam loaded in strong-axis bending. Extracted from (Sonck et al., 2012). 20
2.10 Values of ψ for linearly varying moment considered in this work. 21
2.11 Deflection under double curvature bending ($\psi = -1$). Based on (Trahair, 1993). 22
2.12 Values of factor C_1 for different linearly varying bending moment lines. 23
2.13 Modification factor 1/f in function of reduced slenderness $\overline{\lambda}_{LT}$. 25
2.14 Local buckling, LTB and LDB of plain-webbed members. 27
  a a) Reduced bending capacity under axial force. 28
  b b) Bi-axial bending resistance. 28
2.15 Amendment proposal EC3 for cross-sections class 3. Extracted from (Greiner et al., 2013). 28
2.16 Plastic interaction bending moment-axial force (compression: +, tension: -). 29
2.17 Shear area for simplified cross-section of I profile. 30

2.18 Definition of axes eccentric axial load. 32
2.19 Shape imperfections factors $\overline{w}_0$ and $\overline{v}_0$. 32
2.20 Equivalent moment factor β in function of ψ. 34
2.21 Member with initial sinusoidal shaped imperfection and subjected to M and N. 38
2.22 Biaxial bending and interaction criteria N-M resistance. Extracted from (Boissonnade et al., 2004). 41
2.23 Concept equivalent moment factor C_m. Extracted from (Boissonnade et al., 2004). . . 42
2.24 Characteristics of Method 2 of EC3. Extracted from (Greiner & Lindner, 2006). 43
2.25 Interaction formulae Method 2. Extracted from (Greiner & Lindner, 2006). 44
a a) GMNIA Analysis 45
b b) ECS (EN) 45
2.26 Interaction factor k_y for constant moment. Extracted from (ECCS, 2006). 45
a a) LTB about y-axis 46
b b) LTB about z-axis 46
2.27 Buckling modes as function of restraints for members susceptible to torsional deformation. Extracted from (Greiner & Lindner, 2006). 46
2.28 GMNIA-results interaction factor k_{LT} as function of $\overline{\lambda}_z$. Extracted from (Greiner & Lindner, 2006). 47
2.29 Interaction factor k_{LT} for different moment diagrams. Extracted from (Greiner & Lindner, 2006). 47
2.30 Design approaches for cellular members. 49

3.1 Considered moment distributions ($\psi = M_2/M_1$). 54
3.2 Load displacement diagram of HE300A, L=20.3 m, $\psi = 1$, $\mu = 0.1$. 56
3.3 Considered node for load-displacement diagram. 56
3.4 Load displacement diagram of HE300A, L=20.3 m, $\psi = 1$, $\mu = 10$. 57
3.5 Cross-section numerical model with indication web-flange overlap. 57
3.6 Examined variation of number of elements along the flange width. 58
3.7 Preliminary study mesh size based on LBA analysis HE500A (L=18.3 m). 59
3.8 Boundary conditions at end sections. 59
3.9 Load introduction eccentrically loaded HEA180 (M=1000 Nm; N=822.3 N). 60
3.10 Opposing effects preferential direction geometric in-plane imperfection. 60
3.11 Applied residual stress pattern for profiles of Gevaert ($\sigma_{compression} < 0, \sigma_{tension} > 0$). . 61
3.12 Cross-section classification according to plastic and elastic theory (compression: +, tension: -). 62
3.13 Deviation of LPF following a plastic or elastic theory according to Van Impe method . 64
3.14 Reduced slenderness $\overline{\lambda}$ for 10 different profiles of Gevaert for 4 different lengths (defined by k). 66
3.15 Reduced slenderness for LTB $\overline{\lambda}_{LT}$ for 10 different profiles of Gevaert for 4 different lengths (defined by k; $\psi = 1$). 67
3.16 Observed web distortion for IPE240 ($\psi = -1; L = 2.4\,m$) 68
3.17 First eigenmode of HE300A (L=2.9 m). 69
3.18 Deviation of M_{cr0} for profiles in (Gevaert, 2010). 70
3.19 Determination of M_{cr} based on 4 different methods for IPE240, L=16.8 m, $\mu = \infty$ . . . 71
3.20 Determination of M_{cr} based on 4 different methods for IPE240, L=2.4 m, $\mu = \infty$ . . . 72
3.21 Deviation of LPF based on analytical or numerical value of $M_{cr,0}$. 73
3.22 Deviation between the numerically and analytically obtained LPF according to Vandepitte method ($\psi = 1$). 75

3.23 Deviation between the numerically and analytically obtained LPF according to Vandepitte method ($\psi = -1$). 75
3.25 Comparison design rule ECCS-Vandepitte for IPEO450 and HE500A ($\psi = 1$). 76
3.24 Moment-Normal force interaction diagram IPEO450 under different load configurations and for different lengths 77
3.26 Strength condition in function of load proportionality factor for IPEO450 and HE500A. 78
3.27 Deviation between the numerically and analytically obtained LPF according to ECCS-Van Impe ($\psi = 0$). 79
3.28 Deviation between the numerically and analytically obtained LPF according to ECCS-Van Impe ($\psi = -1$). 79
3.29 Unsafe approach of EC3-Method 1 for IPE120. 80
3.30 Nomenclature box plot. 81
3.31 Deviation of ΔLPF for the Modified General Method for different values of ψ. 82
3.32 Histogram of deviation of LPF according to EC3-Method 1: IPE sections. 83
3.33 Histogram of deviation of LPF according to EC3-Method 1: HE sections. 83
3.34 Comparison approaches Method 1 for IPEO600. 84
3.35 Comparison approaches Method 1 for IPEO600. 85
3.36 Insecurity of EC3 - Method 2 for HE500A. 86
3.37 Economic application of Method 2 for HE180A profile. 87

4.1 Deviation of M_{cr0} for profiles extended parametric study. 90
4.2 Transition elastic-plastic theory HE650A (L=12.6 m, $\psi = 1$). 91
4.3 Normal PDF of members extended parametric study. 93

5.1 Cellular member dimensions. Extracted from (Sonck, 2014). 96
5.2 Illustration of combinations c1-c4 for HE650M. 96
5.3 Equivalent opening cellular member. Extracted from (Sonck, 2014). 101
5.4 Observed web-post buckling for IPE300 (L=2.18 m; $\psi = -1$). 101
5.5 Deviation of $M_{cr,2T}$. 102
5.6 Comparison numerical results with existing buckling curves ($\mu = 0$). 103
5.7 Comparison numerical results with existing buckling curves ($\mu = \infty$; $\psi = 1$). 104
5.8 Comparison numerical results with existing buckling curves ($\mu = \infty$; $\psi = 0$). 105
5.9 Comparison numerical results with existing buckling curves ($\mu = \infty$; $\psi = -1$). 106
5.10 Comparison numerical results with existing buckling curves for all μ values - IPE sections ($\psi = 1$). Data corresponding to $\mu = \infty$ indicated in red; Blue is used for all other μ values. 106
5.11 Comparison numerical results with existing buckling curves for all μ values - HE sections ($\psi = 1$). Data corresponding to $\mu = \infty$ indicated in red; Blue is used for all other μ values. 107
5.12 Deviation of LPF for cellular members as function of length. 108
5.13 Deviation of LPF for cellular members as function of slenderness. 109
5.14 Influence of considered μ value for cellular members. 110
5.15 Moment-Normal force interaction diagram HE650M (L=16.13 m; $\psi = 1$). 111
5.16 Normal PDF of ΔLPF according to method ECCS-Vandepitte ($\psi = 1$). 111
5.17 Normal PDF of ΔLPF according to method ECCS-VI ($\psi = 1$). 112
5.18 Normal PDF of ΔLPF according to Method 1 ($\psi = 1$). 112
5.19 Normal PDF of ΔLPF according to Method 2 ($\psi = 1$). 113
5.20 Normal PDF of ΔLPF according to method ECCS-VDP ($\psi = 0$). 113
5.21 Normal PDF of ΔLPF according to method ECCS-VI ($\psi = 0$). 114

5.22 Normal PDF of ΔLPF according to Method 1 ($\psi = 0$). 114
5.23 Normal PDF of ΔLPF according to Method 2 ($\psi = 0$). 114
5.24 Normal PDF of ΔLPF according to method ECCS-VDP ($\psi = -1$). 115
5.25 Normal PDF of ΔLPF according to method ECCS-VI ($\psi = -1$). 115
5.26 Normal PDF of ΔLPF according to Method 1 ($\psi = -1$). 116
5.27 Normal PDF of ΔLPF according to Method 2 ($\psi = -1$). 116
5.28 Influence dimensions web openings on design rule Method 2. 117
5.29 Normal PDF of ΔLPF according to four different methods. 119

A.1 Dimensions cross-section parent section and cellular member. 127

B.1 Members subjected to strong-axis bending moment M_y and axial load N. 131
B.2 FB curves: Deviations $N_{Rd,Abq}$ with buckling curve a. 137
B.3 FB curves: Deviations $N_{Rd,Abq}$ with buckling curve b. 137
B.4 FB curves: Deviations $N_{Rd,Abq}$ with buckling curve c. 138
B.5 FB curves: Deviations $N_{Rd,Abq}$ with buckling curve d. 138
B.6 LTB curves: Deviations $M_{Rd,Abq}$ with buckling curve a. 140
B.7 LTB curves: Deviations $M_{Rd,Abq}$ with buckling curve b. 140
B.8 LTB curves: Deviations $M_{Rd,Abq}$ with buckling curve c. 141
B.9 LTB curves: Deviations $M_{Rd,Abq}$ with buckling curve d. 141
B.10 Comparison numerical results with existing buckling curves for all μ values - IPE sections ($\psi = 0$). Data corresponding to $\mu = \infty$ indicated in red; Blue is used for all other μ values. 148
B.11 Comparison numerical results with existing buckling curves for all μ values - HE sections ($\psi = 0$). Data corresponding to $\mu = \infty$ indicated in red; Blue is used for all other μ values. 148
B.12 Comparison numerical results with existing buckling curves for all μ values - IPE sections ($\psi = -1$). Data corresponding to $\mu = \infty$ indicated in red; Blue is used for all other μ values. 149
B.13 Comparison numerical results with existing buckling curves for all μ values - HE sections ($\psi = -1$). Data corresponding to $\mu = \infty$ indicated in red; Blue is used for all other μ values. 149

C.1 GMNIA-results interaction factor k_z as function of $\overline{\lambda}_z$. Extracted from (Greiner & Lindner, 2006). 154
C.2 Equivalent moment factor C_m Method 2. 157

D.1 Comparison GMNIA and LBA results for $\mu = \infty$ and $\psi = 1$. 160
D.2 Comparison GMNIA and LBA results for $\mu = \infty$ and $\psi = 0$. 160
D.3 Comparison GMNIA and LBA results for $\mu = \infty$ and $\psi = -1$. 160
D.4 Interaction diagram $M_u/M_{cr,y}$ - $N_u/N_{cr,z}$ of IPE300 section. 161
D.5 Interaction diagram $M_u/M_{cr,y}$ - $N_u/N_{cr,z}$ of IPE600 section. 161
D.6 Deviation of N_{cr} for cellular members. 162
D.7 Yielding of upper flange, lower flange and around web openings of HE320A section (L=4.2 m; $\mu = 0$; $\psi = 1$). 163
D.8 Plastic yielding at corners of web openings of HE320A section (L=4.2 m; $\mu = \infty$; $\psi = -1$). 163
D.9 Web post buckling of HE320A section (L=4.2 m; $\mu = \infty$; $\psi = -1$). 164

List of Tables

2.1 Buckling curves ECCS for S235 and $t_f < 40\,mm$. 16
2.2 Imperfection factor α for buckling curves ECCS. 16
2.3 Yield strength for buckling resistance ECCS. 17
2.4 Imperfection factor α for buckling curves EC3. 17
2.5 Imperfection factor α_{LT} for LTB curves. 23
2.6 General Method: Lateral-torsional buckling curve. 24
2.7 Specific Method: Lateral-torsional buckling curve. 25
2.8 Imperfection factor α_{LT} according to Taras. 26
2.9 Current buckling curves for plain-webbed members (PWM) EC3 for hot-rolled sections (EC3) and proposal for cellular members. 49
2.10 Preliminary proposal for LTB curves per parent section based on existing buckling curves. 50

3.1 Considered values of μ. 54
3.2 Initial load condition. 55
3.3 Overview mesh size for different no. of elements along the flange width. 58
3.4 Cross-sectional properties profiles Gevaert. 61
3.5 Classification of cross-sections Gevaert for $\psi = 1$ (k=1) ($c = h - t_f - 2r$). 63
3.6 Classification of cross-sections Gevaert for $\psi = 0$ and $\psi = -1$ ($c = h - t_f - 2r$). 63
3.7 Classification of cross-sections Gevaert for $\psi = 1$ according to EC3 ($c = h - 2t_f - 2r$). 63
3.8 Classification of cross-sections Gevaert for $\psi = 0$ and $\psi = -1$ according to EC3 ($c = h - 2t_f - 2r$). 63
3.9 Comparison of assumptions in this work with Gevaert. 65
3.10 Profile length plain-webbed members. 66
3.11 Slenderness range $\overline{\lambda_z}$ and $\overline{\lambda}_{LT,min}/\overline{\lambda}_{LT,min}$ for plain-webbed members. 66
3.12 Deviation of N_{cr}. 67
3.13 Deviation of $M_{cr,Abq}$ and $M_{cr,an}$. 68
3.14 Deviation $M_{cr,0} > 10\%$ for profiles in (Gevaert, 2010). 69
3.15 Deviation of LPF based on analytical or numerical value of $M_{cr,0}$. 72
3.16 Overview considered values of μ. 74
3.17 Characteristics profiles IPEO450 and HE500A for comparison strength condition Vandepitte. 78
3.18 Combinations for which design rule ECCS-Van Impe is unsafe. 80
3.19 Combinations for which design rule EC3-Modified General Method 1 is unsafe. Values of μ for which no maximum was reached in the load-displacement diagram are given in brackets after *. 81
3.20 Profiles numbers of geometries examined in Fig. 3.31. 83
3.21 Profiles with largest deviation between General Method and Modified General Method ($\psi = -1$). 84
3.22 Combinations for which design rule EC3-Method 2 is unsafe. 85

3.23 Combinations for which EC3-Method 2 is more economic than EC3-Method1 (Modified General). 86

4.1 Cross-sectional properties parent sections. 89
4.2 Classification of cross-sections extended study for $\psi = 1$ (wire model). 91
4.3 Classification of cross-sections extended study for $\psi = 0$ and $\psi = -1$ (wire model). . . 92
4.4 Classification of cross-sections extended study for $\psi = 1$ according to EC3. 92
4.5 Classification of cross-sections extended study for $\psi = 0$ and $\psi = -1$ according to EC3. 92

5.1 Considered factors f_a and f_w 96
5.2 Considered combinations factors f_a and f_w. 96
5.3 Adapted values considered values factors f_a and f_w. 97
5.4 Profile length cellular members. 98
5.5 Slenderness range $\overline{\lambda}_z$ and $\overline{\lambda}_{min}/\overline{\lambda}_{max}$ for cellular members. 98
5.6 Classification of cellular members for $\psi = 1$ ($c = h - 2t_f - 2_r$). 99
5.7 Classification of cellular members for $\psi = 0$ and $\psi = -1$ ($c = h - 2t_f - 2r$). 99
5.8 Geometries with largest ineffective height h_{ineff}. 100
5.9 Best fitting EC3 buckling curve under pure compression. 103
5.10 Best fitting EC3 buckling curve under pure bending. 105
5.11 Best fitting EC3 buckling curve under bending and compression. 106

A.1 Maximum width-to thickness ratios for compression parts (1) (CEN, 2005). 126
A.2 Maximum width-to thickness ratios for compression parts (2) (CEN, 2005). 127
A.3 Selection of buckling curves for flexural buckling (CEN, 2005). 128

B.1 Overview μ values for which design rule ECCS-Vandepitte is unsafe. Values of μ for which no maximum was reached in the load-displacement diagram are given in brackets after *. 135
B.2 Combinations with large deviations between $M_{cr,Abq}$ and $M_{cr,2T,avg}$ due to web-post buckling. 136
B.3 Deviation of $N_{Rd,2T}$ for cellular members under pure compression. The underlined values indicate the best fitting EC3 buckling curves. 139
B.4 Deviation of $M_{b,Rd}$ for cellular members under pure bending ($\psi = 1$). The underlined values indicate the best fitting EC3 buckling curves. 142
B.5 Deviation of $M_{b,Rd}$ for cellular members under pure bending ($\psi = 0$). The underlined values indicate the best fitting EC3 buckling curves. 143
B.6 Deviation of $M_{b,Rd}$ for cellular members under pure bending ($\psi = -1$). The underlined values indicate the best fitting EC3 buckling curves. 144
B.7 Deviation of $M_{N,b,Rd}$ for cellular members under bending and compression ($\psi = 1$). The underlined values indicate the best fitting EC3 buckling curves. 145
B.8 Deviation of $M_{N,b,Rd}$ for cellular members under bending and compression ($\psi = 0$). The underlined values indicate the best fitting EC3 buckling curves. 146
B.9 Deviation of $M_{N,b,Rd}$ for cellular members under bending and compression ($\psi = -1$). The underlined values indicate the best fitting EC3 buckling curves. 147
B.10 Deviation of LPF for method ECCS-Vandepitte. 150
B.11 Deviation of LPF for method ECCS-Van Impe. 150
B.12 Deviation of LPF for Method 1. 151
B.13 Deviation of LPF for Method 2. 151
B.14 Comparison deviations of four methods. 152

D.1 $\Delta M_{Abq,max}$ for different ψ values. 159
D.2 Minimum deviation of $N_{cr,Abq}$ and $N_{cr,an}$. 162
D.3 Overview results GMNIA and LBA analysis HE320A for pure compression ($\mu = 0$). . . 162
D.4 Overview results GMNIA and LBA analysis HE320A for pure bending ($\mu = \infty$). . . . 163

Acronyms and Symbols

EC3	Eurocode 3 (CEN, 2005)
ECCS	European Convention for Constructional Steelwork
ENV3	European prestandard of EC3 (CEN, 1992)
FB	Flexural Buckling
GMNIA	Geometric and Material Non-linear Analysis with Imperfections
LBA	Linear Buckling Analysis
LDB	Lateral-Distortional Buckling
LPF	Load proportionality factor
LTB	Lateral-Torsional Buckling
M1	EC3 - Method 1
M2	EC3 - Method 2
MNA	Material Non-linear Analysis
PWM	Plain-webbed members
VDP	ECCS - Vandepitte
VI	ECCS - Van Impe

Displacements

ϕ	Rotation of cross-section around x-axis
u	Longitudinal displacement (x-direction)
v	Horizontal displacement (y-direction)
w	Vertical displacement (z-direction)

Material properties

E	Modulus of elasticity
f_y	Yield stress
G	Shear modulus

Geometry

A	Cross-section area
A_{eff}	Effective cross-section area for sections class 4
A_v	Shear area
a	Opening height cellular member
b	Width plain-webbed and cellular member
c	Width or depth of a part of a cross-section (cross-section determination)
h	Height of plain-webbed member or parent section
h_{ineff}	Height ineffective web part sections class 4
H	Height of cellular member
I_y	Second moment of area around the strong axis (y)
I_z	Second moment of area around the weak axis (z)
I_0	Polar moment of area
I_t	Torsional constant
I_w	Warping constant
l_0	Opening diameter
L	Length of the member
n	Number of openings of cellular member
r_b	Cutting width cellular member
r	Fillet radius
t_f	Flange thickness
t_w	Web thickness
w	Web post width (intermediate distance between openings)
W_{el}	Elastic section modulus
w_{end}	Width of web post at end sections
W_{pl}	Plastic section modulus
W_y	Section modulus for strong-axis bending
W_z	Section modulus for weak-axis bending

Stability design rules

a	Ratio of web area to gross area
C_1	Correction factor non-uniform bending moment (EC3)
C_{mLT}	Parameter taking into account the influence of the axial load and the shape of the cross-section on the LTB resistance (design rule EC3 - Method 1)
C_{my}	Equivalent moment factor for strong-axis bending moments (design rule EC3 - Method 1)
C_{mz}	Equivalent moment factor for weak-axis bending moments (design rule EC3 - Method 1)
C_{yy}	Interaction factor taking into account the amount of plasticity in the cross-section at failure (design rule EC3 - Method 1)
C_{zz}	Interaction factor taking into account the amount of plasticity in the cross-section at failure (design rule EC3 - Method 1)
e	Eccentricity of the applied axial force
f	Moment-gradient modification factor for non-uniform bending moments (EC3)
f_{yr}	Reduced yield strength due to shear force
k_c	Factor for determination of f, depending on the shape of the bending moment line
k_w	Effective length factor for out-of-plane buckling (in Eq. of Mcr)

k_z	Effective length factor for in-plane buckling (in Eq. of Mcr)
M	Bending moment
M_{cr}	Critical LTB bending moment
$M_{N,Rd}$	Reduced plastic moment resistance by axial force

$M_{ply,Rd}$	Plastic moment resistance about the strong axis (y)
$M_{plz,Rd}$	Plastic moment resistance about the strong axis (z)
M_{Rd}	Bending resistance
M_u	Moment at failure
N	Axial (compressive) load
$N_{b,Rd}$	Normal buckling resistance
$N_{b,y,Rd}$	Strong-axis normal buckling resistance
$N_{b,z,Rd}$	Weak-axis normal buckling resistance
N_{cr}	Critical buckling load
$N_{cr,y}$	Critical strong-axis flexural buckling load
$N_{cr,z}$	Critical weak-axis flexural buckling load
$N_{cr,t}$	Critical torsional buckling load
N_{pl}	Plastic load
N_u	Axial load at failure
S	First moment of area
V	Shear force
$V_{pl,Rd}$	Plastic shear resistance
v_0	Ideal shape imperfection in XZ-plane
w_0	Ideal shape imperfection in XY-plane

α	Part of a cross section in compression (cross-section determination)
α	Imperfection factor column buckling curves
α	Shape factor for strong-axis bending (y) (design rule ECCS-Vandepitte)
α_{LT}	Imperfection factor LTB curves
β_y	Equivalent moment factor for strong-axis bending moment (y)
β_z	Equivalent moment factor for weak-axis bending moment (z)
γ_{M0}	Partial factor for resistance of cross-sections (independent of Class)
γ_{M1}	Partial factor for 'resistance of members to instability assessed by member checks'
ΔN	Deviation factor numerical-analytical results of members subjected to axial load
ΔM	Deviation factor numerical-analytical results of members subjected to bending moment
ΔLPF	Deviation factor numerical-analytical results of load-proportionality factor
θ	Reduction factor for LTB (design rule ECCS-Vandepitte)
λ	Non-dimensional slenderness
λ	Load proportionality factor (Alternative notation: LPF)
λ_{LT}	Non-dimensional slenderness for LTB
λ_0	Reduced slenderness for LTB under uniform moment (design rule EC3-Method 1)
λ_u	Load proportionality factor at failure
μ	Factor determining the magnitude of the axial load relative to the bending moment
ν	Reduction factor for column buckling (design rule ECCS-Vandepitte)

ρ	Reduction factor taking into account the influence of the shear force on the yield strength
σ_{cr}	Critical elastic LTB stress (design rule ECCS-Vandepittte)
τ	Local shear stress
ϕ	Value to determine reduction factor χ
ϕ_0	Amplitude torsional imperfection for strong-axis bending
χ	Reduction factor for FB
χ_{LT}	Reduction factor for LTB curves
ψ	Ratio of the end moments (Considered values: 1, 0 and -1)

Part I

Introduction and state of the art

Chapter 1

Introduction

When circular web openings with regular spacing are provided along the length of I-section members, the members are designated as cellular members. Also castellated members with hexagonal openings are commonly used, but these will not be focused on in this work. Alternative opening shapes were recently introduced of which Angelina^{TM} beams, a variant of castellated beams but with sinusoidally shaped openings, are most often applied (Fig. 1.1). These alternative opening shapes are outside the scope of this work. For a detailed description on the application and geometry of these specific members, the reader is referred to (ArcelorMittal, 2008b).

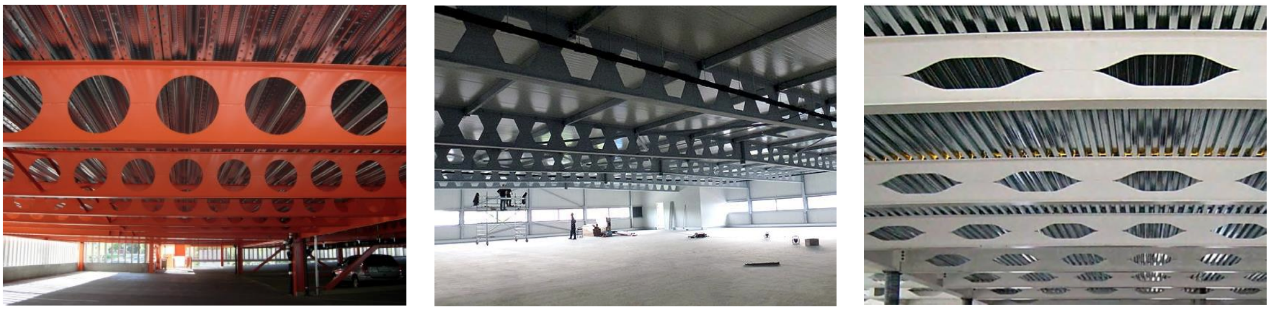

Figure 1.1: Cellular, castellated and Angelina^{TM} beams. Extracted from (ArcelorMittal, 2008b).

1.1 Advantages/disadvantages

The openings of cellular members can have a diameter up to 80% of the member's height with only a limited intermediate distance between the openings, resulting in a transparent design (ArcelorMittal, 2008c). Besides the lighter appearance of cellular members, the most important advantage is that increased spans (in the region of 40 m) are possible due to their higher moment-of-inertia-to-weight ratio. Furthermore, service ducts can be guided through the openings, reducing the floor-to-floor height. Disadvantages are the lower shear capacity, the modified failure pattern and therefore the larger calculation effort. Furthermore, cellular members are less suitable for concentrated loads and despite their more economic material use, the production costs will be higher.

1.2 Application as beam-columns

Cellular members have already been applied for more than thirty years, but principally as beams loaded in strong-axis bending, taking advantage of their increased bending resistance compared to plain-webbed members. In this master thesis however, another application as beam-columns subjected to a combination of bending moment (M) and axial compressive force (N), is being focused on. The

bending moment is possibly arising from the eccentric application of an axial force in longitudinal direction or determined by the boundary conditions and transversal loads.
The specific application as columns is less common and their design mostly based on conservative rules and good engineering judgement. The question can be asked whether applying cellular members vertically is useful, because for lower height columns the presence of the openings will decrease the axial capacity. The contribution of the web to the axial capacity is larger than to the strong-axis bending moment resistance. Therefore, the impact of the web perforations will be larger for columns than for long span beams.
However, for slender columns weak-axis flexural buckling is the dominant factor regarding column design, not the pure axial capacity (Verweij, 2010). One of the factors influencing this buckling capacity is the radius of gyration i ($\sqrt{I/A}$). By introducing openings in the web, the radius of gyration will increase as well as the ratio between the buckling capacity and the pure axial load capacity. In this way, for slender columns this increase will compensate the reduced pure axial load capacity. Therefore, a nearly equal buckling load can be found for cellular columns as for plain-webbed members. However, the use of cellular columns is favourable with regard to the more economical use of materials and the reduced horizontal deflections induced by wind loads. Compared to their parent sections, the height of cellular members is increased and consequently also the second moment of area, minimising the horizontal deflections. On the contrary, for lower height columns, introducing openings is not proven economical and is mainly driven by aesthetics.

1.3 Production method cellular members

Three different manufacturing methods for cellular members are described in (Lawson & Hicks, 2011).

- Isolated openings are cut in the web of symmetric hot-rolled sections. This method is only applicable for isolated openings, not for multiple openings as considered in this work.
- An I-section is formed by welding three steel plates together. Prior to the welding process, openings are cut in the web. This production method is applicable for both isolated and regularly spaced web openings and can also be used for asymmetric or tapered sections. For tapered sections, a linear variation of the height of the web is obtained by cutting the web at an angle to the central axis.
- An existing H- or I-shaped hot-rolled plain-webbed member is cut according to a regular pattern along the web. Afterwards, by shifting and re-welding the separated top and bottom sections, the resulting profiles will be 40-60% higher compared to their parent section (Fig. 1.2). Asymmetric sections can also be achieved by executing the cutting process on two different base sections.

The second method is still applied by Fabsec (UK), although the last manufacturing process is more commonly used by amongst others ArcelorMittal (Luxembourg) and Westok (UK) and will be considered in this work. Other fabricators of cellular and castellated beams are CMC Steel Products (USA), New Millennium (USA), Tata Steel Europe Limited, Peiner Träger GmbH (Germany), Macsteel Trading (South Africa), Grünbauer BV (The Nederlands).

1.4 Residual stresses

Residual stresses can have a detrimental influence on the buckling strength of structural steel members. These longitudinal stresses will introduce a system of forces within the cross-section which are always in internal static equilibrium. Due to uneven cooling or heating during the manufacturing process,

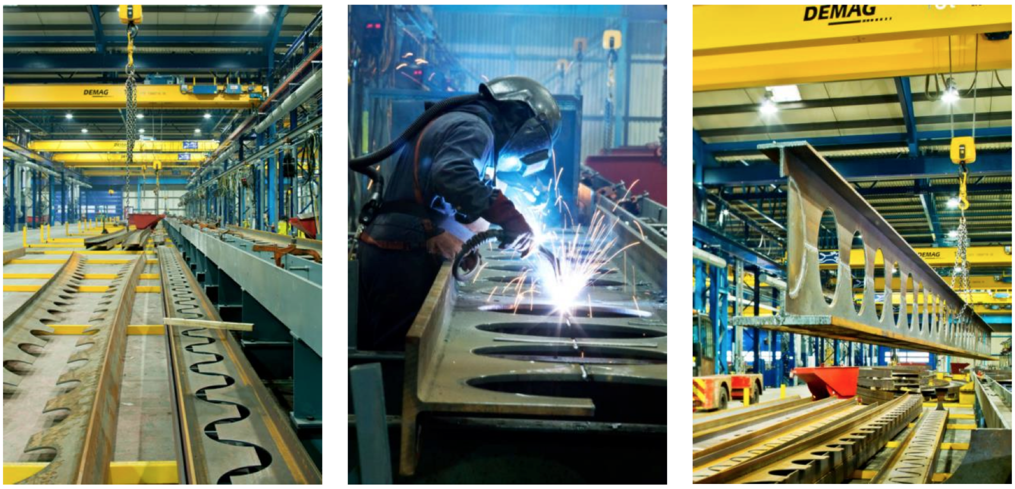

Figure 1.2: Manufacturing process of cellular members according to method 3. Extracted from (Westok, 2013).

residual stresses will be induced. Furthermore, other fabrication operations such as cold-deformation, punching, cambering, welding will influence the formation of residual stresses.

1.4.1 Parent sections

As described in (Young, 1975), residual stresses in I-section members will be generated during the cooling stage of the hot-rolling process. Variability in rolling technique and the corresponding cooling conditions after rolling will introduce different residual stress patterns in the members. The flange tips and the center of the web will cool first; the cooling process at the web to flange junction will be slower. There will be a thermal contraction at the web-to-flange intersection upon cooling. This is however restricted by the already cooled flange tips, resulting in tension at the flange-web intersection.

The residual stress pattern for hot-rolled members proposed in (ECCS, 1984) based on the height-to-width ratio is depicted in Fig. 1.3. A distinction is made between sections with $h/b \leq 1.2$ with a corresponding stress magnitude of $0.5\,f_y$ and sections for which $h/b > 1.2$. For the latter, the stress magnitude is $0.3\,f_y$. Due to plasticity at the compressed tips, the flexibility and consequently the buckling resistance of the member are reduced. Residual stresses have therefore a detrimental influence on the buckling strength, especially on the resistance against weak-axis buckling.

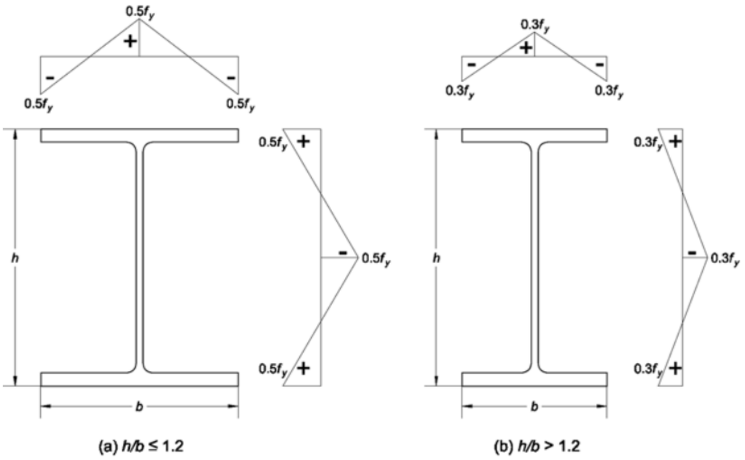

(a) $h/b \leq 1.2$ (b) $h/b > 1.2$

Figure 1.3: Residual stress distribution for hot-rolled members proposed in (ECCS, 1984).

1.4.2 Cellular and castellated members

Due to the additional cutting and welding process of cellular members, an increase of the compressive residual stress in the flanges is possible. Hence, it is expected that the modified residual stress pattern of cellular and castellated members will have a more detrimental effect on the global buckling resistance compared to the residual stresses present in the corresponding parent sections.
In recent research performed by (Sonck, 2014), a proposal was made for this modified residual stress pattern, based on residual stress measurements in both castellated and cellular members with IPE 160 profiles as parent section. The castellated members were fabricated by a standard production procedure, while a deviating fabrication procedure was applied for the cellular members, by cutting circular openings around the hexagonal openings of the castellated members. The cutting procedure was not applied over a length of 1 m at the end of the member, to allow for comparison with the stress pattern of the parent section.
The obtained residual stress patterns of the parent sections showed a good correspondence with the proposed pattern by the ECCS. For the section halves after thermal cutting, a counteracting effect on the residual stress pattern was noticed due to the mechanical effect of the elastic rebound and the thermal effect of the local heat input. Both effects cannot be added linearly due to the non-linear effects of plasticity during the cutting procedure, but the combined influence on the measured stress pattern in the flanges was found to be rather limited.
After welding of the tee sections, the measured residual stresses in the castellated and cellular members were compared with the initial stress pattern proposed by the ECCS (Fig. 1.3). An increase of the compressive stress in the flanges could be noticed. This can be explained by the increased tensile stresses at the web due to the extra heat input during the cutting and welding procedure, which must be balanced by the compressive stresses in the flanges.

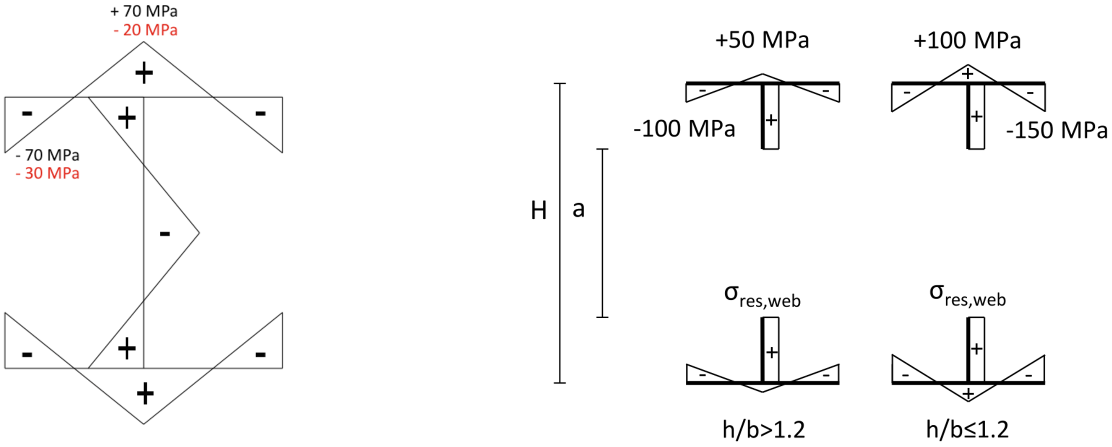

a) Variation of original stress pattern in plain-webbed members h/b>1.2 (ECCS).

b) Cellular and castellated members (Sonck, 2014).

Figure 1.4: Proposed residual stress patterns.

Considering the original stress pattern as proposed by the ECCS for a yield strength f_y of 235 MPa, a stress amplitude of 70 MPa (0.3 f_y) was obtained for h/b >1.2 and 120 MPa (0.5 f_y) for h/b $\leq$ 1.2. The proposal by (Sonck, 2014) implements a stress decrease of 20 MPa at the web-flange connection; for the flange tips, a decrease of 30 MPa is proposed. The suggested adaptations of the original ECCS stress pattern for the specific case of an IPE profile (h/b >1.2) are indicated in Fig. 1.4a. The final proposal of the residual stress pattern by Sonck, depending on the depth to width ratio of the original parent section, is depicted in Fig. 1.4b.
The residual stress pattern is assumed to be constant along the member's length, with a constant

tensile strength in the web at the tee section and at the web post. (Eq. 1.4.1, notation according to Fig. A.1).

$$\sigma_{res,web} = 50\, MPa \cdot \frac{bt_f}{(H - t_f - a)\, t_w} \tag{1.4.1}$$

This adapted residual stress pattern is proposed for both cellular and castellated members based on a standard fabrication procedure. It should be noted that the proposed stress pattern is still preliminary and should be further investigated. However, preference was given to implement the modified stress pattern already in the numerical simulations of the cellular members, since with this pattern a better correspondence of the actual stress pattern could be obtained than in case the stress pattern of plain-webbed members would be used. In case the circular openings are obtained by a non-standard fabrication procedure, a modified stress pattern should be applied (Sonck, 2014).

1.5 Failure modes of cellular members

Two types of failure modes can be identified for cellular members: global and local failure. Global failure modes are essentially similar to those observed for plain-webbed members with lateral-torsional buckling and flexural buckling of main interest in this work. Failure loads can therefore be predicted according to the established methods, but taking into account a few modifications, e.g. the cross-sectional properties should be calculated at the centre of the openings (2T approach) and the buckling curves should be altered to take into account the adapted residual stress pattern. For cellular members however, due to the different shear transfer through the web openings, additional local failure modes can be observed. High shear forces in the member can result in among others the formation of a Vierendeel mechanism, different types of web post failure or shear buckling. This work has however not the aim to give a detailed description of the different failure modes, but is mainly introduced since web-post buckling was observed during the GMNIA analyses.

1.5.1 Vierendeel mechanism

This failure mode is characterized by the formation of four plastic hinges at the corners of the web openings due to local bending. The mechanism is often examined for members with large openings and is most detrimental in case of short length members where shear is dominating. Furthermore, due to the lower plastic resistance of narrow tee sections, the occurrence of the Vierendeel mechanism is more likely. For further information, the reader is referred to (Tsavdaridis et al., 2012); (Kerdal & Nethercot, 1984).

1.5.2 Web post buckling

Web post buckling can be visually observed by an out-of-plane displacement of the web post. The S-shaped displacement of the web post is characteristic for this failure mode (Fig. 1.6a). The web post will be subjected to a combination of horizontal shear and double curvature bending. Both compressive and tensile forces will act across the web post on opposing diagonals. This will result in an inclined compression strut across the member's height (1.6b). Web post buckling can result from the compressive stresses along this compression strut and local buckling was observed adjacent to the openings. This failure mode is further discussed in (Kerdal & Nethercot, 1984); (Durif et al., 2013); (Tsavdaridis et al., 2012); (Tsavdaridis & D'Mello, 2011).

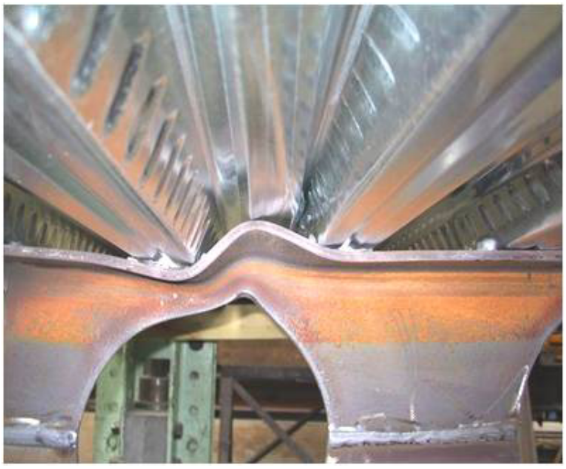

Figure 1.5: Vierendeel mechanism with formation of plastic hinge. Extracted from (Durif et al., 2013).

1.5.3 Shear resistance

To calculate the shear resistance of cellular members, the shear area at the web opening should be taken into account. Under high shear forces, the web can buckle locally and the presence of the web openings will have a detrimental effect on this failure mode, which was also observed for plain-webbed members (Durif et al., 2013).

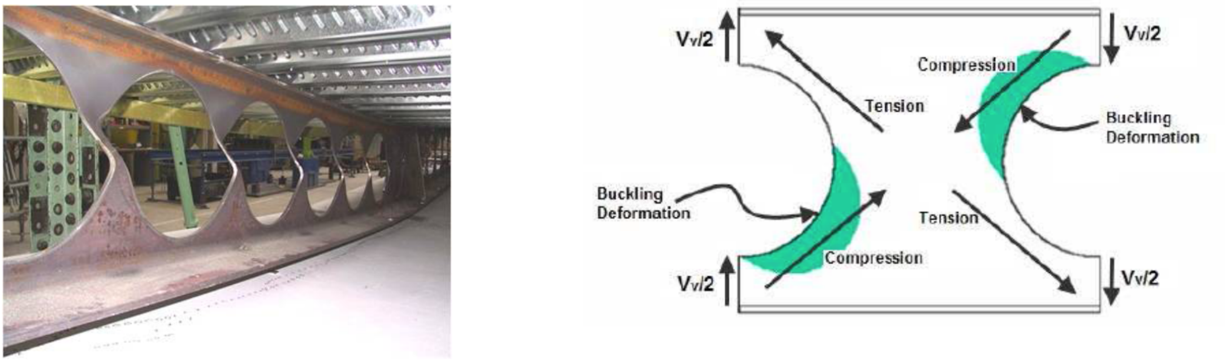

a) Inclined compression line over web post's height. Extracted from (Durif et al., 2013).

b) Compressive and tensile forces across the web post. Extracted from (Durif et al., 2013) and (Tsavdaridis & D'Mello, 2011).

Figure 1.6: Web-post buckling cellular member.

1.6 Previous and recent research

Due to the presence of the openings, the structural behaviour of these members is modified and the global buckling behaviour of members under a compressive force and strong-axis bending moment will be different than for plain-webbed members. To the author's best knowledge, up to now no investigation is carried out on eccentrically loaded cellular or castellated members. Recent research was performed in (Sonck, 2014) for the extreme load cases of only bending or compression of cellular and castellated members with respectively lateral torsion buckling (LTB) and weak-axis flexural buckling (FB) as governing instability modes (Fig. 1.7). Furthermore, in (Gevaert, 2010) the member's resistance of eccentrically loaded plain-webbed members was investigated. A numerical study was performed and the results compared with the analytical results of different design approaches.

The proposed approaches are based on the available resistance calculation methods in the European

Standard EN 1993-1-1 (CEN, 2005), in the remainder referred to as EC3 (Eurocode 3). For the combination of compressive force and bending moment, two different approaches can be found in EC3, Method 1 and 2, of which only Method 1 is applicable in Belgium and Method 2 was therefore not considered by Gevaert. Additionally, the member's resistance was determined according to an alternative set of design rules of the European Convention of Constructional Steelwork (ECCS), although considered less economically compared to the EC3 design rules. However, the theoretical interpretation of the ECCS design rules is more straightforward compared to the complex shaped EC3 design rules of Method 1 including different factors reflecting the physical phenomena. The design rules according to the ECCS approach are listed in (Vandepitte, 1979) and afterwards adapted by Van Impe (Van Impe, 2010) based on the research by Gevaert. A detailed description of the parameters varied in Gevaert's parametric study and the results for the combined compression and bending case on plain-webbed members are given in Chapter 3.

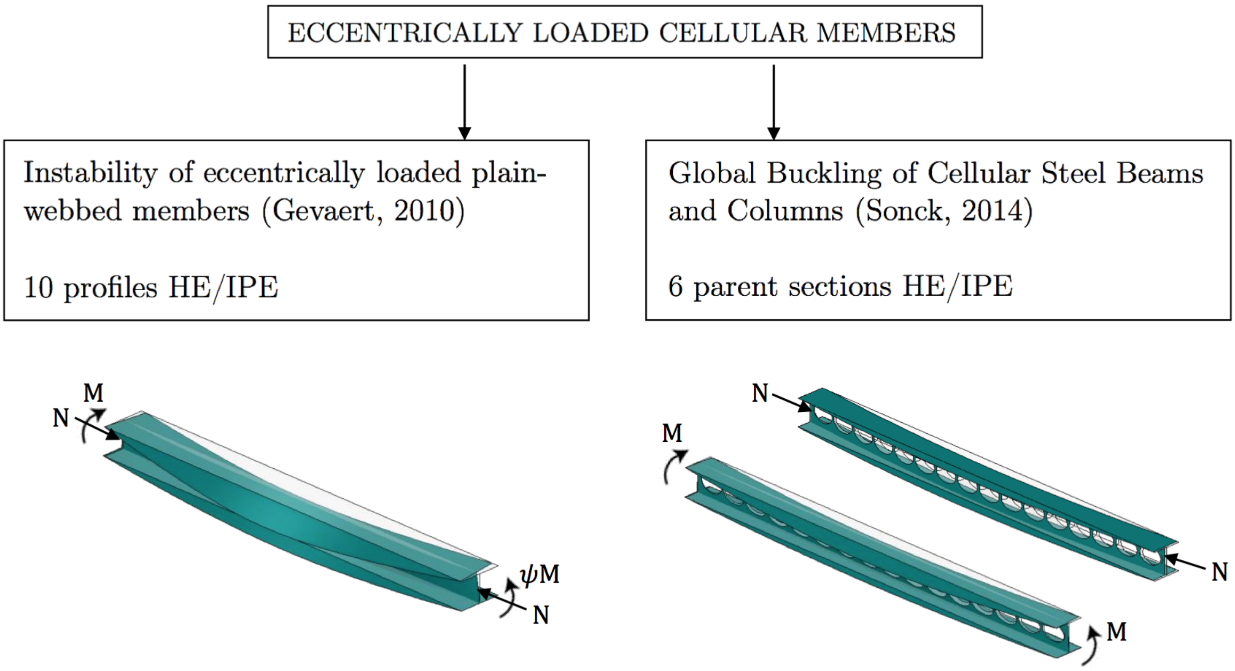
ECCENTRICALLY LOADED CELLULAR MEMBERS
Instability of eccentrically loaded plain-webbed members (Gevaert, 2010)
10 profiles HE/IPE
Global Buckling of Cellular Steel Beams and Columns (Sonck, 2014)
6 parent sections HE/IPE
M
N
ψM
N
N
M
N
M

Figure 1.7: Overview prior research master thesis.

1.7 Overview thesis research

The numerical model in this work will be based on the model used in (Sonck, 2014) for the investigation of global buckling on cellular and castellated members. However, this work will serve as an extended research of the numerical study performed in (Gevaert, 2010) on eccentrically loaded plain-webbed members. Therefore, in order to clarify the assumptions made in Gevaert's work regarding among others the cross-section classification and the exact applied formulation of the design rule ECCS-Van Impe (due to adaptations over the last years), first a parametric study will be performed on the same profiles considered in (Gevaert, 2010). This study was extended with Method 2 of EC3 considering the more user-friendly approach and therefore possible advantage of this method. The available analytical results from Gevaert could also serve as an additional check to avoid mistakes in the Python scripts created for the analytical calculation of the design rules. A detailed interpretation of the results and comparison with both analytical expressions as well as the results of the investigation of Gevaert are given in Chapter 3.

Afterwards, this parametric study on plain-webbed members will be extended with the six profiles, which where considered in (Sonck, 2014) as parent sections for the parametric study of cellular and

castellated members (Fig. 1.8). This additional research is performed as additional validation of the applied model and to extend the limited amount of numerical investigations of plain-webbed members subjected to combined bending and compression. The results of both sets of profiles will be compared and possible additional information or limitations of the study of Gevaert are derived.
Finally, also a parametric study is executed on cellular members with these six profiles as parent sections. The proposed adapted residual stress pattern by Sonck for cellular and castellated members will be implemented in the model. However, it should be noted that experimental measurements of residual stresses were only executed on light parent section geometries (IPE160). Although it can be expected that the production process of cellular and castellated members will have a similar influence on heavier sections, additional residual stress measurements should be performed to confirm the validity of the proposed stress pattern.

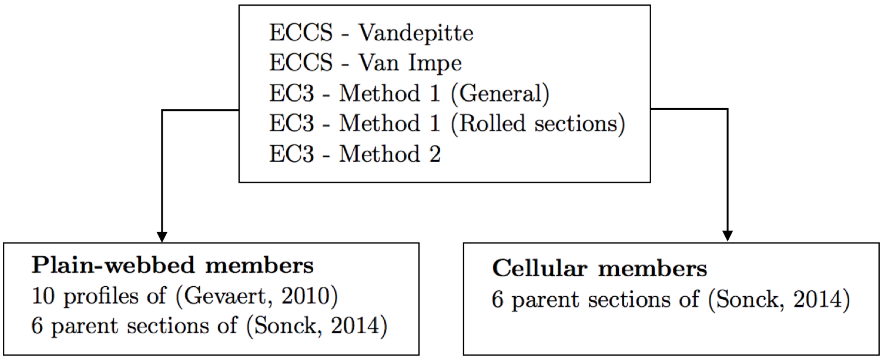
ECCS - Vandepitte
ECCS - Van Impe
EC3 - Method 1 (General)
EC3 - Method 1 (Rolled sections)
EC3 - Method 2
Plain-webbed members
10 profiles of (Gevaert, 2010)
6 parent sections of (Sonck, 2014)
Cellular members
6 parent sections of (Sonck, 2014)

Figure 1.8: Overview thesis research.

Finally, by comparing analytical formulations with the numerical results from the parametric study on cellular members, the following questions will be answered throughout this thesis.

- What is the effect of the web openings of cellular members on the buckling resistance of members subjected to a combination of an axial compressive force and bending moment?
- Is it possible to apply the standard formulations listed in EC3 or alternative expressions proposed by the ECCS, valid for plain-webbed members for the special case of cellular members considering a 2T approach?
- Which of the different expressions shows the best agreement with the numerical results?
- What is the influence of the adapted residual stress pattern proposed in (Sonck, 2014) on the member's buckling resistance of eccentrically loaded members?

1.8 Organisation of the thesis

Part 1 In Chapter 2, first an overview of the stability rules is given for the limit cases of flexural buckling and lateral-torsional buckling. Afterwards, the design rules applicable for eccentrically loaded members are discussed: ECCS-Vandepitte, ECCS-Van Impe, EC3-Method 1 and EC3-Method 2.

Part 2 In Chapter 3, first the determination of the load-proportionality factor is discussed. Afterwards an overview is given on the considered cross-sections for the parametric study on plain-webbed members. Finally, the results of the numerical study are compared with the analytical formulae.

In Chapter 4, a short description of the extended parametric study on the six profiles that are used as parent sections for the cellular members is given.

In Chapter 5, the profiles considered for the parametric study on cellular members are discussed and the numerical results are compared in different ways to the analytical formulae.
Finally, a general conclusion is drawn in Chapter 6 referring to the research questions of Section 1.7 and suggestions for further research are made.

Chapter 2

Stability design rules

2.1 Member behaviour

The response of members loaded by axial forces and bending moments can be characterized by the load-deformation diagram depicted in Fig. 2.1 (Trahair et al., 2007). A linear response until the yield strength is reached can be assumed theoretically for perfectly straight elastic members (curve 1). According to an elastic buckling theory, the elastic member will become unstable at the bifurcation point (intersection curve 1 and 4), corresponding to the critical buckling load. At this critical load sudden failure is caused by the presence of small stress concentrations, imperfections or other disturbances.
In reality, if residual stresses are taken into account, the material will show early non-linearity (curve 2). Depending on the yield stress f_y, a condition of full plasticity can be reached.
Additionally, geometric imperfections or load eccentricities will cause geometric non-linear behaviour (curve 3) of compressed and laterally unsupported members, depending on the modulus of elasticity E and the shear modulus G. The corresponding deformations are quite large, the load-deflection curve approaching the elastic buckling load (curve 4). Global geometric deformations have a detrimental effect on the global buckling resistance; the effect of local geometric deformations is small (Trahair et al., 2007).

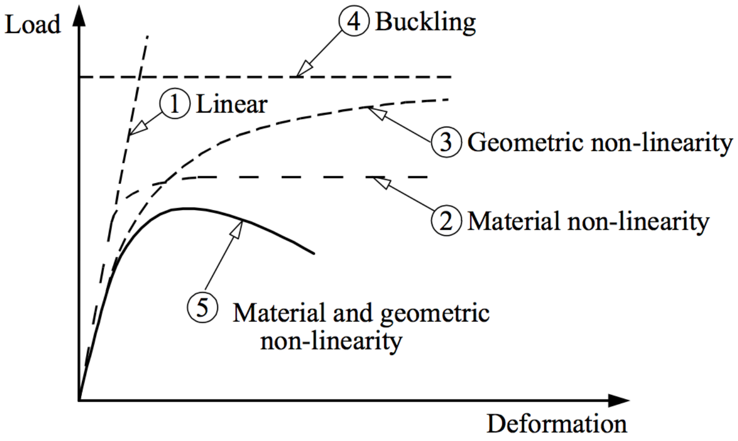

Figure 2.1: General structural behaviour of steel member. Extracted from (Trahair et al., 2007).

For beam-columns subjected to a combination of bending moment and axial load, both material and geometric non-linearities should be considered. Due to material non-linearities a maximum in the load-deflection diagram is reached, i.e. the buckling resistance (curve 5). Therefore for members with combined axial and flexural loads, the failure load is determined by an interaction of yielding and buckling and derived by performing a large number of GMNIA analyses (Geometric Material and Nonlinear Analyses with Imperfections) for different loading conditions. However, due to the stabilizing effect of the pre-buckling deflections the load deflection curve can be constantly increasing without the presence of a maximum in the load-deflection curve. This stabilizing effect can for example be examined for the lateral-torsional buckling behaviour of members subjected to a strong-axis bending moment.

2.2 General

The applied notations of the cross-sectional dimensions for the plain-webbed members and for the parent sections of the cellular members are denoted in Fig. 2.2. Also the applied convention of the principal y- and z-axes is indicated. The x-axis corresponds to the member's direction; the member's length is L. Furthermore, the convention for the extreme load cases corresponding with only strong-axis bending (M) and only a compressive force in longitudinal direction (N) are depicted (Fig. 2.2, a and b).

It should be noted that for the finite element model a numerical model will be used consisting of shell elements without including the fillet (denoted with radius r) at the web-flange intersection (Section 3.5). Therefore, the calculation of the cross-sectional properties will be based on a wire model, in which the omission of the fillet is partly compensated by the overlap at the web-to-flange transition. This simplification will introduce some discrepancies between the analytically calculated and real cross-sectional properties of hot-rolled members. Although in (Taras, 2010) only small differences in buckling curves were obtained for numerical models with or without omission of the fillet, the use of the wire model can have a large effect on the cross-section classification and therefore determine if the calculation should be performed according to an elastic or plastic theory. This influence of the considered model on the cross-section classification will be further discussed in the results of the parametric study on plain-webbed members (Chapter 3). In Fig. 2.2, the total height is denoted with h, including the flanges (with thickness t_f); the thickness of the web is indicated with t_w.

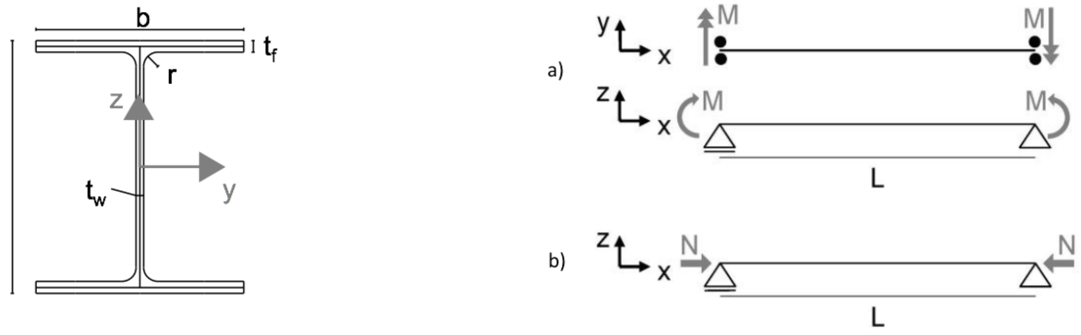

Figure 2.2: Axis conventions, extreme load cases and boundary conditions. Extracted from (Sonck, 2014).

In the remainder of this thesis, to restrict the wide topic of eccentrically loaded members, some limitations will be imposed.

- The members are simply supported with fork-supports at the end. The rotation around the x-axis and well as the translation in y- and z-direction are obstructed, not the rotation around the y- and z-axis;
- Only doubly symmetric I-section members are considered. The principle axes coincide with the axes of symmetry and the shear centre D with the centre of gravity G.

- It is assumed that members are only subjected to a combination of a strong-axis bending moment M and compressive axial load N in longitudinal direction, i.e. in the vertical plane of symmetry XY. Only an eccentricity e_z from the centre of gravity G is considered, $e_y = 0$ (Fig. 2.3).

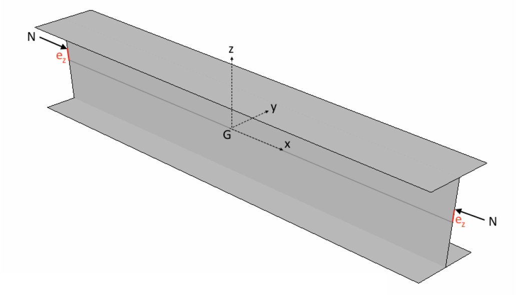

Figure 2.3: Compressive axial load in longitudinal direction with eccentricity e_z.

In Appendix A an overview is given of the standard expressions of the cross-sectional properties for doubly symmetric plain-webbed I-section members.

2.3 Column buckling

Before the available design rules for members under the combined action of axial load and bending moment are discussed, the limit behaviour of beam-columns will be examined more in detail, i.e. lateral torsional buckling of beams under pure bending and flexural buckling of column under pure compression.

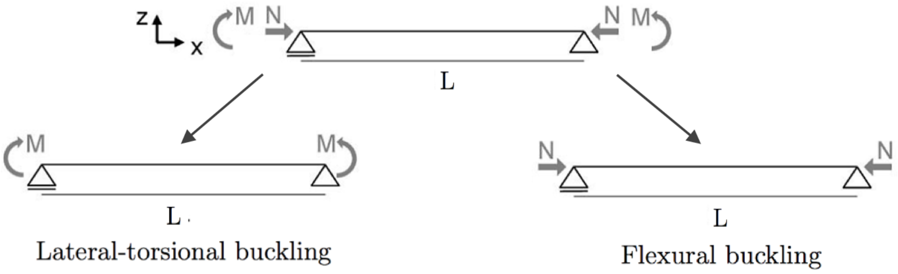

Figure 2.4: Limit behaviour of beam-columns: lateral-torsional buckling and flexural buckling.

2.3.1 Buckling resistance ECCS

In this section the calculation of the buckling resistance that should be applied in the stability design rules of Vandepitte for eccentrically loaded members is described. Different from EC3, according to the ECCS the buckling resistance of members under axial force is determined by the parameters ν and ω (Eq.2.3.1). For hot rolled sections, ω equals 1. The buckling curves are defined based on a similar devision as for the residual stresses. Logically I profiles with small flanges (h/b > 1.2) and lower residual stress values ($\sigma_{res,max} = 0.3 f_y$) correspond with higher buckling curves compared to profiles h/b $\leq$ 1.2 with higher residual stresses (Table 2.1).
The value of ν is determined based on the reduced slenderness $\overline{\lambda}$, listed in tables in (Vandepitte, 1979). The listed values of ν were approximated by the analytical expression (Eq.B.1.8) in (Vandepitte, 1979), for which a good correspondence was found with the actual values. The deviation between the buckling curves obtained by the listed values of the ECCS and those obtained from the analytical approximation is illustrated in Fig. 2.5. Also the Euler curve is depicted corresponding with the buckling behaviour

of a perfectly straight, elastic member without imperfections. The value of α is given in Table 2.2 and depends on the type of buckling curve.

$$N_{b,Rd} = \nu A f_y \omega \tag{2.3.1}$$

$$\overline{\lambda} = \sqrt{\frac{A f_y}{N_{cr}}} \tag{2.3.2}$$

$$\nu = \frac{1}{2\overline{\lambda}^2}\left[1 + \alpha\left(\overline{\lambda} - 0.2\right) + \overline{\lambda}^2 - \sqrt{\left[1 + \alpha\left(\overline{\lambda} - 0.2\right) + \overline{\lambda}^2\right]^2 - 4\overline{\lambda}^2}\right] \tag{2.3.3}$$

It should be noted that for the design formula of Vandepitte the buckling resistance $N_{b,Rd}$ should be determined with an increased yield strength depending on the flange thickness and the real yield strength of the material. This increased value of f_y should be introduced in both Eqs. 2.3.1 and 2.3.2. Attention should be paid that the increased yield stress is only applicable on formulae of Vandepitte. The ECCS formulae adapted by Van Impe and the Eurocode Method 1 and 2 approach are based on the nominal value of f_y.

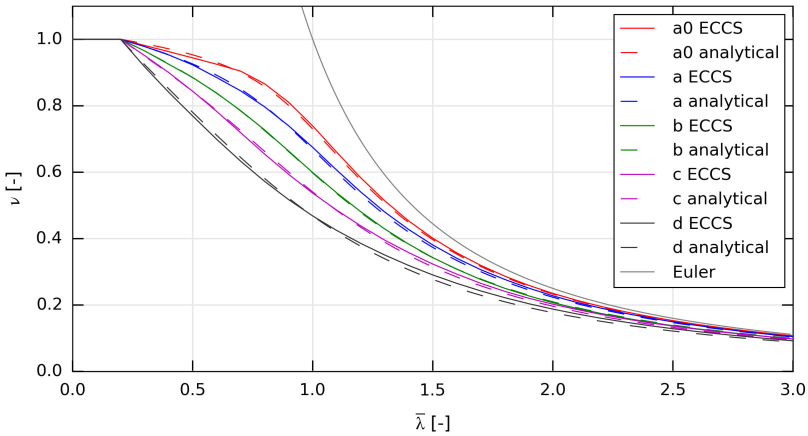

Figure 2.5: Deviation of buckling curves ECCS with analytical approximation.

Table 2.1: Buckling curves ECCS for S235 and $t_f < 40\,mm$.

Buckling axis	h/b	Buckling curve
y-axis	> 1.2	a
	≤ 1.2	b
z-axis	> 1.2	b
	≤ 1.2	c

Table 2.2: Imperfection factor α for buckling curves ECCS.

Buckling curve	a0	a	b	c	d
Imperfection factor α	0.125	0.206	0.339	0.489	0.756

Table 2.3: Yield strength for buckling resistance ECCS.

t_f [mm]	Fe 360/ S235
$t_f \leq 20$	255
$20 < t_f \leq 30$	240
$30 < t_f \leq 40$	225

2.3.2 Buckling resistance EC3

To start with, it should be noted that the design buckling resistance of a compression member according to EC3 is applied in the stability design rules of eccentrically loaded members for all methods, except for the method ECCS-Vandepitte. Also for the method ECCS-Van Impe, a EC3 approach is applied for the buckling resistance, which is given by Eq. 2.3.4, with f_y the yield stress, γ_{M1} the partial factor for the 'resistance of members to instability assessed by members checks' (CEN, 2005), A the cross-section area and χ the reduction factor for the relevant buckling mode as given in Eq.2.3.5.

$$N_{b,Rd} = \frac{\chi A f_y}{\gamma_{M1}} \tag{2.3.4}$$

$$\chi = \frac{1}{\phi + \sqrt{\phi^2 - \overline{\lambda}^2}} \tag{2.3.5}$$

According to the Belgian National Annex, γ_{M1} equals 1. Equation 2.3.4 is only valid for cross-sections of class 1, 2 and 3. For cross-sections of class 4, the effective area should be introduced instead of A. The reduction factor χ is a function of the reduced slenderness $\overline{\lambda}$ (Eq.2.3.6) and the intermediate factor ϕ (Eq. 2.3.7). The same remark for $\overline{\lambda}$ as for Eq.2.3.4 is valid in case of cross-sections class 4.

$$\overline{\lambda} = \sqrt{\frac{A f_y}{N_{cr}}} \tag{2.3.6}$$

$$\phi = 0.5\left[1 + \alpha(\overline{\lambda} - 0.2) + \overline{\lambda}^2\right] \tag{2.3.7}$$

The factor ϕ is determined by the reduced slenderness and the imperfection factor α, which depends on the cross-section geometry, the yield strength, the fabrication process and buckling plane. Appendix A, Table A.3 can be applied for the selection of the buckling curve.

Table 2.4: Imperfection factor α for buckling curves EC3.

Buckling curve	a_0	a	b	c	d
Imperfection factor α	0.13	0.21	0.34	0.49	0.76

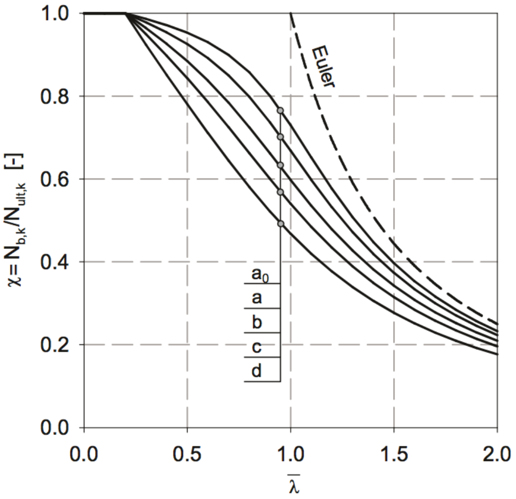

Figure 2.6: Buckling curves according to EC3-1-1. Extracted from (Taras, 2010).

2.3.3 The Ayrton-Perry-Robertson approach

Another important approach to determine the buckling resistance is the Ayrton-Perry-Robertson approach. This method is discussed more in detail here as it forms the basis of the stability design rules of beam-columns according to the ECCS. The most important advantage, compared to the EC3 approach, is that second-order effects due to structural and geometric imperfections can be explicitly introduced in the design formulae.
Consider a simply supported member, subjected to an axial compression force N as indicated in Fig.2.7. An initial sinusoidal shaped imperfection with amplitude e_0 is proposed (Eq.2.3.8).

$$v_0(x) = \bar{e}_0 \sin\frac{\pi x}{L} \tag{2.3.8}$$

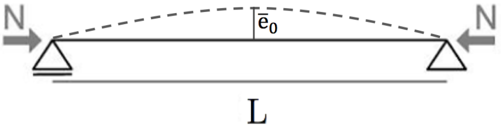

Figure 2.7: Ayrton-Perry derivation for simply supported member.

The Ayrton-Perry formulation that is currently adopted in the Eurocode, is based on the limitation of the elastically calculated compressive stress to the yield stress (Eq. 2.3.9).

$$\frac{N}{A \cdot f_y} + \frac{1}{1 - N/N_{cr}} \cdot \frac{N \cdot \overline{e_0}}{W \cdot f_y} \leq 1.0 \tag{2.3.9}$$

By introducing the following parameters, Eq. 2.3.9 can be rewritten to the normalized form, given in Eq.2.3.11. The factor ϕ is calculated according to Eq.2.3.12, with $\overline{\lambda}$ and η as defined in Eq.2.3.10.

$$\chi = \frac{N}{A \cdot f_y} \qquad \overline{\lambda} = \sqrt{\frac{A \cdot f_y}{N_{cr}}} \qquad \eta = \frac{A \cdot \overline{e_0}}{W} \tag{2.3.10}$$

$$\chi + \eta \cdot \frac{\chi}{1 - \chi \cdot \overline{\lambda}^2} = 1.0 \tag{2.3.11}$$

$$\phi = 0.5 \left[1 + \eta + \overline{\lambda}^2\right] \tag{2.3.12}$$

In Eq.2.3.11, η represents the generalized imperfection, an estimate of the effect of residual stresses, geometrical and material imperfections and eccentrically applied loads on the buckling behaviour. In (Maquoi & Rondal, 1978) 7 possible expressions for η were proposed, of which Eqs.2.3.13-2.3.15 were also considered in (Taras, 2010). All expressions are a function of some order of $\overline{\lambda}$ and of the plateau value $\overline{\lambda_0} = 0.2$, below which no reduction in buckling resistance is applied ($\chi = 1$).

$$\eta_1 = \alpha_1 \cdot (\overline{\lambda} - 0.2) \tag{2.3.13}$$

$$\eta_2 = \alpha_2 \cdot \sqrt{\overline{\lambda}^2 - 0.2^2} \tag{2.3.14}$$

$$\eta_3 = \alpha_3 \cdot (\overline{\lambda} - 0.2)^2 \tag{2.3.15}$$

Small discrepancies (less than 2%) were found between the tabulated buckling curves and the proposed expressions for η_1 and η_2, considering the best fit value of α. Deviations up to 10% were obtained for η_3. In (Maquoi & Rondal, 1978) it was suggested to use η_1, which corresponds with the current used formulation of ϕ in the buckling curve expressions, where the generalized imperfection varies linearly with $\overline{\lambda}$, which is in turn a linear function of the buckling length. The linear relationship was developed based on the assumed imperfection of L/1000, which was adopted for the derivation of the European column buckling curves (Taras, 2010).

2.3.4 Critical buckling load

The critical load resulting in buckling of members subjected to axial loading will be determined by the columns' resistance to torsion and bending. For columns with a doubly symmetric cross-section, as considered in this work, the buckling modes (Eqs. 2.3.17-2.3.19) are independent. Consequently, concentrically loaded columns will fail at the lowest of the critical loads associated with their buckling modes (Eq. 2.3.16).

$$N_{cr} = \min(N_{cr,z}, N_{cr,y}, N_{cr,t}) \tag{2.3.16}$$

a) Weak-axis flexural buckling: displacement v in y-direction

$$N_{cr,z} = \frac{\pi^2 EI_z}{L^2} \tag{2.3.17}$$

b) Strong-axis flexural buckling: displacement w in z-direction

$$N_{cr,y} = \frac{\pi^2 EI_y}{L^2} \tag{2.3.18}$$

c) Torsional buckling: rotation over angle ϕ about the longitudinal x-axis

$$N_{cr,t} = \frac{A}{I_0}\left(GI_t + \frac{\pi^2 EI_w}{L^2}\right) \tag{2.3.19}$$

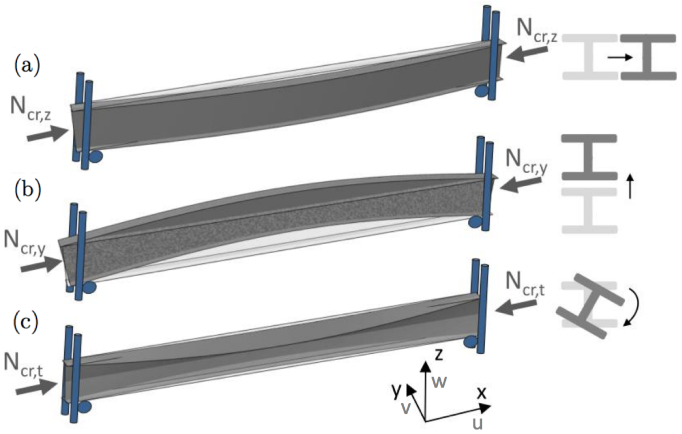

Figure 2.8: Possible buckling modes at N_{cr}: (a) weak-axis flexural buckling, (b) strong-axis flexural buckling, (c) torsional buckling. Extracted from (Sonck, 2014).

For the simply supported I-section members considered in this work, flexural buckling will occur about the weak axis (Eq. 2.3.20), except for columns where weak-axis flexural buckling is prevented. Other exceptions can be found in (Trahair, 1993) for cross-sections with low h/b, t_w/t_f, t_w/h and t_f/b ratios.

$$I_z \leq I_y \rightarrow N_{cr,z} \leq N_{cr,y} \tag{2.3.20}$$

2.4 Lateral-torsional buckling of beams

For beams under pure major axis bending, the lateral-torsional buckling (LTB) phenomenon can be characterized by a combined lateral and torsional movement. The lateral movement of the compressed upper part is partly restricted by the lower part of the beam in tension, creating an additional torsional effect on the member (Fig. 2.9). In this section, first a general formula is given to calculate the critical moment for LTB for members under constant or non-uniform bending moments. Afterwards, different approaches in EC3 applicable to calculate the buckling resistance are discussed: the General, Specific and Modified Specific method. For completeness the new formulation proposed in (Taras, 2010) is mentioned, although this approach won't be applied in the remainder of this work.

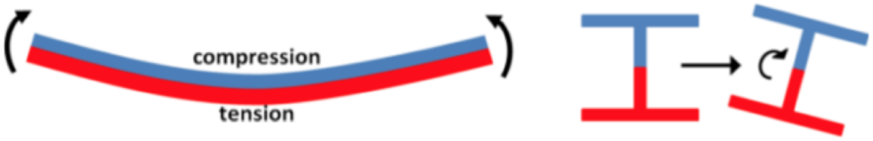

Figure 2.9: Lateral-torsional buckling of beam loaded in strong-axis bending. Extracted from (Sonck et al., 2012).

2.4.1 Critical buckling moment

The critical LTB moment M_{cr} can be considered as the failure load of an elastic, perfectly straight member, i.e. the bending moment at the bifurcation point (intersection curve 1 and 4, Fig. 2.1). Geometric or material non-linearities are not taken into account. The general formula for the practical calculation of the critical moment as adopted in ENV3 is given in Eq.2.4.1.

$$M_{cr} = C_1 \cdot \frac{\pi^2 EI_z}{(k_z \cdot L)^2} \cdot \left[\sqrt{\left(\frac{k_z}{k_w}\right)^2 \cdot \frac{I_w}{I_z} + \frac{(k_z \cdot L)^2 \cdot GI_t}{\pi^2 EI_z} + (C_2 z_g - C_3 z_j)^2} - (C_2 z_g - C_3 z_j) \right] \tag{2.4.1}$$

where

C_1, C_2, C_3	Modification factors depending on restraint conditions and loading
z_g	Distance between (transversal) load application point and shear centre
z_j	$z_s - 0.5 \int_A (y^2 + z^2) \frac{z}{I_y} dA$
z_s	Coordinate of the shear centre
k_z, k_w	Effective length factors for respectively in- and out-of-plane buckling

For doubly symmetric cross-sections with end-fork boundary conditions as considered in this work and with the load acting in the centroid (the shear centre) of the cross-section, the formula can be simplified to Eq. 2.4.2.

$$M_{cr} = C_1 \cdot \frac{\pi^2 EI_z}{L^2} \cdot \sqrt{\frac{I_w}{I_z} + \frac{L^2 \cdot GI_t}{\pi^2 EI_z}} \tag{2.4.2}$$

By definition, C_1 equals 1.0 in case of a uniform bending moment. Non-uniform bending moment diagrams correspond with values larger than 1, depending on the shape of the diagram as discussed in the following section.

2.4.2 Non-uniform bending moments

As mentioned previously, the factor C_1 in the expression of the critical bending moment can be applied as a correction factor for members subjected to a non-uniform bending moment. Of special interest in this work are the linearly varying bending moment lines, defined by the parameter ψ, expressing the ratio between the moment applied at the member's right and left end (M_2/M_1). In this work, the investigation will be limited to three ψ values (1, 0, -1), but the given expressions are generally applicable for linearly varying moment lines.

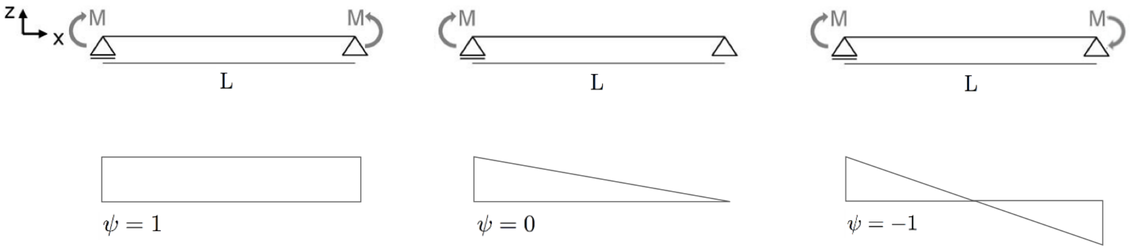

Figure 2.10: Values of ψ for linearly varying moment considered in this work.

From the definition of the non-dimensional slenderness for LTB $\overline{\lambda}_{LT}$ a multiplication factor k_c can be derived to adapt the slenderness value for a uniform bending moment ($\overline{\lambda}_{LT,U}$) to be applicable in case non-uniform bending moments ($\overline{\lambda}_{LT,NU}$) are present (Eq. 2.4.3). This factor k_c is related to the factor C_1 and is mentioned here as the value of k_c will be required to calculate the buckling resistance based on the Modified Specific method of EC3. In (NBN, 2005) the values of k_c for different moment distributions are tabulated. For a linearly varying bending moment, Eq. 2.4.4 is valid.

$$\overline{\lambda}_{LT,NU} = \sqrt{\frac{M_{pl}}{M_{cr,NU}}} = \sqrt{\frac{M_{pl}}{C_1 \cdot M_{cr,U}}} \cdot \overline{\lambda}_{LT,NU} = k_c \cdot \overline{\lambda}_{LT,U} \tag{2.4.3}$$

$$k_c = \frac{1}{1.33 - 0.33\psi} \tag{2.4.4}$$

Lower bound expressions for C_1 were mentioned by (Salvadory, 1955) and (Trahair, 1993), respectively given in Eqs. 2.4.5 and 2.4.6. Both formulae indicate that for beams in double curvature bending (ψ= -1), the corresponding C_1 values are approximately 2.5 times larger than in case of uniform bending (ψ=1). Consequently, for double curved bending, the critical moments M_{cr} will be larger, reducing the normalized slenderness $\overline{\lambda}_{LT}$ and hence increasing the reduction factor χ_{LT}. Therefore, resulting in an increased bending moment resistance for members subjected to double curved bending.

$$C_1 = 1.75 - 1.05\psi + 0.3\psi^2 \leq 2.5 \tag{2.4.5}$$

$$C_1 = \frac{1}{0.6 + 0.4\psi} \leq 2.5 \tag{2.4.6}$$

This can be explained as followed. Under a uniform bending moment (ψ = 1), deflection will occur according to a symmetric sine wave, whereas an anti-symmetric double sine wave will be noticed for double curvature bending (ψ = -1). This results in an anti-symmetric deflection v in case the twist rotation ϕ is symmetric. Consequently, the top and bottom flange will deflect respectively to the left and right side towards the compression zones, enhancing the member's resistance. The reader is referred to (Trahair, 1993) for a more detailed description about simply supported beams under a moment gradient.

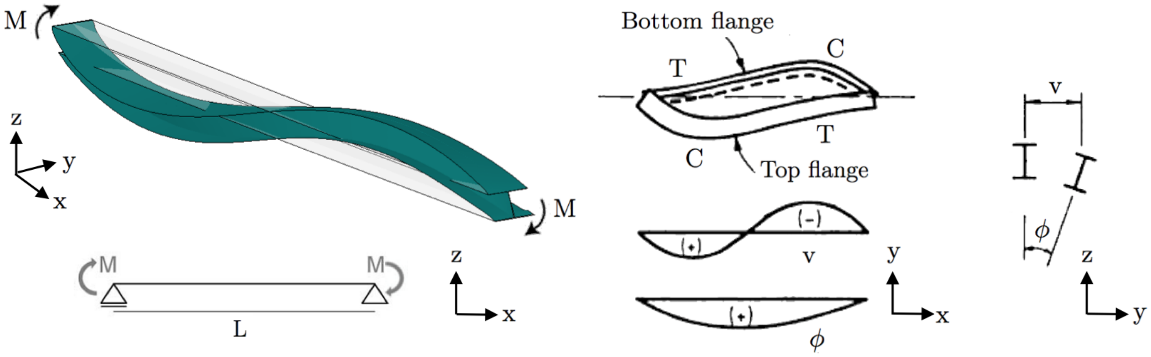

Figure 2.11: Deflection under double curvature bending ($\psi = -1$). Based on (Trahair, 1993).

In this work the formula adopted in (ECCS, 2006) will be used as value of C_1, applicable for any ratio of end loading. The different formulae for C_1 are depicted in Fig. 2.12. Besides the considered linearly varying bending moment in this work, two other load conditions are often found and worth mentioning: (i) a constant distributed line load over the member's length and (ii) a point load applied at mid-span. For these load conditions the corresponding C_1 factor according to EC3 is respectively 1.12 and 1.35 and therefore a lower critical moment will be found than for members under double curvature bending ($\psi = -1$).

$$C_1 = 1.77 - 1.04\psi + 0.27\psi^2 \leq 2.60 \tag{2.4.7}$$

The formula of EC3 is only slightly deviating from the expression proposed by Salvadory, but with a lower upper limit (2.5 instead of 2.6). By applying the equation of Trahair, a higher critical moment is obtained for $\psi \leq -0.3$ compared to Salvadory; values of ψ higher than -0.3 correspond with a lower critical LTB moment. Values of C_1 are ranging from 2.6 to 1.0 for respectively $\psi = -1$ and $\psi = 1$.

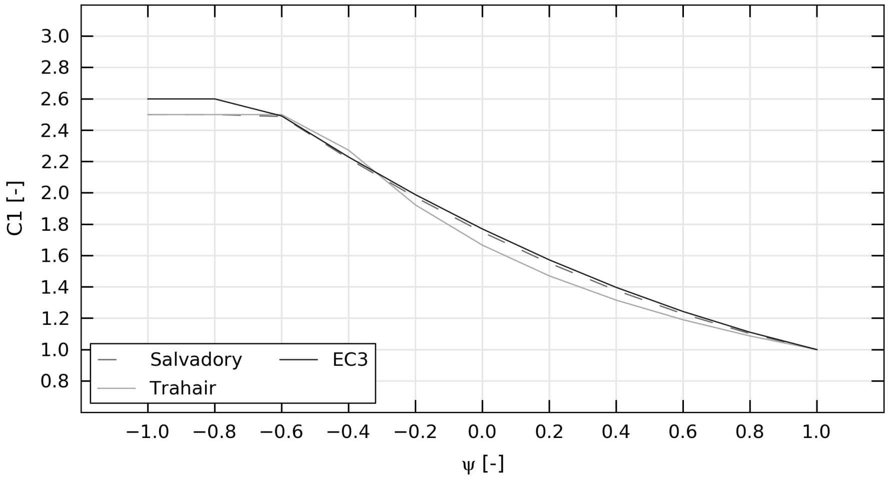

Figure 2.12: Values of factor C_1 for different linearly varying bending moment lines.

2.4.3 Buckling resistance

The critical LTB moment M_{cr} could be regarded as the failure load of an elastic, perfectly straight member. In reality however, the nonlinear geometric and material behaviour as well as the imperfections should be taken into account by the reduction factor χ_{LT} in the design buckling resistance M_{Rd}. For a laterally unrestrained member subjected to major axis bending, the LTB resistance is given by Eq.2.4.8. According to the Belgian National Annex γ_{M1} equals 1.

$$M_{Rd} = \frac{\chi_{LT} W_y f_y}{\gamma_{M1}} \tag{2.4.8}$$

Depending on the cross-section classification, a plastic (class 1-2), elastic (class 3) or effective (class 4) section modulus W_y should be used. Three methods to determine the buckling resistance are proposed in EC3, each method using different sets of formulae for the reduction factor χ_{LT} or another choice of buckling curves. In addition, the alternative approach of Taras is briefly mentioned.

- General Method (EC3, Section 6.3.2.2)
- Specific Method (EC3, Section 6.3.2.3)
- Modified Specific Method (EC3, Section 6.3.2.3)
- Taras Approach (Taras, 2010)

2.4.3.1 EC3 - General method

The general design rules implement the flexural buckling curves, this time related to specific h/b ratios (Table 2.6) which results in a different categorization compared to the column buckling case. The imperfection factor α_{LT} is indicated in Table 2.5. This method is especially used for deep slender beams, which are not considered in the specific method.

Table 2.5: Imperfection factor α_{LT} for LTB curves.

Buckling curve	a	b	c	d
Imperfection factor α_{LT}	0.21	0.34	0.49	0.76

Table 2.6: General Method: Lateral-torsional buckling curve.

Cross-section	Limits	Buckling curve
Rolled I-sections	h/b ≤ 2	a
	h/b > 2	b
Welded I-sections	h/b ≤ 2	c
	h/b > 2	d
Other cross-sections	-	d

The expressions for χ_{LT} and Φ_{LT} have a similar shape as for the column buckling case, but are based on a different value for the normalized slenderness $\overline{\lambda}_{LT}$ and the imperfection factor α_{LT} for LTB. (Eq.2.4.11).

$$\chi_{LT} = \frac{1}{\Phi_{LT} + \sqrt{\Phi_{LT}^2 - \overline{\lambda}_{LT}^2}} \leq 1.0 \tag{2.4.9}$$

$$\Phi_{LT} = \frac{1}{2}\left[1 + \alpha_{LT}(\overline{\lambda}_{LT} - 0.2) + \overline{\lambda}_{LT}^2\right] \tag{2.4.10}$$

$$\overline{\lambda}_{LT} = \sqrt{\frac{W_y f_y}{M_{cr}}} \tag{2.4.11}$$

2.4.3.2 EC3 - Specific method

For the 'special' case of rolled sections or equivalent welded sections, this method is proposed by EC3. The method is an extension of the general method, with the implementation of an additional factor β in the formulas of χ_{LT} and Φ_{LT}. According to the National Annex NBN EN 1993-1-1 ANB:2010, $\beta = 1$ and $\overline{\lambda}_{LT,0} = 0.2$. Although in EC3 $\beta = 0.75$ and $\overline{\lambda}_{LT,0} = 0.4$ are the recommended values, the national values were modified to take into account the criticisms on the specific method. Unsafe results up to 12% were obtained in (Snijder & Hoenderkamp, 2007) with this method and therefore a careful choice of β and $\overline{\lambda}_{LT,0}$ is required. With the nationally assumed values for these parameters, the specific method is reduced to the general method, but with a different choice of buckling curves.

$$\chi_{LT} = \frac{1}{\Phi_{LT} + \sqrt{\Phi_{LT}^2 - \beta \cdot \overline{\lambda}_{LT}^2}} \leq \frac{1}{\overline{\lambda}_{LT}^2} \leq 1.0 \tag{2.4.12}$$

$$\Phi_{LT} = \frac{1}{2}\left[1 + \alpha_{LT}(\overline{\lambda}_{LT} - \overline{\lambda}_{LT,0}) + \beta \cdot \overline{\lambda}_{LT}^2\right] \tag{2.4.13}$$

where

$\overline{\lambda}_{LT,0}$	Plateau value for LT buckling
β	Curve shape modification factor
α_{LT}	Imperfection factor Specific method (Table 2.5)

Table 2.7: Specific Method: Lateral-torsional buckling curve.

Cross-section	Limits	Buckling curve
Rolled I-sections	h/b ≤ 2	b
	h/b > 2	c
Welded I-sections	h/b ≤ 2	c
	h/b > 2	d

2.4.3.3 EC3 - Modified Specific method

The LT-buckling curves used for the derivation of the lateral torsional buckling resistance are based on a constant bending moment along the member. A higher LTB resistance can however be obtained for a non-uniform bending moment due to the increased critical moment M_{cr}, which results in a reduced value of $\overline{\lambda}_{LT}$ and finally in a larger value of the reduction factor χ_{LT}. A second beneficial effect on the buckling resistance will be present due to the reduction of the plastic zones due to the variable bending moment along the member. EC3 takes this into account by introducing a moment-gradient modification factor f. It should be noted that although this modification for the General Method is not longer adopted in EC3, the modification for non-uniform bending moments was originally proposed by the ECCS for both the General and Specific Method.

$$\chi_{LT,mod} = \frac{\chi_{LT}}{f} \leq 1 \tag{2.4.14}$$

$$f = 1 - 0.5(1 - k_c)\left[1 - 2(\overline{\lambda}_{LT} - 0.8)^2\right] \leq 1 \tag{2.4.15}$$

The non-uniform shape of the moment diagram is taken into account by the correction factor k_c, as defined in paragraph 2.4.2. It should be noticed that the factor f has no mechanical justification (Taras, 2010). The factor was proposed by (Lindner, 2000) as the best-fitting curve for a large set of GMNIA numerical calculations based on Specific Method formulations. As the buckling curves for the General Method are generally lower, applying the modification factor for this general case was found to be a conservative approach, although this is not longer adopted in EC3. In (Gevaert, 2010) both the general and specific method of EC3 are applied without taking into account the modification factor f.

For the extended parametric study in this work however, only the modified general method will be considered. This application of the general method, accounted for the moment distribution along the member, was also in (Rebelo et al., 2009) stated as the most suitable method.

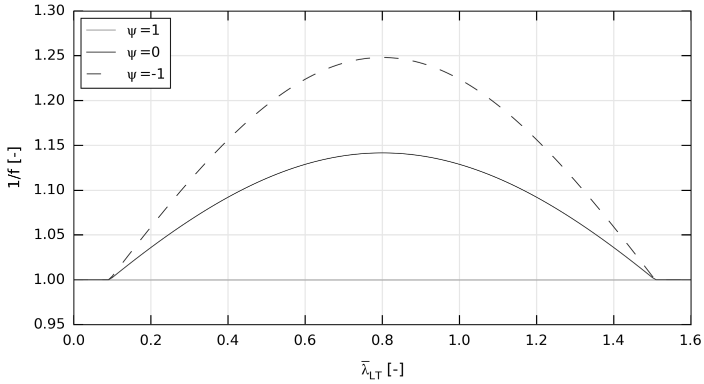

Figure 2.13: Modification factor 1/f in function of reduced slenderness $\overline{\lambda}_{LT}$.

When plotting the factor 1/f over $\overline{\lambda}_{LT}$, a parabolic shape can be found with a maximum at $\overline{\lambda}_{LT}$=0.8 and a corresponding value of $2/(k_c+1)$. The plot indicates the increased values of the LTB factor

χ_{LT} compared to the general formulation of the reduction factor for a constant bending moment. The unmodified value is valid outside the $\overline{\lambda}_{LT}$ interval [0.1;1.5].

As stated in paragraph 2.4.2, the largest increase of χ_{LT} can be obtained for double curved bending. An increase in lateral torsional buckling resistance of 25% can be noticed compared to the case of uniform bending.

2.4.3.4 Taras Approach

A new formulation was proposed in (Taras, 2010) showing a higher accuracy within the practical ranges of length and a better consistency with the physical behaviour (Table 2.8). It is based on a generalized imperfection of the form $\eta = \alpha_{LT}(\overline{\lambda}_z - 0.2)$ with $\overline{\lambda}_z$ the slenderness for weak-axis buckling. This formulation reflects underlying assumptions made for the derivation of the numerical buckling curves regarding material and geometrical imperfections. The reduction factor χ_{LT} for LTB is altered with a factor f_M taking into account the moment distribution. The factor is also adopted in Eq.2.4.17 with $f_M = 1$ as conservative approach. The formulation of χ_{LT} is the solution of an Ayrton-Perry equation, limiting the sum of the first and second-order stresses to the yield stress. The eigenmode imperfection is proportional to the length due to the proportionality with $\overline{\lambda_z}$ in Eq.2.4.17.

An additional factor should be included in the expression of the imperfection factor α_{LT} to reflect the transition in residual stress at a depth-to-width ratio of h/b = 1.2. In this way the inconsistency that sections with lower residual stresses correspond with higher α_{LT} values can be avoided. It was found that the amplification of α_{LT} should be proportional to the square root of $W_{y,el}/W_{z,el}$.

$$\chi_{LT} = \frac{f_M}{\Phi_{LT}^2 + \sqrt{\Phi_{LT}^2 - f_M \overline{\lambda}_{LT}^2}} \leq 1.0 \tag{2.4.16}$$

$$\phi_{LT} = 0.5 \left[1 + f_M \left(\frac{\overline{\lambda}_{LT}^2}{\overline{\lambda}_z^2} \alpha_{LT}(\overline{\lambda}_z - 0.2) + \overline{\lambda}_{LT}^2 \right) \right] \tag{2.4.17}$$

The maximum value of α_{LT}, as indicated in Table 2.8, is given by α_z, the generalized imperfection amplitude for out-of-plane flexural buckling. This limit value can be explained by the similarity in behaviour of the flange of a deep section with low torsional rigidity and weak-axis bucking of a column. The imperfection factor α_z for weak-axis flexural buckling was derived for both hot-rolled and welded columns, although the residual stresses were based on rolled sections. Therefore for welded sections an accurate description of the column buckling curves can only be obtained by considering a higher α_z value to implement the 'welded' residual stresses. This limiting value of $\alpha_{LT,max}$ is set to 0.64, 31% higher than for rolled section $h/b \leq 1.2$ ($\alpha_z = 0.49$). A similar increase was also incorporated in the expression for α_{LT}, where $\alpha_{LT} = 0.21\sqrt{W_{el,y}/W_{el,z}}$ for welded sections is 31% higher than for rolled sections: $\alpha_{LT} = 0.16\sqrt{W_{el,y}/W_{el,z}}$.

Table 2.8: Imperfection factor α_{LT} according to Taras.

Cross-section	Limits	α_{LT}
Hot-rolled I & H	h/b ≤ 2	$0.16\sqrt{\frac{W_{el,y}}{W_{el,z}}} \leq 0.49$
	h/b > 2	$0.12\sqrt{\frac{W_{el,y}}{W_{el,z}}} \leq 0.34$
Welded I & H	h/b ≤ 2	$0.21\sqrt{\frac{W_{el,y}}{W_{el,z}}} \leq 0.64$

2.4.4 Lateral distortional buckling

In both design rules, lateral-distortional buckling (LDB) is not taken into account. Typical for this failure mode is the distortion of the cross-section, as an interaction between lateral-torsional buckling and local buckling typically for respectively short and long members (Fig. 2.14). Web distortion is therefore mainly observed for members with intermediate length and members with slender webs are most susceptible to the phenomenon. Due to the S-shaped distortion the torsional stiffness is reduced and a lower critical moment is obtained (Eq. 2.4.2). The effect of web distortion is examined for both plain-webbed members and members with web openings. The LDB strength can be estimated by inserting 0 as value for the torsion constant in the equation of the critical moment. This approach is only accurate for slender webs and overly conservative for more compact webs.

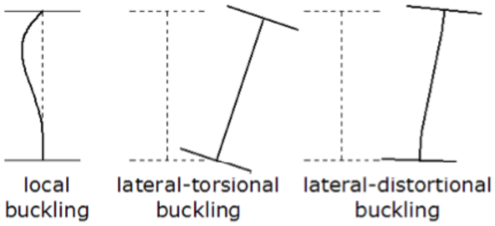

Figure 2.14: Local buckling, LTB and LDB of plain-webbed members.

In previous work (Sonck et al., 2009), numerical simulations on a wide variety of realistic cellular beam geometries were performed in Abaqus to compare the numerically obtained critical moment with the critical moment obtained from the ENV3 design rule, i.e. using the cross-sectional properties at the centre of the openings (2T approach) for the expression of M_{cr} (Eq. 2.4.2). Comparable results were obtained for the numerical and theoretical calculations, except for HEM320 and HEA320 parent sections in case of short-length members. For short-length members, the ENV3 design rule led to an overestimation and therefore an unsafe estimation of the critical moment due to web distortion. However, short members will fail by plastic yielding rather than elastic instability, decreasing the detrimental effects of web distortion. The largest web distortion was observed near the edges and around mid-span of the considered members.

The cross-sectional properties for both plain-webbed members and cellular members are given in Appendix A. By comparing the expressions it can be concluded that mainly a reduction of the effective torsional stiffness is obtained, the reduction in bending stiffness is limited. The difference between $M_{cr,2T}$ and $M_{cr,0}$ is therefore mainly determined by I_t. This difference will increase with increasing length, based on the classical LTB critical moment of a doubly symmetric I-section, supported by fork bearings at its ends (Eq. 2.4.2). The above considerations concerning LDB, which is not covered by the current desing rules, will be taken into account during the parametric study on plain-webbed and cellular members.

2.5 Beam-columns

The resistance of steel members subjected to an axial force and bending moment is varying with slenderness. For short members (low slenderness), the behaviour is dominated by the cross-section resistance. With increasing slenderness, residual stresses and geometrical imperfections will induce pronounced second-order effects. The design of members with high slenderness will therefore be governed by their elastic behaviour, i.e. failure due to instability phenomena: flexural and lateral-torsional buckling, typically for respectively members in pure compression and bending.

2.5.1 Cross-section resistance

The cross-section resistance will be based on the plastic resistance for sections class 1-2 or on the elastic or effective resistance for cross-sections of respectively class 3 and 4. The cross-section classification is further discussed in Appendix A. A disadvantage of this distinction in cross-section resistance based on the classification is indicated in Fig. 2.15b, where a sudden loss of capacity can be noticed at the transition between sections class 2 and 3. Therefore, as a result of two recent European research projects, an alternative set of design rules for cross-sections class 3 (semi-compact sections) was proposed in considering a partly-plastic capacity (Greiner, 2011). This proposal to allow an increased design resistance of sections class 3 is based on the examined increased capacity compared to the elastic resistance due to an internal plastic redistribution. The improved design rules are applicable for doubly-symmetric cross-sections (rolled or welded) and allow for a more economic design compared to the current conservative design approach in EC3. However, since this is not yet included in EC3, this will not be further considered in this work.

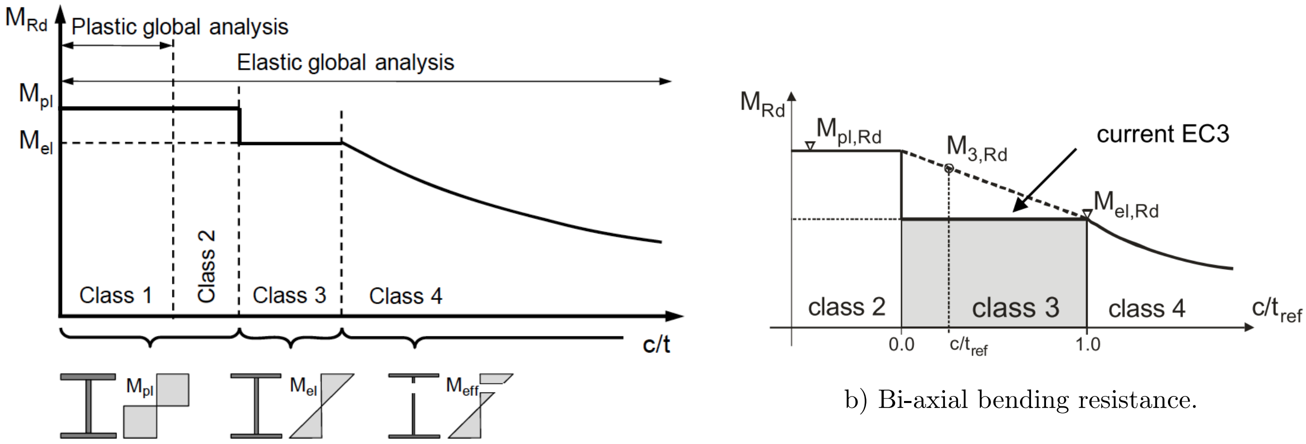

a) Reduced bending capacity under axial force.

b) Bi-axial bending resistance.

Figure 2.15: Amendment proposal EC3 for cross-sections class 3. Extracted from (Greiner et al., 2013).

2.5.2 Plastic resistance

Specific formulae for I and H sections can be applied to evaluate the plastic cross-section resistance for sections class 1 or 2. For the general case where a cross-section with section area A and yield strength f_y is subjected to N+M, the central area $A_N = N/f_y$ can be defined in such a way that the remaining upper and lower area (A_1 and A_2) are equal (Fig. 2.16).

$$A_1 = A_2 = \frac{A - N/f_y}{2} \tag{2.5.1}$$

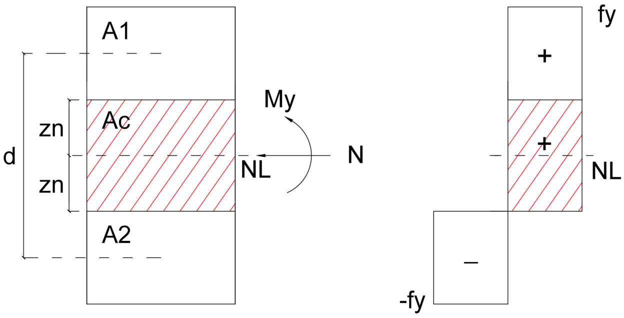

Figure 2.16: Plastic interaction bending moment-axial force (compression: +, tension: -).

The central part of the cross-section is considered under compression due to the centrically applied axial force N; the remaining cross-section will take up the additional bending moment arising from the eccentric application of N. The reduced plastic bending moment resistance $M_{N,Rd}$ is given by Eq. 2.5.2, with d the distance between the centroid of the areas A_1 and A_2.

$$M_{N,Rd} = A_1 f_y d = A_2 f_y d \tag{2.5.2}$$

2.5.2.1 Reduced plastic moment resistance $M_{N,Rd}$

According to EC3, the reduction of the plastic moment is not significant and therefore not required for doubly symmetric I or H sections if the following conditions are satisfied (Eq.2.5.3) and 2.5.4).

- No reduction in plastic moment resistance $M_{N,y,Rd}$ if:

$$N_{Ed} \leq 0.25 N_{pl,Rd} \text{ and } N_{Ed} \leq \frac{0.5 h_w t_w f_y}{\gamma_{M0}} \tag{2.5.3}$$

- No reduction in plastic moment resistance $M_{N,z,Rd}$ if:

$$N_{Ed} \leq \frac{h_w t_w f_y}{\gamma_{M0}} \tag{2.5.4}$$

with h_w the height and t_w the thickness of the web.
If the previous conditions are not fulfilled, the reduced plastic moment resistances for rolled or welded I or H sections about the y and z axis, respectively $M_{N,y,Rd}$ and $M_{N,z,Rd}$ can be obtained by Eqs.2.5.5-2.5.7 (CEN, 2005).

$$M_{N,y,Rd} = M_{pl,y,Rd} \cdot \frac{1-n}{1-0.5a} \qquad \text{but} \quad M_{N,y,Rd} \leq M_{pl,y,Rd} \tag{2.5.5}$$

$$M_{N,z,Rd} = M_{pl,z,Rd} \qquad \text{if } n \leq a \tag{2.5.6}$$

$$M_{N,z,Rd} = M_{pl,z,Rd} \left[1 - \left(\frac{n-a}{1-a} \right)^2 \right] \qquad \text{if } n > a \tag{2.5.7}$$

Where

$$a = \frac{A - 2bt_f}{A}, \text{ but } a \leq 0.5 \text{ and } n = \frac{N_{Ed}}{N_{pl,Rd}} \tag{2.5.8}$$

2.5.2.2 Influence of shear force

Only if $V_{Ed} > 0.5V_{pl,Rd}$, the influence of the shear force should be taken into account by calculating the design resistance $M_{N,Rd}$ under bending moment and axial force with a reduced yield strength f_{yr} for the shear area according to Eq. 2.5.9. It should be noted that in this case also the plastic moment resistance (Eq. 2.5.5) is calculated with the reduced yield strength: $W_{pl,y}f_{yr}$. For $V_{Ed} \leq V_{pl,Rd}$, the reduction is not significant and counterbalanced by strain-hardening of the steel.

$$f_{yr} = (1-\rho)f_y \tag{2.5.9}$$

$$\text{where } \rho = \left(\frac{2V_{Ed}}{V_{pl,Rd}} - 1\right)^2 ; \quad V_{pl,Rd} = \frac{A_v f_y}{\sqrt{3}\gamma_{M0}} \tag{2.5.10}$$

The shear surface of the cross-section A_v in 2.5.10 is determined based on the simplified cross-section used in the numerical model (Fig. 2.17):

$$A_v = A - 2bt_f + t_w t_f \geq h_w t_w \tag{2.5.11}$$

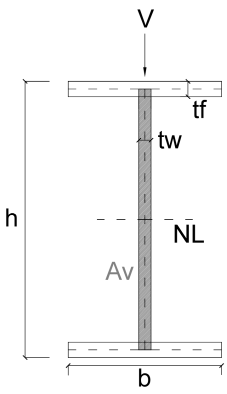

Figure 2.17: Shear area for simplified cross-section of I profile.

2.5.2.3 ECCS - Vandepitte

Only in the formulae of the ECCS according to Vandepitte an alternative definition is used for the reduced plastic moment resistances depending on the considered cross-section.

IPE profiles:

$$\frac{M_{N,y,Rd}}{M_{pl,y}} = 1 \text{ if } \frac{N_{Ed}}{N_{pl}} \geq 0.18; \qquad \frac{M_{N,y,Rd}}{M_{pl,y}} = 1.22\left(1 - \frac{N_{Ed}}{N_{pl}}\right) \text{ if } \frac{N_{Ed}}{N_{pl}} \geq 0.18 \tag{2.5.12}$$

HE profiles:

$$\frac{M_{N,y,Rd}}{M_{pl,y}} = 1 \text{ if } \frac{N_{Ed}}{N_{pl}} \leq 0.1; \qquad \frac{M_{N,y,Rd}}{M_{pl,y}} = 1.11\left(1 - \frac{N_{Ed}}{N_{pl}}\right) \text{ if } \frac{N_{Ed}}{N_{pl}} \geq 0.1 \tag{2.5.13}$$

$$\text{where } N_{pl} = Af_y \quad \text{and} \quad M_{pl,y} = W_{pl,y}f_y \tag{2.5.14}$$

2.5.2.4 General formula plastic resistance

For a cross-section under an axial force and bi-axial bending $N + M_y + M_z$, the following interaction formula (Eq. 2.5.15) can be applied:

$$\left[\frac{M_{y,Ed}}{M_{N,y,Rd}}\right]^{\alpha} + \left[\frac{M_{z,Ed}}{M_{N,z,Rd}}\right]^{\beta} \leq 1.0 \tag{2.5.15}$$

The parameters α and β are determined by the shape of the cross-section. For I or H sections, α=2 and β=5n with $\beta \geq 1$ and $n = N_{Ed}/N_{pl,Rd}$.

2.5.3 Elastic resistance

To determine the elastic cross-section capacity, general interaction formulae can be used, valid for all cross-section classes. These formulae are based on a conservative approximation by considering a linear summation on the basis of resistance for the different stress resultants. For a cross-section subjected to an axial force N and bi-axial bending (M_y, M_z), the following criterion can be applied (Eq. 2.5.16).

$$\frac{N_{Ed}}{N_{Rd}} + \frac{M_{y,Ed}}{M_{y,Rd}} + \frac{M_{z,Ed}}{M_{z,Rd}} \leq 1 \tag{2.5.16}$$

where $M_{y,Ed}/M_{z,Ed}$ and $M_{y,Rd}/M_{z,Rd}$ represent respectively the design and resisting bending moments about the strong and weak axis. N_{Rd} is the resisting axial force corresponding to the applied load N_{Ed}.

2.5.3.1 Combined shear and bending

For cross-sections class 3 or 4 the interaction between bending moment and axial force should be checked by applying a yield criterion.

$$\sigma_{von-Mises} = \sqrt{\sigma^2 + 3\tau^2} \leq \frac{f_y}{\gamma_{M0}} \tag{2.5.17}$$

$$\text{with} \quad \tau_{Ed} = \frac{VS}{I_y t_w} \tag{2.5.18}$$

where V is the shear force, S the first moment of area about the neutral axis of the part of the cross-section between a considered point and the cross-section boundary.
The normal and shear stresses σ and τ are based on an elastic stress analysis with a reduced effective cross-section for section members class 4. This verification in combination with Eq. 2.5.16 will be performed for all 4 methods in this chapter at the web-flange transition of the member's end sections.

2.5.4 ECCS - Vandepitte

2.5.4.1 Design formula

The design rules of the ECCS expressing the interaction of an axial force and bending moment were developed based on the formula of Perry-Robertson, limiting the elastically calculated compressive stresses at the ultimate fiber to the yield stress (Eq.2.5.19).

$$\frac{N}{A} + \frac{1}{1 - N/N_{cr,y}} \frac{Ne}{W_{el,y}} \leq f_y \quad \text{or} \quad \frac{N}{N_{pl}} + \frac{1}{1 - N/N_{cr,y}} \frac{|M_1|}{M_{el,y}} \leq 1 \tag{2.5.19}$$

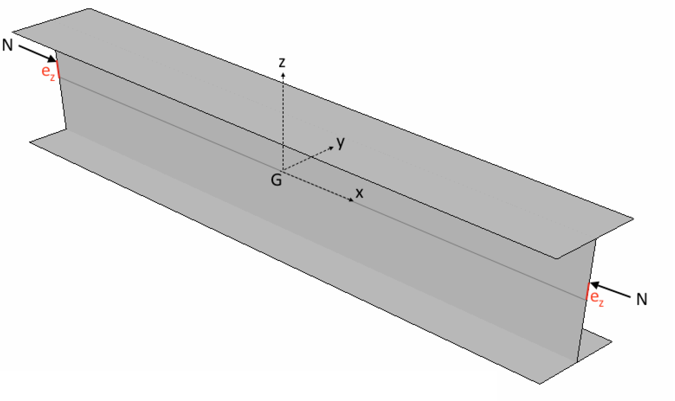

Figure 2.18: Definition of axes eccentric axial load.

where M_1 = -Ne_z and $M_{el,y} = W_{el,y}f_y$. Equation 2.5.19 is valid for members with two planes of symmetry and an axial load applied with eccentricity e_z in the vertical plane of symmetry XZ resulting in a strong-axis bending moment M_y.
The first order moment M_1 is multiplied by the magnification factor $\frac{1}{1-N/N_{cr}}$. The factor is introduced to include second order effects as a result of the applied axial force on the member, deflected due to the first order moment M_1. This magnification factor was already introduced in section 2.3.3 where the reduction factor χ for the flexural buckling resistance was derived based on an Ayrton-Perry Robertson approach.

2.5.4.2 Ideal shape imperfections

The ideal shape imperfections with amplitude $\overline{v}_0$ (XY-plane) and $\overline{w}_0$ (XZ-plane) applied in the ECCS formulae are chosen such that the highest compressive stress in the elastic member with imperfections is equal to the yield stress at the same load which results in buckling for the case of the real axially-loaded compressed beam (incl. its material and shape imperfections). It should be noted that the ideal shape factor is determined by the dimensions of the cross-section, the method of fabrication, the slenderness of the beam and the yield stress, but independent of the load acting on the member.

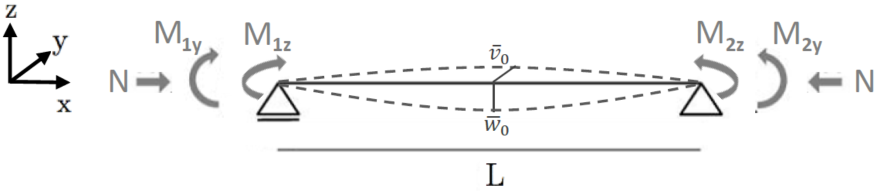

Figure 2.19: Shape imperfections factors $\overline{w}_0$ and $\overline{v}_0$.

The ideal shape imperfection $\overline{w}_0$ is found by introducing $N = N_{b,y,Rd}$ in Eq.2.5.19.

$$\frac{N_{b,y,Rd}}{A} + \frac{1}{1 - \frac{N_{b,y,Rd}}{N_{cr,y}}} \frac{N_{b,y,Rd}\overline{w_0}}{W_y} = f_y \tag{2.5.20}$$

$$\overline{w}_0 = \left(1 - \frac{N_{b,y,Rd}}{N_{cr,y}}\right)\left(f_y - \frac{N_{b,y,Rd}}{A}\right)\frac{W_y}{N_{b,y,Rd}} = \left(1 - \frac{N_{b,y,Rd}}{N_{cr,y}}\right)\left(\frac{N_{pl}}{N_{b,y,Rd}} - 1\right)\frac{W_y}{A} \tag{2.5.21}$$

Similarly $\overline{v}_0$ corresponds to $N = N_{b,z,Rd}$. It should be noted that by introducing $N_{b,y,Rd}$ or $N_{b,z,Rd}$in the expressions of $\overline{w}_0$ and $\overline{v}_0$, the shape imperfections are calculated with an increased yield strength (Section 2.3.1).

$$\frac{N_{b,z,Rd}}{A}+\frac{1}{1-\frac{N_{b,z,Rd}}{N_{cr,z}}}\frac{N_{b,z,Rd}\overline{v}_0}{W_z}=f_y \tag{2.5.22}$$

$$\overline{v}_0=\left(1-\frac{N_{b,z,Rd}}{N_{cr,z}}\right)\left(f_y-\frac{N_{b,z,Rd}}{A}\right)\frac{W_z}{N_{b,z,Rd}}=\left(1-\frac{N_{b,z,Rd}}{N_{cr,z}}\right)\left(\frac{N_{pl}}{N_{b,z,Rd}}-1\right)\frac{W_z}{A} \tag{2.5.23}$$

2.5.4.3 Adaptations design formula

The design formula (Eq.2.5.19) should be adapted in two ways.

- In reality the eccentricities at both end sections will have a different magnitude or even an opposite sign. Therefore an equivalent effective uniform bending moment is introduced: $M_{eff}=\beta|M_1|$. This effective moment should have the same influence on the buckling behaviour as the real acting moments M_1 and M_2 at the end sections with $|M_1|\geq|M_2|$. Different empirical formulae can be applied for β (cf. section 2.5.4.4).

- The special case where $e_z=0$ and therefore $M_1=0$, would result in N $=N_{pl}$. As indicated before, failure of short members is governed by yielding of the cross-section, but for slender members elastic buckling is the determining failure mode. To take into account the risk for buckling, N_{pl} should be reduced to $N_{b,Rd}=\chi N_{pl}$. This failure compressive force $N_{b,Rd}$ can be determined based on the buckling curves of the ECCS that are applicable for the assumed compression member.

Considering the two limitations of design formula 2.5.19 discussed in this section, the formula should be adapted as followed.

$$\frac{N}{N_{b,Rd}}+\frac{1}{1-N/N_{cr,y}}\frac{|M_{eff}|}{M_{el,y}}\leq 1 \tag{2.5.24}$$

2.5.4.4 Equivalent moment factor β

Different empirical formulae for the equivalent moment factor β are listed below (Van Impe, 2010). Equal moments at both ends ($\psi=M_2/M_1=1$) logically result in $\beta=1$. Smaller values of β are obtained for $M_2=0$. For moments with opposite sign ($M_2=-M_1$) the risk of reaching the failure state is even smaller. It should be noted that the proposed values of β are only applicable for linear bending moment lines. The widely used formula of Austin will be used in the remainder of this work.

Campus and Massonnet	$\beta=\sqrt{0.3+0.4\psi+0.3\psi^2}$
Austin	$\beta=0.6+0.4\psi$ with $\beta\geq 0.4$
Van Impe	$\beta=0.4+0.15(1+\psi)^2$

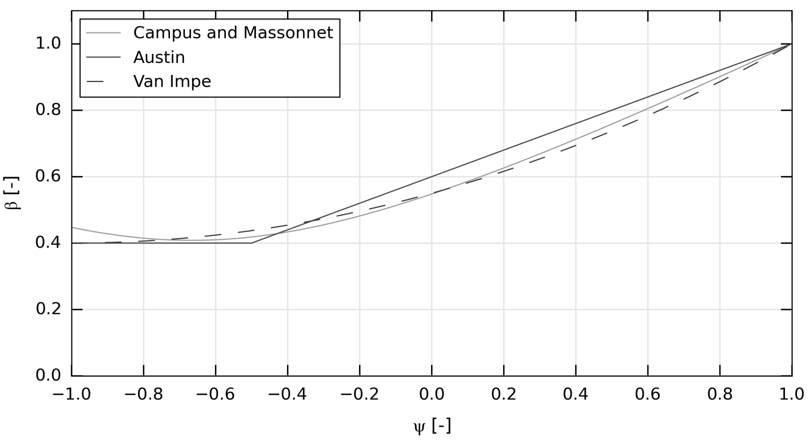

Figure 2.20: Equivalent moment factor β in function of ψ.

2.5.4.5 Members susceptible to lateral torsional buckling

For profiles susceptible to torsional deformations (e.g. I and H-sections), the strong-axis bending moment is multiplied by an additional factor θ, defined according to Eq. 2.5.25, where α is the shape factor for buckling around the strong axis and σ_{cr} the elastic critical stress for LTB. If $\alpha f_y/\sigma_{cr} \leq 0.16$, θ equals 1. In (Vandepitte, 1979) it is proposed to exclude the factor $1/\alpha$ from the expression of θ.

$$\theta = \frac{1}{\alpha}\left[1 + \left(\frac{\alpha f_y}{\sigma_{cr}}\right)^{2.5}\right]^{\frac{1}{2.5}} \qquad \sigma_{cr} = \frac{M_{cr}}{W_{el,y}} \text{ and } \alpha = \frac{W_{pl,y}}{W_{el,y}} \tag{2.5.25}$$

The resulting design rules of the ECCS for the general case of members subjected to bi-axial bending and susceptible to torsional deformations are given by Eqs. B.1.1 and B.1.2. Depending on a verification according to a plastic (class 1 or 2) or elastic (class 3 or 4) theory, the values of respectively W_{pl} and W_{el} should be used for the section modulus. As the distinction between plastic or elastic theory was not prescribed by the design rules of Vandepitte, the classification is adopted from the Eurocode.

$$\text{Buckling in XZ-plane:} \quad \frac{N}{A} + \frac{\theta\beta_y|M_{1y}|+N\overline{w_0}}{\left(1-\frac{N}{N_{cr,y}}\right)W_y} + \frac{\beta_z|M_{1z}|}{\left(1-\frac{N}{N_{cr,z}}\right)W_z} \leq f_y \tag{2.5.26}$$

$$\text{Buckling in XY-plane:} \quad \frac{N}{A} + \frac{\theta\beta_y|M_{1y}|}{\left(1-\frac{N}{N_{cr,y}}\right)W_y} + \frac{\beta_z|M_{1z}|+N\overline{v_0}}{\left(1-\frac{N}{N_{cr,z}}\right)W_z} \leq f_y \tag{2.5.27}$$

It should be noted that for purely compressed members ($M_{1y} = M_{2y} = 0$), a stricter condition is obtained than was proposed for column buckling: $N_{b,Rd} = \nu A f_y \omega$. This can be explained as the shape imperfections $\overline{w}_0$ and $\overline{v}_0$ in Eqs. B.1.1-B.1.2 were calculated with an increased yield strength (Section 2.3.1), whereas the real yield strength is introduced on the right-hand side, resulting in an underestimation of the member's strength. Therefore the strength conditions in this section will be used for members under combined axial force and bending moment; for pure compressive members $N_{b,Rd}$ (Eq. 2.3.1) is used. Consequently, a discontinuity will be noticeable between these different loading conditions. Additionally, the stress at the ultimate fiber of the member's end sections should be limited to the yield stress. This can be verified according to an elastic theory similarly as in Eq. 2.5.16; the formula for cross-sections following a plastic theory is derived from Eq.2.5.15 with $\alpha = \beta = \mu$.

$$\text{Elastic theory (Class 1-2):} \quad \frac{N}{A} + \frac{|M_{1y}|}{W_{el,y}} + \frac{|M_{1z}|}{W_{el,z}} \leq f_y \tag{2.5.28}$$

$$\text{Plastic theory (Class 3-4):} \quad \left(\frac{|M_{1y}|}{M_{N,y,Rd}}\right)^{\mu} + \left(\frac{|M_{1z}|}{M_{N,z,Rd}}\right)^{\mu} \leq 1 \text{ with } \mu = 1.6 - \frac{N_{Ed}/N_{pl}}{2ln\left(N_{Ed}/N_{Pl}\right)} \tag{2.5.29}$$

2.5.5 ECCS - Van Impe

Compared to the design rules listed by Vandepitte, the rules were adapted by Van Impe to obtain a better correspondence with the design rules adopted in the Eurocode. $N_{b,Rd}$ and $M_{b,Rd}$ are determined based on the buckling curves from the Eurocode. The equivalent moment factor β and the shape imperfections $\overline{w}_0$ and $\overline{v}_0$ are determined similarly as in the formulae ECCS-Vandepitte. The resistance of the end cross-sections following a plastic theory is defined differently.

2.5.5.1 General strength conditions

The general strength conditions for members subjected to a combination of biaxial bending and axial compression are given by Eqs. B.1.22-B.1.23. The stress due to the axial load N and the weak-axis bending moments M_{1z} and M_{2z} is expressed by respectively the first and third term of Eq. B.1.22. Verification of buckling around the strong axis is included by the second term. Comparable to the reduction factor θ in the formulae of Vandepitte, the factor χ_{LT} is introduced for members susceptible to torsional deformations. The choice of the section modulus (W_{el} or W_{pl}) is again based on the member's cross-section classification.

$$(i-a) \quad \text{Buckling y-y:} \quad \frac{N}{A} + \frac{\beta_y|M_{1y}|+N|\overline{w_0}|}{\chi_{LT}\left(1-\frac{N}{N_{cr,y}}\right)W_y} + \frac{\beta_z|M_{1z}|}{\left(1-\frac{N}{N_{cr,z}}\right)W_z} \leq f_y \tag{2.5.30}$$

$$(ii-a) \quad \text{Buckling z-z} \quad \frac{N}{A} + \frac{\beta_y|M_{1y}|}{\chi_{LT}\left(1-\frac{N}{N_{cr,y}}\right)W_y} + \frac{\beta_z|M_{1z}|+N|\overline{v_0}|}{\left(1-\frac{N}{N_{cr,z}}\right)W_z} \leq f_y \tag{2.5.31}$$

The interaction between lateral-torsional buckling and weak-axis flexural buckling can be expressed alternatively by a set of equations without the reduction factor χ_{LT}, but by considering a torsional imperfection $\phi(x)$ for strong-axis bending with amplitude ϕ_0 (Eqs.2.5.32-2.5.33). The amplitude ϕ_0 is determined such that for a member only subjected to a uniform moment, M_y equals the LTB resistance $M_{b,Rd}$ $=\chi_{LT}W_yf_y$. Therefore ϕ_0 can be calculated from Eq. 2.5.35, obtained by setting N=0, $\beta_y = 1$ and $M_{1z} = 0$ in Eq. 2.5.33.

$$(i-b) \quad \text{Buckling y-y:} \quad \frac{N}{A} + \frac{\beta_y|M_{1y}|+N|\overline{w_0}|}{\left(1-\frac{N}{N_{cr,y}}\right)W_y} + \frac{\beta_z|M_{1z}|}{\left(1-\frac{N}{N_{cr,z}}\right)W_z} \leq f_y \tag{2.5.32}$$

$$(ii-b) \quad \text{Buckling z-z:} \quad \frac{N}{A} + \frac{\beta_y|M_{1y}|}{\left(1-\frac{N}{N_{cr,y}}\right)W_y} + \frac{\beta_z|M_{1z}|+N|\overline{v_0}|+\phi_0\beta_y|M_{1y}|}{\left(1-\frac{N}{N_{cr,z}}-\frac{M_{1y}^2}{M_{cr}^2}\right)W_z} \leq f_y \tag{2.5.33}$$

$$\overline{\phi}(x) = \phi_0 \sin\left(\frac{\pi x}{L}\right) \tag{2.5.34}$$

$$\frac{M_{b,Rd}}{W_y f_y} + \frac{M_{b,Rd}\phi_0}{\left(1 - \frac{M_{b,Rd}^2}{M_{cr}^2}\right) W_z f_z} = 1 \tag{2.5.35}$$

For the specific case of members subjected only to a strong-axis bending moment M_{1y} ($\beta_y < 1$), $M_z = 0$ and in case the interaction with the axial force is negligible (N is small), condition (i-a) can be reduced according to Eq. 2.5.36. The resulting value of M_{1y} obtained from Eq.2.5.33 might be larger than the resistance against lateral-torsional buckling $M_{b,Rd}$ and the ultimate moment M_u even larger than M_{cr}. To avoid this anomaly an additional third condition (Eq.2.5.37) is required.

$$\frac{\beta_y |M_{1y}|}{\chi_{LT} W_y} \leq f_y \rightarrow \beta_y |M_{1y}| \leq \chi_{LT} W_y f_y \rightarrow \beta_y |M_{1y}| \leq M_{b,Rd} \tag{2.5.36}$$

$$(iii) \quad \left(\frac{N}{N_{bz,Rd}}\right)^2 + \left(\frac{M_{1y}}{\left(1 - \frac{N}{N_{cr,y}}\right) M_{b,Rd}}\right)^2 + \left(\frac{M_{1z}}{\left(1 - \frac{N}{N_{cr,z}} - \frac{M_{1y}^2}{M_{cr}^2}\right) W_z f_z}\right)^2 \leq 1 \tag{2.5.37}$$

where $M_{b,Rd} = \chi_{LT} W_y f_y$. By introducing this third condition the M/N-interaction diagram is capped, avoiding moments $M_u > M_{cr}$. However, by introducing this horizontal branch, the resisting moment M_u is independent of the magnitude of the normal force, which is in contrast to the real member's behaviour. It should be noted that this third condition is only required in case of $\beta_y \leq 1$, i.e. for non-uniform bending moments ($\psi = 0$ or $\psi = -1$).
Furthermore, again the compressive stresses at the ultimate fiber of the end sections should be limited to the yield stress, which can be verified by Eq.2.5.38 for an elastic approach or with Eq.2.5.39 following a theory of plasticity.

$$\text{Elastic theory (Class 1-2):} \quad \frac{N}{A} + \frac{|M_{1y}|}{W_{el,y}} + \frac{|M_{1z}|}{W_{el,z}} \leq f_y \tag{2.5.38}$$

$$\text{Plastic theory (Class 3-4):} \quad \left(\frac{|M_{1y}|}{M_{N,y,Rd}}\right)^2 + \left(\frac{|M_{1z}|}{M_{N,z,Rd}}\right)^{5n} \leq 1 \text{ with } n = \frac{N}{N_{pl}} \tag{2.5.39}$$

2.5.5.2 Strong-axis bending

For completeness, in this section an overview is given of the simplified conditions for members subjected to strong-axis bending where axial-torsional and flexural-torsional buckling do not occur, i.e. torsionally stiff members (e.g. rectangular box profile, torsionally restrained profile,..).
Three strength conditions should be fulfilled (Eq. 2.5.40-2.5.42).
(i) Strength verification eccentrically loaded beam, prevention of buckling around the strong axis y (in the XZ-plane):

$$\frac{N}{A} + \frac{\beta_y |M_{1y}| + N\overline{w_0}}{\left(1 - \frac{N}{N_{cr,y}}\right) W_y} \leq f_y \tag{2.5.40}$$

(ii) Prevention of buckling around the weak axis z (in the XY-plane):

$$N \leq N_{bz,Rd} \tag{2.5.41}$$

(iii) Strength verification eccentrically most-heavily loaded cross-sections:

$$\frac{N}{A} + \frac{|M_{1y}|}{W_y} \leq f_y \tag{2.5.42}$$

In case $|M_{2y}| \leq |M_{1y}|$ or M_{2y} and M_{1y} have a different sign, $\beta_y < 1$ and for short members the left-hand term of expression (i) can be smaller than the one of equation (iii). Therefore, expression (iii) is required to avoid yielding of the edge fiber at both ends of the member. Following a plastic theory, equation (iii) should be replaced by $|M_{1y}| \leq M_{N,y,Rd}$ (Eq.2.5.5).

2.5.5.3 Weak-axis bending

Similarly simplified expressions can be obtained for weak-axis bending without axial-torsional buckling. Again three strength conditions should be fulfilled (Eq. 2.5.43-2.5.45)
(i) Strength verification eccentrically loaded beam, prevention of buckling around the weak axis z (in the XY-plane):

$$\frac{N}{A} + \frac{\beta_z |M_{1z}| + N\overline{v_0}}{\left(1 - \frac{N}{N_{cr,z}}\right) W_y} \leq f_y \tag{2.5.43}$$

(ii) Prevention of buckling around the strong axis y (in the XZ-plane) in case $l_z < l_y$:

$$N \leq N_{by,Rd} \tag{2.5.44}$$

(iii) Strength verification eccentrically most-heavily loaded cross-sections:

$$\frac{N}{A} + \frac{|M_{1z}|}{W_z} \leq f_y \tag{2.5.45}$$

Following the theory of plasticity, equation (iii) should be replaced by $|M_{1z}| \leq M_{N,z,Rd}$ (Eqs. 2.5.6 and 2.5.7).

2.5.6 Eurocode

For the verification of members subjected to a combination of bending and axial compression, two different design approaches are incorporated in EN 1993-1-1(CEN, 2005).
Pronounced second order effects due to residual stresses, material and geometrical imperfections will appear. The effects of the bending moments and the axial force can be linearly summed; specific interaction factors can be used for the non-linear effects. Based on this concept, two sets of formulae were derived: the first one by a French-Belgian team (Method 1), the second one was developed by an Austrian-German team (Method 2) (ECCS, 2006).
In Method 1 individual factors are introduced to reflect the influence of different physical phenomena with a high level of accuracy. In contrast to the transparency of Method 1, simplicity is enhanced with Method 2 by using one compact interaction factor. By this globalisation of several effects, Method 2 is more user-friendly, focussing on direct design. Although only Method 1 is applicable in Belgium, both methods will be considered in the remainder of this thesis, to compare Method 1 with the more user-friendly approach of Method 2.

2.5.7 Method 1

2.5.7.1 Derivation of general formulae

The structure of the formulae of Method 1 can be easily understood by considering a simply supported member with an initial sinusoidal shaped geometrical imperfection with amplitude $\overline{e_0}$ and subjected to moment M and axial force N, expressed in the equations with their design values M_{Ed} and N_{Ed}. As indicated in section 2.3.3, an Ayrton-Perry approach can be used, verifying the resistance of the most heavy-loaded cross-section according to an elastic second-order theory. For members subjected to a first order bending moment M_{Ed}, second order bending moments will be introduced, amplifying the existing bending moment as well as the deflection. Therefore, an additional third term is added (Eq.2.5.46).

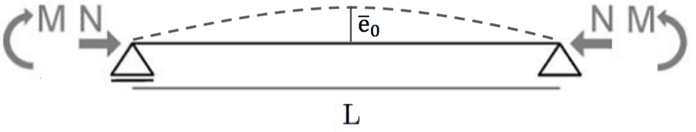

Figure 2.21: Member with initial sinusoidal shaped imperfection and subjected to M and N.

The classical amplification factor $1/(1 - N_{Ed}/N_{cr})$ for second order effects was introduced in both the second and third term, although it should be noted that for the third term this is only an approximation of $1/\left[\cos(\pi/2)\sqrt{N_{Ed}/N_{cr}}\right]$. The equivalent moment factor C_m was discussed in section 2.5.4.4.

$$\frac{N_{Ed}}{N_{pl,Rd}} + \frac{1}{1 - N_{Ed}/N_{cr}} \frac{N_{Ed} \cdot \overline{e_0}}{M_{el,Rd}} + \frac{1}{1 - N_{Ed}/N_{cr}} \frac{C_m M_{Ed}}{M_{el,Rd}} \leq 1.0 \tag{2.5.46}$$

This formula can be rearranged into the so-called μ format, which can be reduced to the classical buckling check ($N_{Ed} \leq N_{b,Rd}$) for members in pure compression ($M_{Ed} = 0$). For the exact derivation of this formula, the reader is referred to (ECCS, 2006); (Boissonnade et al., 2004).

$$\frac{N_{Ed}}{\chi N_{pl,Rd}} + \mu \frac{1}{1 - N_{Ed}/N_{cr}} \frac{C_m M_{Ed}}{M_{el,Rd}} \leq 1 \tag{2.5.47}$$

$$\mu = \frac{1 - N_{Ed}/N_{cr}}{1 - \chi N_{Ed}/N_{cr}} \tag{2.5.48}$$

2.5.7.2 Beam-column under biaxial bending and axial force

The previously derived Eq.2.5.47 can be extended to the general formulae expressing the complex coupling of axial compression and bending based on an elastic second-order theory.

$$\text{Buckling y-y:} \quad \frac{N_{Ed}}{\chi_y N_{pl,Rd}} + \mu_y \left[\frac{C_{my} M_{y,Ed}}{\left(1 - \frac{N_{Ed}}{N_{cr,y}}\right) M_{el,y,Rd}} + \frac{C_{mz} M_{z,Ed}}{\left(1 - \frac{N_{Ed}}{N_{cr,z}}\right) M_{el,z,Rd}} \right] \leq 1.0 \tag{2.5.49}$$

$$\text{Buckling z-z:} \quad \frac{N_{Ed}}{\chi_z N_{pl,Rd}} + \mu_z \left[\frac{C_{my} M_{y,Ed}}{\left(1 - \frac{N_{Ed}}{N_{cr,y}}\right) M_{el,y,Rd}} + \frac{C_{mz} M_{z,Ed}}{\left(1 - \frac{N_{Ed}}{N_{cr,z}}\right) M_{el,z,Rd}} \right] \leq 1.0 \tag{2.5.50}$$

To make the expressions also applicable for cross-sections class 1 and 2, the elastic bending resistance $M_{el,Rd}$ is replaced by an elastic-plastic resistance C$M_{pl,Rd}$, where the additional parameters C_{yy}, C_{yz}, C_{zy} and C_{zz} are introduced to reflect plasticity effects. The factors $\alpha*$ and $\beta*$ simulate the material's non-linear behaviour and are chosen as $0.6\sqrt{\frac{w_z}{w_y}}$ and $0.6\sqrt{\frac{w_y}{w_z}}$ to be applicable for any type of cross-section. The meaning of the different factors will be explained in the next section (2.5.7.3).

$$\text{Buckling y-y:} \quad \frac{N_{Ed}}{\chi_y N_{pl,Rd}} + \mu_y \left[\frac{C_{my,0} M_{y,Ed}}{\left(1 - \frac{N_{Ed}}{N_{cr,y}}\right) C_{yy} M_{pl,y,Rd}} + \alpha* \frac{C_{mz,0} M_{z,Ed}}{\left(1 - \frac{N_{Ed}}{N_{cr,z}}\right) C_{yz} M_{pl,z,Rd}} \right] \leq 1.0 \tag{2.5.51}$$

$$\text{Buckling z-z:} \quad \frac{N_{Ed}}{\chi_z N_{pl,Rd}} + \mu_z \left[\beta* \frac{C_{my,0} M_{y,Ed}}{\left(1 - \frac{N_{Ed}}{N_{cr,y}}\right) C_{zy} M_{pl,y,Rd}} + \frac{C_{mz,0} M_{z,Ed}}{\left(1 - \frac{N_{Ed}}{N_{cr,z}}\right) C_{zz} M_{pl,z,Rd}} \right] \leq 1.0 \tag{2.5.52}$$

2.5.7.3 Members susceptible to lateral-torsional buckling

Different from the design rules of the ECCS, where it should be decided (by adding the factor θ or χ_{LT}) if flexural-torsional buckling should be taken into account, in Method 1 the values of I_t and I_y determine if the member is susceptible to torsional deformations. Torsional deformation is typically relevant in case of open I or H sections without torsion restraint; hollow sections are assumed to be not susceptible to torsional deformations.

- The member is not susceptible to torsional deformations if:

  1) $I_t \geq I_y$
  2) $I_t \leq I_y$ and if

$$\overline{\lambda}_0 \leq 0.2\sqrt{C_1}\sqrt[4]{\left(1-\frac{N_{Ed}}{N_{cr,z}}\right)\left(1-\frac{N_{Ed}}{N_{cr,T}}\right)} \quad \text{with} \quad \overline{\lambda}_0 = \sqrt{\frac{W_y f_y}{M_{cr,0}}} \tag{2.5.53}$$

  With $N_{cr,T}$ the critical load for torsional buckling:

$$N_{cr,T} = \frac{A}{I_y + I_z}\left(GI_t + \frac{\pi^2 E I_w}{L_{LT}^2}\right) \tag{2.5.54}$$

- The member is susceptible to torsional deformations if:

$$\overline{\lambda}_0 > 0.2\sqrt{C_1}\sqrt[4]{\left(1-\frac{N_{Ed}}{N_{cr,z}}\right)\left(1-\frac{N_{Ed}}{N_{cr,T}}\right)} \tag{2.5.55}$$

In Eqs. 2.5.53 - 2.5.55, $\overline{\lambda}_0$ expresses the reduced slenderness for LTB with constant bending moment. Factor C_1 takes into account a non-uniform bending moment distribution as discussed in paragraph 2.4.2. The critical load for weak-axis flexural buckling is indicated by $N_{cr,z}$ (Eq.2.3.17).
For members susceptible to lateral-torsional buckling, an additional factor C_{mLT}/χ_{LT} should be added to the strong bending term. The influence of the axial load and the shape of the cross-section is accounted for by C_{mLT} (Eq.B.1.43). The reduction factor χ_{LT} is introduced on the bending resistance $M_{pl,y,Rd}$ for torsionally flexible profiles subjected to strong-axis bending. The resulting conditions in case of double bending for members susceptible to LTB are given by Eqs. B.1.38-2.5.59.

$$C_{mLT} = \frac{C_{my}^2 a_{LT}}{\sqrt{\left(1-\frac{N_{Ed}}{N_{cr,z}}\right)\left(1-\frac{N_{Ed}}{N_{cr,T}}\right)}} \geq 1 \tag{2.5.56}$$

Buckling around the strong axis y-y:

$$\frac{N_{Ed}}{\chi_y N_{pl,Rd}} + \mu_y\left[\frac{C_{mLT}}{\chi_{LT}}\frac{C_{my}M_{y,Ed}}{\left(1-\frac{N_{Ed}}{N_{cr,y}}\right)C_{yy}W_y f_y} + 0.6\sqrt{\frac{w_z}{w_y}}\frac{C_{mz}M_{z,Ed}}{\left(1-\frac{N_{Ed}}{N_{cr,z}}\right)C_{yz}W_z f_y}\right] \leq 1 \tag{2.5.57}$$

Buckling around the weak axis z-z:

$$\frac{N_{Ed}}{\chi_z N_{pl,Rd}} + \mu_z\left[0.6\sqrt{\frac{w_y}{w_z}}\frac{C_{mLT}}{\chi_{LT}}\frac{C_{my}M_{y,Ed}}{\left(1-\frac{N_{Ed}}{N_{cr,y}}\right)C_{zy}W_y f_y} + \frac{C_{mz}M_{z,Ed}}{\left(1-\frac{N_{Ed}}{N_{cr,z}}\right)C_{zz}W_z f_y}\right] \leq 1 \tag{2.5.58}$$

Resistance check of the end cross-sections:

$$\left(\frac{M_{1y,Ed}}{M_{N,y,Rd}}\right)^2 + \left(\frac{M_{1z,Ed}}{M_{N,z,Rd}}\right)^{5n} < 1 \quad \text{(Class 1-2)} \qquad \frac{N_{Ed}}{A} + \frac{|M_{1y,Ed}|}{W_{el,y}} + \frac{|M_{1z,Ed}|}{W_{el,z}} \leq f_y \quad \text{(Class 3)} \tag{2.5.59}$$

The factors μ_y and μ_z are defined according to Eq. B.1.40. To include the influence of lateral-torsional buckling, the expression for C_{my0} is modified. The adapted value is denoted with C_{my}.

$$\mu_y = \frac{1 - N_{Ed}/N_{cr,y}}{1 - \chi_y N_{Ed}/N_{cr,y}}; \quad \mu_z = \frac{1 - N_{Ed}/N_{cr,z}}{1 - \chi_z N_{Ed}/N_{cr,z}} \tag{2.5.60}$$

$$C_{mz} = C_{mz,0} \tag{2.5.61}$$

$$C_{my} = C_{my,0} + (1 - C_{my,0}) \frac{\sqrt{\epsilon_y} a_{LT}}{1 + \sqrt{\epsilon_y} a_{LT}} \tag{2.5.62}$$

$$\text{where} \quad \epsilon_y = \frac{M_{y,Ed}}{N_{Ed}} \frac{A}{W_{el,y}} \quad \text{(class 1-3);} \quad a_{LT} = 1 - \frac{I_T}{I_y} \geq 0 \tag{2.5.63}$$

The elastic-plastic coefficients C_{ii} and C_{ij} are introduced (i and j referring to the main directions), expressing the elastic-plastic interaction under bending and compression, i.e. the amount of plasticity in the cross-section at the moment of failure. The coefficients are function of (i) the reduced slenderness (or N_{Ed}/N_{cr}) and (ii) the bending moment distribution (expressed by C_m) (Boissonnade et al., 2004). The N-M elastic-plastic interaction will be different for slender members subjected to high axial force compared to stocky members under low compression.

$$C_{yy} = 1 + (w_y - 1) \left[2 - \frac{1.6}{w_y} C_{my}^2 \left(\overline{\lambda}_{max} + \overline{\lambda}_{max}^2 \right) n_{pl} - b_{LT} \right] \geq \frac{1}{w_y} \tag{2.5.64}$$

$$C_{yz} = 1 + (w_z - 1) \left[\left(2 - 14 \frac{C_{mz}^2 \overline{\lambda}_{max}^2}{w_z^5} \right) n_{pl} - c_{LT} \right] \geq \frac{0.6}{\sqrt{w_y w_z}} \tag{2.5.65}$$

$$C_{zy} = 1 + (w_y - 1) \left[\left(2 - 14 \frac{C_{my}^2 \overline{\lambda}_{max}^2}{w_y^5} \right) n_{pl} - d_{LT} \right] \geq \frac{0.6}{\sqrt{w_y w_z}} \tag{2.5.66}$$

$$C_{zz} = 1 + (w_z - 1) \left[2 - \frac{1.6}{w_z} C_{mz}^2 \left(\overline{\lambda}_{max} + \overline{\lambda}_{max}^2 \right) - e_{LT} \right] n_{pl} \geq \frac{1}{w_z} \tag{2.5.67}$$

where

$$\text{Class 1-2:} \quad w_y = \frac{W_{pl,y}}{W_{el,y}} \leq 1.5; \quad w_z = \frac{W_{pl,z}}{W_{el,z}} \leq 1.5; \tag{2.5.68}$$

$$\text{Class 3-4:} \quad w_y = w_z = 1.0 \tag{2.5.69}$$

$$n_{pl} = \frac{N_{Ed}}{N_{pl,Rd}}; \quad \overline{\lambda_{max}} = max(\overline{\lambda_y}, \overline{\lambda_z}) \tag{2.5.70}$$

With factor $(w - 1)$ indicating the bending potential available from from pure elasticity to plasticity. For cross-sections class 3, preference is given to replace W_{pl} by W_3 to allow for a more continuous transitions between sections class 2 and 3, as discussed in section 2.5.1. In the expressions of C_{ii}/C_{ij}, the factors b_{LT}, c_{LT}, d_{LT} and e_{LT} are 0 if lateral-torsional buckling is prevented.
Class 1-2:

$$b_{LT} = 0.5 a_{LT} \overline{\lambda_0}^2 \frac{M_{y,Ed}}{\chi_{LT} M_{pl,y,Rd}} \frac{M_{z,Ed}}{M_{pl,z,Rd}} \tag{2.5.71}$$

$$c_{LT} = 10 a_{LT} \overline{\lambda_0}^2 \frac{\overline{\lambda_0}^2}{5 + \overline{\lambda}_z^4} \frac{M_{y,Ed}}{C_{my} \chi_{LT} M_{pl,y,Rd}} \tag{2.5.72}$$

$$d_{LT} = 2 a_{LT} \overline{\lambda_0} \frac{\overline{\lambda_0}}{0.1 + \overline{\lambda}_z^4} \frac{M_{y,Ed}}{C_{my} \chi_{LT} M_{pl,y,Rd}} \frac{M_{y,Ed}}{C_{mz} M_{pl,z,Rd}} \tag{2.5.73}$$

$$e_{LT} = 1.7a_{LT}\overline{\lambda_0}\frac{\overline{\lambda_0}}{0.1+\overline{\lambda}_z^4}\frac{M_{y,Ed}}{C_{my}\chi_{LT}M_{pl,y,Rd}} \tag{2.5.74}$$

Class 3-4:

$$C_{yy} = C_{zz} = 1; \;\; C_{yz} = C_{zy} = 0.6 \tag{2.5.75}$$

2.5.7.4 Continuity to cross-sectional resistance

For members of which the slenderness approaches 0, i.e. $N_{cr,y}$ and $N_{cr,z}$ are infinitely large (and therefore $C_{my} = C_{mz} = 1$), the member's failure behaviour is no longer determined by instability effects and only cross-sectional checks should be performed. For class 1 and 2 cross-sections, the C_{ii} and C_{ij} factors are equal to 1 and Eqs. B.1.38-B.1.39 are reduced to the following expressions:

$$\frac{M_{y,Ed}}{M_{pl,y,Rd}} + \alpha*\frac{M_{z,Ed}}{M_{pl,z,Rd}} \leq 1 \tag{2.5.76}$$

$$\beta*\frac{M_{y,Ed}}{M_{pl,y,Rd}} + \frac{M_{z,Ed}}{M_{pl,z,Rd}} \leq 1 \tag{2.5.77}$$

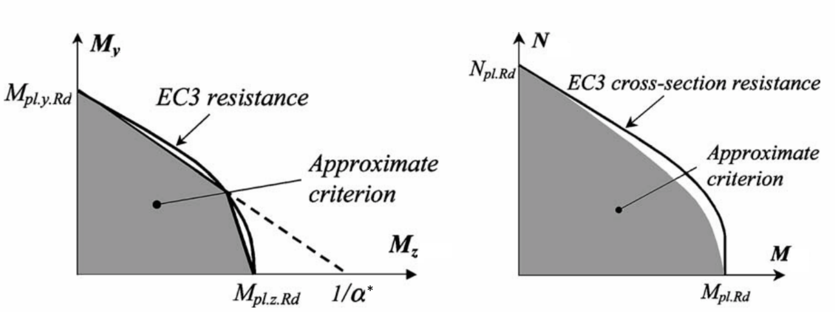

Figure 2.22: Biaxial bending and interaction criteria N-M resistance. Extracted from (Boissonnade et al., 2004).

These approximate interaction formulae are visualised in Fig. 2.22 and compared with the cross-sectional resistance to biaxial bending according to EC3 (Eq. 2.5.78), where the factors α and β are function of the cross-sectional shape. Similarly the plastic cross-section check for members subjected to an axial load an mono-axial bending ($M_z = 0$) is represented and compared to the formula adopted in EC3.

$$\left(\frac{M_{y,Ed}}{M_{pl,y,Rd}}\right)^{\alpha} + \left(\frac{M_{z,Ed}}{M_{pl,z,Rd}}\right)^{\beta} \leq 1 \tag{2.5.78}$$

2.5.7.5 Equivalent uniform moment factor C_m

Similarly as the equivalent moment factor β for the ECCS formulae, the factor C_m is introduced for Method 1. It should be noted that the factors listed in this section represent the factors $C_{my,0}$ and $C_{mz,0}$ for members not susceptible to LTB. To simplify the determination of the most heavy-loaded cross-section, the equivalent moment concept is introduced: the maximum amplified moment due to an axial compression force on the real member is equal to the maximum amplified moment in a column under an equivalent sinusoidal moment distribution (Boissonnade et al., 2004).

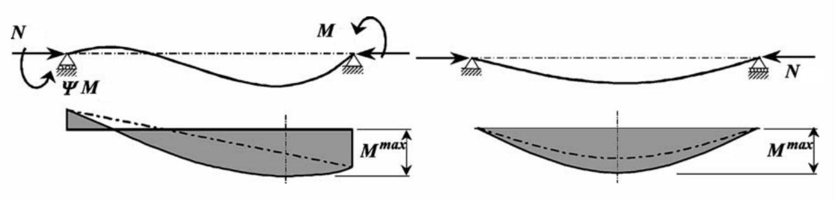

Figure 2.23: Concept equivalent moment factor C_m. Extracted from (Boissonnade et al., 2004).

Different approximate formulae are proposed in (ECCS, 2006) for C_m for linearly distributed moments. A first expression is due to Villette (Eq.2.5.79), for which it should be noted that for ψ=1 no correspondence can be found with the expression for a uniform moment as given in (Taras, 2010) (Eq.2.5.80).

$$C_m = 0.79 + 0.21\psi + 0.36(\psi - 0.33)\frac{N_{Ed}}{N_{cr}} \tag{2.5.79}$$

$$C_m = 1 + 0.27\frac{N_{Ed}}{N_{cr}} \tag{2.5.80}$$

Based on numerical calculations, it was concluded by Taras that with this formulation a conservative, but yet acceptable approach is obtained. This conservative behaviour can be explained by the elastic second-order moment amplification on which the formula is based. In contrast, GMNIA calculations will include plasticity effects. Alternative expressions are therefore shown to describe more accurately the elastic-plastic buckling strength of beam-columns. Commonly, the expression proposed by Austin is used, which was already introduced for the ECCS design rules.

$$C_m = 0.6 + 0.4\psi \geq 0.4 \tag{2.5.81}$$

An alternative equivalent uniform moment factor was introduced by Campus and Massonnet.

$$C_m = \sqrt{0.3(1+\psi^2) + 0.4\psi} \geq \frac{1}{2.3} \tag{2.5.82}$$

Equations 2.5.81 and 2.5.82 are both expressed relative to a constant bending moment and have the advantage to be independent of the axial force N_{Ed}. In reality however, Eq. 2.5.83 for a linearly varying bending moment will dependent on N_{Ed}.

$$C_m = \left(1 - \frac{N_{Ed}}{N_{cr}}\right)\frac{\sqrt{1 - 2\psi\cos(\pi\sqrt{N_{Ed}/N_{cr}}) + \psi^2}}{\sin(\pi\sqrt{N_{Ed}/N_{cr}})} \tag{2.5.83}$$

It should be noted that the expressions of Austin and Campus and Massonnet (Eq.2.5.81-2.5.82) are both relative to a constant reference equivalent moment, while Villette (Eq.2.5.79) and the theoretical expression 2.5.83 are expressed relative to a sinusoidal bending moment. More information on the influence of this different reference moment and on the C_m factor for different moment distributions is given in (ECCS, 2006),(Taras, 2010) and (CEN, 2005), Table A.2.

2.5.8 Method 2

Although the format of Method 2 is also based on the theoretical buckling equations, various specific coefficients will be summarized in a few factors. This aim for simplicity will reduce the accuracy of the formulations, but for practical standard design cases the influence is not considered to be significant. The derivation of the general interaction formulae of Method 2 will be based on formulation 2.5.84, expressing the resistance of members subjected to an axial force N and bending moment M, as derived in section 2.5.7.1. By considering Eq.2.5.85, this expression can be reformulated resulting in the theoretical expression 2.5.86.

$$\frac{N_{Ed}}{N_{pl,Rd}} + \frac{1}{1-\frac{N_{Ed}}{N_{cr}}} \frac{C_m M_{Ed} + N_{Ed} e}{M_{pl,Rd}} \leq 1 \tag{2.5.84}$$

$$e = \left(\frac{1}{\chi} - 1\right)(1 - \chi\overline{\lambda}^2)\frac{W_{pl}}{A} \tag{2.5.85}$$

$$\frac{N_{Ed}}{\chi N_{pl,Rd}} + k\frac{C_m M_{Ed}}{M_{pl,Rd}} \leq 1 \quad \text{with} \quad k = \frac{1}{1 - \frac{N_{Ed}}{N_{pl,Rd}}\chi\overline{\lambda}^2} \tag{2.5.86}$$

Similarly as for Method 1, a distinction can be made between members susceptible or not susceptible to lateral torsional buckling. A complete overview of the design rules adopted in (ECCS, 2006) is given in Appendix C. This section will focus on the background of the interaction formulae of Method 2.

The formulation of the interaction factor k, as introduced in Eq. 2.5.86, is the result of an extensive GMNIA analysis carried out by Abaqus for different cross-sections and moment distributions. Also the effect of geometrical and material non-linearities on the buckling behaviour was investigated. The Method 2 interaction coefficients are applicable for doubly symmetric sections as considered in this work, but extension to mono-symmetric sections is possible.

2.5.8.1 Characteristics buckling rules Method 2

Different sets of formulae are available depending on whether the member is susceptible to lateral-torsional buckling or not. Hot-rolled I and H-sections forming the scope of this work are torsionally flexible; torsionally restrained I-sections restrict out-of-plane deformations. Furthermore, also hollow sections are torsionally stiff.

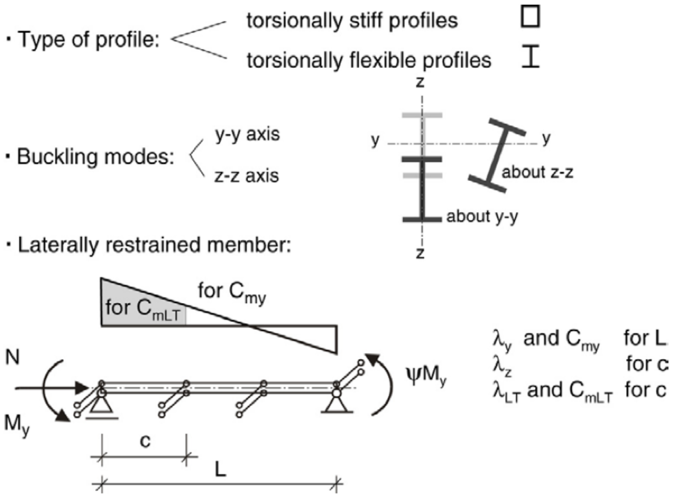
• Type of profile:
torsionally stiff profiles
torsionally flexible profiles
• Buckling modes:
y-y axis
z-z axis
z
y
y
about z-z
about y-y
z
• Laterally restrained member:
for C_mLT
for C_my
λ_y and C_my for L
λ_z for c
λ_LT and C_mLT for c
N
M_y
ψM_y
c
L

Figure 2.24: Characteristics of Method 2 of EC3. Extracted from (Greiner & Lindner, 2006).

For members subjected to an axial load and uniaxial or biaxial bending, two expressions are available of which the first is corresponding with the strong-axis buckling mode; weak axis-buckling is described by the second expression.
In contrast to Method 1, with Method 2 also members with intermediate lateral restraints are covered (Greiner & Lindner, 2006). The equivalent uniform moment factors C_{mLT} and C_{mz} (cf. infra) are therefore determined by the segmental moment diagram between lateral restraints. Factor C_{my} is however always related to the total span length. A clear overview (Fig. 2.24) on the available interaction formulae was provided in (Greiner & Lindner, 2006). For the torsionally stiff profiles, only flexural buckling will be of concern. Torsionally flexible profiles will be susceptible to LTB. The axis about which buckling takes place is influenced by the presence of intermediate restraints.

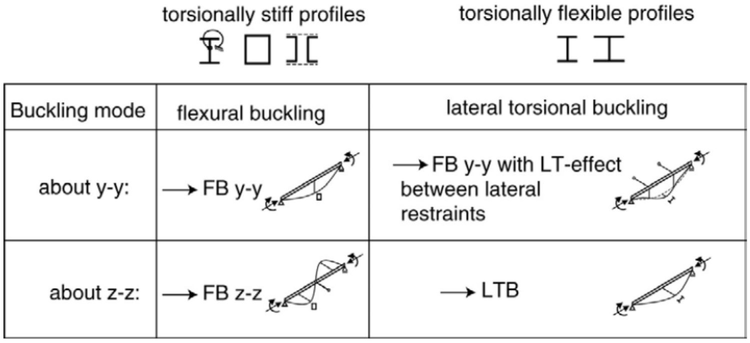
torsionally stiff profiles
torsionally flexible profiles
Buckling mode
flexural buckling
lateral torsional buckling
about y-y:
→ FB y-y
→ FB y-y with LT-effect between lateral restraints
about z-z:
→ FB z-z
→ LTB

Figure 2.25: Interaction formulae Method 2. Extracted from (Greiner & Lindner, 2006).

2.5.8.2 Members not susceptible to lateral torsional buckling

If lateral deformation is sufficiently restrained, the governing buckling mode will be in-plane buckling. Out-of-plane buckling is examined for unrestrained members. The formulae given are valid for cross-sections class 1 and 2.

In-plane buckling under N+M_y The interaction behaviour is determined by the parameters $\overline{\lambda}_y$ and n_y. A graphical representation of the derived interaction factor k_y for a constant moment is presented in Fig. 2.27a. The effect of the cross-section shape was found to be very limited, only affecting the results for higher n_y values.

$$\frac{N_{Ed}}{\chi_y N_{pl,Rd}} + k_y \frac{C_{my} M_{y,Ed}}{M_{pl,y,Rd}} \leq 1 \tag{2.5.87}$$

$$k_y = 1 + (\overline{\lambda}_y - 0.2) n_y \leq 1 + 0.8 n_y \tag{2.5.88}$$

$$C_{my} = 0.6 + 0.4\psi \geq 0.4 \tag{2.5.89}$$

$$n_y = \frac{N_{Ed}}{\chi_y N_{pl,Rd}} \tag{2.5.90}$$

Values of k_y below 1.0 can be noticed in the range of $\overline{\lambda} \approx 0$ and express the plastic cross-section interaction of moment M_y and axial force N. Numerical analysis showed increased k_y values for increasing relative slenderness up to $\overline{\lambda} \approx 1.0$ due to the increase of second-order effects with the axial compression parameter n_y. For a slenderness $\overline{\lambda_y}$ larger than 1.0, a constant level of k_y is reached as compensation for the used plastic moment resistance $M_{pl,y,Rd}$ in Eq. 2.5.87 throughout the complete slenderness range, wheras members for $\overline{\lambda_y} > 1.0$ show increasing elastic behaviour and the use of $M_{el,y,Rd}$ is required. The GMNIA results are translated into a bi-linear diagram with a plateau value at $\overline{\lambda}_y = 1$ (Fig. 2.27b). From the GMNIA results however, it can be noticed that beyond $\overline{\lambda}_z \approx 1.0$ for large n_y-values k_y is still decreasing with increasing $\overline{\lambda}_z$, different from the assumed bi-linear diagram with constant level for $\overline{\lambda}_z = 1$. This is however acceptable as differences in k_y occur mainly at larger values of n_y where the member's behaviour is determined by the normal force N and the moment term in Eq. 2.5.87 is less pronounced, reducing the influence of the k_y-factor. An Austin formulation is used for the factor C_{my} with $C_{my} = 1.0$ for a constant moment and lower values for non-uniform moment diagrams.

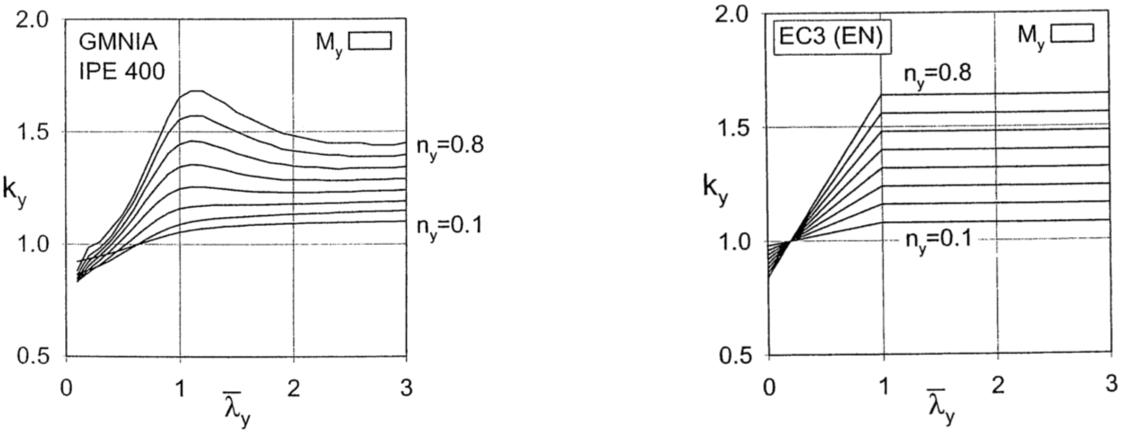

a) GMNIA Analysis

b) ECS (EN)

Figure 2.26: Interaction factor k_y for constant moment. Extracted from (ECCS, 2006).

Out-of-plane buckling under N+M_y The design formulae for members subjected to out-of-plane buckling are given by Eq. 2.5.91. It can be noticed that in the second term the interaction factor $0.6k_y$ was introduced, assuming that the out-of-plane buckling is affected by 60% of the in-plane buckling. This formula can be simplified to Eq. 2.5.92, for which the level of unsafety (maximum of 7% to 9%) was considered tolerable (Greiner & Lindner, 2006).

$$\frac{N_{Ed}}{\chi_z N_{pl,Rd}} + 0.6k_y \frac{C_{my} M_{y,Ed}}{M_{pl,y,Rd}} \leq 1 \tag{2.5.91}$$

$$\frac{N_{Ed}}{\chi_z N_{pl,Rd}} \leq 1 \tag{2.5.92}$$

2.5.8.3 Members susceptible to lateral torsional buckling

In case no lateral restraints are present (as considered in this work), buckling about the z-axis will dominate. If lateral restraints are provided, failure can be dominated by LTB about the y-axis for the segmental part between the restraints (Fig. 2.27). The formulae discussed in this section are valid for sections class 1 and 2.

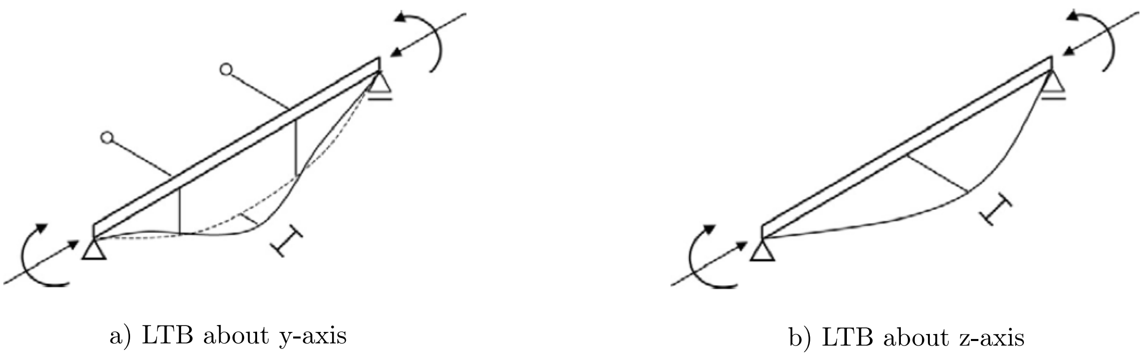

a) LTB about y-axis

b) LTB about z-axis

Figure 2.27: Buckling modes as function of restraints for members susceptible to torsional deformation. Extracted from (Greiner & Lindner, 2006).

In-plane buckling under N + M_y Compared to the interaction formula for torsionally stiff members (Eq. 2.5.87), for torsionally flexible profiles the bending resistance is replaced by the buckling resistance $\chi_{LTpl,y,Rd}$ (Eq. B.1.53). It should be noted that for short members with low slenderness values $\overline{\lambda_{LT}}$, this formula for torsionally stiff members is again reduced to Eq. 2.5.87. as $\chi_{LT} \approx 1.0$. Flexural in-plane buckling is than the corresponding failure mode. As in this thesis simply supported members with fork-supports are considered without intermediate lateral restraints, Eq. B.1.53 is irrelevant and should not be checked.

$$\frac{N_{Ed}}{\chi_y N_{pl,Rd}} + k_y \frac{C_{my} M_{y,Ed}}{\chi_{LT} M_{pl,y,Rd}} \leq 1 \tag{2.5.93}$$

Out-of-plane buckling under N+M_y In a similar way as for the k_y-factors, the interaction factor k_{LT} in Eq. B.1.54 was again determined based on GMNIA simulations (Fig. 2.28). For a constant bending moment values for k_{LT} in the range 0.6 to slightly below 1.0 are obtained, with an initial increase of k_{LT} up to $\overline{\lambda}_z \approx 1.0$. The influence of the shape of the moment diagram is taken into account by the uniform moment factor C_{mLT} (Eq. B.1.55). Although the non-uniformity is beneficial, the k_{LT}-factor is reduced significantly for high n_z-values. However, a similar comment as for torsionally stiff members can be made: due to the reduced magnitude of the bending moment for higher n_z values the influence of the second term (Eq. B.1.54) and therefore of k_{LT} will be reduced.

$$\frac{N_{Ed}}{\chi_z N_{pl,Rd}} + k_{LT} \frac{M_{y,Ed}}{\chi_{LT} M_{pl,y,Rd}} \leq 1 \tag{2.5.94}$$

$$k_{LT} = 1 - \frac{0.1\overline{\lambda}_z n_z}{C_{mLT} - 0.25} \geq 1 - \frac{0.1 n_z}{C_{mLT} - 0.25} \tag{2.5.95}$$

$$k_{LT} = 0.6 + \overline{\lambda}_z \leq 1 - \frac{0.1\overline{\lambda}_z}{C_{mLT} - 0.25} n_z \qquad \left[\overline{\lambda}_z < 0.4\right] \tag{2.5.96}$$

$$C_{mLT} = 0.6 + 0.4\psi \geq 0.4 \tag{2.5.97}$$

$$n_z = \frac{N_{Ed}}{\chi_z N_{pl,Rd}} \tag{2.5.98}$$

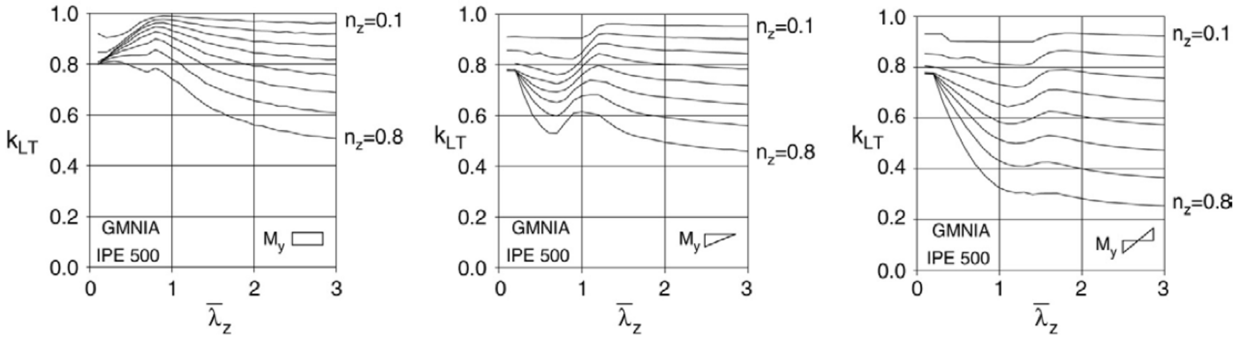

Figure 2.28: GMNIA-results interaction factor k_{LT} as function of $\overline{\lambda}_z$. Extracted from (Greiner & Lindner, 2006).

As for $\overline{\lambda}_z \rightarrow 0$ according to the bi-lineair interaction formula, k_{LT} equals 1.0 and the transition to the plastic cross-section interaction for $\overline{\lambda}_z = 0$ is not included in the formula. Therefore the cut-off formula (Eq. B.1.56) has been introduced (Fig. 2.29) for $\overline{\lambda_z} < 0.4$, approaching $k_{LT} = 0.6$ in the low slenderness range. As mentioned in section 2.5.8.1, the C_{mLT} factor is related to the full span for laterally free members, but restricted to a segmental part in case relevant lateral restraints are present.

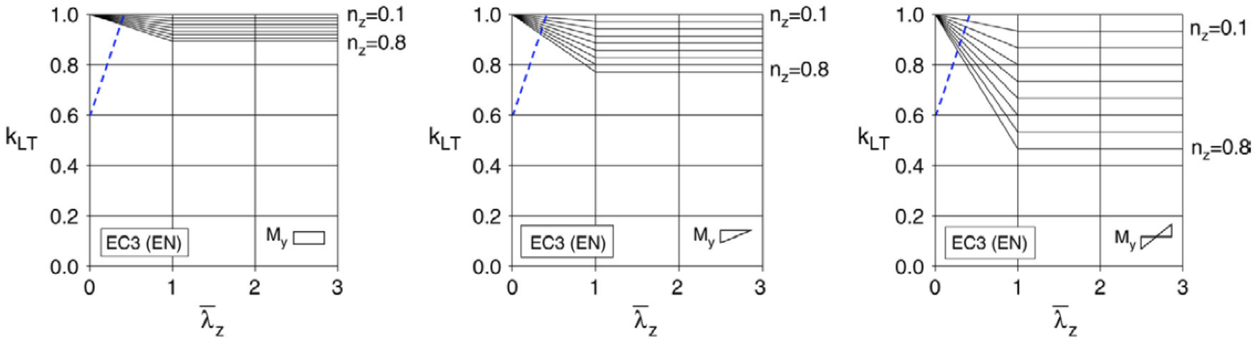

Figure 2.29: Interaction factor k_{LT} for different moment diagrams. Extracted from (Greiner & Lindner, 2006).

2.5.8.4 Members of class 3 or 4

As explained previously in section 2.5.1, for cross-sections of class 3 also a partial-plastic resistance can be considered. The interaction formulae for cross-sections class 3 or 4 will therefore by analogous with the expressions discussed in paragraphs 2.5.8.2 and 2.5.8.3, but with the plastic moment resistance M_{pl} replaced by M_{el} or M_{eff} (class 3 or 4). The resulting shift of the neutral axis due to the considered effective cross-section for members class 4 should also be taken into account by $\Delta M = e_N \cdot N$. An overview of the interaction formulae for members class 3 and 4 is given in Appendix C. Also the formulae for in-plane buckling under N+M_y as well as for the combination of axial compression and biaxial bending (N + M_y + M_z) are listed.

Buckling y-y:

$$\frac{N_{Ed}}{\chi_y N_{pl,Rd}} + k_y \frac{C_{my} M_{y,Ed}}{\chi_{LT} M_{el,y,Rd}} \leq 1 \tag{2.5.99}$$

Buckling z-z:

$$\frac{N_{Ed}}{\chi_z N_{pl,Rd}} + k_{LT} \frac{C_{my} M_{y,Ed}}{\chi_{LT} M_{el,y,Rd}} \leq 1 \tag{2.5.100}$$

Interaction factors k_y, k_z:

$$k_y = 1 + (\overline{\lambda}_y - 0.2)n_y \leq 1 + 0.8n_y \tag{2.5.101}$$

$$k_{LT} = 1 - \frac{0.05\overline{\lambda}_z n_z}{C_{mLT} - 0.25} \geq 1 - \frac{0.05n_z}{C_{mLT} - 0.25} \quad [\overline{\lambda}_z \geq 0.4] \tag{2.5.102}$$

$$k_{LT} = 0.6 + \overline{\lambda}_z \leq 1 - \frac{0.1\overline{\lambda}_z}{C_{mLT} - 0.25} n_z \quad [\overline{\lambda}_z < 0.4] \tag{2.5.103}$$

Equivalent moment factor:

$$C_{mLT} = 0.6 + 0.4\Psi \geq 0.4 \tag{2.5.104}$$

Axial compression parameter:

$$n_z = \frac{N_{Ed}}{\chi_z N_{pl,Rd}} \tag{2.5.105}$$

For linear moment distributions, the C_m factor according to Austin is applied. The formulation shows a bilinear shape with a conservative lower bound of 0.4. For non-linear bending diagrams, expressions for C_{my}, C_{mz} and C_{mLT} are tabulated based on the coefficients α_s and α_h (ECCS, 2006). These coefficients are determined based on the largest (absolute) value of the two hogging moments M_h at the beam extremities and the sagging moment M_s at mid-span. This is not necessarily the maximum sagging moment. The table providing the additional equations for uniformly distributed loads and for a concentrated transversal load at mid-span can be found in (CEN, 2005).

2.6 Application to cellular members

2.6.1 Design approach for cellular members

The design rules listed in the previous section are generally applicable for plain-webbed members. To apply these analytical rules on cellular members, two different design approaches are proposed, the 1T and 2T Approach. Only the 2T Approach will be considered in the remainder of this work. The cross-sectional properties based on this 2T approach can be found in Appendix A.

2.6.1.1 2T Approach

The 2T approach is based on experimental findings of Nethercot (Nethercot & Kerdal, 1982) and is adopted in the European pre-standard ENV 1993-1-1 (further referred to as ENV3), Annex N (CEN, 1998). Based on these limited number of test results, the critical LTB failure moment of cellular members can be calculated similarly as for plain-webbed cross-sections, but with the cross-sectional properties at the centre of the openings. According to this 2T approach, referring to the two tees of which the cross-section with web openings is formed, the effect of the openings on the lateral stability is negligible.

2.6.1.2 1T Approach

The 1T approach, adopted in the software program ARCELOR Cellular Beams, only takes into account the compressed tee section at the openings for the calculation of the lateral torsional resistance. By neglecting the stabilizing effect of the tee-section in tension, very conservative results are obtained.

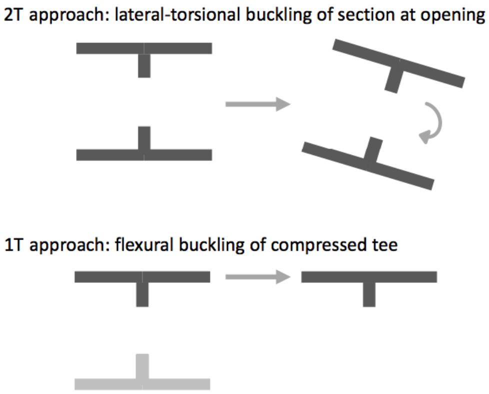
2T approach: lateral-torsional buckling of section at opening
1T approach: flexural buckling of compressed tee

Figure 2.30: Design approaches for cellular members.

2.6.2 Buckling curves

To take into account the adapted residual stress pattern of cellular members, the FB and LTB resistance should be calculated based on a different set of buckling curves. In (Sonck, 2014), a preliminary proposal was made for the modification of the buckling curves by derivation of the best fitting buckling curve to the numerical results.

2.6.2.1 Buckling curves for FB

Similarly as for the choice of the residual stress pattern, the selection of buckling curve is based on the height-to-width ratio of the parent section ($h/b > 1.2$ or $h/b \leq 1.2$). The current and for cellular members adapted EC3 buckling curve formulation, using existing buckling curves is given in Table 2.9. It can be concluded that the modified residual stress pattern for cellular members due the adapted manufacturing process will result in a lowering of approximately one buckling curve. Consequently, the buckling resistance N_{Rd} is decreased due to the lower value of the reduction factor χ.

Table 2.9: Current buckling curves for plain-webbed members (PWM) EC3 for hot-rolled sections (EC3) and proposal for cellular members.

	buckling axis	PWM	Cellular member
$h/b \geq 1.2$ $t_f \leq 40\,mm$	z	b	c
$h/b \leq 1.2$ $t_f \leq 100\,mm$	z	c	d

In (Sonck, 2014) preference was given to maintain the standard imperfection factors α (Table 2.4) corresponding with each buckling curve, although in this way slightly unsafe results were obtained for the HE650A profile.

2.6.2.2 Buckling curves for LTB

In (Sonck, 2014) a preliminary proposal for the selection of the buckling curves for LTB was made, using the current EC3 formulation (Table 2.10). Satisfactory results were obtained for all listed profiles, although even better results could be obtained for the profiles HE320A, IPE300, HE650A and IPE600 by considering a modified optimal imperfection factor α_{opt}. Finally, as conservative assumption it was proposed to perform the calculation of all profiles with $\alpha = 0.6$. A distinction based on the height-to-width ratio H/b (≤ 2 or ≥ 2) as in the current EC3 LTB curve selection was not recommended do to the large difference in results between the HE320A and HE320M sections, although for both geometries H/b<2.0.

Table 2.10: Preliminary proposal for LTB curves per parent section based on existing buckling curves.

parent section	H/b	buckling curve	α	α_{opt}
HE320A	≤ 2.0	d	0.76	0.6
HE320M	≤ 2.0	a	0.21	-
IPE300	≥ 2.0	d	0.76	0.55
HE650A	≥ 2.0	d	0.76	0.55
HE650M	≥ 2.0	c	0.49	-
IPE600	≥ 2.0	d	0.76	0.55

Part II

Numerical research

Chapter 3

Eccentrically loaded plain-webbed members

As already mentioned briefly in Chapter 1, the finite element model used is based on the model in (Sonck, 2014) for the investigation of global buckling of cellular and castellated members. In Sonck's work the model was first validated by performing a linear and linear bucking analysis (LA and LBA) on plain-webbed members loaded in bending or compression. Afterwards, the model was further validated for the specific case of cellular and castellated members under axial force or bending moment by comparing the numerically obtained buckling resistance with two sets of experiments. Experimental results obtained at Ghent University and results from experiments at the EIA-FR in Fribourg were used for the validation. It can be concluded that numerical and experimental results show a good correspondence, except for longer beams where failure was initiated by plasticity at extreme large deformations instead of the LTB phenomenon. In this master thesis however, members are subjected to a combination of bending moment and axial load. This work will therefore serve as an extension of the numerical study on eccentrically loaded members in (Gevaert, 2010), but performed for cellular members. In this chapter the principles and results of the numerical study of Gevaert are discussed.

3.1 Scope of Chapter 3

Although this work is focusing on cellular members, the study of Gevaert on plain-webbed members will be partly repeated for following reasons:

- To check the analytical values of the load proportionality factor obtained by means of Python scripts with numerical values.
- To clarify the assumptions of Gevaert regarding the considered boundary conditions, the use of kinematic coupling restraints, the applied imperfections, the analytical expressions used for the determinations of the load-proportionality factor.
- To extend the limited research on eccentrically loaded members (Chapter 4) and draw more general conclusions, since only interaction diagrams were available in (Gevaert, 2010).
- To verify the numerical model used in (Sonck, 2014) for the changed load condition of bending and compression.

Next, an overview of general principles will be given.

3.2 Analytical determination of load proportionality factor

To limit the number of simulations, three types of bending moment lines were considered: constant bending moment ($\psi = 1$), one-sided bending moment ($\psi = 0$) and moment at both supports ($\psi = -1$) equal in absolute value but opposite in sign.

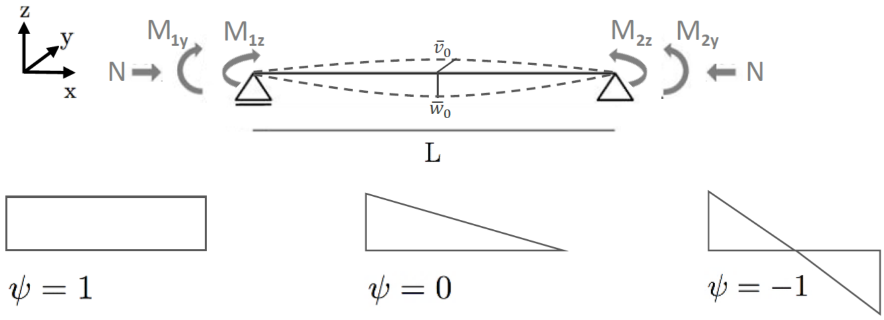

Figure 3.1: Considered moment distributions ($\psi = M_2/M_1$).

The magnitude of the normal force relative to the strong-axis bending moment can be expressed by the parameter μ. This parameter is a function of the critical buckling load $N_{cr,z}$ and the critical LTB moment M_{cr}. Low values of μ will therefore correspond to failure due to flexural buckling, whereas large values will result in a LTB failure mechanism. For the limit value $\mu = 0$, only an axial load is present, for $\mu = \infty$ the member is only subjected to a bending moment. In (Gevaert, 2010) as well as in this work, seven different values of μ are considered (Table 3.1).

$$\mu = \frac{M/M_{cr,LTB}}{N/N_{cr,z}} \leftrightarrow e = \frac{M}{N} = \mu \frac{M_{cr,LTB}}{N_{cr,z}} \tag{3.2.1}$$

Table 3.1: Considered values of μ.

μ						
0	0.1	0.5	1	5	10	∞

For the GMNIA analyses, first the initial load condition of the member is determined, i.e. the value of the initial axial load N and bending moment M (at both supports) to which the member is subjected. The initial load condition is indicated with the load proportionality factor λ_{start} and will be determined by the choice of the parameters μ and ψ.

$$M_{left} = \lambda_{start} \cdot M_{left,start} \tag{3.2.2}$$

$$M_{right} = \lambda_{start} \cdot M_{right,start} \tag{3.2.3}$$

$$N = \lambda_{start} \cdot N_{start} \tag{3.2.4}$$

Except for the limit cases $\mu = 0$ and $\mu = \infty$, the value of the axial load N_{start} can be determined based on Eq. 3.2.1 with an assumed starting value of $M_{left,start}$ equal to 1 kNm.

$$\mu = \frac{\frac{M_{left,start}}{M_{cr}}}{\frac{N_{start}}{N_{cr,z}}} \rightarrow N_{start} = \frac{N_{cr,z} M_{left,start}}{\mu M_{cr}} \rightarrow N_{start} = \frac{N_{cr,z}}{\mu M_{cr}} \tag{3.2.5}$$

An overview of the different initial load conditions is given in Table 3.2.

Table 3.2: Initial load condition.

	$M_{start,left}$ [kNm]	$M_{start,right}$ [kNm]			N_{start} [kN]
μ		$\psi = 1$	$\psi = 0$	$\psi = \text{-}1$	
0	0	0	0	0	1
0.1 to 10	1	1	0	-1	$\frac{N_{cr,z}}{\mu M_{cr}}$
∞	1	1	0	-1	0

In a specified number of increments, depending on the considered cross-section and corresponding resistance to failure, the value of λ_{start} is increased to the ultimate value λ_u at failure. With this proportionality factor, the load condition resulting in failure (M_u and N_u) can be determined.

$$M_{u,left} = \lambda_u \cdot M_{left,start} \tag{3.2.6}$$

$$M_{u,right} = \lambda_u \cdot M_{right,start} \tag{3.2.7}$$

$$N_u = \lambda_u \cdot N_{start} \tag{3.2.8}$$

In Section 2.5, four different methods with their corresponding conditions were discussed to check the cross-section resistance of members under a combination of bending moment and axial force.

For the analytical calculation of λ_u, each strength condition is written with 1 as upper limit. The load proportionality factor λ can be increased to its ultimate value λ_u, reached if the maximum of the strength conditions equals 1. The value of λ is therefore determined by iteration according to Eq. 3.2.10, by which the value of λ is initially varying strongly due to the low values of the strength conditions. With increasing values of λ and the strength conditions approaching 1, the variation of λ is limited. In this way the determination of λ can occur easily and efficiently. To limit the calculation time, the number of iterations will be limited to 500 as higher numbers resulted in a negligible deviation ($\leq 1\%$).

$$\text{Strength condition} \leq 1 \rightarrow \max(\text{Strength conditions}) = 1 \tag{3.2.9}$$

$$\lambda_{new} = \frac{\lambda_{old}}{\max(\text{strength conditions})} \quad \text{while } \max(\text{strength conditions}) \neq 1 \tag{3.2.10}$$

3.3 Levels of numerical analysis

The software package Abaqus was used for three types of analysis:

- Linear Buckling Analysis (LBA): Elastic, critical buckling load
  An eigenvalue analysis on a perfectly straight, elastic member is performed to determine the critical loads and eigenvalues. No imperfections nor residual stresses are introduced.

- Material Non-linear Analysis: First order plastic limit load
  No specific MNA analyses will be performed in this thesis, only a preliminary study was executed to examine if local deformations at the end sections were observed in the MNA analyses and if therefore a kinematic coupling constraint was strictly required.

- Geometrically and Materially Non-linear Analysis with imperfections: Ultimate buckling strength
  The resistance of the member subjected to a compression force, bending moment or both, depending on the values of μ and ψ (Section 3.2), is determined by the modified Riks method. Both imperfections and material non-linearities are considered.

3.4 Numerical determination of load proportionality factor

According to an analytical approach, the member will fail if one of the strength conditions of the ECCS or the Eurocode (as discussed in Chapter 2) is no longer fulfilled. Numerically, the member is considered to reach its failure mode if the maximum in the load displacement diagram is obtained, so no restriction is applied on the maximum deformation. However, it should be noted that in this way the failure load can correspond with large deformations and therefore in reality the failure state of this member is already reached before a maximum in the load displacement diagram is obtained. The load displacement diagram (of node indicated in Fig. 3.3) resulting from a GMNIA analysis on a HE300A profile with a length of 20.3 m and subjected to a uniform moment is given in Fig. 3.2.

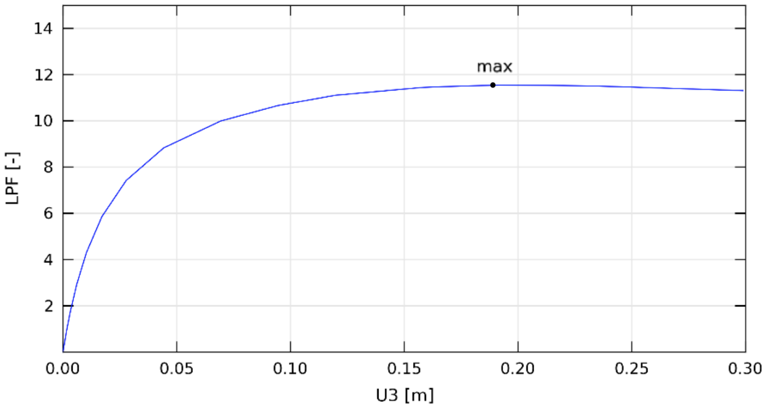

Figure 3.2: Load displacement diagram of HE300A, L=20.3 m, $\psi = 1$, $\mu = 0.1$.

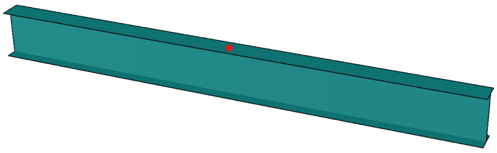

Figure 3.3: Considered node for load-displacement diagram.

As already mentioned in Section 2.1, it is possible that the load deflection curve is constantly increasing and that no maximum is reached due to the stabilizing effect of the pre-buckling deflections. This effect was at least noticeable for the largest considered length of all profiles (k=4, Section 3.11.1) subjected to a constant bending moment ($\psi = 1$, $\mu = \infty$). As members under a non-uniform bending moment ($\psi = 0$, $\psi = -1$) can be considered to behave as members with reduced buckling length, this stabilizing effect will be more pronounced under a constant bending moment. Although the effect is larger under pure bending ($\mu = \infty$), it was also examined for $\mu = 5$ and $\mu = 10$ (Fig. 3.4), where the influence of the axial load compared to the bending moment is already small. It should however be noted that by not including the kinematic coupling constraint, in some cases a maximum in the load displacement diagram could be reached. The effect of this kinematic coupling constraint is further discussed in Section 3.7.

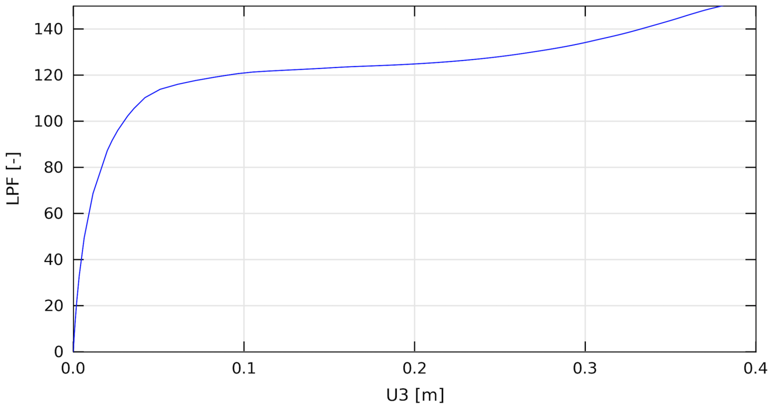

Figure 3.4: Load displacement diagram of HE300A, L=20.3 m, $\psi = 1$, $\mu = 10$.

3.5 Element type

The considered model for the plain-webbed members is depicted in Fig. 3.5. For the selection of the shell elements, to obtain accurate results at a reasonable cost the preference is given to quadratic shell elements S8R5 with reduced integration. Quadrilateral shell elements S4R are not considered as they are prone to hourglassing. A greater solution accuracy could be obtained by considering S4 elements, although increasing the calculation time considerably. With continuum elements the cross-section can be modelled more accurately, but again with a detrimental effect on the calculation time (Dassault Systèmes, 2012). Considering these drawbacks, the use of elements S8R5 is proposed.

The fillet at the web-to-flange intersection was not taken into account. Consequently, the torsion constant and plastic section modulus will be lower than in reality. This is partially compensated by the overlap of material at the web-to-flange transition. Earlier investigations were performed by D. Sonck where the fillet was implemented in the numerical model by means of an additional set of elements at the upper and lower part of the web with a variable thickness. Results of these test simulations showed however a limited improvement and still a lack of correspondence with the real cross-section geometry at the web-to-flange interface.

Based on the considerations above, the simplified model will be used for both the numerical simulations and for the cross-section characteristics in the theoretical formulations. As shown in (Taras, 2010), the omission of the fillet is justified as buckling curves similar in shape are obtained, depending on the dimensionless parameters $\overline{\lambda}$ and χ. For the determination of the buckling strength in absolute terms, the fillet must be included.

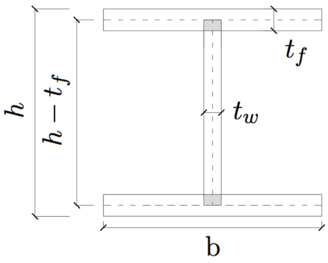

Figure 3.5: Cross-section numerical model with indication web-flange overlap.

3.6 Mesh size

Not only the type of element (S8R5), but also the mesh size will have a large influence on the accuracy and calculation time. In this work a preliminary refinement study was performed on different profiles for which the element size was defined as b/n, with b the flange width and n $\in [2, 4, 6, 8]$. In this way the number of elements was varied along the flange width from 2 to 8 (Fig. 3.6). The study was limited to members subjected to pure bending, but a constant ($\psi = 1$) as well as a non-uniform bending moment ($\psi = 0; \psi = -1$) were considered.

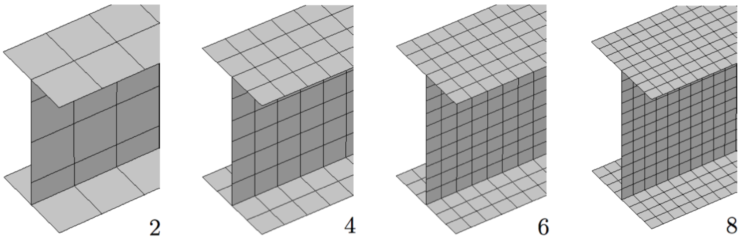

Figure 3.6: Examined variation of number of elements along the flange width.

The critical LTB moment was determined by means of an LBA analysis. The results on a HE500A profile (L=18.3 m) are depicted in Fig. 3.7, from which a convergence of M_{cr} can be observed starting from six elements along the flange width. A slightly higher value of M_{cr} can even be observed for eight elements per flange width due to the large mesh density. It should be noted that in (Gevaert, 2010) a mesh size of 4 elements along the flange width was chosen based on a similar refinement study for an LBA and MNA analysis. The maximum difference (obtained for $\psi = 1$) in critical LTB moment for a model with four or six elements per flange width for the described HE500A profile is indeed only 0.036%. In this work however the parametric study was performed with the model of six elements along the flange, the same amount as will be used for the model of the cellular members. This larger accuracy can compensate for the fact that in this study only an out-of-plane imperfection is applied, whereas also an in-plane imperfection was considered by Gevaert. In this way, a larger calculation time will however be required as illustrated in Fig. 3.7, where a maximum increase from 60.1 s to 107 s was obtained for $\psi = 1$ by changing the elements per flange width from 4 to 6. An overview of the considered mesh size for the refinement study is given in Table 3.3.

Table 3.3: Overview mesh size for different no. of elements along the flange width.

No. elements/ flange width [-]	No. Elements along member's length [-]	Mesh size [m]
2	122	0.150
4	244	0.075
6	366	0.050
8	488	0.038

3.7 Boundary conditions and load application

To meet the theoretical assumption of fork supports as boundary condition, the displacement of all nodes in y- and z- direction (indicated with U2 and U3, Fig. 3.8) at both ends of the member is prevented, as well as the rotation about the x-axis (UR1). Furthermore, the translation in x-direction at the central node of the web of one end is restricted (U1). In this work also a kinematic coupling

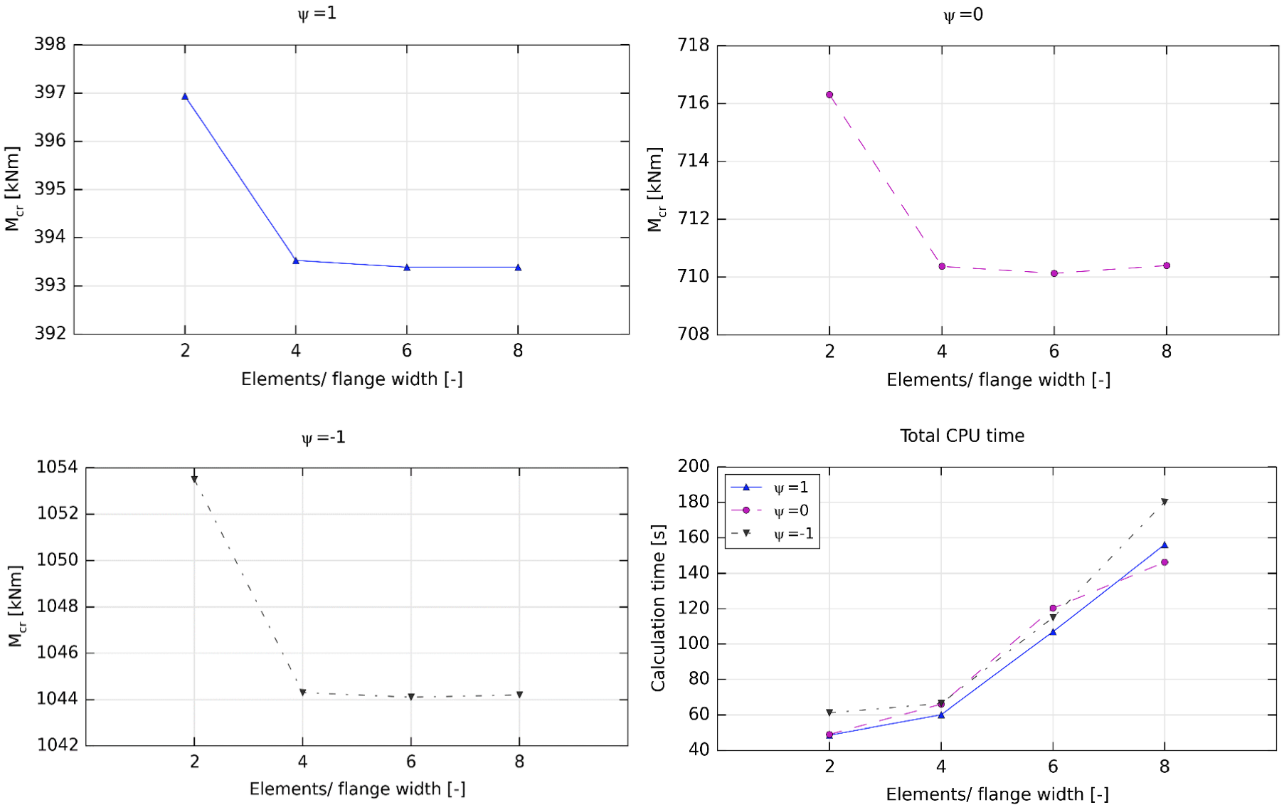

Figure 3.7: Preliminary study mesh size based on LBA analysis HE500A (L=18.3 m).

constraint was implemented in the numerical model similarly as in (Sonck, 2014), due to the observed local deformations during MNA analyses, which could be avoided by the coupling restraint. Local deformations at the end sections are prevented, but not the warping of the flanges. This coupling constraint was however not incorporated by Gevaert in his model used for the parametric study on plain-webbed members.

Both the axial load and bending moment are introduced as line loads at both ends of the member acting on the flanges as well as on the web. For members under combined moment and compressive force, the sum of both contributing line loads (M and N) is taken. This load introduction is illustrated in Fig. 3.9 for an eccentrically loaded HE180A profile subjected to non-uniform bending ($\psi = -1$) and for $\mu = 5$, indicating that the influence of the axial load is rather small. Therefore, for the resulting line load the same direction as for the pure bending case is examined.

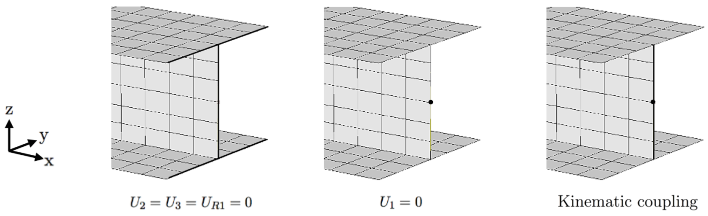

Figure 3.8: Boundary conditions at end sections.

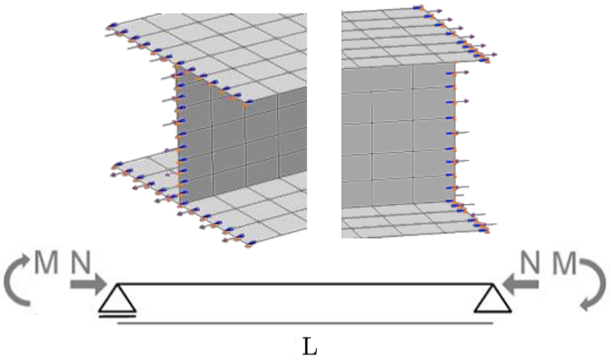

Figure 3.9: Load introduction eccentrically loaded HEA180 (M=1000 Nm; N=822.3 N).

3.8 Geometric imperfection

For the GMNIA analysis, a half-sine wave geometric imperfection with amplitude L/1000 was introduced. In (Gevaert, 2010) both an in-plane and out-of-plane imperfection were applied. As the considered members are subjected to a combination of axial load and strong-axis bending moment, the direction in which the out-of-plane imperfection is applied (positive or negative y-coordinate) has no influence. For the geometric imperfection according to the z-axis (in-plane), two opposing effects should be taken into account to determine the most detrimental direction. This was investigated by Gevaert.

For members subjected to pure bending ($\mu = \infty$), the direction of the in-plane geometric imperfection will have an influence on the critical LTB moment. Members for which the direction of the imperfection is opposite from the deflections due to the applied bending moment will result in lower values of M_{cr} and these members will therefore be more susceptible to LTB compared to members with an opposite or no in-plane imperfection (Fig. 3.10). As an example, an upward (positive z-coordinate) geometric imperfection is most detrimental for members under uniform bending.

For eccentrically loaded members, also the influence of the axial load N should be considered. For members with a downward geometric in-plane imperfection, the bending moment at mid-span will increase with $\Delta M = N\bar{e}_0$. This will result in larger stresses and earlier failure of the member. This effect is however opposed by the larger favourable critical LTB moment under a downward imperfection. For members with an upward imperfection, the bending moment at mid-span is decreased with ΔM, increasing the member's strength, but this favourable effect is opposed by a lower value of M_{cr} for an upward imperfection.

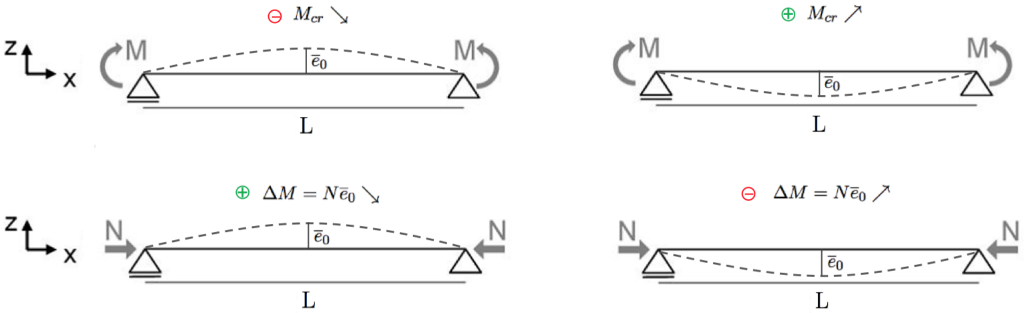

Figure 3.10: Opposing effects preferential direction geometric in-plane imperfection.

3.9 Residual stress pattern for plain-webbed members

The residual stress pattern is applied according to section 1.4.1 as function of the height to width ratio of the profiles. The residual stresses were implemented in the model by means of a user subroutine by which the longitudinal stresses are defined in function of the coordinates of the nodes of the model with imperfections. The residual stresses are only implemented for the GMNIA analysis in contrast to the LBA analysis, which is performed on a perfectly straight, elastic member.

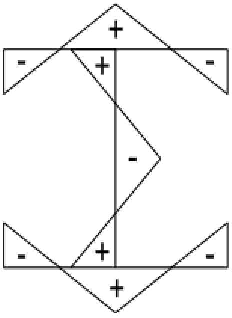

h/b $\leq$ 1.2: $|\sigma_{res}|_{max} = 0.5\ f_y$
HEA180/ HEA300

h/b $\geq$ 1.2: $|\sigma_{res}|_{max} = 0.3\ f_y$
IPE120/IPE240/IPEO360/HEA400/
IPEO450/HEA500/IPEO600/HEM700

Figure 3.11: Applied residual stress pattern for profiles of Gevaert ($\sigma_{compression} < 0, \sigma_{tension} > 0$).

3.10 Profiles

3.10.1 Classification cross-section

In (Gevaert, 2010), ten different doubly-symmetric I-section profiles with steel grade S235 were considered, of which the cross-section characteristics are given in Table 3.4.

Table 3.4: Cross-sectional properties profiles Gevaert.

	h [m]	b [m]	t_f [m]	t_w [m]
IPE120	0.120	0.064	0.0063	0.0044
HE180A	0.171	0.180	0.0095	0.0060
IPE240	0.240	0.120	0.0098	0.0062
HE300A	0.290	0.300	0.0140	0.0085
IPEO360	0.364	0.172	0.0147	0.0092
HE400A	0.390	0.300	0.0190	0.0110
IPEO450	0.456	0.192	0.0176	0.0110
HE500A	0.490	0.300	0.0230	0.0120
IPEO600	0.610	0.224	0.0240	0.0150
HE700M	0.716	0.304	0.0400	0.0210

The most detrimental classification is obtained when the web is only subjected to a compressive force ($\mu = 0$). When also a bending moment is present, it is assumed that the compressive force will be taken by the central part of the cross-section (hatched in Fig.3.12), while the bending moment is taken by the outermost parts.

For $\psi = 1$ and $\mu \neq 0$, there is always a combination of compressive force and constant bending moment. For these sections the relative height α of the compressive zone is determined based on z_n, the distance between the centre of gravity and the end of the compressive zone. The distance z_n can be calculated by expressing a constant ratio between bending moment and axial force until failure (Eq.3.10.3), i.e the ultimate value of the load proportionality factor λ_u is equal for M and N. It should be noted that for cross-sections class 3, an elastic approach is required with parameter ψ indicating the stress distribution over the web (Eq.3.10.4). For the double symmetric I section members considered in this work the stress ratio ψ is always larger than -1. For members under constant bending moment the classification is depending on the members' length. This is due to the variation of M_{cr} and $N_{cr,z}$ for different lengths resulting in different values for the ratio of M_{start} and N_{start} influencing the value of α for the classification.

$$N_{max} = 2 z_n f_y t_w \tag{3.10.1}$$

$$M_{max} = 2 b t_f f_y \left(\frac{h}{2} - \frac{t_f}{2}\right) + 2 f_y t_w \left(h/2 - t_f - z_n\right) \left[z_n + \frac{(h/2 - t_f - z_n)}{2}\right] \tag{3.10.2}$$

$$\frac{M_{max}}{N_{max}} = e = \frac{M_{start}}{N_{start}} \tag{3.10.3}$$

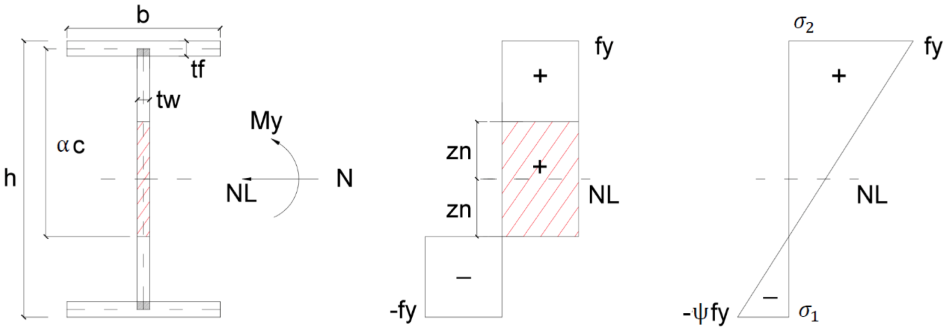

Figure 3.12: Cross-section classification according to plastic and elastic theory (compression: +, tension: -).

$$\psi = \frac{\sigma_1}{\sigma_2} \quad \text{with} \quad \sigma_1 = \frac{N_{Ed}}{A} + \frac{M_{Ed}}{W_{el}}; \quad \sigma_2 = \frac{N_{Ed}}{A} - \frac{M_{Ed}}{W_{el}} \tag{3.10.4}$$

If the cross-section is only subjected to a bending moment ($\mu = \infty$), at least half of the cross-section is in compression, considering that the neutral line (NL) is situated at half the height of the cross-section for doubly-symmetrical profiles. The compressive zone will increase with increasing values of N. For both $\psi = -1$ and $\psi = 0$, one cross-section can be found where only a compressive force is acting, which will be determining for the classification. For these sections, the classification is independent of the length of the considered members.

The numerical research in (Gevaert, 2010) was limited to cross-sections class 1 till 3. Although the classical HEA and IPE profiles belong to this range, for the classification based on the numerical model also sections class 4 were obtained. This can be explained by the larger web height of the wire model ($h - t_f$), where the fillet is not taken into account, compared to the standard classification based on $h - t_f - 2r$. Therefore, in (Gevaert, 2010), it was decided to deviate from the standard HEA and IPE profiles. Due to the larger web and and flange thickness of IPEO and HEM profiles compared to IPE and HEA sections, the width-to-thickness ratios for the compression parts are sufficiently low to obtain maximum class 3. An overview of the classification for the 10 profiles considered by Gevaert as function of the load distribution is given in Tables 3.5 and 3.6. For members under constant bending moment ($\psi = 1$), the most detrimental classification is listed, obtained for the shortest members (k=1, Section 3.11.1). For IPE120, HE180A, HE300A and HE700M profiles, the classification is valid for all considered lengths.

Table 3.5: Classification of cross-sections Gevaert for $\psi = 1$ (k=1) ($c = h - t_f - 2r$).

μ	IPE120	HE180A	IPE240	HE300A	IPEO360	HE400A	IPEO450	HE500A	IPEO600	HE700M
0	1	2	2	3	2	2	3	3	3	1
0.1	1	2	2	3	2	2	3	3	3	1
0.5	1	2	2	3	2	2	3	3	3	1
1	1	2	2	3	2	2	3	3	2	1
5	1	2	1	3	1	1	1	1	1	1
10	1	2	1	3	1	1	1	1	1	1
∞	1	2	1	3	1	1	1	1	1	1

Table 3.6: Classification of cross-sections Gevaert for $\psi = 0$ and $\psi = -1$ ($c = h - t_f - 2r$).

μ	IPE120	HE180A	IPE240	HE300A	IPEO360	HE400A	IPEO450	HE500A	IPEO600	HE700M
0	1	2	2	3	2	2	3	3	3	1
0.1	1	2	2	3	2	2	3	3	3	1
0.5	1	2	2	3	2	2	3	3	3	1
1	1	2	2	3	2	2	3	3	3	1
5	1	2	2	3	2	2	3	3	3	1
10	1	2	2	3	2	2	3	3	3	1
∞	1	2	1	3	1	1	1	1	1	1

The classification of the web and flange are performed according to EC3 (CEN, 2005) ($c = h - 2t_f - 2r$), whereas based on a wire model ($c = h - t_f - 2r$) in (Gevaert, 2010). Only for comparison of results with Gevaert, the wire model will be considered. By considering a wire model, a better correspondence can be obtained with the numerical study where the fillets were also omitted from the model. A critical remark can however be made on this cross-section classification. Due to the larger web height of the wire model compared to the real profiles, a higher classification is obtained compared to the classification according to EC3 (Tables 3.8 - 3.7). For profiles HE300A, IPEO450, HE500A and IPEO600 the maximum class obtained by including the fillets is only 2 and these sections can therefore be calculated according to a plastic theory, whereas for the wire model an elastic calculation is required as class 3 was obtained. The differences between the classification according to a wire model (Tables 3.5-3.6) and according to EC3 (Tables 3.8-3.7) are indicated in bold. Differences between elastic and plastic theory are underlined.

Table 3.7: Classification of cross-sections Gevaert for $\psi = 1$ according to EC3 ($c = h - 2t_f - 2r$).

μ	IPE120	HE180A	IPE240	HE300A	IPEO360	HE400A	IPEO450	HE500A	IPEO600	HE700M
0	1	**1**	**1**	$\underline{\mathbf{1}}$	2	**1**	$\underline{\mathbf{2}}$	$\underline{\mathbf{2}}$	$\underline{\mathbf{2}}$	1
0.1	1	**1**	**1**	$\underline{\mathbf{1}}$	2	**1**	$\underline{\mathbf{2}}$	$\underline{\mathbf{2}}$	$\underline{\mathbf{2}}$	1
0.5	1	**1**	**1**	$\underline{\mathbf{1}}$	2	**1**	$\underline{\mathbf{2}}$	$\underline{\mathbf{2}}$	$\underline{\mathbf{2}}$	1
1	1	**1**	**1**	$\underline{\mathbf{1}}$	2	**1**	$\underline{\mathbf{2}}$	$\underline{\mathbf{2}}$	2	1
5	1	**1**	1	$\underline{\mathbf{1}}$	1	1	1	1	1	1
10	1	**1**	1	$\underline{\mathbf{1}}$	1	1	1	1	1	1
∞	1	**1**	1	$\underline{\mathbf{1}}$	1	1	1	1	1	1

Table 3.8: Classification of cross-sections Gevaert for $\psi = 0$ and $\psi = -1$ according to EC3 ($c = h - 2t_f - 2r$).

μ	IPE120	HE180A	IPE240	HE300A	IPEO360	HE400A	IPEO450	HE500A	IPEO600	HE700M
0	1	**1**	**1**	$\underline{\mathbf{1}}$	2	**1**	$\underline{\mathbf{2}}$	$\underline{\mathbf{2}}$	$\underline{\mathbf{2}}$	1
0.1	1	**1**	**1**	$\underline{\mathbf{1}}$	2	**1**	$\underline{\mathbf{2}}$	$\underline{\mathbf{2}}$	$\underline{\mathbf{2}}$	1
0.5	1	**1**	**1**	$\underline{\mathbf{1}}$	2	**1**	$\underline{\mathbf{2}}$	$\underline{\mathbf{2}}$	$\underline{\mathbf{2}}$	1
1	1	**1**	**1**	$\underline{\mathbf{1}}$	2	**1**	$\underline{\mathbf{2}}$	$\underline{\mathbf{2}}$	$\underline{\mathbf{2}}$	1
5	1	**1**	**1**	$\underline{\mathbf{1}}$	2	**1**	$\underline{\mathbf{2}}$	$\underline{\mathbf{2}}$	$\underline{\mathbf{2}}$	1
10	1	**1**	**1**	$\underline{\mathbf{1}}$	2	**1**	$\underline{\mathbf{2}}$	$\underline{\mathbf{2}}$	$\underline{\mathbf{2}}$	1
∞	1	**1**	1	$\underline{\mathbf{1}}$	1	1	1	1	1	1

It should be noted that the model according to EC3 ($c = h - 2t_f - 2r$) is only used for the cross-section classification and not for the cross-sectional properties appearing in the design rules, for which the wire model is still used. This reasoning can be substantiated in the following way based on the design rule of Van Impe, but a similar reasoning is possible for other methods.
The design rule of Van Impe for buckling about the weak axis is repeated here in the form used to determine the load proportionality factor analytically. In this formula, the influence of introducing a plastic or elastic section modulus is clearly noticeable. The same reasoning can be applied on the design rule of Vandepitte. Under pure compression ($\mu = 0$, Fig. 3.13), members fail by weak-axis flexural buckling (N $\leq N_{bz,Rd}$). This flexural buckling resistance is independent of the considered section modulus and therefore no difference is obtained between a plastic or elastic calculation, as visualized in Fig. 3.13. In this figure the deviation in LPF between a plastic or elastic calculation is plotted for an HE300A profile for a range of forty μ values between 0 and 100. The determination of these μ values is discussed in Section 3.16. Two different lengths (L=2.9 m; L=20.3 m) and three different ψ values are considered. For the profile HE300A class 3 was obtained for the wire model; without omission of the fillet the cross-section classification is 1.

$$\frac{\lambda N_{start}}{A} + \frac{\beta_y \lambda |M_{1y,start}|}{\chi_{LT}\left(1 - \frac{\lambda N_{start}}{N_{cr,y}}\right) W_y} + \frac{\lambda N_{start} |\overline{v_0}|}{\left(1 - \frac{\lambda N_{start}}{N_{cr,z}}\right) W_z} \leq f_y \tag{3.10.5}$$

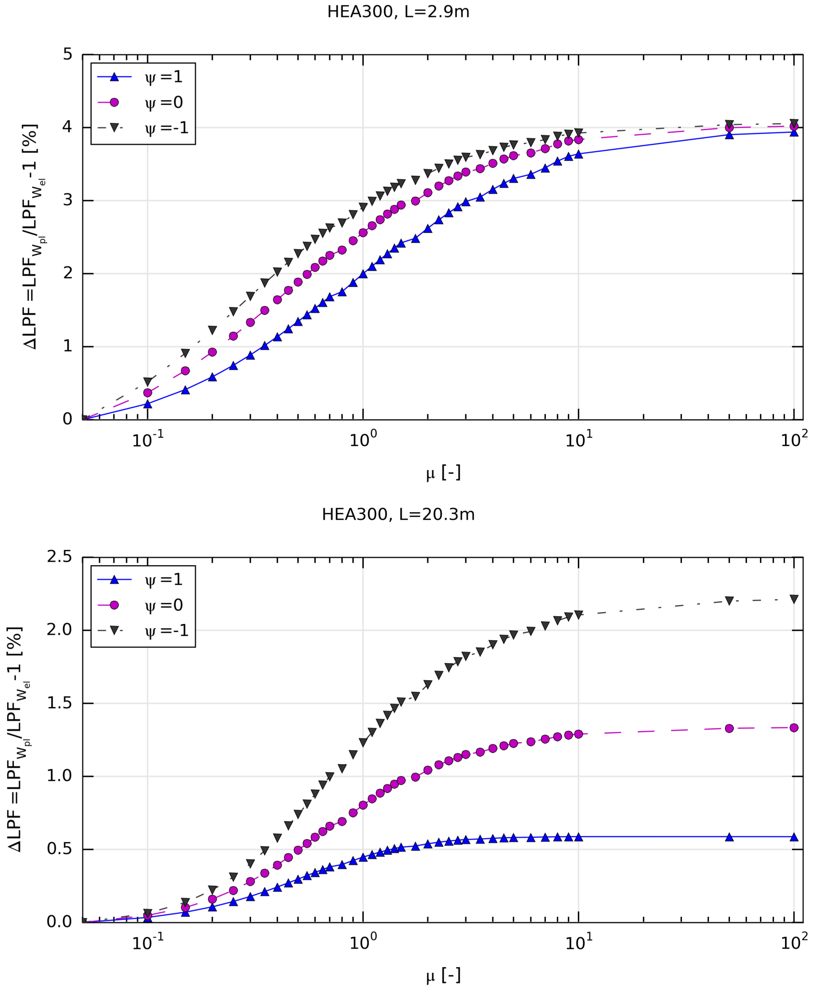

Figure 3.13: Deviation of LPF following a plastic or elastic theory according to Van Impe method

It can be concluded that calculation according to a plastic theory would result in a higher LPF for both considered lengths. The deviation is increasing with increasing μ value and largest for the shortest members and for $\psi = -1$. The largest obtained deviation is 4.1%. That the deviation will be positive can be directly derived from Eq. 3.10.5, which can be reduced as followed for the limit case of pure bending ($\mu = \infty$; N=0):

$$\frac{\beta_y \lambda |M_{1y,start}|}{\chi_{LT} W_y} \leq f_y \tag{3.10.6}$$

Since $W_{pl} > W_{el}$, the value of the load proportionality factor should be larger for a calculation according to a plastic theory.
Due to the larger value of the load proportionality factor λ_u, the failure moment M_u and compressive force N_u are larger and therefore by calculation according to a plastic theory it is assumed that the cross-section can resist a higher bending moment and axial load.

Although criticism on calculation according to a plastic theory is therefore possible, it should be noted that deviations are small, that in reality the cross-section does have a fillet with radius r and that these short length members will behave plastically. Furthermore, in this master thesis only the global instability of eccentrically loaded members is addressed, not failure due to local instabilities. Therefore, only a global shape imperfection was introduced without inclusion of local imperfections. Since in the modified Riks method elastic behaviour can only be introduced by local folding effects, which are not modelled, members will behave plastically. As a result, calculation according to an elastic theory by considering a wire model would be safe, but not economic and not better corresponding with the obtained Abaqus results. However, for the cross-sectional properties in the stability design rules themselves, the fillet is omitted as in this way a better correspondence is obtained with the numerical model.

3.11 Differences with D. Gevaert

An overview of the assumptions made in this work regarding the numerical model, compared to Gevaert, is given in Table 3.9.

Table 3.9: Comparison of assumptions in this work with Gevaert.

	Section	Assumptions	(Gevaert, 2010)
Mesh: elements/flange width	3.6	6	4
Kinematic coupling	3.7	Yes	No
Imperfection	3.8	Out-of-plane	In-plane and out-of-plane
Classification	3.10.1	EC3 ($c = h - 2t_f - 2r$)	wire model ($c = h - t_f - 2r$)
CS properties design rules	3.10.1	wire model ($c = h - t_f - 2r$)	wire model ($c = h - t_f - 2r$)

3.11.1 Length

The determination of the length was based on Gevaert, with the length chosen to cover a sufficient range of slendernesses for the different profiles. Preference was given to examen four different lengths with a maximum length of 25 m to obtain lengths in the normal range of application. However, due to the large variation in dimensions of the four different I-section types (IPE, IPEO, HEA, HEM), the length of the lower-height profiles (70 h $\leq$ 25) was calculated differently than for the larger profiles (70 h>25), where the length was determined based on interpolation between the lower boundary of 10 h and the maximum considered length of 25 m (Table 3.10). With the notation h is referred to the total cross-section height. An overview of the dimensionless slendernesses λ_z (FB) and λ_{LT} (LTB) is given in

Table 3.11. It can be noticed that due to the higher second moment of area I_z for equal height profiles HEA/HEM compared to IPE/IPEO profiles, the corresponding critical weak-axis flexural buckling load $N_{cr,z}$ for these HE profiles is higher, reducing the member's slenderness. To make it possible to examen also lower slenderness values of IPE profiles, a lower boundary of 5 h could have been introduced in (Gevaert, 2010). The reduced slenderness values $\overline{\lambda}$ and $\overline{\lambda}_{LT}$ are represented in Figs. 3.14-3.15, where the lower values for HE compared to IPE profiles are clearly noticeable. The profile numbers are mentioned in Table 3.11.

Table 3.10: Profile length plain-webbed members.

k	70 h $\leq$ 25	70 h $>$ 25
1	10 h	10 h
2	30 h	10 h + (25-10 h)(1/3)
3	50 h	10 h + (25-10 h)(2/3)
4	70 h	25

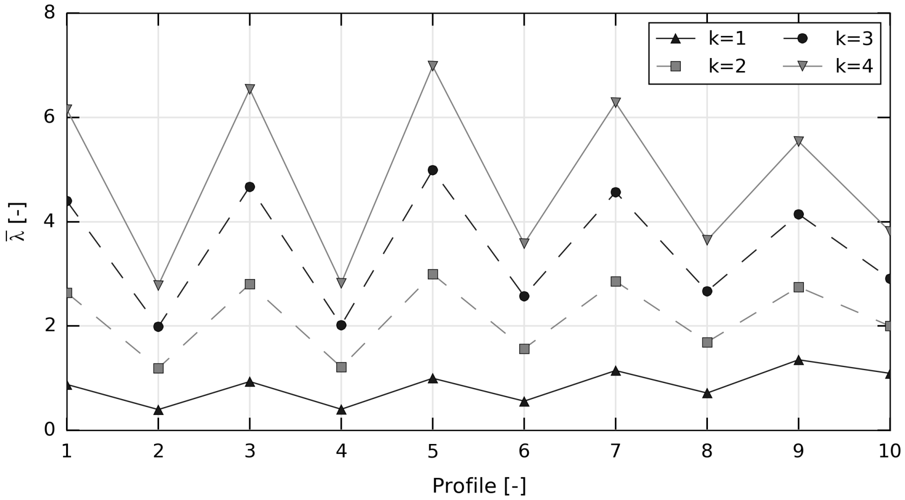

Figure 3.14: Reduced slenderness $\overline{\lambda}$ for 10 different profiles of Gevaert for 4 different lengths (defined by k).

Table 3.11: Slenderness range $\overline{\lambda_z}$ and $\overline{\lambda}_{LT,min}/\overline{\lambda}_{LT,min}$ for plain-webbed members.

k		1	2	3	4		
		$\overline{\lambda}_z$				$\overline{\lambda}_{LT,min}$	$\overline{\lambda}_{LT,max}$
			70 h $\leq$ 25				
1	IPE120	0.88	2.64	4.40	6.15	0.41	2.18
2	HEA180	0.40	1.19	1.98	2.78	0.22	1.43
3	IPE240	0.93	2.80	4.67	6.54	0.46	2.58
4	HEA300	0.40	1.21	2.02	2.72	0.22	1.54
5	IPEO360	1.00	3.00	4.99	6.98	0.48	2.68
			70 h>25				
6	HEA400	0.56	1.57	2.57	3.58	0.29	1.75
7	IPEO450	1.15	2.86	4.57	6.28	0.54	2.59
8	HEA500	0.71	1.69	2.67	3.64	0.37	1.81
9	IPEO600	1.35	2.75	4.14	5.54	0.61	2.40
10	HEM700	1.09	2.00	2.91	3.81	0.49	1.70

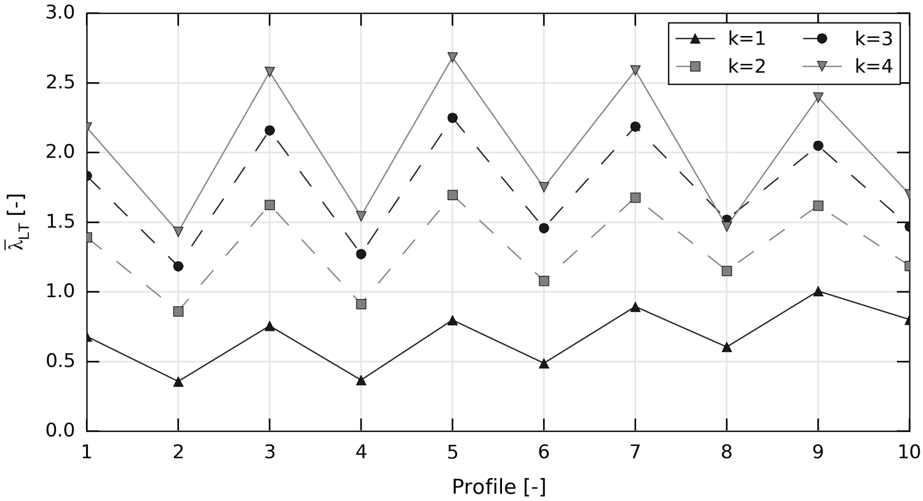

Figure 3.15: Reduced slenderness for LTB $\overline{\lambda}_{LT}$ for 10 different profiles of Gevaert for 4 different lengths (defined by k; $\psi = 1$).

3.12 Critical load N_{cr}

Correct modelling will be governed by the complex LTB behaviour rather than failure due to flexural buckling. Therefore only a preliminary study was performed comparing numerical results from Abaqus of this model with those obtained by D. Gevaert. The critical load was determined by an LBA analysis on perfectly elastic members without imperfections. A further verification occurred by comparison with analytical expressions, the difference between both expressed by the deviation factor Δ_N, defined according to Eq. 3.12.1.

$$\Delta_N = \left(\frac{N_{abq}}{N_{an}} - 1\right) \cdot 100\% \tag{3.12.1}$$

The deviations obtained for both models (Table 3.12) are negative indicating that the theoretical expression of the critical flexural buckling load is slightly unsafe. However, the maximum measured deviations are only 0.33%.

Table 3.12: Deviation of N_{cr}.

	L [m]	$N_{an}[kN]$	$N_{cr,Abq,GD}[kN]$	$\Delta_{N,GD}$	$N_{Abq}[kN]$	$\Delta_N[\%]$
IPE120	6.00	15.89	15.88	-0.06	15.88	-0.09
HEA180	8.55	261.89	261.04	-0.32	261.02	-0.33
IPE240	12.00	40.69	40.65	-0.10	40.65	-0.10
HEA300	14.50	621.18	619.19	-0.32	619.16	-0.33
IPEO360	18.20	78.15	78.08	-0.09	78.08	-0.09
HEA400	17.97	549.24	547.99	-0.23	547.97	-0.23
IPEO450	18.19	130.40	130.28	-0.09	130.28	-0.09
HEA500	18.30	640.97	639.59	-0.22	639.27	-0.27
IPEO600	18.70	267.44	267.16	-0.10	267.16	-0.10
HEM700	19.05	1072.30	1070.3	-0.19	1070.30	-0.19

3.13 Deviation of $M_{cr,0}$

From an LBA analysis, a deviation factor $\Delta M_{cr,0}$ is determined, indicating the deviation of the numerical results for the critical LTB bending moment M_{abq} with the analytically obtained values $M_{cr,an}$. For the theoretical expressions, the cross-sectional properties according to a wire model were used.

$$\Delta M_{cr,0} = \left(\frac{M_{cr,Abq}}{M_{cr,an}} - 1 \right) \cdot 100\% \tag{3.13.1}$$

An overview of the minimum and maximum deviations for different load configurations is given in Table 3.13. For members subjected to a constant bending moment ($\psi = 1$), the observed deviations for longer members are limited, as depicted in Fig. 3.18. For shorter members however unsafe deviations are obtained due to web distortion, but these deviations can be considered insignificant as the governing failure mode of short members will be plastic yielding instead of elastic buckling. For a non-uniform bending moment ($\psi = 0, \psi = -1$), positive deviations are obtained indicating that the expressions for the critical LTB bending moment are safe and more conservative than for members subjected to a constant moment. Again, short members are prone to lateral-distortional buckling, which is even more pronounced than under a uniform moment. Under a non-uniform bending moment, the behaviour is comparable to members with reduced buckling length, resulting in an increased critical LTB moment and increased importance of other failure modes such as lateral-distortional buckling or other local buckling phenomena. For these local effects, load configuration $\psi = -1$ is most detrimental.

Table 3.13: Deviation of $M_{cr,Abq}$ and $M_{cr,an}$.

ψ	Δ_{min} [%]	Δ_{max}[%]	Δ_{mean} [%]	Δ_{median} [%]
1	-4.16	0.14	-0.66	-0.28
0	-3.09	2.34	1.24	1.34
-1	-7.65	2.36	0.26	1.04

The observed web distortion is illustrated for section IPE240 showing the largest deviation (7.65%) of all profiles for $\psi = -1$ and a length of 2.4 m. From Fig. 3.16 the S shape of the distorted web is clearly visible. Furthermore, it can be noticed that over this section the yield strength is fully reached and the plastic capacity will determine the member's failure behaviour.

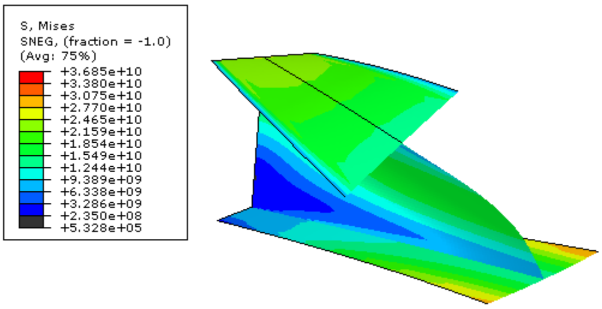

Figure 3.16: Observed web distortion for IPE240 ($\psi = -1; L = 2.4\,m$)

It should however be noted that for some of the shortest considered lengths of profiles HE180A, HE300A, HE400A and HE500A, much larger deviations (>10 %) were obtained. These configurations, listed in Table 3.21, failed by local plastic yielding, not in a lateral-torsional buckling mode. The plastic moment M_{pl} of these sections is much lower than the critical LTB bending moment $M_{cr,LTB}$ as illustrated by the low values of $M_{pl}/M_{cr,An}$ and $\overline{\lambda}_{LT}$. Therefore, the member's behaviour will be governed by plastic yielding and elastic buckling is considered unlikely. Consequently, although the observed deviations are large, they can be considered insignificant, similarly as for the examined web distortion. The first eigenmode of an HE300A profile is given in Fig. 3.17.

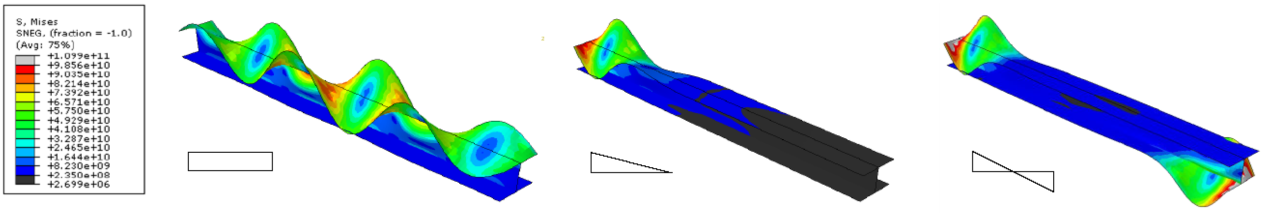

Figure 3.17: First eigenmode of HE300A (L=2.9 m).

Table 3.14: Deviation $M_{cr,0} > 10\%$ for profiles in (Gevaert, 2010).

	ψ	L [m]	CS	M_{pl} [kNm]	$M_{cr,Abq}$ [kNm]	$M_{cr,An}$ [kNm]	$\Delta M_{cr,0}$ [%]	$\bar{\lambda}_{LT}$ [-]	$M_{pl}/M_{cr,An}$ [-]
HE180A	1	1.71	1	74.09	385.29	581.47	-33.74	0.36	0.127
	0	1.71	1	74.09	449.55	1029.20	-56.32	0.27	0.072
	-1	1.71	1	74.09	487.17	1511.83	-67.78	0.22	0.049
HE300A	1	2.90	1	310.45	1241.30	2308.78	-46.24	0.37	0.134
	0	2.90	1	310.45	1446.20	4086.54	-64.61	0.28	0.076
	-1	2.90	1	310.45	1565.80	6002.82	-73.92	0.23	0.052
HE400A	-1	3.90	1	585.91	4745.80	6404.37	-25.90	0.30	0.091
HE500A	-1	4.90	1	910.99	5497.50	6485.02	-15.23	0.37	0.140

3.14 Determination critical LTB moment

For the analytical calculation of the load proportionality factor λ_u of members susceptible to torsional deformations, the value of the critical LTB moment $M_{cr,0}$ should be known. As mentioned previously (Section 3.2), this value is also required to determine the start value of the axial force acting on the member. Different methods are applicable to calculate this critical moment analytically or numerically.

3.14.1 Numerical determination

LTBeam This software program was developed by CTICM (Centre Technique Industriel de la Construction Métallique) and can be used to determine the critical LTB moment of plain-webbed members. In this work it will only be used as a fast check of the obtained results by Abaqus and those from analytical expressions. The cross-sectional properties entered in the program are based on the simplified numerical model (Fig. 3.5).

Abaqus The critical LTB moment is determined by a linear buckling analysis (LBA).

3.14.2 Analytical determination

Variation equation and Ritz method An analytical result can be obtained by integration of the variation equation on which the method of Ritz can be applied. The variation equation is obtained by expressing the equilibrium between the virtual work performed by the internal and external forces. For a detailed description on the derivation of this equation, the reader is referred to (Van Impe, 2010) According to the Ritz method, both the translation in y-direction and the angular rotation around the longitudinal x-axis are replaced by linearly independent functions fulfilling the kinematic boundary conditions. By integrating the variation equation, a closed but complex theoretical expression can be obtained. In (Gevaert, 2010) and also in this work, this method will only be used as a reference

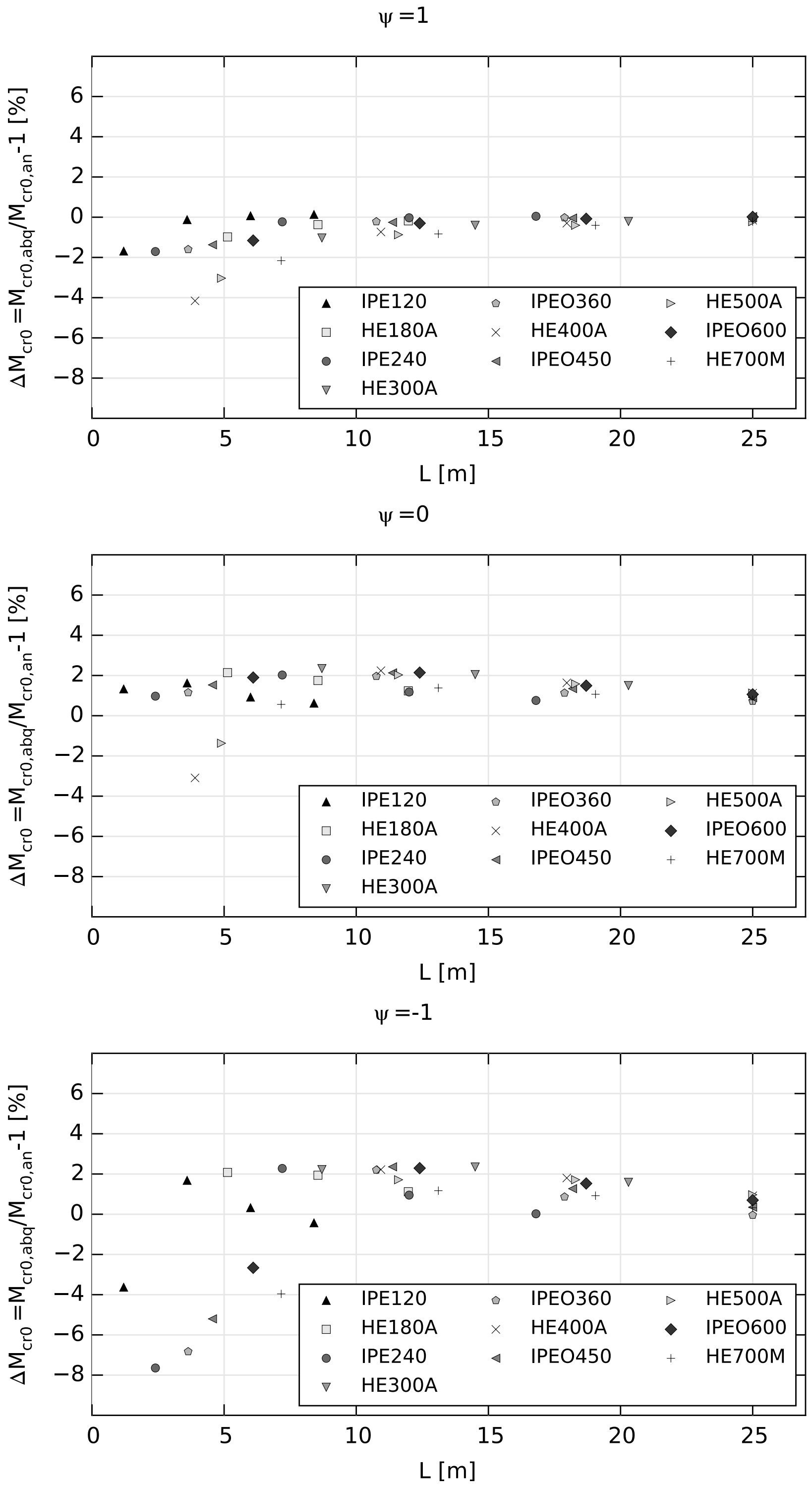

Figure 3.18: Deviation of M_{cr0} for profiles in (Gevaert, 2010).

value to check the numerically obtained results and to easily notice Abaqus results deviating from this theoretical value due to distortion or local yielding.

Eurocode 3 The expressions for the critical moment adopted in EC3 for uniform and non-uniform moments were already mentioned in sections 2.4.1 and 2.4.2.

3.14.3 Comparison different methods

The described methods for the determination of M_{cr} are compared for an IPE240 profile subjected to different load configurations by varying the value of ψ between -1 and 1 with a step size of 0.25 (Figs. 3.19-3.20). Two different lengths were considered: L=2.4 m and L=16.8 m.

For the longest considered members (L=16.8 m) the values for M_{cr} obtained by Abaqus and LTBeam are almost perfectly coinciding. The values of EC3 are only slightly deviating from and always lower than or equal to these numerically obtained results. The expression for M_{cr} (Eq. 2.4.2) adopted in EC3 is therefore a safe estimate. The application of the Ritz method is safe for $\psi \geq 0.25$; for lower values the graph is situated above the numerical results and therefore an unsafe estimate.

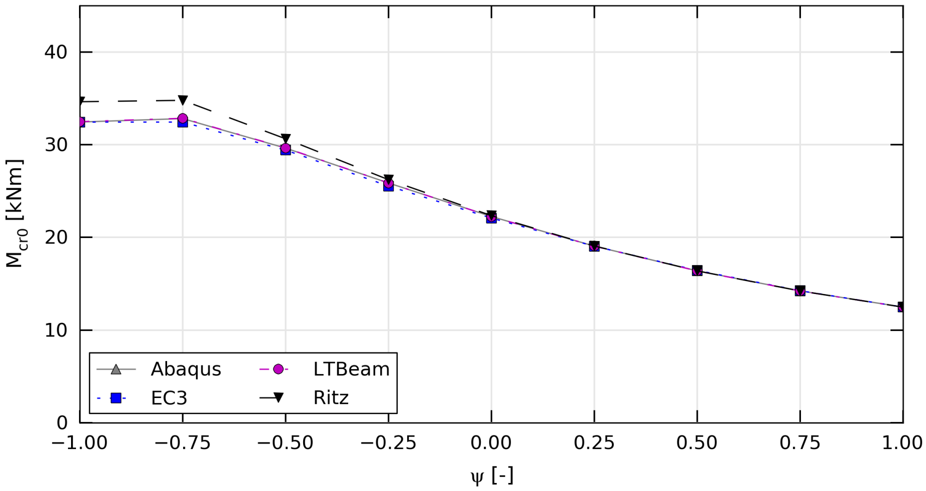

Figure 3.19: Determination of M_{cr} based on 4 different methods for IPE240, L=16.8 m, $\mu = \infty$

For the short length member (L=2.4 m), the best correspondence is found between the values of LTBeam and the Ritz method, with again slightly higher values obtained following the Ritz method and therefore unsafe. In contrast to the longer members, a deviation is found between the numerical results of Abaqus and LTBeam. This is due to the observed web distortion, as mentioned in Section 3.13, with a maximum deviation of 4.8% between the Abaqus and LTBeam results for M_{cr}. The expression of EC3, which does not cover the lateral-distortional buckling behaviour, is therefore only safe for $\psi > 0.5$.

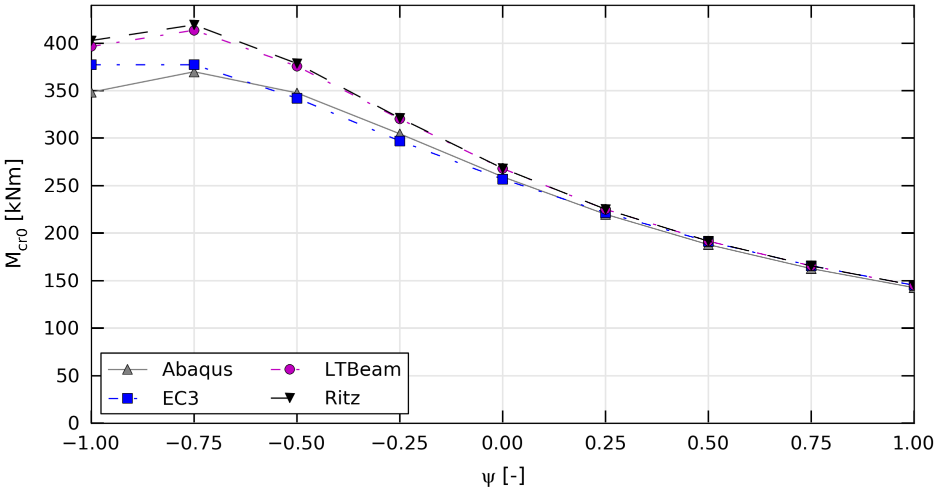

Figure 3.20: Determination of M_{cr} based on 4 different methods for IPE240, L=2.4 m, $\mu = \infty$

3.15 Influence numerical or analytical determination $M_{cr,0}$ on LPF

In (Gevaert, 2010), the values of $M_{cr,0}$ obtained by LT-Beam were used to determine the start value of the applied axial load and were also used in the analytical formulae according to the four discussed methods (Chapter 2) to determine the member's resistance. From practical point of view however, if one wants to determine the resisting moment and axial load of eccentrically loaded members theoretically, no set of LBA simulations will be performed in advance to determine the critical load. Furthermore, the LT-Beam software is only applicable for plain-webbed members and therefore for cellular members theoretical expressions of the critical LTB moment should be applied anyway. The deviation of the load proportionality factor obtained by an analytical or numerical value of $M_{cr,0}$ for the ten considered profiles is plotted in Fig. 3.21. The plots are based on the General Method 1 as analytical approach, but similar findings can be derived from application of other methods. For each profile and every ψ value, seven different μ values are plotted per considered length of the profile. For this specific case, largest deviations were obtained for the different ψ values for μ equal to 0.1.

It can be noticed that under a constant bending moment the deviation is insignificant. For members subjected to a linear varying bending moment ($\psi = 0$, $\psi = -1$), the largest deviation is as expected examined for short-length members, for which the deviation of $M_{cr,0}$ was also largest due to the observed web distortion. An overview of the maximum and minimum obtained deviations is given in Table 3.15. Since the deviations are mainly negative (the positive deviation is insignificant), lower values of the LPF will be obtained for an analytical value of M_{cr} than in case the numerical values are introduced, i.e. the estimated member's resistance is lower, which is a safe estimate.

Table 3.15: Deviation of LPF based on analytical or numerical value of $M_{cr,0}$.

ψ	Δ_{min} [%]	Δ_{max}[%]	Δ_{mean} [%]	Δ_{median} [%]
1	-0.165	0.035	-0.009	0
0	-5.647	0	-1.484	-1.145
-1	-4.429	0.228	-1.040	-0.937

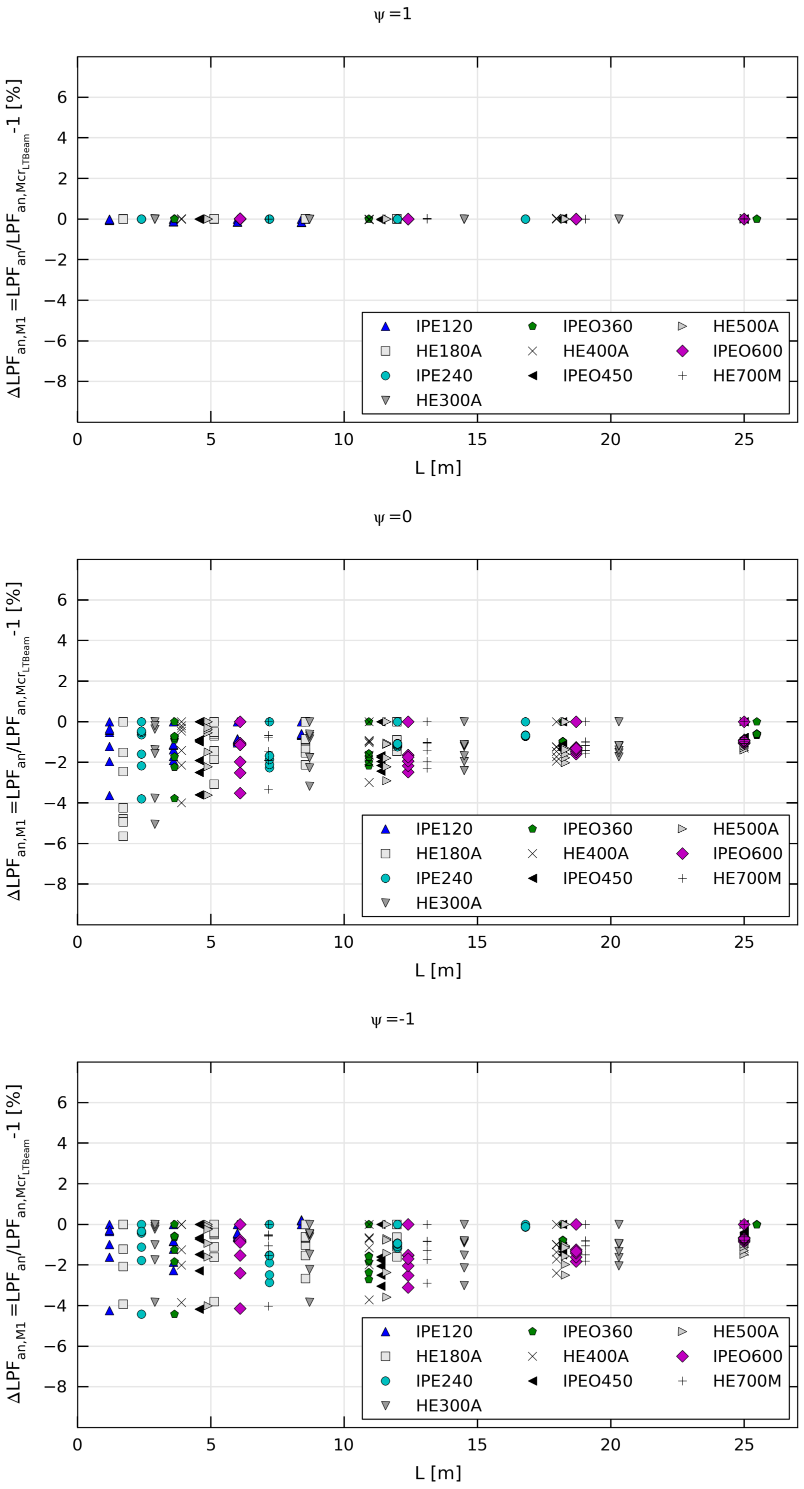

Figure 3.21: Deviation of LPF based on analytical or numerical value of $M_{cr,0}$.

3.16 Parametric study: results and discussion

The results of the parametric study will be represented in moment-normal force interaction diagrams with $N_u/N_{b,Rd}$ as abscissa and $M_u/M_{b,Rd}$ as ordinate. On these interaction diagrams (provided on an additional CD), the Abaqus results are represented as well as the results obtained from the different analytical methods available for the stability of eccentrically loaded members, which were mentioned in Chapter 2 and listed as reminder:

- ECCS - Vandepitte
- ECCS - Van Impe
- EC3 - Method 1: Modified General Method
- EC3 - Method 2

The normal buckling resistance $N_{b,z,Rd}$ and the bending resistance $M_{b,y,Rd}$ are calculated as prescribed according to their corresponding method. This means that the buckling resistance should be calculated differently for the method ECCS-Vandepitte (Eq. 2.3.1) than for the other methods, for which EC3 is used (Eq. 2.3.4). As described in Section 2.4.3, for Method 1 different approaches are adopted in EC3 to determine the buckling resistance. Starting from the General Method, the Specific Method was obtained by applying the same expressions, but with a different set of buckling curves. For the method to be also applicable for members subjected to a non-uniform bending moment, a modification factor f was introduced and the method was referred to as the Modified Specific Method. It should be noted however that for Method 1 depicted on the interaction diagrams, the so-called Modified General Method was used, where the modification factor f was applied to the General Method, since this was concluded to be the most suitable method (Section 2.4.3.3). For all other methods (ECCS-Vandepitte, ECCS-Van Impe, EC3-Method 2), the buckling resistance $M_{b,y,Rd}$ is calculated according to the General Method of EC3. It should be noted that although in this way the ultimate moment M_u and axial load N_u are scaled differently for different methods, this representation is preferred due to its clear compilation of both the analytical and numerical results.

For each length only seven different μ values were considered to perform the numerical simulations in Abaqus, represented as discrete points on the interaction diagrams. As mentioned previously (Section 3.4), for some load configurations no maximum is obtained in the load displacement diagram and the results obtained from these configurations are not included in the interaction diagrams. For the analytical expressions the number of μ values was extended to 40 to get a smoother and more accurate representation of the stability rules (Table 3.16).

Table 3.16: Overview considered values of μ.

0.00	0.25	0.50	0.80	1.30	2.25	4.00	9.00
0.05	0.30	0.55	0.90	1.40	2.50	4.50	10.00
0.10	0.35	0.60	1.00	1.50	2.75	5.00	20.00
0.15	0.40	0.65	1.10	1.75	3.00	6.00	40.00
0.20	0.45	0.70	1.20	2.00	3.50	7.50	∞

3.16.1 ECCS - Vandepitte

At first, general conclusions can be drawn about the safety and validity of the design rules by comparing the numerical (LPF_{Abq}) and fully analytical (LPF_{an}) (i.e. based on an analytical determination of $M_{cr,0}$) results of the load proportionality factor. The results are represented by the deviation factor ΔLPF, defined according to Eq. 3.16.1.

$$\Delta LPF = \left(\frac{LPF_{Abq}}{LPF_{an}} - 1 \right) \cdot 100\% \tag{3.16.1}$$

Again for every ψ value seven different μ values are depicted for each considered length. It can be easily noticed that under a constant bending moment ($\psi = 1$) the design rule ECCS-Vandepitte is unsafe over a certain range of μ values for all considered profiles and lengths. Observation of the deviation for $\psi = 0$ results in similar findings. For $\psi = -1$ however, the amount of positive deviations is larger and therefore application of the design rule is safer, especially for larger lengths. An overview of the μ values for which this design rule is not applicable is given in Appendix B, Table B.1.

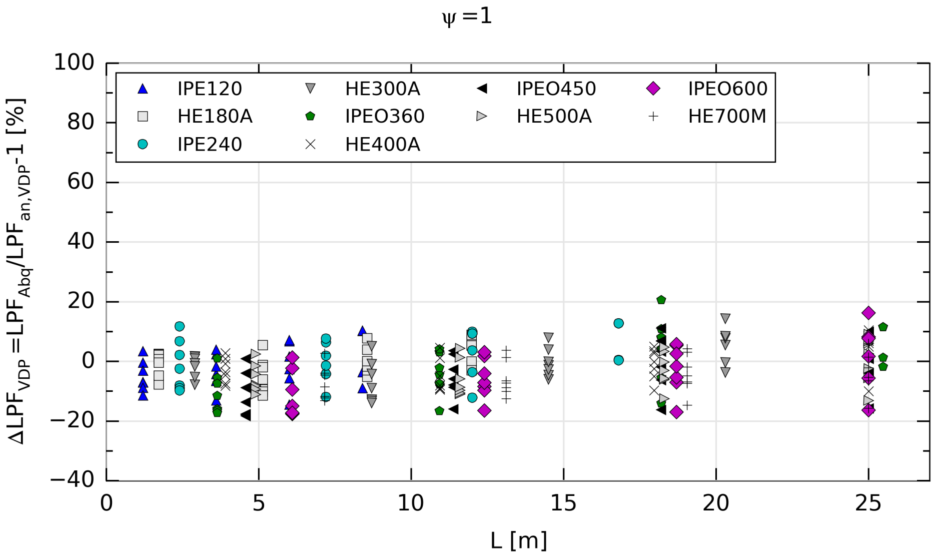

Figure 3.22: Deviation between the numerically and analytically obtained LPF according to Vandepitte method ($\psi = 1$).

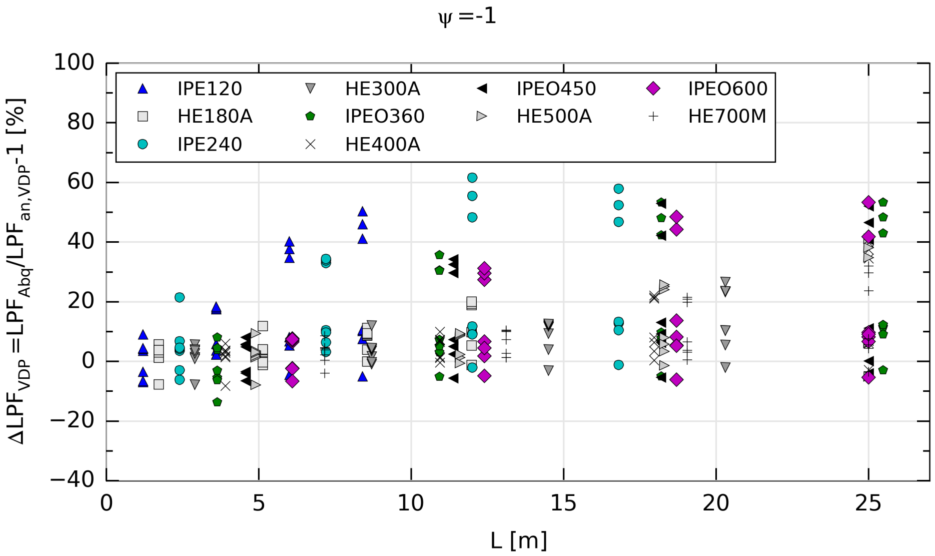

Figure 3.23: Deviation between the numerically and analytically obtained LPF according to Vandepitte method ($\psi = -1$).

It can be examined that the interaction diagrams according to Vandepitte are very dissimilar in shape compared to the other design rules and in most cases the interaction diagram is situated higher than the one obtained by Abaqus and therefore unsafe. A more rectangular shape is observed with increasing length of the members and especially for a non-uniform bending moment ($\psi = 0$; $\psi = -1$). By this rectangular shape, it is reflected that members subjected to a large bending moment ($\mu \to \infty$) can resist an axial load as large as if the member would only be subjected to this compressive force. This effect is illustrated here in Fig. 3.24 for an IPEO450 profile with L=4.56 m (k=1) and L=11.37 m (k=2) subjected to a constant bending moment. It is clearly visible that for the longest member the shape of the interaction diagram is more rectangular. Also the interaction diagram for $\psi = -1$ is given for L=11.37 m, from which it can be noticed that the rectangular shape is even more pronounced than under a uniform bending moment. Due to the rectangular shape, the Vandepitte design rule can be economically interesting for low and high μ values, but unsafe for intermediate values. This can be examined in Fig. 3.24 for L=11.37 m and $\psi = -1$, where the design rule is not applicable for $\mu = 1$, but an economic approach for all other μ values.

Furthermore, it is examined that this rectangular shape of the interaction diagram is more pronounced for IPE than for HE profiles with equal length. This is illustrated in Fig. 3.25 where the interaction diagrams for $\psi = 1$ of both an IPEO450 (L=11.37 m) and HE500A (L=11.6 m) profile are presented. By considering these two profiles, the best correspondence in length and height (h-t_f) is obtained.

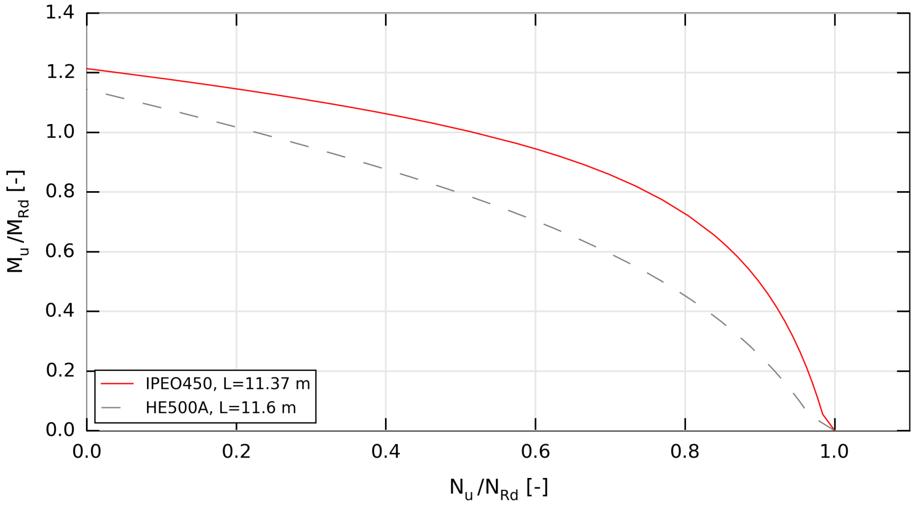

Figure 3.25: Comparison design rule ECCS-Vandepitte for IPEO450 and HE500A ($\psi = 1$).

The observed difference in shape of the interaction diagrams will be explained based on the governing condition of weak-axis buckling for members subjected to an axial load and strong-axis bending moment, in the adapted form used to determine the load proportionality factor analytically.

$$\frac{\lambda N_{start}}{Af_y} + \frac{\theta \beta_y \lambda |M_{1y,start}|}{\left(1 - \frac{\lambda N_{start}}{N_{cr,y}}\right) W_y f_y} + \frac{\lambda N_{start} \overline{v}_0}{\left(1 - \frac{\lambda N_{start}}{N_{cr,z}}\right) W_z f_y} \leq 1 \tag{3.16.2}$$

The contribution of the axial load is expressed by the first and third term, while the contribution of the bending moment is represented by the second term. Both parts contributing to the total strength condition are indicated in Fig. 3.26. In this figure the strength condition in function of the load proportionality factor is depicted for the IPEO450 and HE500A profile for which a difference in shape of the interaction diagram was observed. Only the chart for $\mu = 1$ is given; Similar findings can be derived from other load configurations with an increased contribution of the bending moment for increasing μ values. The corresponding curve will therefore be situated closer to the curve representing the total strength condition. It should be noted that for the third term an asymptotic value is reached

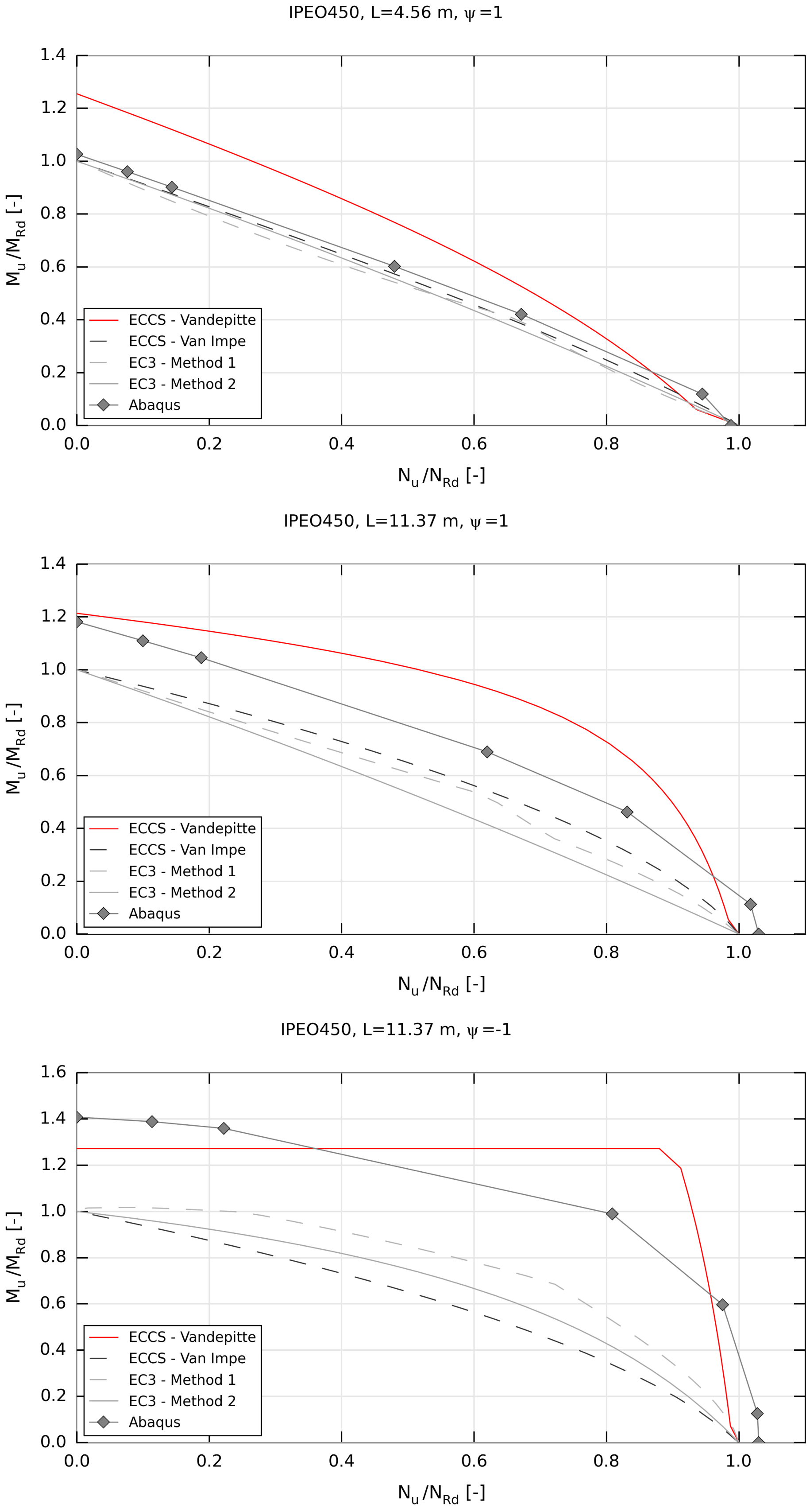

Figure 3.24: Moment-Normal force interaction diagram IPEO450 under different load configurations and for different lengths

for $\lambda = N_{cr,z}/N_{start}$. Therefore, for values of the ultimate buckling load $\lambda_u N_{start}$ approaching $N_{cr,z}$ an increased slope of the contribution of N near λ_u, the ultimate value of the LPF, should be noticed. Although differences are small (Table 3.17) due to the almost equal and even slightly lower length of the IPEO450 profile, it can be noticed that the slope of the curve expressing the contribution of the axial load is slightly increased for the IPEO450 profile while reaching λ_u, while the curve remains more or less straight for the HE500A profile.

Table 3.17: Characteristics profiles IPEO450 and HE500A for comparison strength condition Vandepitte.

	IPEO450	HE500A
L [m]	11.37	11.60
λ_z [-]	2.86	1.69
N_u [kN]	218.84	807.57
$N_{cr,z}$ [kN]	333.45	1595.24
$N_u/N_{cr,z}$ [-]	0.66	0.51

The curve 'Contribution M' is situated closer to the curve of the total strength condition for an IPEO450 profile than for HE500A. Therefore, the corresponding point on the moment-normal force interaction diagram of an IPEO450 will be positioned more to the right compared to $\mu = 1$ for HE500A, as illustrated on Fig. 3.25. This is generally observed when making the comparison between IPE and (the most corresponding) HE profiles and explains the more pronounced rectangular shape of the IPE profiles. The length of the profiles was defined based on the height only (Section 3.11.1) and due to the larger reduced slenderness $\overline{\lambda}_z$ for IPE than for HE profiles with equal height, resulting in a larger ratio of $N_u/N_{cr,z}$ for IPE profiles.

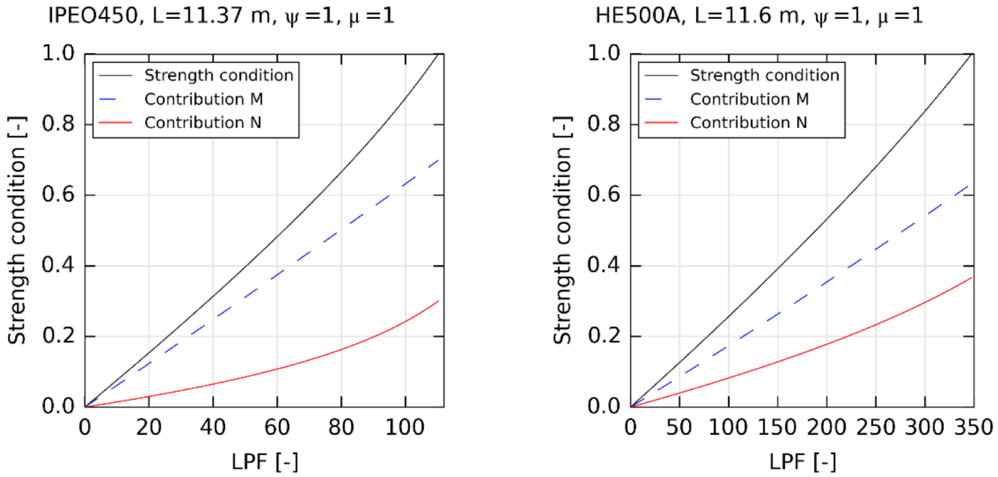

Figure 3.26: Strength condition in function of load proportionality factor for IPEO450 and HE500A.

3.16.2 ECCS - Van Impe

Similarly as for the Vandepitte method, first graphs indicating the difference in LPF between numerical and analytical results are given (Figs. 3.27 - 3.28). Similarly as for the Vandepitte method, a wider range of deviations is obtained for $\psi = -1$ than for $\psi = 1$. In contrast to the Vandepitte method however, a large improvement in safety can be examined for the Van Impe design rule, except for short length members, where still negative deviations can be observed. The combinations for which application of the ECCS-Van Impe design rule is unsafe are listed in Table 3.18.

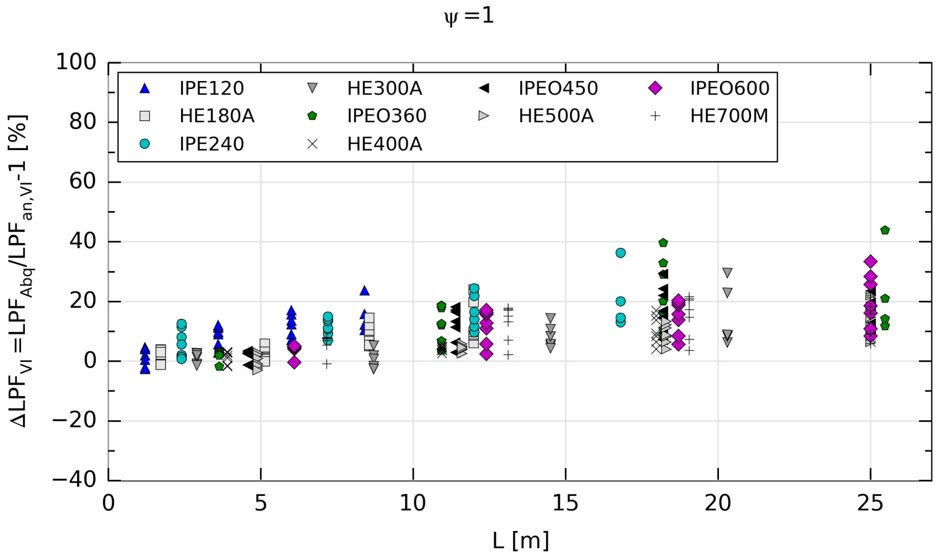

Figure 3.27: Deviation between the numerically and analytically obtained LPF according to ECCS-Van Impe ($\psi = 0$).

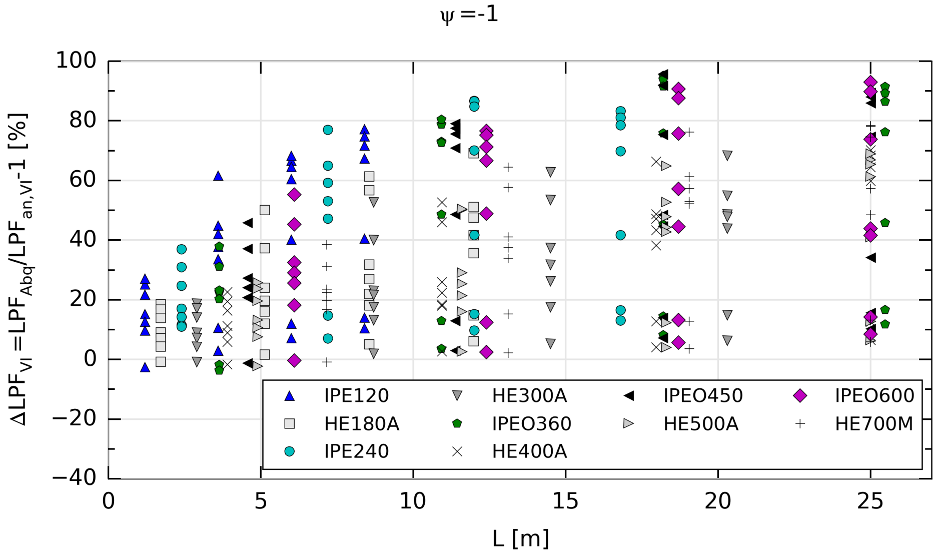

Figure 3.28: Deviation between the numerically and analytically obtained LPF according to ECCS-Van Impe ($\psi = -1$).

Table 3.18: Combinations for which design rule ECCS-Van Impe is unsafe.

	L [m]	ψ	μ [-]		L [m]	ψ	μ [-]
IPE120	1.20	1	0 - ∞	HE400A	3.90	1	0 - ∞
	1.20	0	0		3.90	0	0
	1.20	-1	0		3.90	-1	0
HE180A	1.71	1	0 - ∞	IPEO450	4.56	1	0
	1.71	0	0		4.56	0	0
	1.71	-1	0		4.56	-1	0
HE300A	2.90	1	0 - ∞	HE500A	4.90	1	0 - 5 - 10 - ∞
	2.90	-1	0		4.90	0	0
	8.70	1	1 - 5 - 10 - ∞		4.90	-1	0
IPEO360	3.64	1	0				
	3.64	0	0				
	3.64	-1	0				

3.16.3 EC3 - Method 1

By comparison with the numerically obtained moment-normal force interaction diagrams, it can be concluded that application of design rule EC3-Method 1 is mostly a safe approach, except for the combinations listed in Table 3.19. It can be noticed that the design rule is only unsafe for the shortest considered members (k=1) and especially for members subjected to a non-uniform bending moment ($\psi = 0$; $\psi = -1$). Unsafe results were mainly obtained for low or high values of μ as illustrated in Fig. 3.29 for the profile IPE120, where the design rule is not applicable for $\mu = 0, 0.5$ or 1.

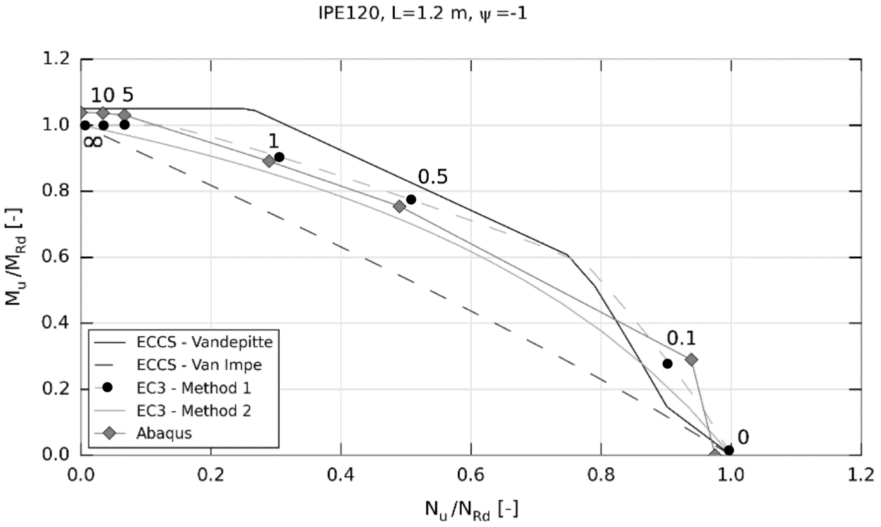

Figure 3.29: Unsafe approach of EC3-Method 1 for IPE120.

For this method the results are represented in an alternative manner by means of box plots (Fig. 3.31) indicating the first (Q1) and third quartiles (Q3), the median (second quartile Q2, indicated in red) and the whiskers within 1.5 IQR (Interquartile range) of the lower and upper quartile (Fig. 3.30). The outliers outside this range are plotted as individual points. The numbers on the horizontal axis refer to the different profiles and are given in Table 3.20. Three plots were made for the different ψ values and on each plot the seven different μ values are considered. Similar findings as for the Van Impe method are possible with for all ψ values mainly positive deviations, indicating the safety of this method, except for short length members for which negative deviations corresponding with the lower

Table 3.19: Combinations for which design rule EC3-Modified General Method 1 is unsafe. Values of μ for which no maximum was reached in the load-displacement diagram are given in brackets after *.

	L [m]	$\psi[-]$	$\mu[-]$
IPE120	1.20	-1	0 - 0.5 - 1
HE180A	1.71	1	0 - 0.1 - ∞
	1.71	0	0 - 0.1
	1.71	-1	0 - 1
IPE240	2.40	-1	0.5 - 1
HE300A	2.90	1	0 - 0.1
	2.90	0	0 - 0.1 *(∞)
	2.90	-1	1
IPEO360	3.64	-1	0 - 0.5 - 1 - ∞
HE400A	3.90	1	0 - 0.1 - ∞
	3.90	0	0 - 0.1
	3.90	-1	0 - 0.1 - 0.5 - 1
IPEO450	4.56	-1	0 - 1
HE500A	4.90	1	0 - 10 - ∞
	4.90	-1	0 - 0.5 - 1
HE700M	7.16	-1	0 - 0.5 - 1

whisker were measured. The maximum deviations are again obtained for the longest members with for example for $\psi = 1$ two outliers for IPE240 (L=16.80 m; $\mu = 1$) and for IPEO360 (L=25.48 m; $\mu = \infty$). Although the maximum deviations were obtained for different μ values, it should be noted that for the IPE240 profile, $\mu = 1$ is the largest of the seven considered values of μ for which a maximum was obtained in the load-displacement diagram. Therefore, it is of further interest if the design rules are indeed more conservative towards the limit case of members under pure bending ($\mu = \infty$). This will be further discussed in the next paragraph.

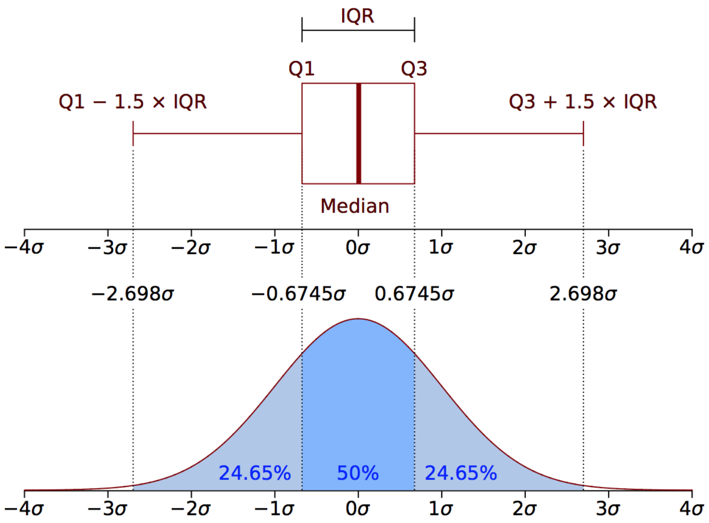

Figure 3.30: Nomenclature box plot.

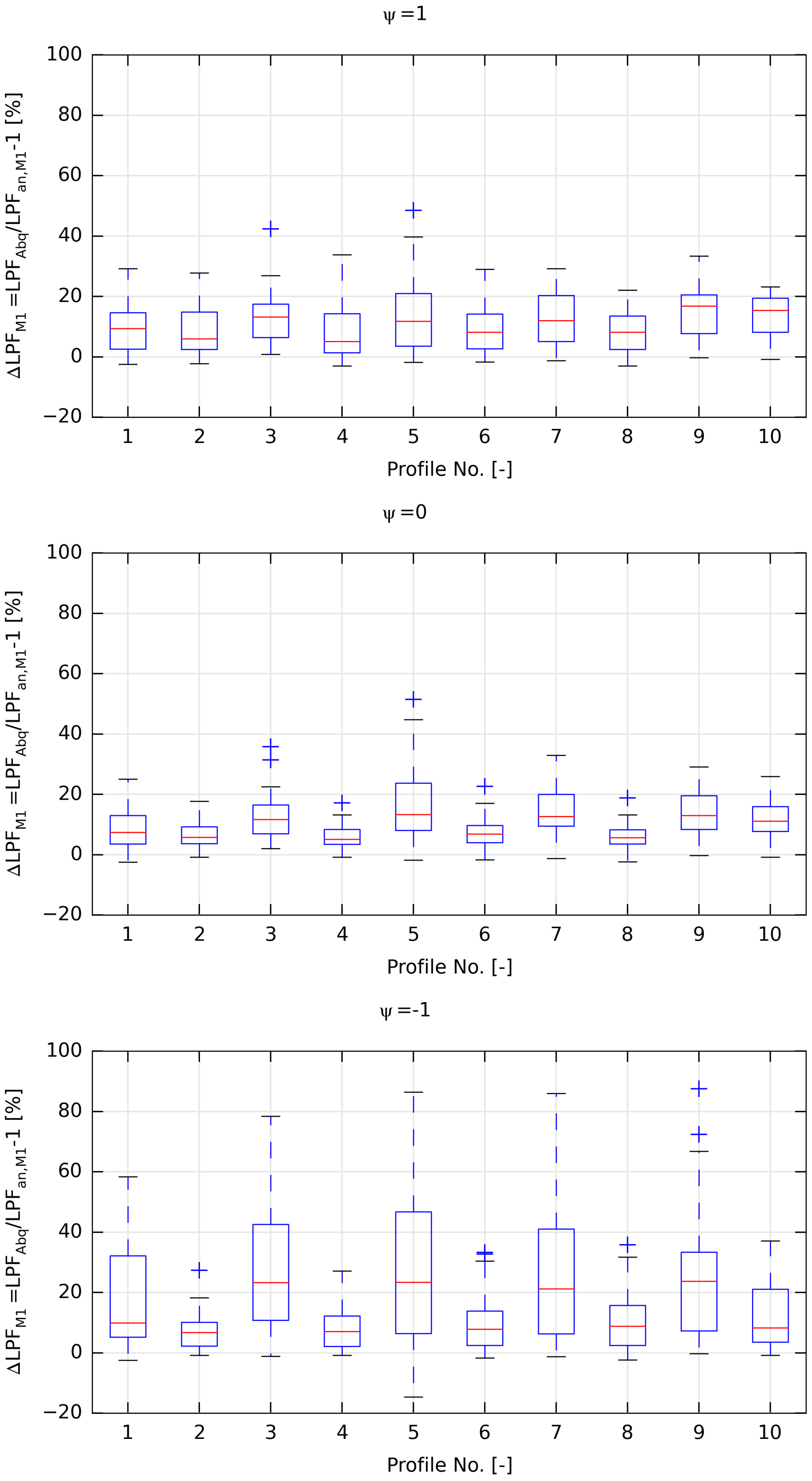

Figure 3.31: Deviation of ΔLPF for the Modified General Method for different values of ψ.

Table 3.20: Profiles numbers of geometries examined in Fig. 3.31.

1	2	3	4	5	6	7	8	9	10
IPE120	HE180A	IPE240	HE300A	IPEO360	HE400A	IPEO450	HE500A	IPEO600	HE700M

Furthermore, it can be emphasized that for $\psi = 0$ and especially for $\psi = -1$ a larger variation is examined than for members under a constant bending moment. This is most pronounced for IPE sections, where a maximum positive deviation of 88.5% is obtained for the IPEO600 section for $\psi = -1$ (L=25 m; $\mu = \infty$).

3.16.4 Influence of the considered μ value

In Figs. 3.32-3.33 histograms of the deviations of the load proportionality factor according to EC3-Method 1 for respectively the five considered IPE and HE sections are given. For the histograms, a binwidth of 10 was chosen; the sum of all surface areas equals 1. It can be concluded that for both IPE and HE sections larger deviations were obtained for $\mu = \infty$ than for $\mu = 0$ (max. of 85% for IPE). In general, for $\mu = \infty$, the histograms show a larger varibility, which is more pronounced for IPE than for HE sections.

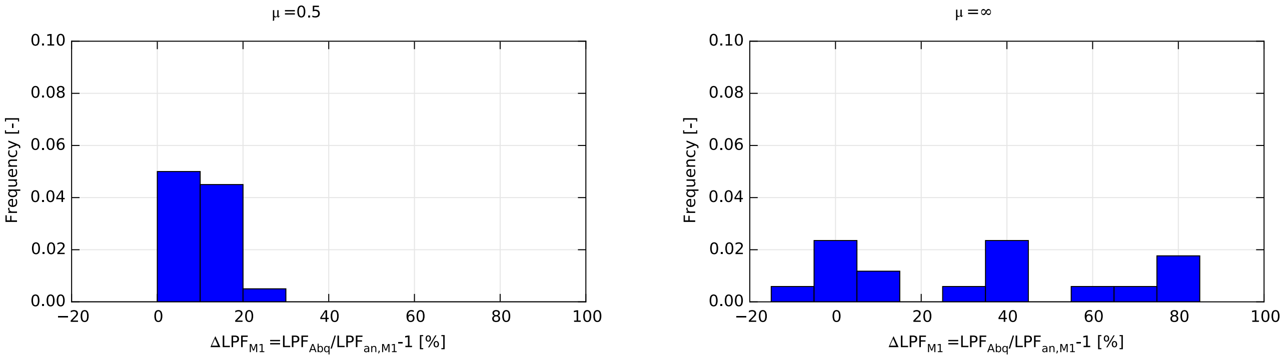

Figure 3.32: Histogram of deviation of LPF according to EC3-Method 1: IPE sections.

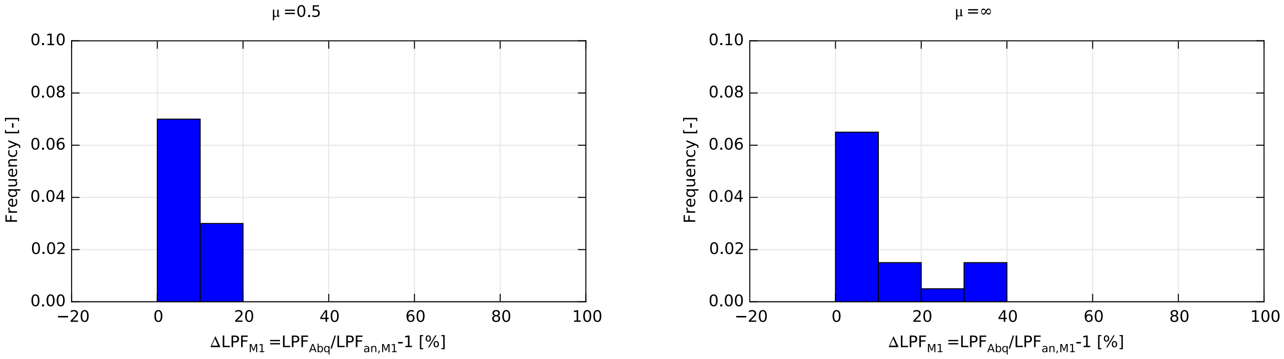

Figure 3.33: Histogram of deviation of LPF according to EC3-Method 1: HE sections.

3.16.5 Comparison different approaches Method 1

As mentioned in the introduction of Section 3.16, preference was given to the representation of the Modified General Method on the interaction diagram. In this paragraph results obtained by the General Method, the Modified General Method and Modified Specific Method are compared. It should be noted that under pure compression ($\mu = 0$) there is no deviation between the three methods as they are based on the same buckling curves.

As already mentioned in paragraph 2.4.3.3, the influence of the application of the Modified General Method will be largest for $\psi = -1$ and for a reduced slenderness for LTB $\overline{\lambda}_{LT}$ near 0.8. It was indeed clearly noticeable that the largest deviations between the General Method and the Modified General Method were obtained for members with a value of $\overline{\lambda}_{LT}$ closest to 0.8 (Table 3.21). Due to the larger values of $\overline{\lambda}_{LT}$ for IPE profiles than for HE profiles with similar height and length (Section 3.11.1), the value $\overline{\lambda}_{LT} = 0.8$ is for IPE profiles already reached for shorter length members than for HE profiles. For the Modified Specific Method, additionally lower buckling curves are used compared to the General Method corresponding with a larger imperfection factor α and a lower reduction factor for LTB χ_{LT}. This is opposing the effect of the increased buckling resistance due to the modification factor f.

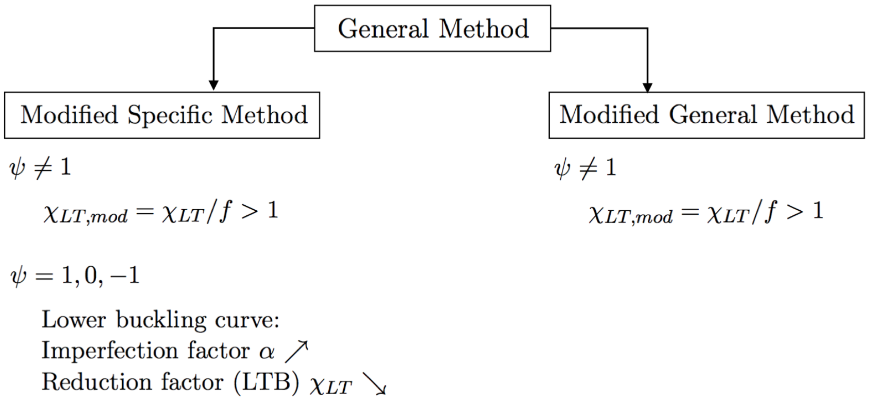
General Method
Modified Specific Method
Modified General Method
$\psi \neq 1$
$\chi_{LT,mod} = \chi_{LT}/f > 1$
$\psi = 1, 0, -1$
Lower buckling curve:
Imperfection factor $\alpha \nearrow$
Reduction factor (LTB) $\chi_{LT} \searrow$
$\psi \neq 1$
$\chi_{LT,mod} = \chi_{LT}/f > 1$

Figure 3.34: Comparison approaches Method 1 for IPEO600.

Table 3.21: Profiles with largest deviation between General Method and Modified General Method ($\psi = -1$).

Profile	L [m]	$\overline{\lambda}_{LT}$ [-]
IPE120	3.60	0.85
HE180A	11.97	0.88
IPE240	7.20	0.99
HE300A	14.50	0.78
IPEO360	10.92	1.04
HE400A	17.97	0.89
IPEO450	11.37	1.02
HE500A	18.30	0.93
IPEO600	12.40	0.99
HEM700	13.11	0.72

Also marked in paragraph 2.4.3.3, an increase in lateral torsional buckling resistance $M_{b,Rd}$ of 25% was obtained for $\psi = -1$ by introduction of the modification factor f. Due to this increased buckling resistance, the curve of the Modified General Method will be positioned lower and therefore more conservative values are obtained than for the General Method. The Modified Method can therefore certainly be preferable for short length members, for which unsafe results were obtained for the General Method.

The differences between the different approaches is illustrated in Fig. 3.35 for a short length IPEO600 profile (L=6.1 m). Safe results are obtained over the complete range of considered μ values by applying the Modified General Method, whereas the General Method would result in an unsafe approach for

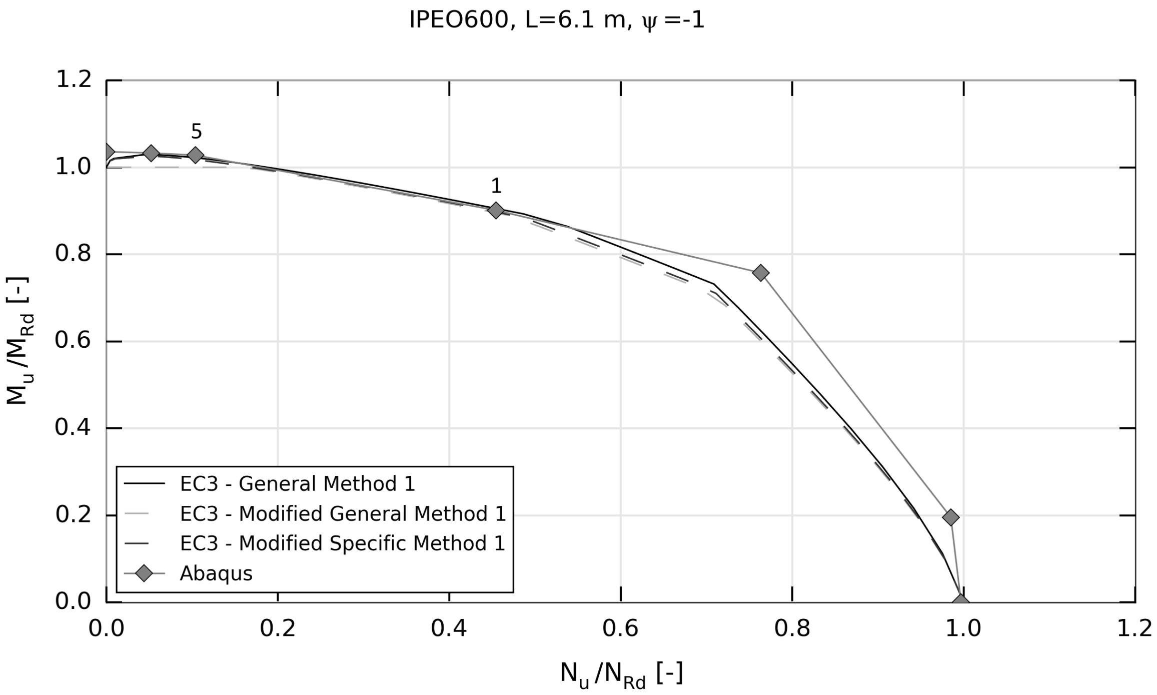

Figure 3.35: Comparison approaches Method 1 for IPEO600.

values of μ ranging from 1 to 5.

3.16.6 EC3 - Method 2

Although a good agreement with the numerical results was obtained for the EC3-Method 1, a possible criticism is certainly the unpredictable and complex combination of different specific interaction factors giving the user a black box feeling. A good alternative could therefore be the more user-friendly approach of Method 2, but the question is if this method is as accurate and economic as Method 1 of EC3. It will be tried to provide an answer to this question by examination of the results.

In general it can be concluded that Method 2 is a safe and mostly more conservative approach than the Modified General Method 1. In contrast to the latter, Method 2 is therefore also applicable for short length members under a non-uniform bending moment. Only for two combinations application of the method would be an unsafe estimate (Table 3.22). It can be noticed that these unsafe results were obtained in the range of intermediate to high μ values (0.5-∞) and for members subjected to a constant moment ($\psi = 1$). The interaction diagram of the HE500A profile is given as example in Fig. 3.36, where the unsafe part of the interaction diagram of Method 2 is indicated in red.

Table 3.22: Combinations for which design rule EC3-Method 2 is unsafe.

	L [m]	$\psi[-]$	$\mu[-]$
HE300A	8.70	1	0.5 - 1 - 5 - 10 - ∞
HE500A	4.90	1	1 - 5 - 10 - ∞

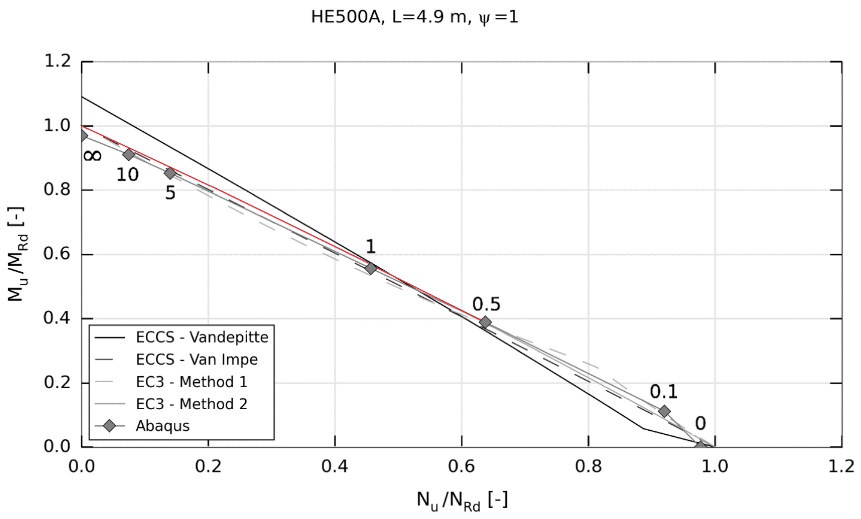

Figure 3.36: Insecurity of EC3 - Method 2 for HE500A.

Although the general behaviour of Method 2 is more conservative than Method 1, certain combinations are of interest for which application of Method 2 is more economic. From Table 3.23 it can be observed that these combinations mostly correspond with a uniform bending moment ($\psi = 1$), except for the profiles HE180A and HE300A where for the shortest length members the economic trend was also observed for $\psi = -1$ for larger μ values (5, 10, ∞). The economic approach of Method 2 is illustrated in Fig. 3.37 for a HE180A profile for $\psi = 1$ (L=5.13 m) and $\psi = -1$ (L=1.71 m), where the economic range of μ values is indicated in green.

Table 3.23: Combinations for which EC3-Method 2 is more economic than EC3-Method1 (Modified General).

	L [m]	ψ	μ [-]
IPE120	1.20	1	1 - 5 - 10
HE180A	1.71	1	1 - 5 - 10
	1.71	-1	5 - 10 - ∞
	5.13	1	0.1 - 0.5 - 1 - 5 - 10
	8.55	1	1 - 5 - 10
	11.97	1	1 - 5 - 10
IPE240	2.40	1	0.1 - 1 - 5 - 10
HE300A	2.90	1	0.5 - 1 - 5 - 10
	2.90	-1	5 -10 - ∞
	8.70	1	0.1 - 0.5
	14.50	1	1 - 5 - 10
	20.30	1	5 - 10
IPEO360	3.64	1	0.1 - 1 - 5 - 10
HE400A	3.90	1	0.5 - 1 -5 -10
	10.93	1	1 - 5 - 10
IPEO450	4.56	1	0.1 - 1 - 5 - 10
HE500A	11.60	1	5 - 10
IPEO600	6.10	1	0.1 - 5 - 10
HEM700	7.16	1	0.1 - 1 - 5 - 10

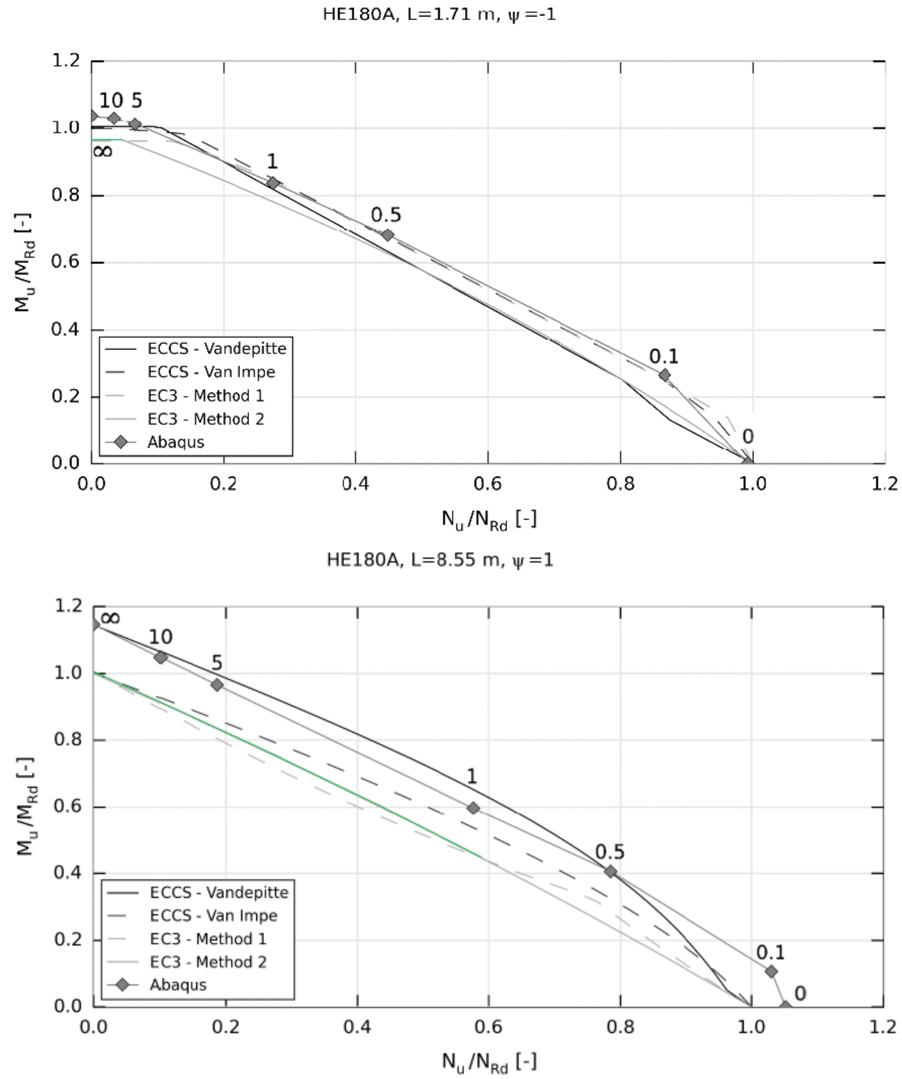

Figure 3.37: Economic application of Method 2 for HE180A profile.

3.17 Conclusion applicability of the design rules

Considering all μ values, the largest variability in the deviation between the numerical and analytical values of the load proportionality factor was obtained for $\psi = -1$. Looking at the different μ values in particular, largest deviations were obtained for $\mu = \infty$, i.e. for members subjected to pure bending. Deviations are generally increasing with increasing length. Application of the design rules is in general unsafe (negative deviations) for short length members, while deviations up to 100% were observed for the longest members (25 m; $\psi = -1$).

From observation of the interaction diagrams, it can be concluded that the design rule of Vandepitte is mostly unsafe, even for longer members. A large increase in safety was indeed examined for the the improved design rule of Vandepitte. For Method 1, the Modified General Method was considered taking into account the influence of a non-uniform bending moment. With this method, mostly safe results were obtained, except for short length members and especially under a non-uniform bending moment. Method 2 was observed to be more conservative than the General Modified Method and therefore also much safer for short length members, except for sections HE300A and HE500A under a constant bending moment ($\psi = 1$).

Chapter 4

Extended parametric study on plain-webbed members

The same profiles that will be used as parent sections to examen the resistance of eccentrically loaded cellular members, were also used to extend the limited research on plain-webbed members under combined bending and axial load. However, since the six additional sections are very similar to the ones of Gevaert, similar findings are possible. Therefore only a few interesting observations will be highlighted. A detailed description on the choice of these specific profiles as parent sections of the cellular members is given in section 5.1. An overview of the profiles with their principal dimensions is given in Table 4.1.

Table 4.1: Cross-sectional properties parent sections.

Section	h [m]	b [m]	t_f [m]	t_w [m]
IPE300	0.300	0.150	0.0071	0.0107
IPE600	0.600	0.220	0.0120	0.0190
HE320A	0.310	0.300	0.0090	0.0155
HE650A	0.640	0.300	0.0135	0.0260
HE320M	0.359	0.309	0.0210	0.0400
HE650M	0.668	0.305	0.0210	0.0400

4.1 Deviation of $M_{cr,0}$

Similarly as for the ten plain-webbed members in the parametric study of Gevaert, a deviation factor $\Delta M_{cr,0}$ is defined indicating the correspondence of the theoretical expressions for the critical LTB bending moment with the numerically obtained results. Lateral-distortional buckling was again observed for the short length members and large deviations were obtained for the shortest considered lengths of profiles HE320A and HE650A. As mentioned previously (section 3.13), the large deviations can be explained by the observed plastic failure instead of elastic buckling failure.

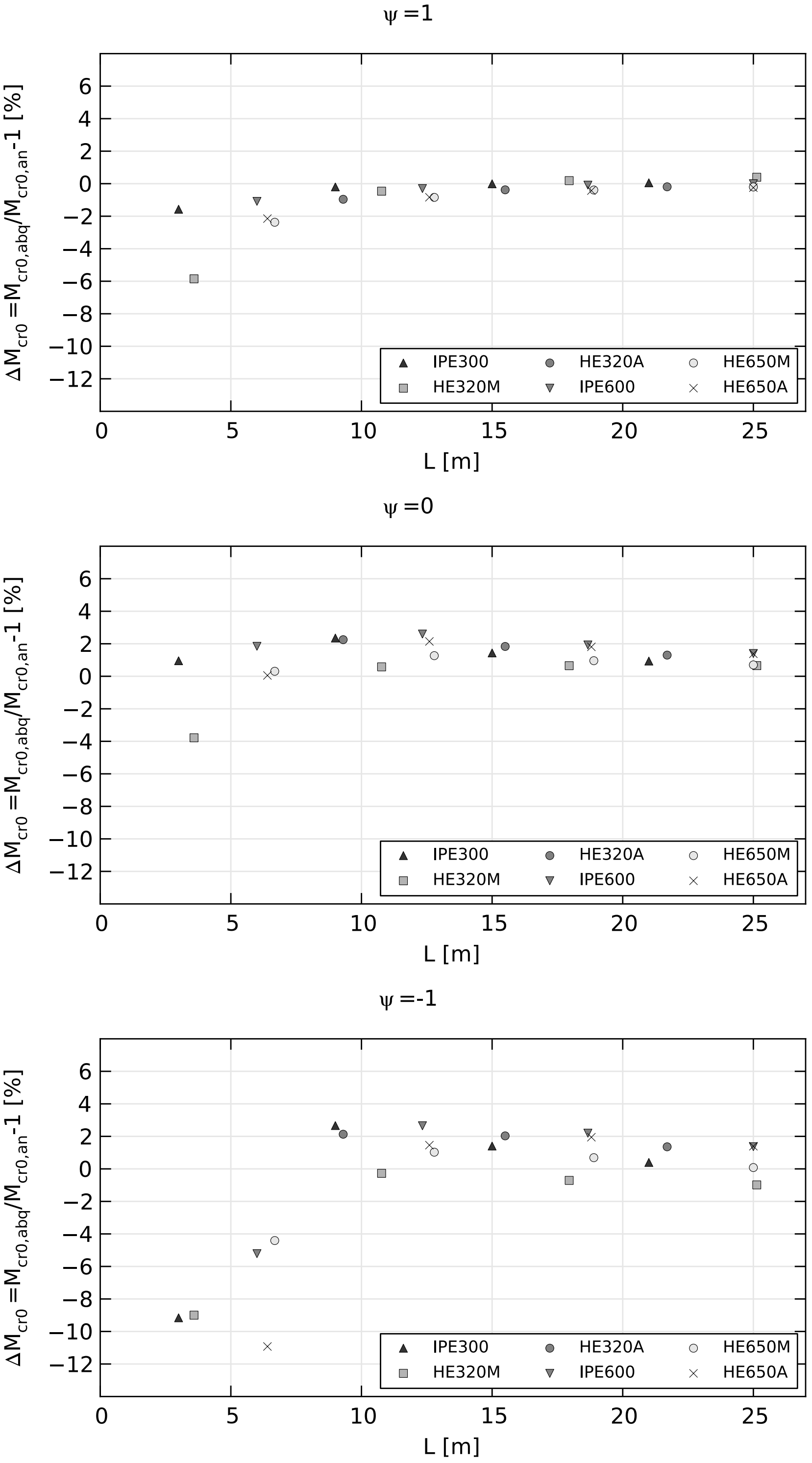

Figure 4.1: Deviation of M_{cr0} for profiles extended parametric study.

4.2 Classification cross-section

The cross-section classification is again performed according to EC3 (CEN, 2005) ($c = h - 2t_f - 2r$) and for the different μ values given in Tables 4.4-4.5. Different from the study of Gevaert, cross-sections Class 4 are obtained for sections IPE600 and HE650A. Since the classification has an important influence on the application of the design rules (as mentioned in Section 3.10.1), comparison is again made with the classification based on a wire model ($c = h - t_f - 2r$) (Tables 4.2-4.3). The most important difference can be found for IPE300 profiles, where (different from the wire model) according to EC3 a plastic theory can be applied. Furthermore, it can be emphasized that for sections IPE600 and HE650A, class 1 is obtained under pure bending whereas class 3 or 4 is found for other μ values. Consequently, a shift in the interaction diagram from elastic (low μ values) to plastic (high μ values) theory is noticeable. According to a plastic theory, sections will reach a larger value of the ultimate axial load N_u compared to an elastic theory and also the failure moment M_u is larger. This is illustrated for a HE650A section subjected to a constant bending moment ($\psi = 1$). The transition between the elastic and plastic theory is clearly noticeable for three methods: ECCS-Vandepitte, EC3-Method 1 and EC3-Method 2. The influence of the cross-section classification on the design rule Vandepitte was already discussed in Section 3.10.1. Also for Method 2, in the governing condition of buckling around the weak axis (Eq. 4.2.1), the influence of the cross-section classification is clearly noticeable since depending on this classification the elastic or plastic bending resistance is used. This is less straightforward for Method 1, where several interaction factors are calculated differently depending on an elastic or plastic theory.

$$\frac{N_{Ed}}{\chi_z N_{pl,Rd}} + k_{LT}\frac{M_{y,Ed}}{\chi_{LT} M_{y,Rd}} \leq 1 \tag{4.2.1}$$

The above considerations will be important for cellular members where due to their increased height compared to the parent sections cross-sections Class 4 will be obtained for all profiles for one or more μ values. Consequently, the same transition in the interaction diagram from elastic to plastic theory can be observed.

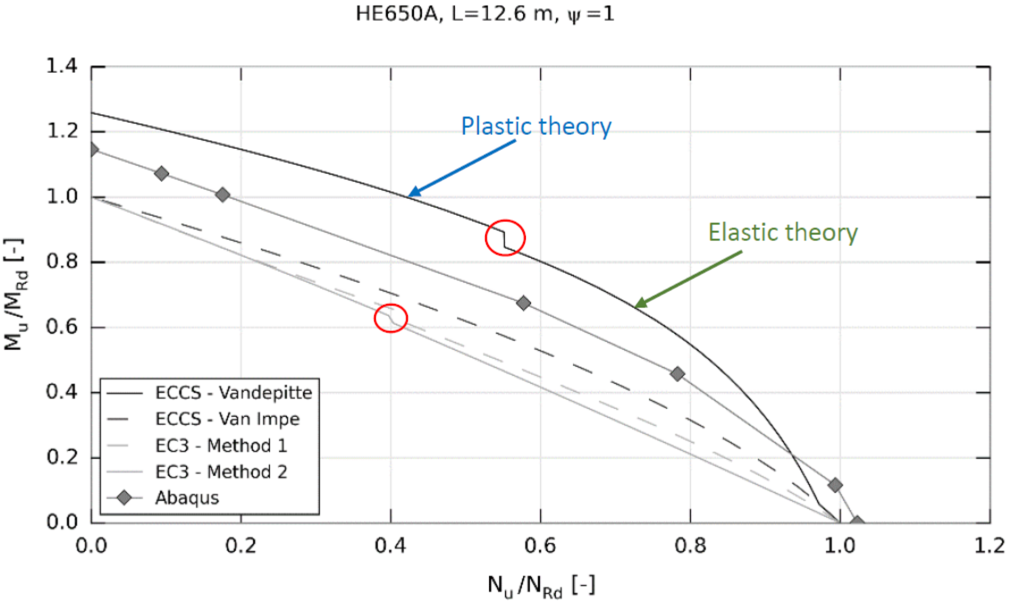

Figure 4.2: Transition elastic-plastic theory HE650A (L=12.6 m, $\psi = 1$).

Table 4.2: Classification of cross-sections extended study for $\psi = 1$ (wire model).

μ	IPE300	IPE600	HE320A	HE650A	HE320M	HE650M
0	3	4	2	4	1	1
0.1	3	4	2	3	1	1
0.5	3	3	2	3	1	1
1	3	3	2	3	1	1
5	1	1	2	1	1	1
10	1	1	2	1	1	1
∞	1	1	2	1	1	1

Table 4.3: Classification of cross-sections extended study for $\psi = 0$ and $\psi = -1$ (wire model).

μ	IPE300	IPE600	HE320A	HE650A	HE320M	HE650M
0	3	4	2	4	1	1
0.1	3	4	2	4	1	1
0.5	3	4	2	4	1	1
1	3	4	2	4	1	1
5	3	4	2	4	1	1
10	3	4	2	4	1	1
∞	1	1	2	1	1	1

Table 4.4: Classification of cross-sections extended study for $\psi = 1$ according to EC3.

μ	IPE300	IPE600	HE320A	HE650A	HE320M	HE650M
0	**2**	4	**1**	**3**	1	1
0.1	**2**	**3**	**1**	3	1	1
0.5	**2**	3	**1**	3	1	1
1	**2**	3	**1**	3	1	1
5	1	1	**1**	1	1	1
10	1	1	**1**	1	1	1
∞	1	1	**1**	1	1	1

Table 4.5: Classification of cross-sections extended study for $\psi = 0$ and $\psi = -1$ according to EC3.

μ	IPE300	IPE600	HE320A	HE650A	HE320M	HE650M
0	**2**	4	**1**	**3**	1	1
0.1	**2**	4	**1**	**3**	1	1
0.5	**2**	4	**1**	**3**	1	1
1	**2**	4	**1**	**3**	1	1
5	**2**	4	**1**	**3**	1	1
10	**2**	4	**1**	**3**	1	1
∞	1	1	**1**	1	1	1

4.3 Alternative representation of the results

An alternative representation of the interaction diagrams is possible by means of normal probability density functions (Fig. 4.3). In this way easier comparison between the deviations of the different methods is possible. The distributions are characterized by their mean value and standard deviation σ_Δ, of which the latter gives an idea of the variability of the results. It can be concluded that application of design rules ECCS-Van Impe, EC3-Method 1 and 2 is safe, except for short length members, corresponding to the negative deviations in the probability density functions. For Vandepitte, unsafe results are obtained over a wider range of lengths, showing the insecurity of this method. It should however be noted that for larger lengths the method can be a good alternative to the conservative results obtained by the other methods.

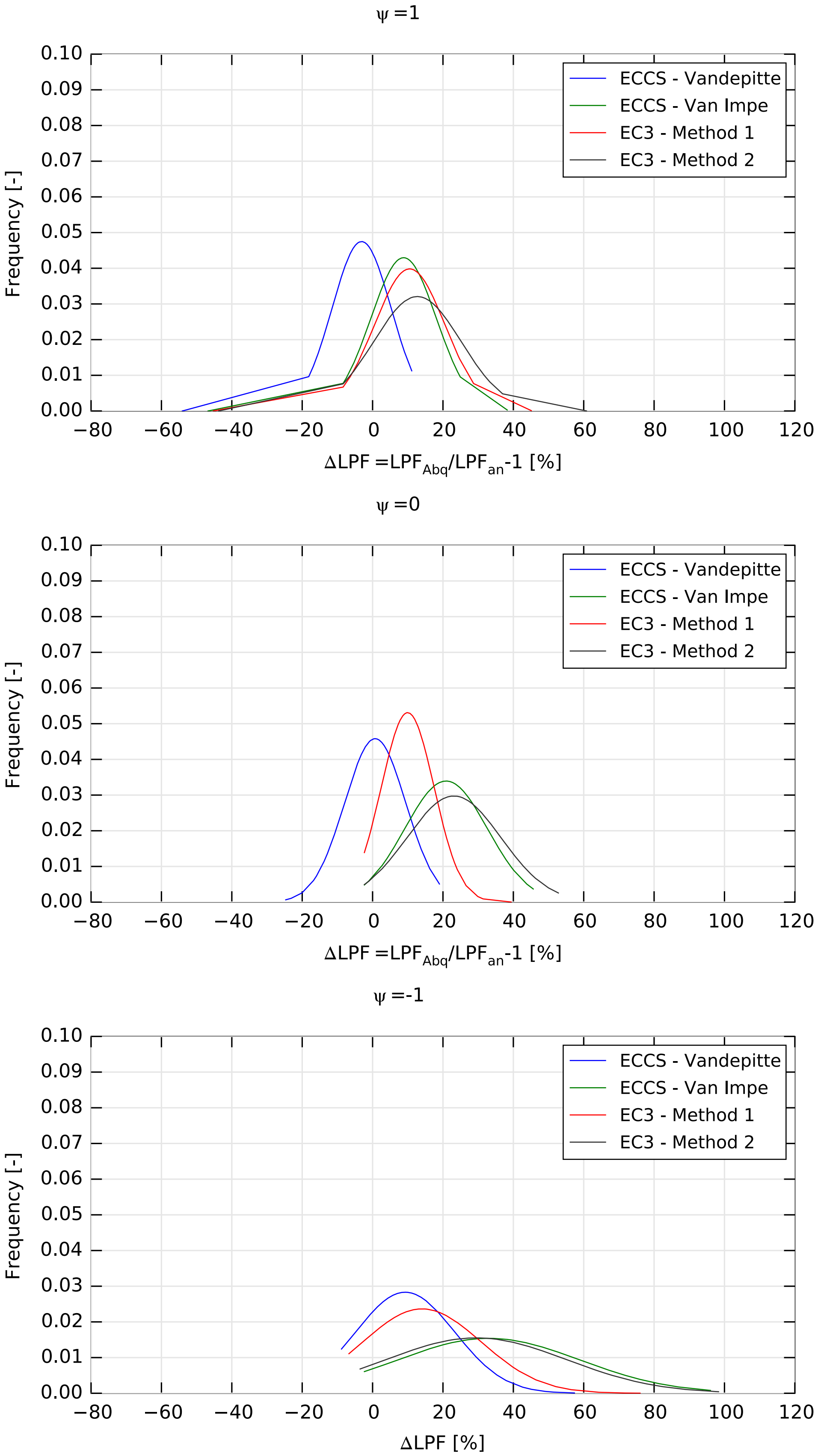

Figure 4.3: Normal PDF of members extended parametric study.

Chapter 5

Parametric study on cellular members

Referring to the scope of this thesis (Section 1.7), a parametric study will be performed to determine the buckling resistance of cellular members subjected to a combination of bending moment and compressive force. In this chapter first the different parameters considered in the parametric study will be discussed.

5.1 Parent sections

For plain-webbed members, a parametric study was already executed on the profiles considered in (Gevaert, 2010). This served as a verification of the numerical model that is based on the model used in (Sonck, 2014) under the changed load condition of bending and compression. The six profiles that were used to extend the research on plain-webbed members will now be considered as parent sections for the cellular members.
With the choice of parent sections, it was tried to cover a range of regularly used profiles starting from three different I-section types (IPE, HEA and HEM). Representative parent sections for the cellular members were selected based on the available profiles in (ArcelorMittal, 2008). The dimensions of the profiles were chosen to vary in the normal range of application: IPE200-IPE750 for IPE profiles and HE260-HE1000 for HE profiles. It should be noted that adapted residual stress pattern proposed by Sonck for cellular members, which was only experimentally validated for light parent sections (IPE160), will be implemented in the model. Therefore, the extremely heavy HE sections where excluded from the parametric study. Based on the same reasoning, the heavy HL sections, only ranging from HL900 to HL1100, were not considered. Although the application of HEB sections is common, the choice of HEA and HEM sections was chosen to cover a larger range of section properties. As final criterium, sections were chosen with a limited variation in web height (h-2t_f).
The above considerations were also made in (Sonck, 2014) for the investigation of the global buckling on castellated and cellular members. As a result, the same profiles will be considered for the parametric study (Table 4.1).

5.1.1 Parameters cellular openings

To determine the buckling resistance of members under the combined action of bending moment and normal force, a sufficient number of different geometries should be considered. For cellular members, the dimension of the openings a is determined by the factor f_a. To characterize the web post width w the factor f_w is introduced. Similarly, the width of the web post at the end of the cellular member can by varied by $f_{w,end}$, although this width will be considered constant throughout the parametric study. The relations between the factors f and the dimensions of the cellular members are given by Eqs. 5.1.1-5.1.3 (Fig. 5.1).

$$a = f_a \cdot h \tag{5.1.1}$$

$$w = f_w \cdot a \tag{5.1.2}$$

$$w_{end} = f_{w,end} \cdot w \tag{5.1.3}$$

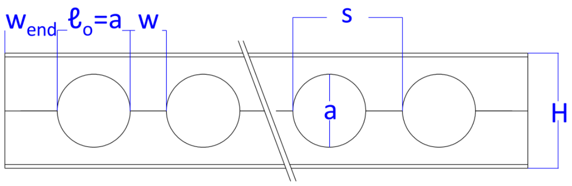

Figure 5.1: Cellular member dimensions. Extracted from (Sonck, 2014).

The choice of the factors f_a and f_w is based on values of normal application in (ArcelorMittal, 2008). To limit the number of simulations, two different values will be considered for both parameters. The considered values for both factors are given in Table 5.1. However, also the geometrical constraints found in the Detailed Technical Description of ARCELOR Cellular Beams (CTICM, 2006) should be fulfilled, possibly reducing the number of possible geometries for one or more of the considered values for f_a and f_w. The values in Table 5.1 are therefore starting values, that are altered per profile to obtain four parameters that meet the geometrical constraints.

Table 5.1: Considered factors f_a and f_w

Factor	Considered values.	
f_a	0.8	1.2
f_w	0.1	0.7

An overview of the geometrical constraints for cellular members is given in Appendix A.5. To illustrate the adaptations that will be made to the factors f_a and f_w, first an overview of the considered combinations (denoted with c_1 till c_4) is given in Table 5.2.

Table 5.2: Considered combinations factors f_a and f_w.

Combination	f_a	f_w
c1	0.8	0.1
c2	1.2	0.1
c3	0.8	0.7
c4	1.2	0.7

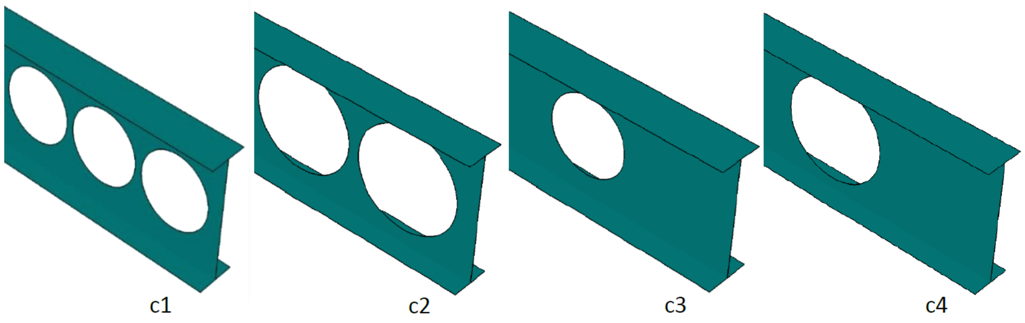

Figure 5.2: Illustration of combinations c1-c4 for HE650M.

Constraint 3 (w $\geq$ 50 mm) was not fulfilled for combination c1 for all profiles except for the higher HE650A and HE650M profiles. This can be explained by the low value of factor f_a and its direct relation with the web post width w according to Eq. 5.1.2. To allow for a wider range of applicable geometries, constraint 3 was not used to determine the possible geometries for the parametric study. Consequently, the originally proposed factors for f_a and f_w of combination c1 (Table 5.2) were maintained. For combination c2 the proposed value of 1.2 for factor f_a was adapted to 1.1 to fulfill constraint 7. All geometrical constraints for combination c3 were met for all profiles.

Table 5.3: Adapted values considered values factors f_a and f_w.

Section	Combination	f_a	f_w	Failing constraint
IPE300	c4	1.1	0.65	constraint 4/7/8
IPE600	c4	1.15	0.6	constraint 4
HE320A	c4	1	0.65	constraint 4/7/8
HE650A	c4	1.15	0.6	constraint 4
HE320M	c2	1.05	0.1	constraint 7
	c4	0.9	0.6	constraint 4/7/8
HE650M	c4	1.15	0.6	constraint 4/7/8

Most restrictions on factors f_a and f_w were obtained for combination c4. An overview of the final considered values and the failing constraints for the originally proposed values (Table 5.2) for the different sections is given in Table 5.3. It should be noted that for the adapted values of f_a and f_w the preference was given to values of f_a with a minimal deviation of the original value 1.2 in order to obtain a diameter of the openings that is as large as possible. By aiming for a maximum web opening area, the dead load is lowest with a larger possibility to integrate services in the openings. An overview of the considered combinations for HE650M is given in Fig. 5.2, where the larger openings for combinations c2 and c4 are clearly noticeable, as well as

Limitations were mainly obtained for geometrical constraints 4, 7 and 8. For combination c4 all profiles failed on constraint 4, which imposes a lower limit of 1.25 on H/a. Difficulties for this constraint can be explained by the combination of high f_a and f_w values considering Eqs. 5.1.1-5.1.2. Constraints 7 and 8 were introduced to facilitate the cutting of the web of the parent section during the fabrication process and are based on $h_{web,TS}$, the height of the remaining part of the web at the location of the opening (Fig. A.1).

5.1.2 Profile length

The variation of the member's length was determined similarly as for the plain-webbed members, i.e. by interpolation between two set boundaries for the minimum and maximum length. The height H is now referring to the total height of the cellular member. In contrast to the profiles considered in (Gevaert, 2010), the variation in web height for the two groups of profiles IPE300/HE320A/HE320M and IP600/HE650A/HE650M is limited. As a reminder, the devision made by Gevaert (section 3.11.1) was mainly introduced for low-height profiles to limit the non-dimensional slenderness $\overline{\lambda}$ (Eq.5.1.4) for long lengths due to the considerable decrease of the critical weak-axis flexural buckling load $N_{cr,z}$ for these members. For large values of $\overline{\lambda}$, the critical flexural buckling load becomes determining, since N approaches $N_{cr,z}$. Based on this consideration and the smaller variation of the cross-sectional properties of the profiles in this work, only the length determination based on interpolation was retained. However, to allow for a wider variation of corresponding slenderness of the members, an additional length was introduced. A few other adaptations were required due the larger height of the cellular members. First, a minimum length $f_{L,min}$ of 5H was introduced for the higher profiles IPE600/HE650A/HE650M

so that also for these profiles lower slenderness values $\overline{\lambda}_z$ could be examined. The lower boundary of 5H was also introduced for IPE300 profiles due to their higher slenderness for equal lengths compared to HE320A and HE320M profiles. As already mentioned in section 3.11.1, for high values of $\overline{\lambda_{LT}}$ (Eq.), it is not possible to obtain a load proportionality factor from the GMNIA analyses as deformations are increasing with increasing load and no maximum is obtained.
Therefore, for IPE300 and IPE600 profiles an additional limitation will be set to the length of respectively 15 m and 20 m. The subdivision for the different profiles is given in Table 5.4.

Table 5.4: Profile length cellular members.

k	IPE300	IPE600	HE650A/HE650M	HE320A/HE320M
1	5H	5H	5H	10H
2	5H + (15-5H)(1/4)	5H + (20-5H)(1/4)	5H + (25-5H)(1/4)	10H + (25-10H)(1/4)
3	5H + (15-5H)(2/4)	5H + (20-5H) (2/4)	5H + (25-5H)(2/4)	10H + (25-10H)(2/4)
4	5H + (15-5H)(3/4)	5H + (20-5H) (3/4)	5H + (25-5H)(3/4)	10H + (25-10H)(3/4)
5	15	20	25	25

Table 5.5: Slenderness range $\overline{\lambda}_z$ and $\overline{\lambda}_{min}/\overline{\lambda}_{max}$ for cellular members.

	$\overline{\lambda}_z$	$\overline{\lambda}_{LT,min}$	$\overline{\lambda}_{LT,max}$
IPE300	0.6 - 1.5 - 2.4 - 3.3 - 4.2	0.35	2.75
IPE600	0.9 - 1.7 - 2.4 - 3.2 - 3.9	0.49	2.77
HE650A	0.7 - 1.4 - 2.1 - 2.7 - 3.5	0.37	2.37
HE650M	0.7 - 1.4 - 2.0 - 2.7 - 3.4	0.36	2.01
HE320A	0.6 - 1.3 - 1.9 - 2.6 - 3.3	0.3	2.07
HE320M	0.6 - 1.3 - 1.9 - 2.5 - 3.2	0.28	1.39

$$\overline{\lambda}_z = \sqrt{\frac{f_y A_{2T}}{N_{crz,2T}}} \tag{5.1.4}$$

$$\lambda_{LT} = \sqrt{\frac{f_y W_{pl,2T}}{M_{cr,2T,avg}}} \tag{5.1.5}$$

It should be noted that the lengths specified in Table 5.4 are the minimum lengths L_{min} of the cellular members. The length L is determined using Eq. 5.1.6 with n indicating the smallest number of whole openings (Eq. 5.1.7) and the dimensions of the cellular member as indicated in Fig. A.1.

$$L = n(a + w) - w + 2w_{end} \tag{5.1.6}$$

$$n = \left\lceil \frac{L_{min} + w - 2w_{end}}{a + w} \right\rceil \tag{5.1.7}$$

5.1.3 Cross-section classification cellular members

The classification of the web post between the openings will be performed in the same manner as discussed in detail for the plain-webbed members, i.e. by applying the classification rules of EC3 without omission of the fillets. It should again be emphasized that for the cross-sectional properties themselves a wire model is used. Also for the classification of the flanges, the rules of (CEN, 2005) are applied. For cellular members however, an additional check of local buckling of the web at the tee section is required according to (CEN, 1998) (Annex N). Based on the following rules, a distinction is made between profiles Class 2 or 3 (Figs. 5.1-A.1).

$$\text{Class 2:} \quad l^* \leq 32\epsilon t_w \quad \text{or} \quad h_{web,TS} \leq \frac{10\epsilon t_w}{\sqrt{1-\left(\frac{32\epsilon t_w}{l^*}\right)^2}} \tag{5.1.8}$$

$$\text{Class 3:} \quad l^* \leq 36\epsilon t_w \quad \text{or} \quad h_{web,TS} \leq \frac{14\epsilon t_w}{\sqrt{1-\left(\frac{36\epsilon t_w}{l^*}\right)^2}} \tag{5.1.9}$$

$$\text{where} \quad l^* = 0.7a; \;\; h_{web,TS} = \frac{H - 2t_f - 2r - a_0}{2} \tag{5.1.10}$$

Due to large height of the web post of cellular members, Class 4 was obtained for all profiles, except for HE320M (Class 2). The most detrimental classification for all profiles was obtained for the largest web opening (defined by f_a) and the smallest web post width (defined by f_w), i.e. combination c2 (Table 5.2 and 5.3). The most detrimental classification for different load configurations is given in Table 5.6 and 5.7. Although for class 4, an effective cross-section should be considered with an ineffective central part of the web (h_{ineff}), this central part was always smaller than the opening height a, which is already included in the cross-sectional properties when applying a 2T approach. The ineffective height h_{ineff} is largest for the combinations with the most detrimental classification and given in Table 5.8.

Table 5.6: Classification of cellular members for $\psi = 1$ $(c = h - 2t_f - 2_r)$.

μ	IPE300	IPE600	HE320A	HE650A	HE320M	HE650M
0	4	4	4	4	2	4
0.1	4	4	4	4	2	4
0.5	4	4	3	4	2	3
1	3	4	3	4	2	3
5	3	4	2	3	2	2
10	3	4	2	3	2	2
∞	3	4	2	3	2	2

Table 5.7: Classification of cellular members for $\psi = 0$ and $\psi = -1$ $(c = h - 2t_f - 2r)$.

μ	IPE300	IPE600	HE320A	HE650A	HE320M	HE650M
0	4	4	4	4	2	4
0.1	4	4	4	4	2	4
0.5	4	4	4	4	2	4
1	4	4	4	4	2	4
5	4	4	4	4	2	4
10	4	4	4	4	2	4
∞	3	4	2	3	2	2

Table 5.8: Geometries with largest ineffective height h_{ineff}.

	IPE300	IPE600	HE320A	HE650A	HE320M	HE650M
f_a	1.20	1.20	1.20	1.20	1.05	1.20
f_w	0.10	0.10	0.10	0.10	0.10	0.10
H	0.471	0.950	0.487	1.014	0.539	1.059
a	0.360	0.720	0.372	0.768	0.377	0.802
h_{ineff}	0.230	0.466	0.236	0.494	0.249	0.509

5.1.4 Types of analyses

First, an LBA analysis will be performed to determine the critical lateral-torsional buckling moment $M_{cr,abq}$ and the deviation from the analytical formula $M_{cr,an}$ according to a 2T approach. In total, 420 LBA analyses should be executed on every profile, i.e. for each of the 5 lengths, the 4 combinations (c1 →c4), the seven μ values and the three ψ-values defining the load condition. Similarly as in the study of Gevaert, this value of M_{cr} will be required for the GMNIA analyses to define the initial axial load on the members. However, due to the observed web post buckling for short length members (Section 5.1.5), resulting in a large deviation between the numerically and theoretically obtained results, the theoretical expressions will be used to determine the initial axial load. For each of the LBA analyses, a corresponding GMNIA analysis will be performed.

5.1.5 Critical bending moment M_{cr}

For all considered members subjected to a constant bending moment ($\psi = 1$) lateral-torsional buckling was examined as failure mode. For the non-uniform bending moments however, local web post-buckling was observed for the short-length members. By means of LBA analyses, the deviation factor Δ_M between the numerical and analytical results will be examined (Eq.5.1.11).

$$\Delta_M = \left(\frac{M_{abq}}{M_{an}} - 1\right) \cdot 100\% \tag{5.1.11}$$

For the analytical expression of the critical buckling moment, it should be noted that the torsional constant I_t will be the determining factor. Therefore, a weighted average approach was proposed for I_t according to Eq. 5.1.12, resulting in a value intermediate between the underestimated value $I_{t,2T}$ and the overestimated value $I_{t,0}$. With this expression, an equivalent rectangular opening is considered with horizontal dimension $l_{0,avg}$ (Eq. 5.1.12) and vertically the diameter of the circular opening (Fig.5.3). The factor β_{cell} in the expression of the equivalent length $l_{0,avg}$ based on examination of $\Delta_{M_{cr}}$, are obtained by best fitting of the factors β_{cell} with the numerical results. This was studied in (Sonck, 2014) and a value of 0.9 was proposed for cellular members. Although this value was only derived for members subjected to a constant bending moment, based on further investigation in this work it could be concluded that also satisfactory results were obtained in case of non-uniform bending moments ($\psi = 0$; $\psi = -1$). It should be noted that (as investigated by Sonck) the introduction of $I_{t,avg}$ compared to $I_{t,0}$ will only affect the deviations for larger lengths significantly, considering the smaller influence of the torsional constant $I_{t,avg}$ for shorter lengths in the expression of M_{cr}.

$$I_{t,avg} = n\frac{l_{0,avg}}{L} \cdot I_{t,2T} + \left(1 - \frac{nl_{0,avg}}{L} \cdot I_{t,0}\right) l_{0,avg,cell} = \beta_{cell} l_0 = \beta_{cell} a \tag{5.1.12}$$

The deviations $\Delta M_{cr,2T}$ for different ψ values are represented in Fig. 5.5. The combinations for which large deviations were obtained due to web-post buckling are listed in Table B.2. An example of the observed web-post buckling for section IPE300 (L=2.18 m; $\psi = -1$) is given in Fig. 5.4.

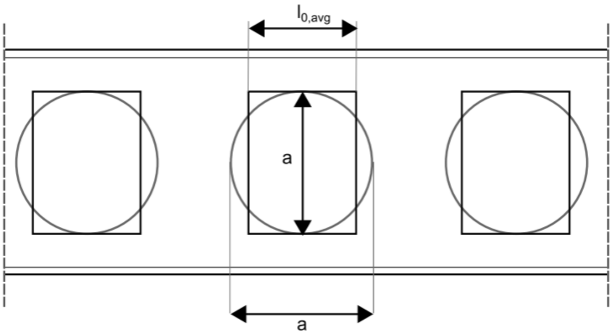

Figure 5.3: Equivalent opening cellular member. Extracted from (Sonck, 2014).

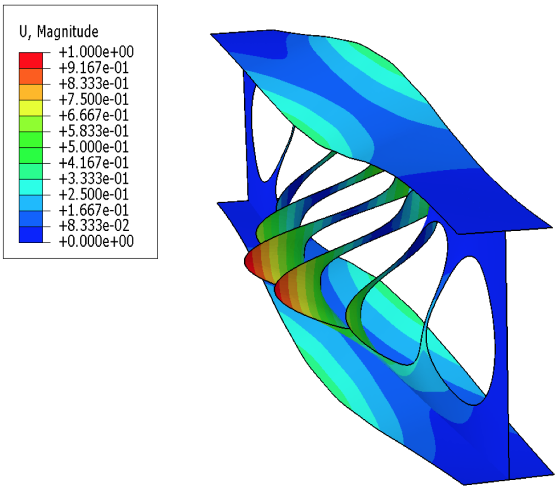

Figure 5.4: Observed web-post buckling for IPE300 (L=2.18 m; $\psi = -1$).

5.2 Comparison numerical results with buckling curves for limit cases

5.2.1 Flexural buckling

In (Sonck, 2014) a design rule proposal was made for the adapted weak-axis flexural buckling curves of cellular members due to the more detrimental residual stress pattern. The best buckling curve fit with existing EC3 buckling curves was determined for the same six geometries as considered in this work. The additional GMNIA results for the different set of slendernesses examined here will therefore serve as an additional verification of this preliminary design rule. Comparison of the numerical results with the different existing buckling curves is given in Fig. 5.6, where the non-dimensionless slenderness $\overline{\lambda}$ was calculated analytically according to Eq. 5.1.4. The reduction factor χ_{Abq} was determined numerically using Eq. 5.2.1, based on $N_{b,Rd} = \lambda_u N_{start}$.

$$\chi_{Abq} = \frac{N_{Rd,abq}}{f_y A_{2T}} \tag{5.2.1}$$

For each buckling curve, the deviations ΔN_{Rd} from the existing EC3 buckling curves are given in Appendix B, Table B.3, of which the minimal deviations and best fitting buckling curves are also represented in Table 5.9. The profiles HE320A and HE320M show the best correspondence with buckling curve d, whereas for the other geometries best fitting was obtained with buckling curve c. This can be explained by the higher residual stresses in the parent sections due to which also for the

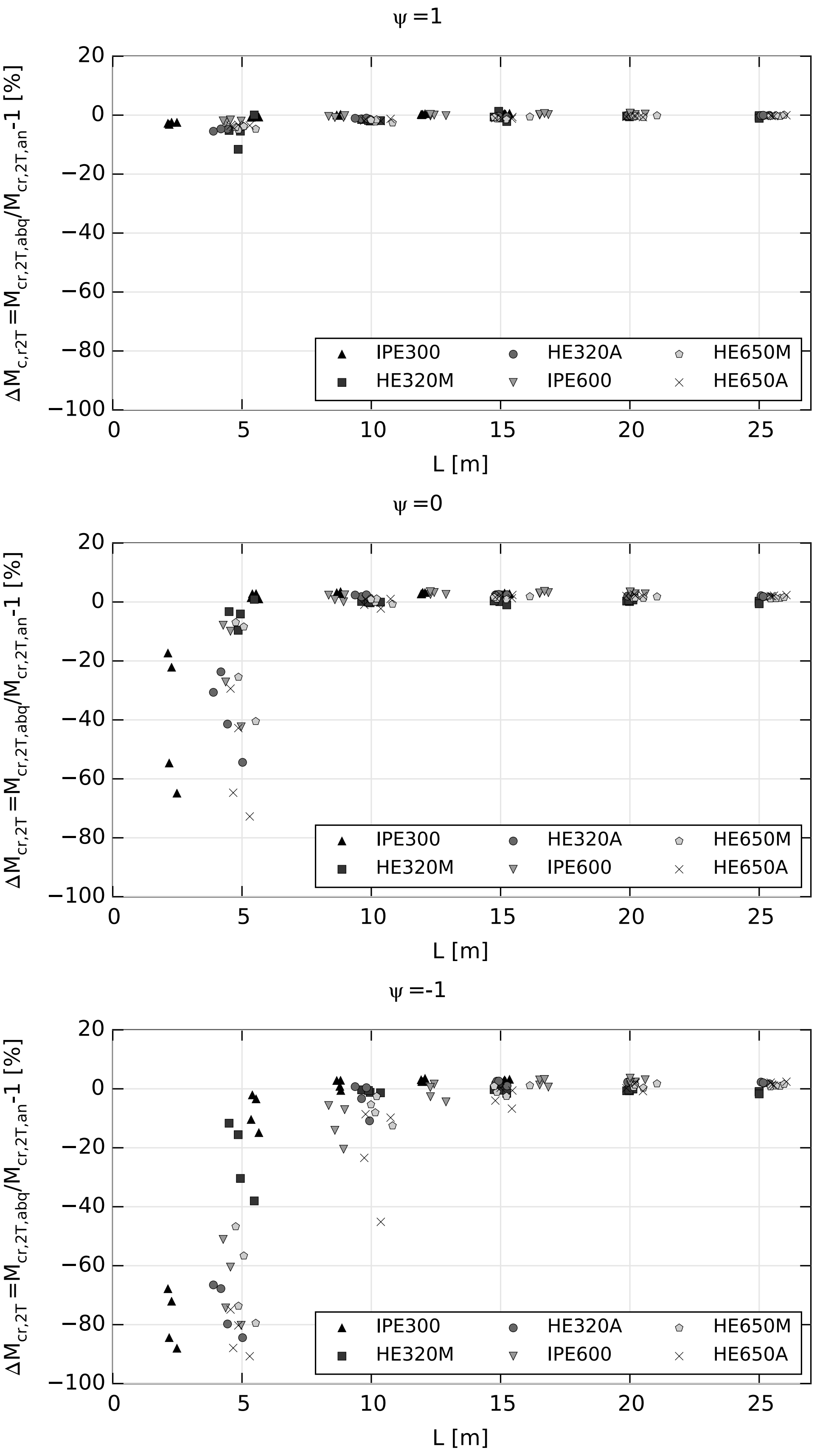

Figure 5.5: Deviation of $M_{cr,2T}$.

cellular members a higher residual stress pattern was assumed. Detailed examination is outside the scope of this work, but based on these results, it can be concluded that the FB curve proposal for cellular members made in (Sonck, 2014) is also applicable for the different range of slendernesses in this work.

Table 5.9: Best fitting EC3 buckling curve under pure compression.

parent section	h/b [-]	H/b [-]	$\Delta N_{Rd,EC3,min}$[%]	buckling curve
IPE300	≥ 1.2	≥ 1.2	-2.13	c
IPE600	≥ 1.2	≥ 1.2	-0.32	c
HE320A	≤ 1.2	≥ 1.2	-0.46	d
HE650A	≥ 1.2	≥ 1.2	-3.28	c
HE320M	≤ 1.2	≥ 1.2	-0.46	d
HE650M	≥ 1.2	≥ 1.2	-2.49	c

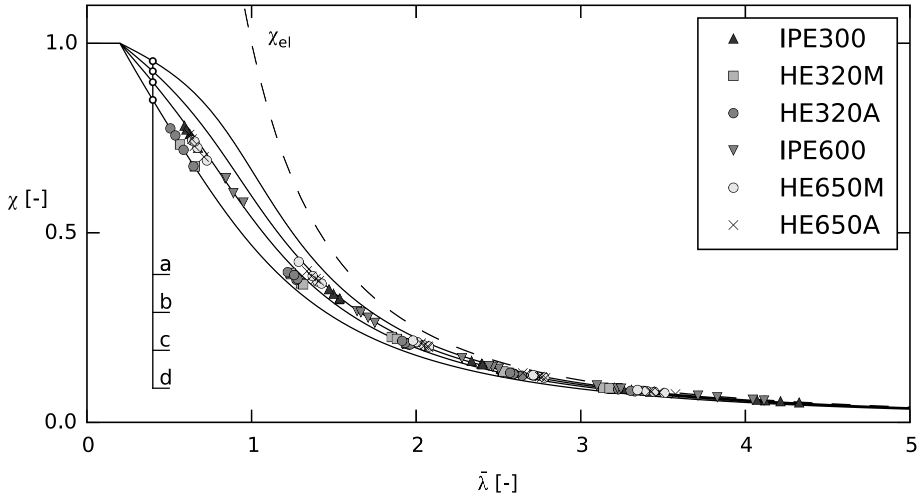

Figure 5.6: Comparison numerical results with existing buckling curves ($\mu = 0$).

5.2.2 Lateral-torsional buckling

According to (CEN, 2005), a global non-dimensional slenderness $\overline{\lambda}_{op}$ can be defined according to Eq. 5.2.2 for structural components subjected to lateral and lateral-torsional buckling.

$$\overline{\lambda}_{op} = \sqrt{\frac{\alpha_{ult,k}}{\alpha_{cr,op}}} \tag{5.2.2}$$

The factor $\alpha_{ult,k}$ is the minimum amplification factor that should be applied to the design loads (moment and axial load) to obtain the characteristic resistance of the most critical cross-section of the considered member. It is defined here specifically as the factor by which both moment and axial force should be multiplied to obtain full plastic yielding of the cross-section. It should be noted that the initially applied bending moment M and normal force N were defined based on a constant ratio between both (e=M/N, Eq. 3.2.1). Therefore it is possible to define a general multiplication factor for the combined action of M and N. The factor $\alpha_{ult,k}$ was determined theoretically based on Eq. 5.2.3, with N_{Rk} and $M_{y,Rk}$ respectively the normal buckling and bending resistance.

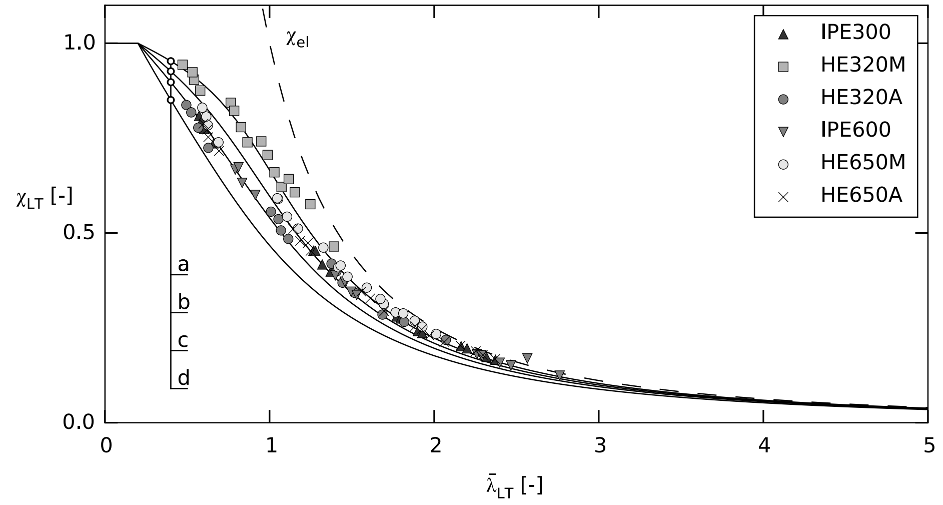

Figure 5.7: Comparison numerical results with existing buckling curves ($\mu = \infty$; $\psi = 1$).

$$\alpha_{ult,k}\left(\frac{N_{Ed}}{N_{Rk}}+\frac{M_{y,Ed}}{M_{y,Rk}}\right)=1 \tag{5.2.3}$$

On the other hand, for the multiplication factor $\alpha_{cr,op}$ the results of an LBA analysis executed for all combinations will be used, since this factor represents the elastic critical lateral or lateral torsional buckling resistance of the considered member.

This alternative formulation of the non-dimensionless slenderness will be used to compare the numerical results with the buckling curves proposed in EC3. In this way, not only members under pure bending or compression can be considered, but representation of all results of members subjected to a combination of bending and compression is possible. The reduction factor $\chi_{Abq,LT}$ was defined according to Eq. 5.2.4, where the resistances $M_{Rd,Abq}$ are obtained from GMNIA analysis; factor $\alpha_{ult,k}$ results again from Eq. 5.2.3.

$$\chi_{Abq}=\frac{M_{Rd,abq}}{\alpha_{ult,k}} \tag{5.2.4}$$

First, only members subjected to pure (uniform or non-uniform) bending are considered. The obtained resistances in the GMNIA analysis will be compared with the resistances $M_{Rd,2T,avg} = \chi_{LT} W_{pl} f_y$, in which a 2T approach is used for all cross-sectional properties, but a weighted average expression for the torsional constant. Similarly as for flexural buckling (Section 5.2.1), the deviations ΔM_{Rd} from the existing EC3 buckling curves can be determined. An overview of the deviations and best fitting buckling curves for three different ψ values is given in Table 5.10. The corresponding best fit buckling curves for $\psi = 1$, corresponding to the smallest value of $\sum(\chi_{Abq} - \chi)^2$, are identical as in (Sonck, 2014), where a similar study was performed. For section HE650M, the best fit buckling curve is b, but since the minimum deviation $\Delta M_{Rd,EC3,min}$ (-7.7%) is smaller than -5%, the choice of this buckling curve is considered unsafe. Therefore, buckling curve c is recommended.

As indicated in Section 2.4.3.2, an increased lateral-torsional buckling resistance can be obtained members subjected to an non-uniform bending moment compared to members under constant bending. This can be clearly noticed from the higher buckling curves that were obtained for $\psi = 0$ (Fig. 5.8). For all considered sections, the highest buckling curve a was therefore most suitable, although deviations with buckling curve a are still large for all HE sections. This effect is even more pronounced for $\psi = -1$

where, although a higher variation of the results can be noticed (Fig. 5.9), most values of χ_{LT} for all sections are situated at a significant distance above buckling curve a.

Table 5.10: Best fitting EC3 buckling curve under pure bending.

	h/b [-]	H/b [-]	$\psi = 1$		$\psi = 0$		$\psi = -1$	
			$\Delta M_{Rd,EC3,min}$[%]	curve [-]	$\Delta M_{Rd,EC3,min}$[%]	curve [-]	$\Delta M_{Rd,EC3,min}$[%]	curve [-]
IPE300	≥ 2	≥ 2	-2.4	c	-4.7	a	-84.5	a*
IPE600	≥ 2	≥ 2	-3.3	c	-3.2	a	-35.9	a*
HE320A	≤ 2	≥ 2	-6.7	c	-20.5	a*	-26.7	a*
					-3.9	c		
HE650A	≥ 2	≥ 2	-4.5	c	-29.2	a*	-67.9	a*
					0.2	d		
HE320M	≤ 2	≥ 2	-3.2	a	9.2	a*	-17.2	a*
HE650M	≥ 2	≥ 2	-7.7	b*	-6.9	a*	-43.8	a*
			-0.5	c	-3.4	b		

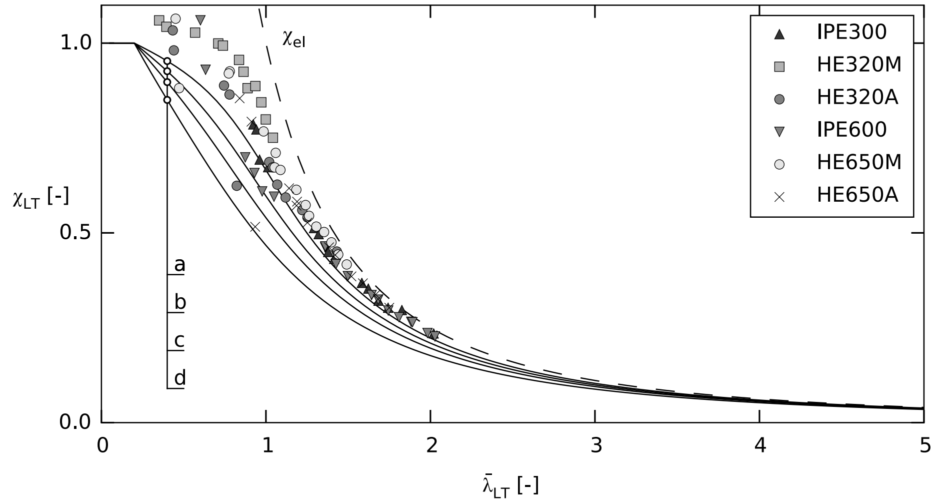

Figure 5.8: Comparison numerical results with existing buckling curves ($\mu = \infty$; $\psi = 0$).

5.2.3 Members subjected to bending and axial load

Finally, it is possible to compare the results obtained for all seven μ values of Table 3.1 with the buckling curves of EC3. This is illustrated in Figs. 5.10-5.11 for $\psi = 1$, where the data corresponding to $\mu = \infty$ are indicated in red; Blue is used for all other μ values. Best fitting buckling curves can again be derived of which a summary is given in Table 5.11. The charts for $\psi = 0$ and $\psi = -1$ as well as the corresponding deviations in M_{Rd} are given in Appendix B.

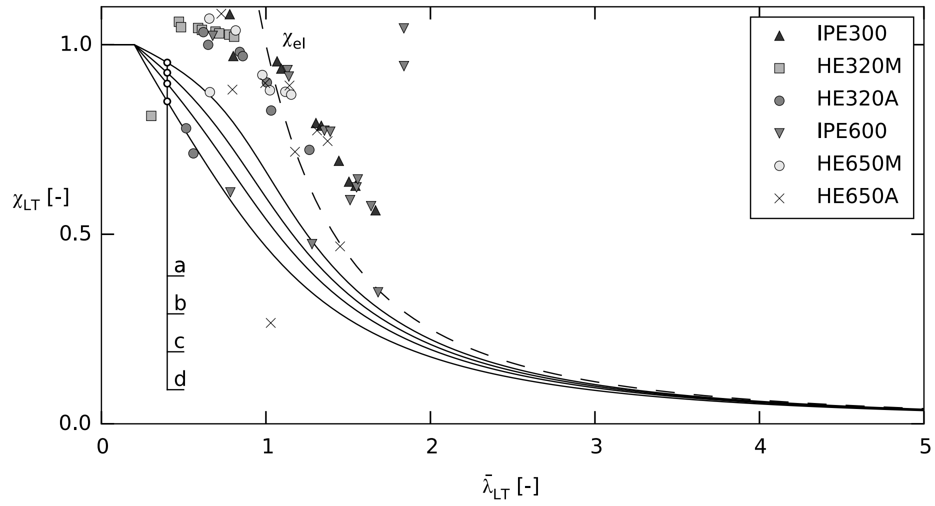

Figure 5.9: Comparison numerical results with existing buckling curves ($\mu = \infty$; $\psi = -1$).

Table 5.11: Best fitting EC3 buckling curve under bending and compression.

parent section	h/b [-]	H/b [-]	$\Delta M_{N,Rd,EC3,min}$[%]	buckling curve
IPE300	≥ 1.2	≥ 1.2	-2.4	c
IPE600	≥ 1.2	≥ 1.2	-3.2	c
HE320A	≤ 1.2	≥ 1.2	-6.7	c*
			3.6	d
HE650A	≥ 1.2	≥ 1.2	-4.5	c
HE320M	≤ 1.2	≥ 1.2	-3.2	a
HE650M	≥ 1.2	≥ 1.2	-7.7	b*
			-0.5	c

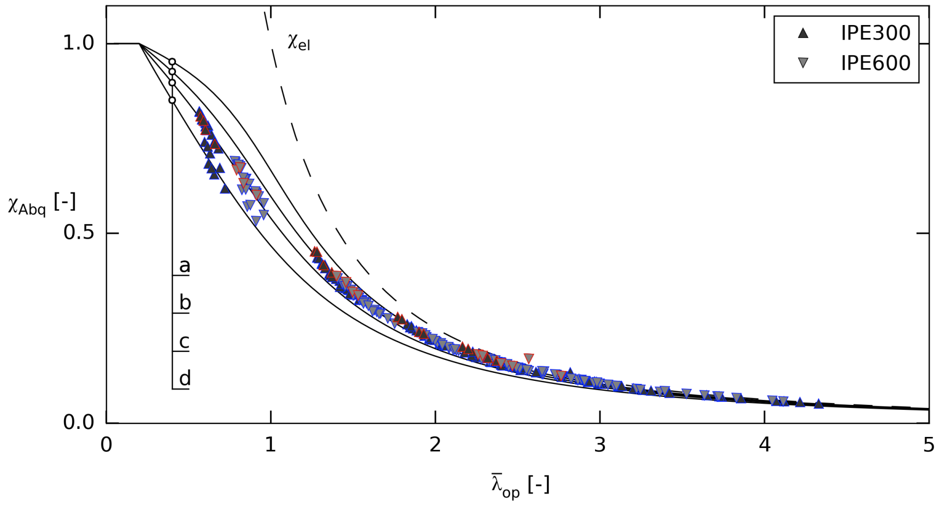

Figure 5.10: Comparison numerical results with existing buckling curves for all μ values - IPE sections ($\psi = 1$). Data corresponding to $\mu = \infty$ indicated in red; Blue is used for all other μ values.

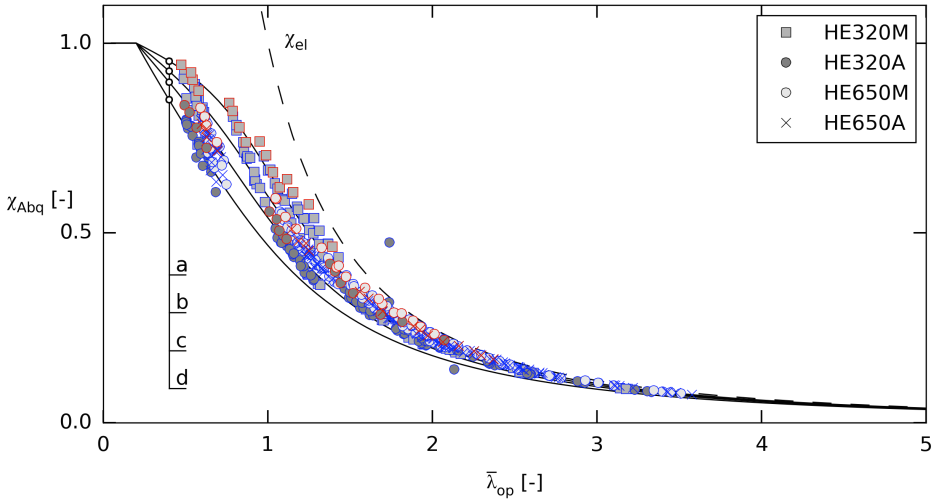

Figure 5.11: Comparison numerical results with existing buckling curves for all μ values - HE sections ($\psi = 1$). Data corresponding to $\mu = \infty$ indicated in red; Blue is used for all other μ values.

5.3 Deviation of LPF for different lengths

Similarly as for plain-webbed members, the deviation between the numerically and analytically obtained load-proportionality factor is represented by ΔLPF (Eq. 3.16.1). Figure 5.12 shows the results for Method 1 based on a modified optimal imperfection factor α of 0.6 for the LTB curves, but similar findings are possible for other methods. The seven different μ values of Table 3.1 are represented in the graphs. Similar findings as for plain-webbed members are possible where also negative deviations were observed for short length members indicating the insecurity of the design rules for shorter lengths. Largest negative deviations were again obtained for $\psi = -1$ (-85%). Long length members on the other hand show large positive deviations (up to 140% for IPE600; $\psi = -1$) and application of the design rule for these members is therefore very conservative. As remarked for the plain-webbed members, a larger variation of the results can be noticed for $\psi = -1$ than for members subjected to a constant bending moment.

5.4 Deviation of LPF for different slendernesses

Alternatively, the deviation in load proportionality factor for seven μ values (Table 3.1) can be given as function of the slenderness $\bar{\lambda}_{op}$ (Eq. 5.2.2). Comparable results are obtained for three methods: ECCS-Van Impe, Method 1 and Method 2 of EC3. The results for Method 2 are represented in Fig. 5.13. Under a constant bending moment ($\psi = 1$), deviations are increasing with increasing slenderness up to $\bar{\lambda}_{op} \approx 2.5$. For higher slendernesses ($\bar{\lambda}_{op} > 2.5$), especially obtained for profiles IPE300 and IP600 (Fig. 5.13), the observed deviations are smaller. For members under a non-uniform bending moment ($\psi = 0$ or $\psi = -1$), a similar effect can be noticed with all large deviations obtained for $\bar{\lambda}_{op} < 2$. Reference is made to Section 5.3, where it was concluded that deviations in LPF were increasing with increasing length of the members. For longer lengths, the obtained values of the elastic critical buckling resistance were indeed lower, increasing the member's slenderness $\bar{\lambda}_{op}$.

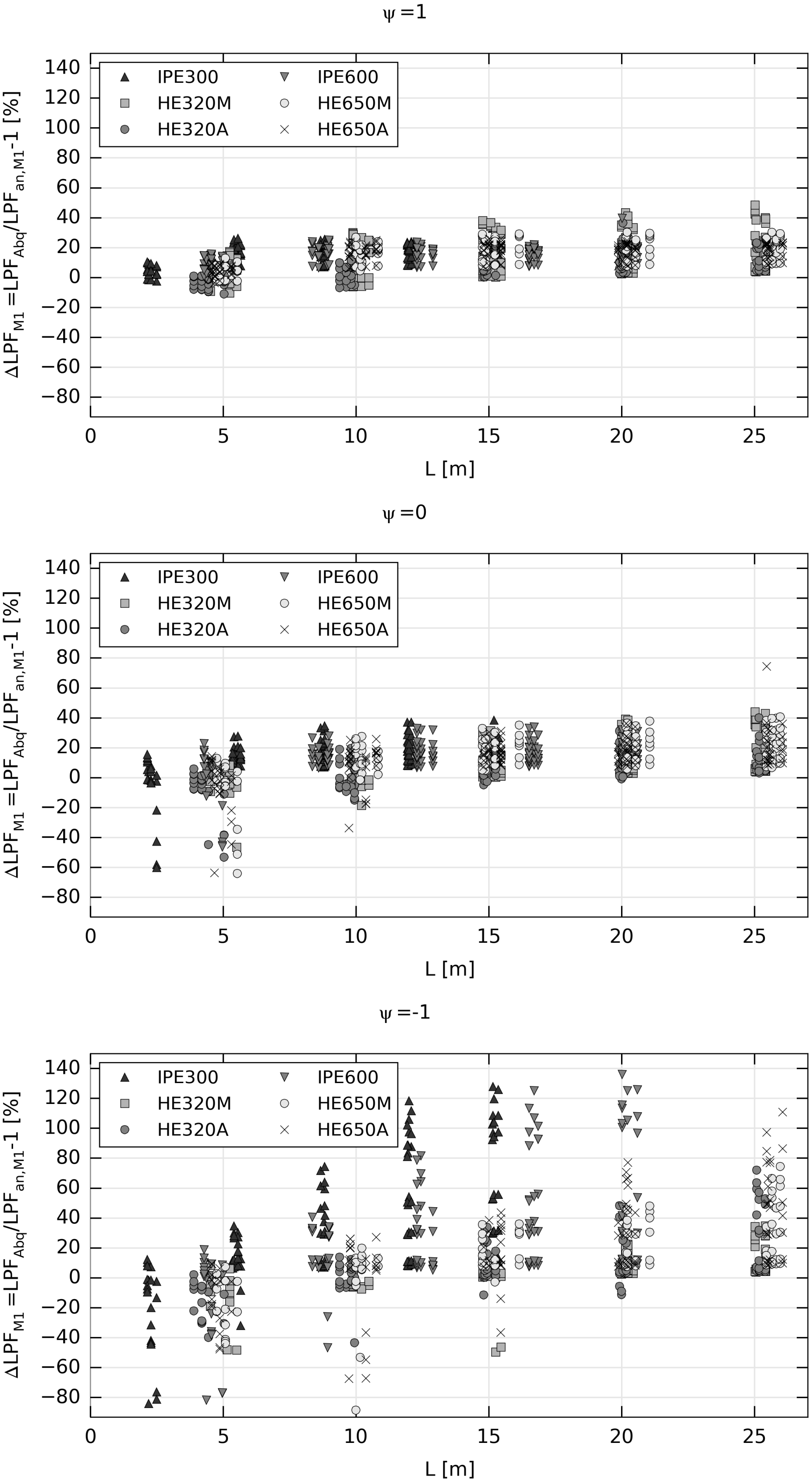

Figure 5.12: Deviation of LPF for cellular members as function of length.

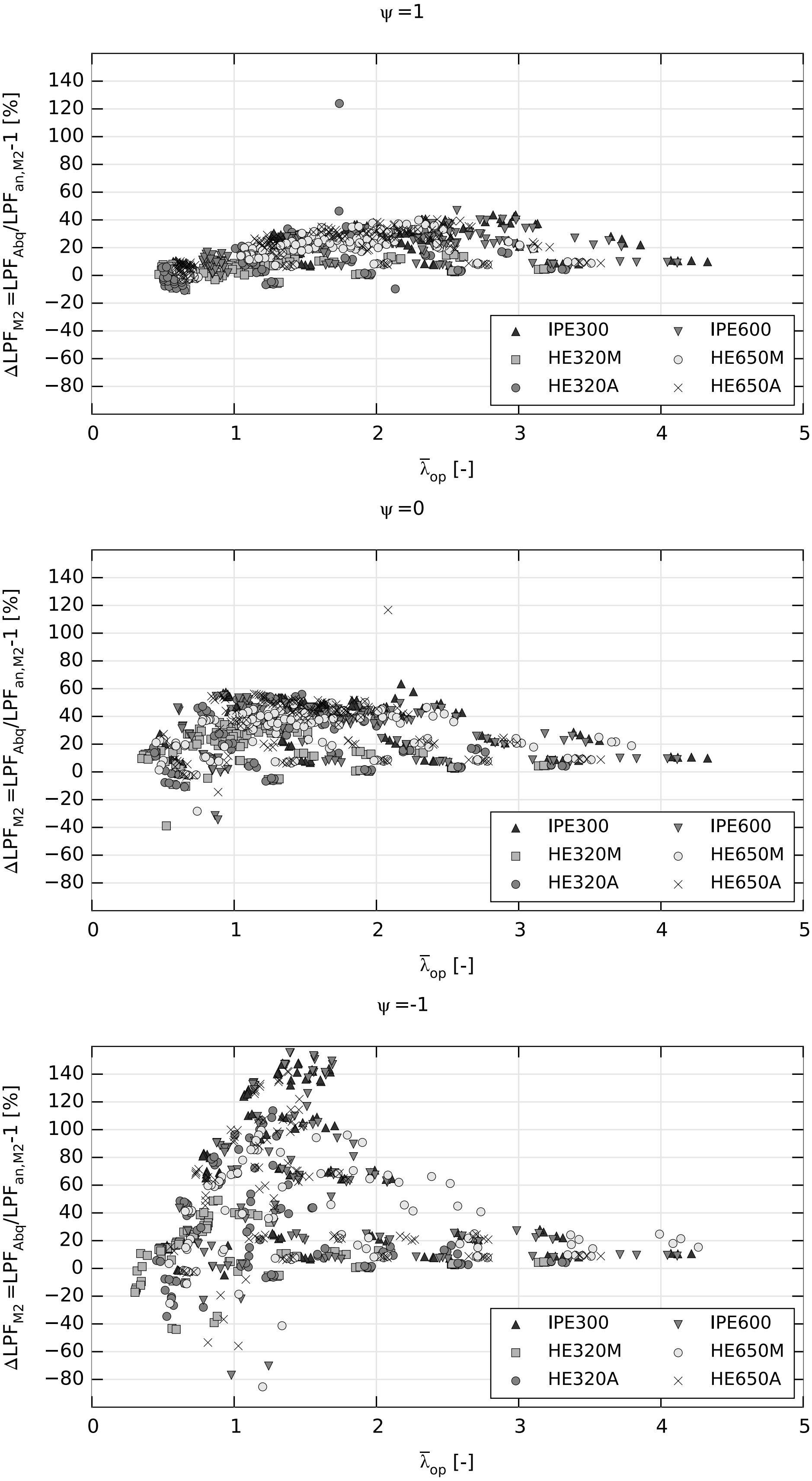

Figure 5.13: Deviation of LPF for cellular members as function of slenderness.

5.5 Influence of the considered μ value

As concluded for plain-webbed members, also for cellular members largest deviations are obtained for members subjected to pure bending ($\mu = \infty$). The plot of Fig. 5.12 for $\psi = -1$ is repeated here, but only for $\mu = 0$ and $\mu = \infty$. It can be concluded that for both values of μ application of design rule Method 1 is unsafe for short length members and conservative for longer lengths. However, the deviation and variability of the results is much larger for $\mu = \infty$ than for $\mu = 0$. Although the focus in this part is only on Method 1, it should be noted that other methods lead to similar findings.

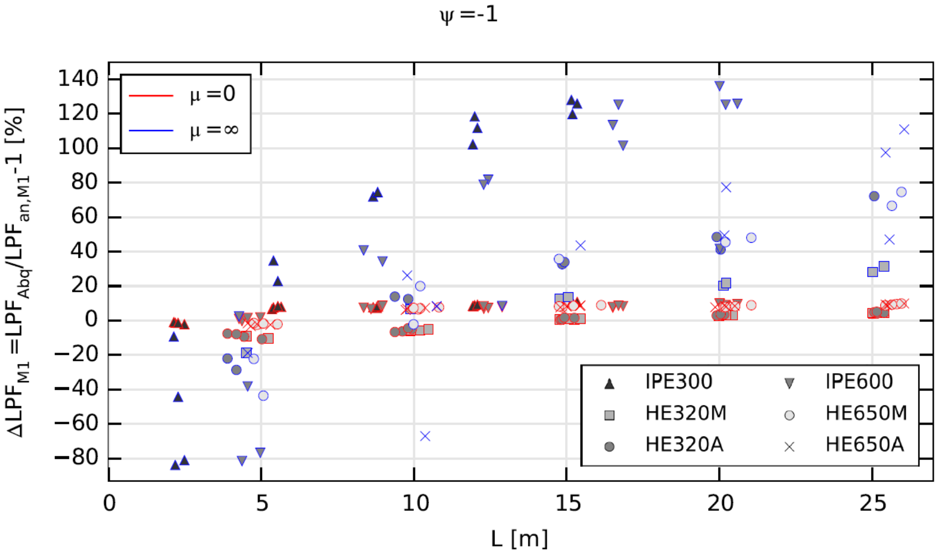

Figure 5.14: Influence of considered μ value for cellular members.

5.6 Influence of the cross-section classification

The influence of the cross-section classification, again based on EC3, is represented by a moment-normal force interaction diagram (Fig. 5.15). All moment-normal force interaction diagrams are provided on CD. Similarly as observed in the extended study on plain-webbed members, a shift from elastic to plastic theory is clearly noticeable (for Method 1 and 2) with increasing values of μ. However, comments can be made on this classification and possibly the calculation could be performed according to a plastic theory (considering the comments of Section 3.10.1) for all μ values. Still, preference was given by the author to follow the classification of EC3 according to an elastic-plastic theory due to the increased height and therefore more pronounced elastic behaviour of cellular members.

5.7 Influence of the choice of parent section

In this section the influence of the choice of parent section on the applicability and insecurity of the design rules is of further interest. This will be discussed based on the normal probability density function of the deviation of the load proportionality factor of each of the profiles, repeated for the four considered methods. An overview of the minimum, maximum, mean, median and standard deviation is given in Appendix B, Section B.7. In this part, a qualitative interpretation of the results is given. The results will be discussed separately for different ψ values.

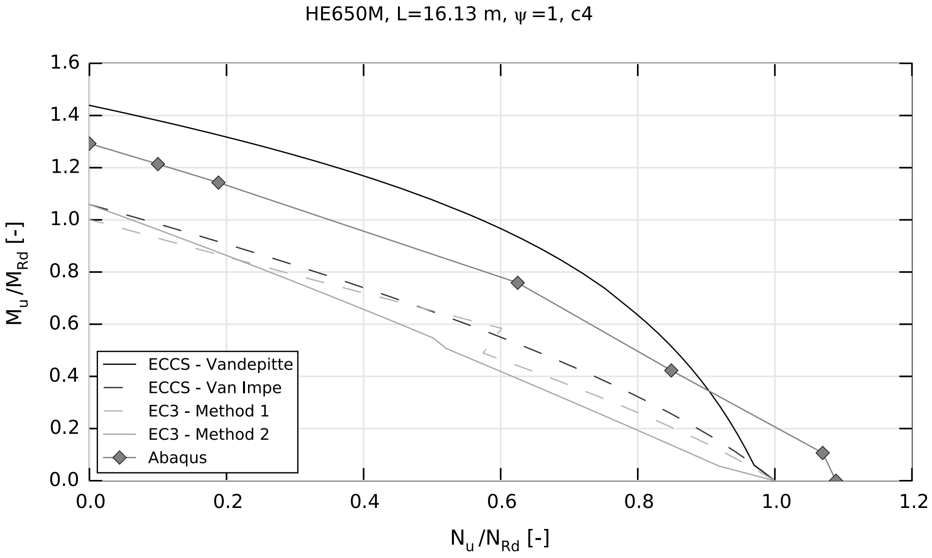

Figure 5.15: Moment-Normal force interaction diagram HE650M (L=16.13 m; $\psi = 1$).

5.7.1 Members subjected to a constant bending moment ($\psi = 1$)

Although in this paragraph only members subjected to a constant bending moment are considered, for which the smallest deviations are expected, the larger insecurity of the Vandepitte design rule is already clearly noticeable (Fig. 5.16) with a minimum deviation of -36.9% for section HE320A. For this section, also the maximum deviation (46.3%) of all profiles was observed. For this profile, the standard deviation σ_Δ is 10.9%, which is the largest of all profiles. The deviations of HE320M show the smallest variability with a standard deviation σ_Δ of 5.8% and the smallest negative deviation (-4.8%) as mean value. The distributions of the five other profiles are quite comparable and for each of them a larger variability can be observed.

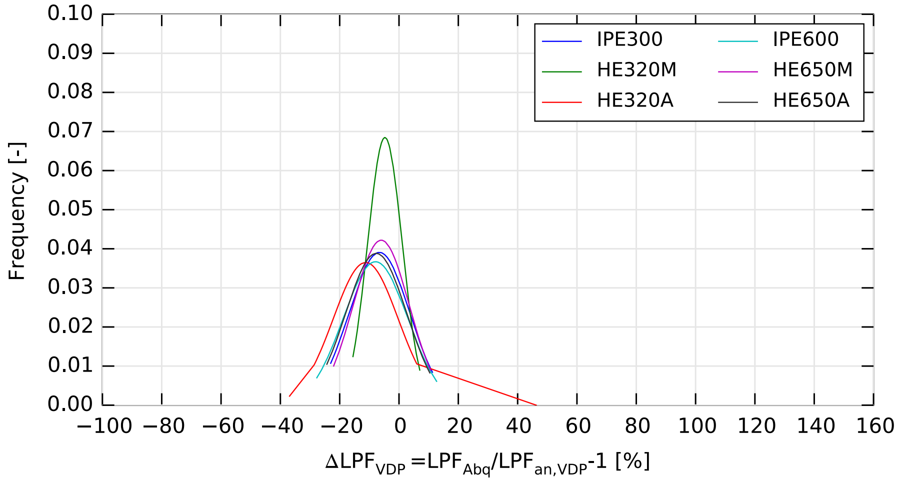

Figure 5.16: Normal PDF of ΔLPF according to method ECCS-Vandepitte ($\psi = 1$).

Similar findings are possible for the Van Impe method (Fig. 5.17) concerning section HE320M, for which the distribution shows an even smaller variability (4.3%). Similarly as for the Vandepitte method, other profiles show a larger variability with the largest variability on the deviations again obtained for HE320A (14.9%). It should be noted that the obtained distribution functions are quite comparable to the ones of Method 2 (as can be observed in Fig. 5.19), from which similar conclusions can be drawn. In contrast to the previous methods, the distribution function of the deviations in LPF of Method 1 has a wider variability for section HE320M (15.3%). Similarly as for the other methods, the largest maximum deviation was obtained for HE320A (109.1%). It should be noted that although negative deviations were obtained for method Vandepitte, a better correspondence can be found with the numerical results compared to the other methods, for which application of the design rule is conservative.

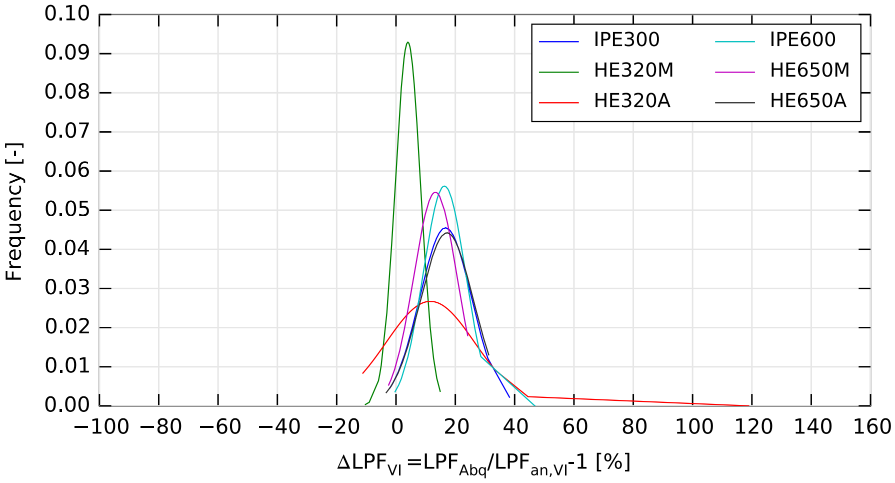

Figure 5.17: Normal PDF of ΔLPF according to method ECCS-VI ($\psi = 1$).

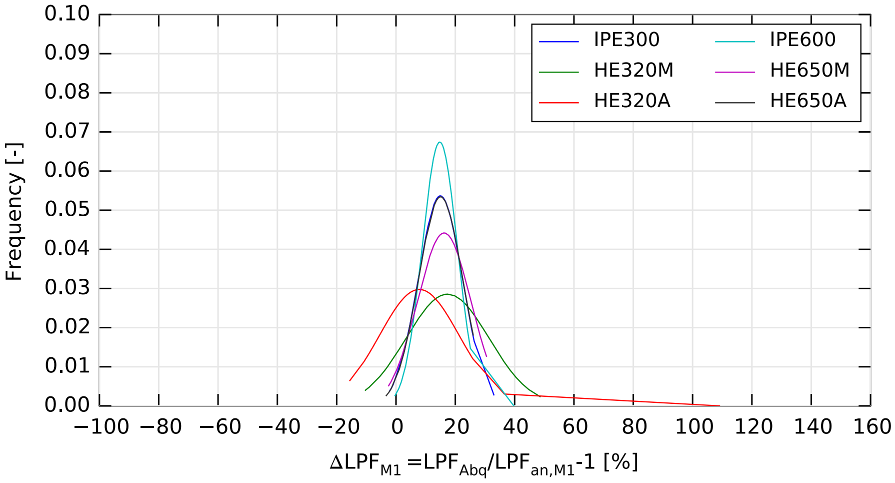

Figure 5.18: Normal PDF of ΔLPF according to Method 1 ($\psi = 1$).

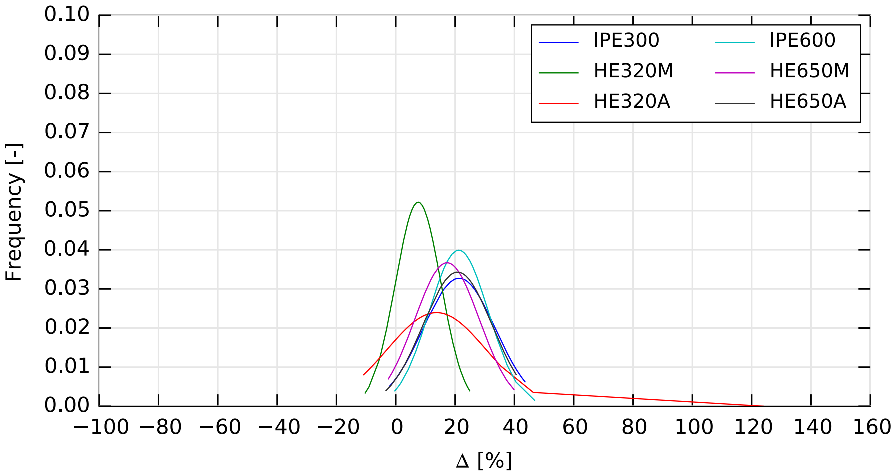

Figure 5.19: Normal PDF of ΔLPF according to Method 2 ($\psi = 1$).

5.7.2 Members subjected to a non-uniform bending moment ($\psi = 0$ or $\psi = -1$)

For members subjected to a bending moment at one of the member's end sections ($\psi = 0$), the obtained distribution functions of the deviations in LPF are very similar for the four methods. As indicated for $\psi = 1$, negative deviations are observed for method Vandepitte (Fig. 5.20), which are even larger in absolute value (up to 66.3% for HE650M) than for members subjected to a uniform bending moment ($\psi = 1$). The distribution function of profile HE320M shows the largest frequency with a mean value of -2.7%. Mean values of the distribution functions of other profiles are comparable, but lower.

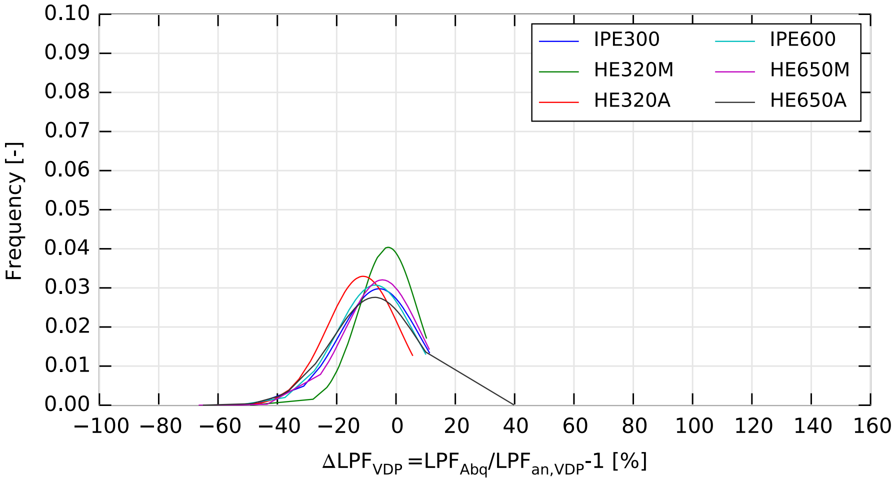

Figure 5.20: Normal PDF of ΔLPF according to method ECCS-VDP ($\psi = 0$).

For the three other methods, negative deviations in the same order of magnitude of method Vandepitte can be noticed. As remarked in Section 5.3, these large deviations were observed for short length members. In contrast to the design rule Vandepitte however, the distribution functions of the other methods show a larger variability, which was already observed in Section 5.3. For Method 2, a maximum standard deviation σ_Δ of 22.6% was found for section HE650A, whereas only 14.5% for method Vandepitte.

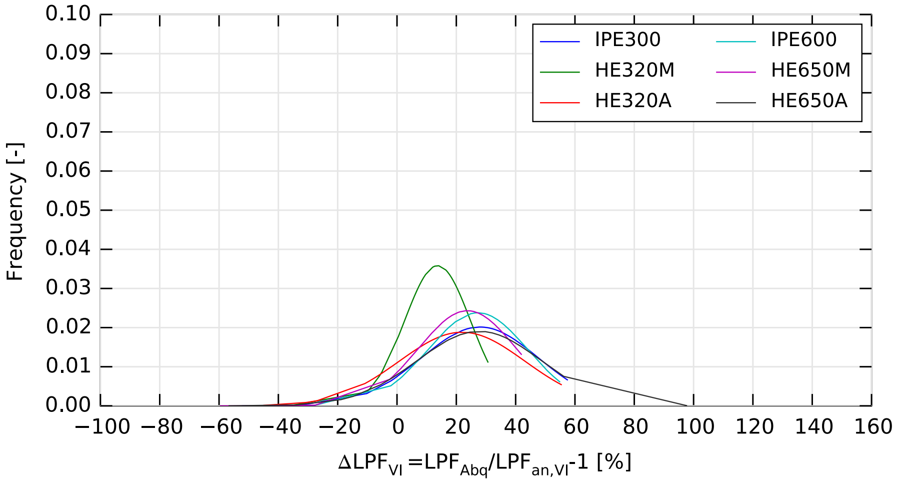

Figure 5.21: Normal PDF of ΔLPF according to method ECCS-VI ($\psi = 0$).

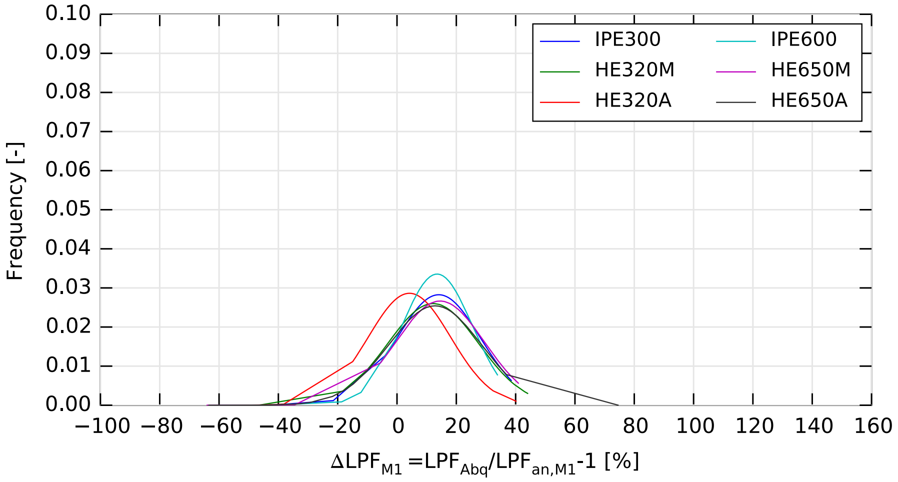

Figure 5.22: Normal PDF of ΔLPF according to Method 1 ($\psi = 0$).

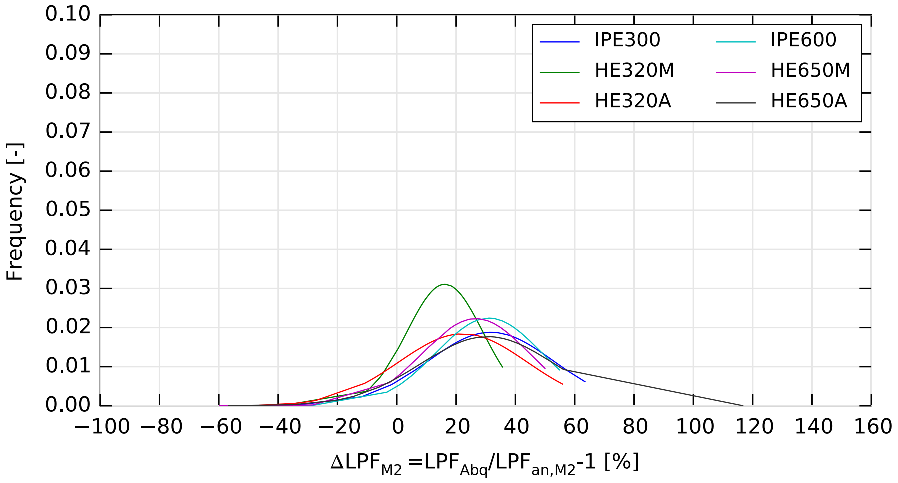

Figure 5.23: Normal PDF of ΔLPF according to Method 2 ($\psi = 0$).

When an equal moment, but opposite in sign ($\psi = -1$) is applied at both member's end sections, the distribution functions of all methods show again a larger variability. Largest standard deviations σ_Δ were obtained for method ECCS-Van Impe, Method 1 and Method 2 (Figs. 5.25 - 5.27) with a maximum of 155.5% for profile IPE600 according to Method 2. Although method Vandepitte was proved to be unsafe for different μ values, due to the smaller variability on the deviations of the LPF and with mean values of the different profiles close to 0, it should be noted the Vandepitte method (Fig. 5.24) is less conservative compared to the other methods, for which a large safety is obtained for longer length members. Finally, it can be remarked that a lower mean value and standard deviation are obtained for profiles HE320M and that in general the variability of the deviations according to Method 1 is lower for all considered sections.

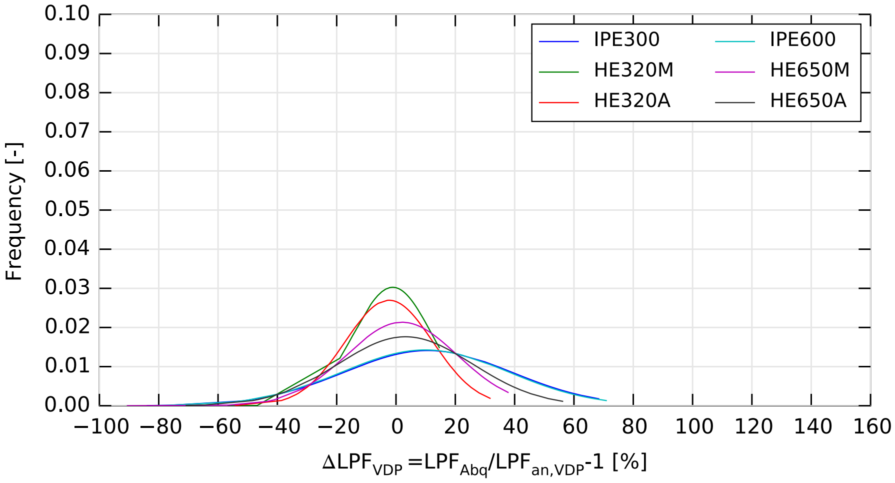

Figure 5.24: Normal PDF of ΔLPF according to method ECCS-VDP ($\psi = -1$).

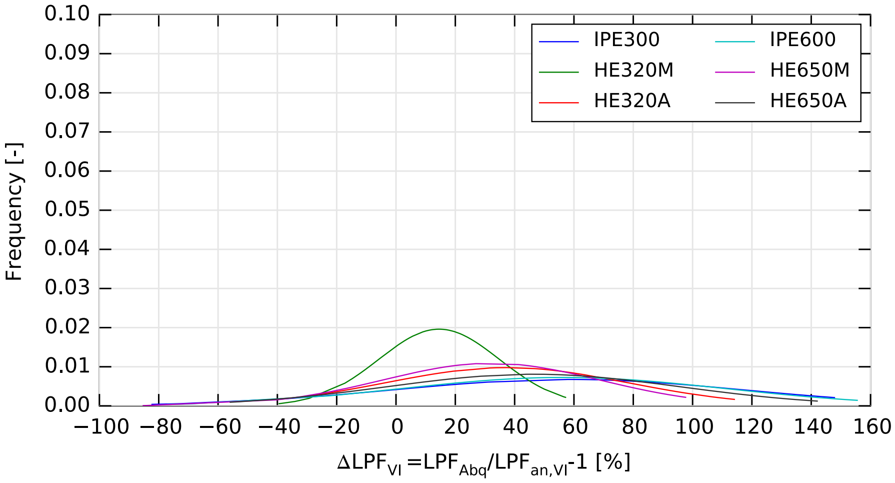

Figure 5.25: Normal PDF of ΔLPF according to method ECCS-VI ($\psi = -1$).

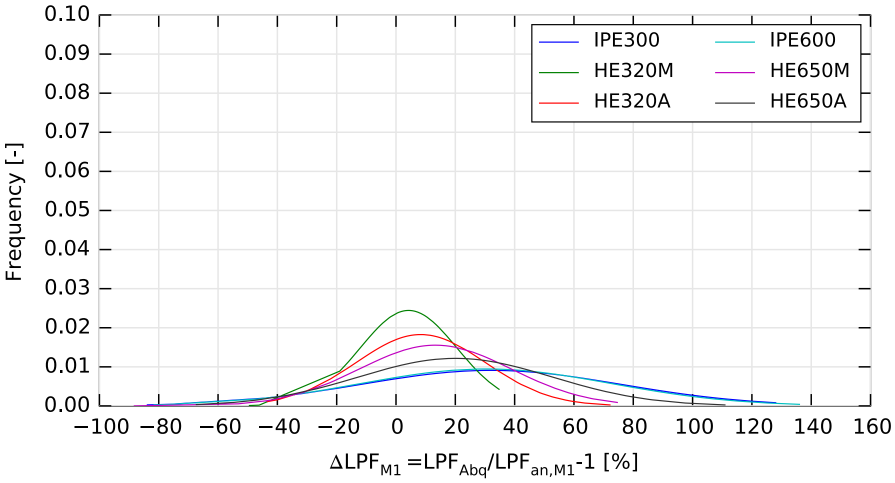

Figure 5.26: Normal PDF of ΔLPF according to Method 1 ($\psi = -1$).

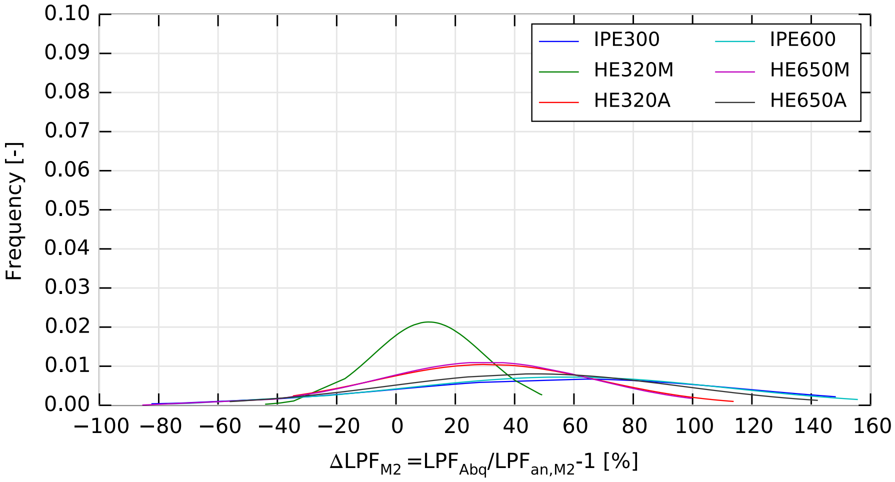

Figure 5.27: Normal PDF of ΔLPF according to Method 2 ($\psi = -1$).

5.8 Influence of the dimensions of the web openings and web post width

As indicated in Section 5.1.1, four different combinations were considered for each profile (Table 5.2). The factors were altered per profile to meet the geometrical restrictions, but in general combinations c_2 and c_4 correspond to large web openings ($f_a = 1.2$), whereas a large web post between the openings and at the end sections is aimed for with combinations c_3 and c_4. A possible influence of the cross-section geometry on the design rules is illustrated in Fig. 5.28 for Method 2, but similar observations are possible for other methods. In general, it can be concluded that there are no significant differences between the observed combinations, due to which general conclusions regarding design rules can be drawn for all combinations. Minor remarks: for $\psi = 0$ and $\psi = -1$, a larger variability can be noticed for combination c_2. Furthermore, for combination c_4, distribution functions of all ψ values show the largest mean value.

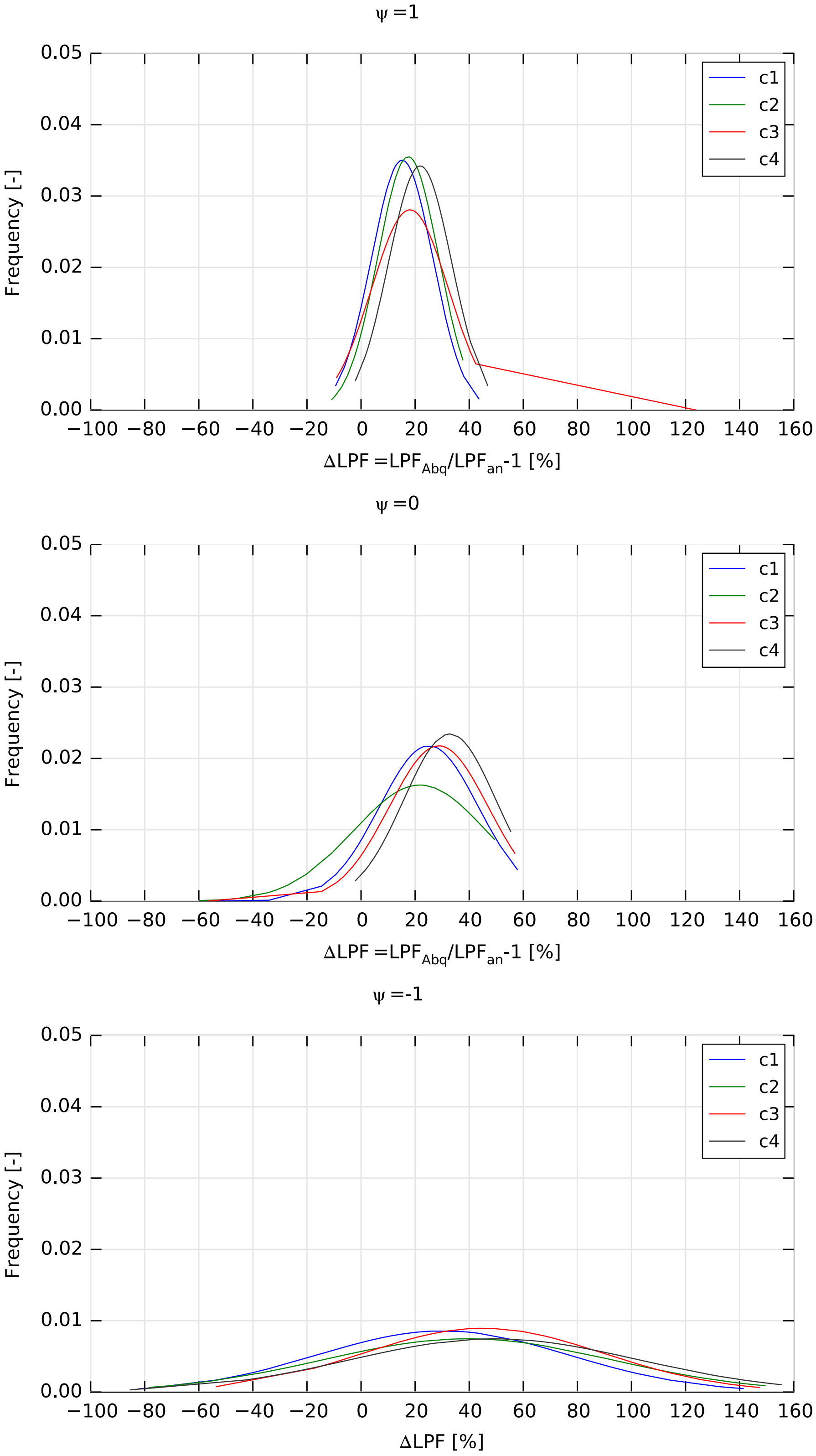

Figure 5.28: Influence dimensions web openings on design rule Method 2.

5.9 Comparison of the different methods

In this section the deviations between the numerical and analytical values of the load proportionality factor are compared for the four considered methods. The results are again plotted by means of normal probability density functions. It should be noted that the plots are made based on results of all profiles and considering the seven different μ values of Table 3.1, but that a distinction was made between different ψ values. What follows is a summary of the safety and applicability of the different design rules based on Fig. 5.29. An overview of the parameters characterizing the probability density functions is given in Appendix B.
As observed in Section 5.7, the largest insecurity is obtained for method Vandepitte with the largest negative deviations (-90.6%) for $\psi = -1$. It should however be noted that with this design rule the smallest standard deviation is obtained for all ψ values. Although application of the method is unsafe for short length members, a better correspondence with the numerical results is obtained for longer lengths.

Comparable results are obtained from application of method Van Impe and Method 2, where it can be remarked that these design rules are very conservative for short length members with a maximum deviation of 155.5% for Method 2. Method 1 can therefore serve as a good alternative since the analytically obtained results are less conservative, although application of the method is only unsafe in the range of shorter lengths.

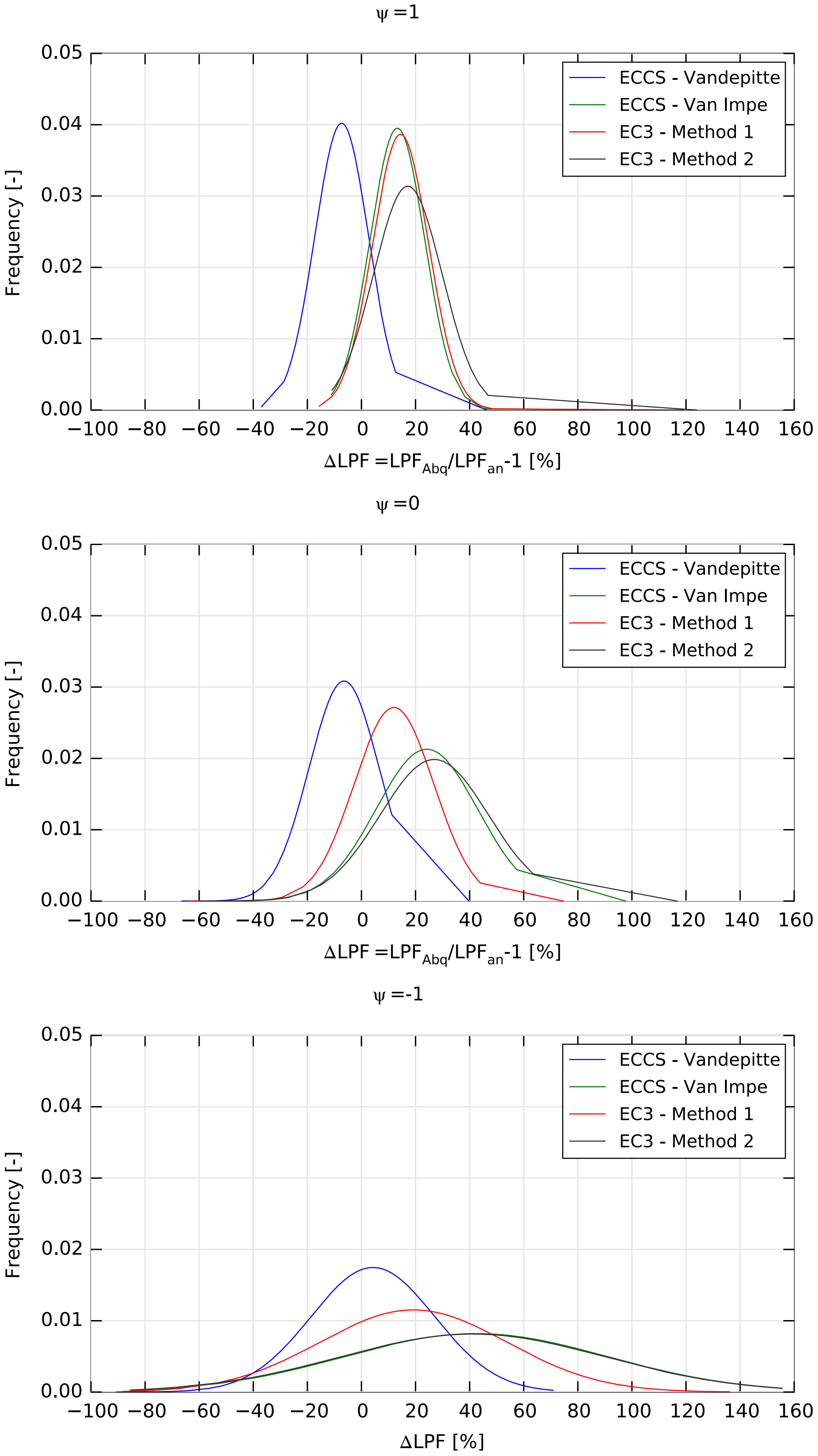

Figure 5.29: Normal PDF of ΔLPF according to four different methods.

Chapter 6

General conclusions and further research

As conclusion, general answers will be provided to the research questions of Chapter 1, Section 1.7. The formulations provided by the ECCS (ECCS-Vandepitte and ECCS-Van Impe) and the design rules adopted in EC3 (EC3-Method 1 and EC3-Method 2) regarding eccentrically loaded members can be applied for both plain-webbed members and cellular members. It should however be noticed that additional failure modes might be observed for cellular members, such as web-post buckling. For cellular members, a 2T approach was applied considering the cross-section characteristics at the centre of the openings. Adapted buckling curves were used (Section 2.6) to take into account the adapted residual stress pattern of cellular members. Best fitting buckling curves for members subjected to combined bending and compression were also derived in Section 5.2.3. It can be concluded that the the four considered design rules are unsafe for short length members and conservative for longer lengths. Design rule Vandepitte was observed to be still unsafe for intermediate lengths, but can serve as a good alternative for longer lengths, due to the conservative results obtained by other methods.

In this work the preliminary residual stress pattern proposed in (Sonck, 2014) for cellular members was already implemented in the numerical model, although further research should be performed, especially to confirm if the proposed pattern is still applicable for heavier parent sections. Furthermore, further research can be performed to adapt the four proposed design rules for eccentrically loaded members considering the unsafe results for short length members and the conservative approach for long lengths. Finally, one should be aware of the impact of the cross-section classification on the proposed design rules and the conclusions made in this work should be reconsidered in case of further adaptations to the existing cross-section classification of EC3.

Part III

Appendices

Appendix A

Sectional properties

A.1 Plain-webbed members

Based on the notations in Fig. 2.2, the formulas for the second moments of area around the y- and z-axis (I_y and I_z), the polar moment of area I_0, the torsional constant I_t and the warping constant I_w are given by Equations A.1.1-A.1.5.

$$I_y = 2\frac{bt_f^3}{12} + 2bt_f\left(\frac{h-t_f}{2}\right)^2 + \frac{(h-t_f)^3\,t_w}{12} \tag{A.1.1}$$

$$I_z = 2\frac{b^3t_f}{12} + \frac{(h-t_f)\,t_w^3}{12} \tag{A.1.2}$$

$$I_0 = I_y + I_z \tag{A.1.3}$$

$$I_t = \frac{(h-t_f)t_w^3}{16}\left[\frac{16}{3} - 3.36\frac{t_w}{(h-t_f)}\left(1 - \frac{t_w^4}{12(h-t_f)^4}\right)\right] + 2\frac{bt_f^3}{16}\left[\frac{16}{3} - 3.36\frac{t_f}{b}\left(1 - \frac{t_f^4}{12b^4}\right)\right] \tag{A.1.4}$$

$$I_w = \frac{(h-t_f)^2 I_z}{4} \tag{A.1.5}$$

The elastic section moduli $W_{y,el}$ and $W_{z,el}$ for respectively strong- and weak-axis bending are given in Equations A.1.6 and A.1.7. The plastic section moduli are determined by Eqs. A.1.8 - A.1.9.

$$W_{y,el} = \frac{2I_y}{h-t_f} \tag{A.1.6}$$

$$W_{z,el} = \frac{2I_z}{b} \tag{A.1.7}$$

$$W_{y,pl} = bt_f(h-t_f) + \left(\frac{h-t_f}{2}\right)^2 t_w \tag{A.1.8}$$

$$W_{z,pl} = t_f\frac{b^2}{2} + (h-t_f)\frac{t_w^2}{4} \tag{A.1.9}$$

$$A = 2bt_f + (h-t_f)t_w \tag{A.1.10}$$

A.2 Cross-section classification plain-webbed members according to (CEN, 2005)

Table A.1: Maximum width-to thickness ratios for compression parts (1) (CEN, 2005).

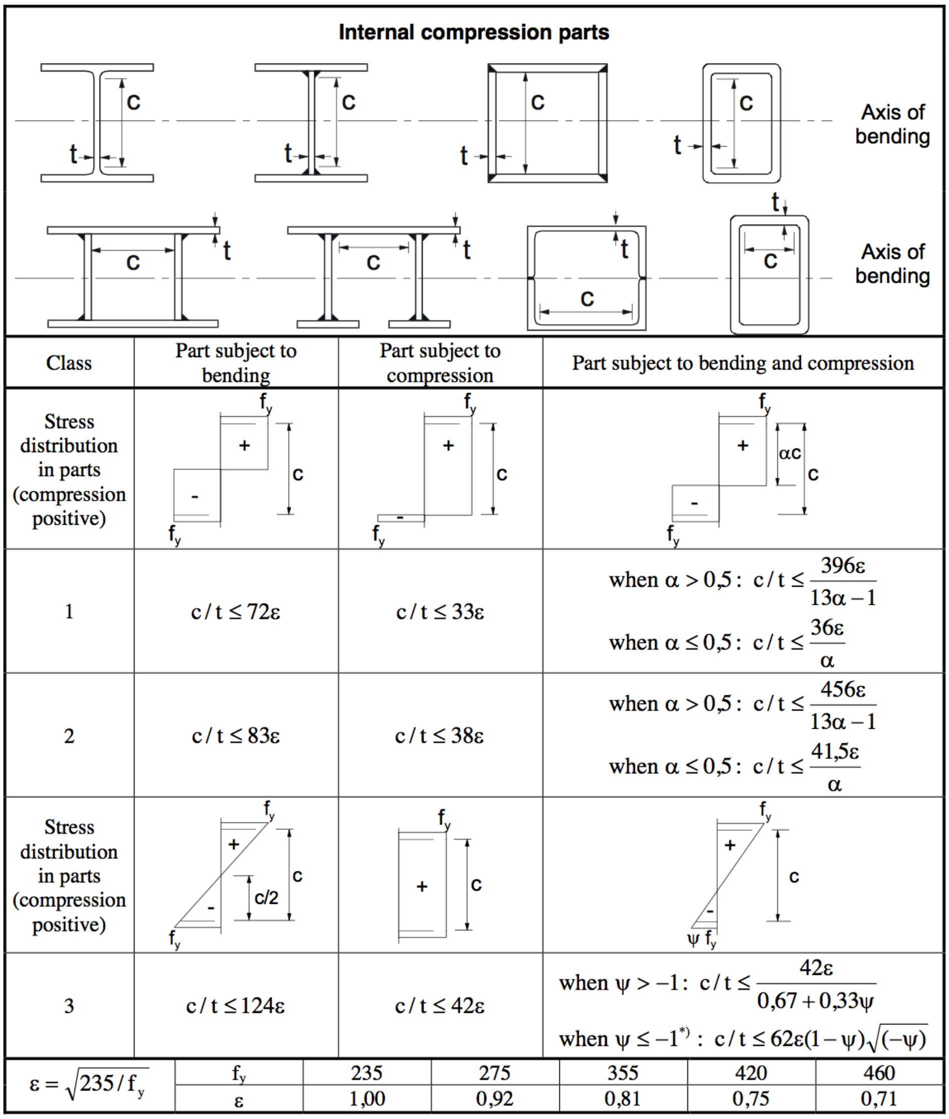

Internal compression parts
c
t
Axis of bending
c
t
Axis of bending
+
-
f_y
c
αc
c/2
ψf_y

Class	Part subject to bending	Part subject to compression	Part subject to bending and compression
Stress distribution in parts (compression positive)			
1	$c/t \leq 72\varepsilon$	$c/t \leq 33\varepsilon$	when $\alpha > 0{,}5$: $c/t \leq \frac{396\varepsilon}{13\alpha - 1}$ when $\alpha \leq 0{,}5$: $c/t \leq \frac{36\varepsilon}{\alpha}$
2	$c/t \leq 83\varepsilon$	$c/t \leq 38\varepsilon$	when $\alpha > 0{,}5$: $c/t \leq \frac{456\varepsilon}{13\alpha - 1}$ when $\alpha \leq 0{,}5$: $c/t \leq \frac{41{,}5\varepsilon}{\alpha}$
Stress distribution in parts (compression positive)			
3	$c/t \leq 124\varepsilon$	$c/t \leq 42\varepsilon$	when $\psi > -1$: $c/t \leq \frac{42\varepsilon}{0{,}67 + 0{,}33\psi}$ when $\psi \leq -1^{*)}$: $c/t \leq 62\varepsilon(1-\psi)\sqrt{(-\psi)}$

$\varepsilon = \sqrt{235/f_y}$	f_y	235	275	355	420	460
	ε	1,00	0,92	0,81	0,75	0,71

*) $\psi \leq -1$ applies where either the compression stress $\sigma \leq f_y$ or the tensile strain $\varepsilon_y > f_y/E$

A.3 FB curve selection according to (CEN, 2005)

A.4 Cellular members

The 2T approach is adopted in the European pre-standard ENV3, Annex N (CEN, 1998). The formulas of the cross-sectional properties corresponding to this approach are given by Equations A.4.2-A.4.5 for a height H of the cellular member.

$$H = h + \frac{\sqrt{(a + 2r_b)^2 - w^2}}{2} \tag{A.4.1}$$

Table A.2: Maximum width-to thickness ratios for compression parts (2) (CEN, 2005).

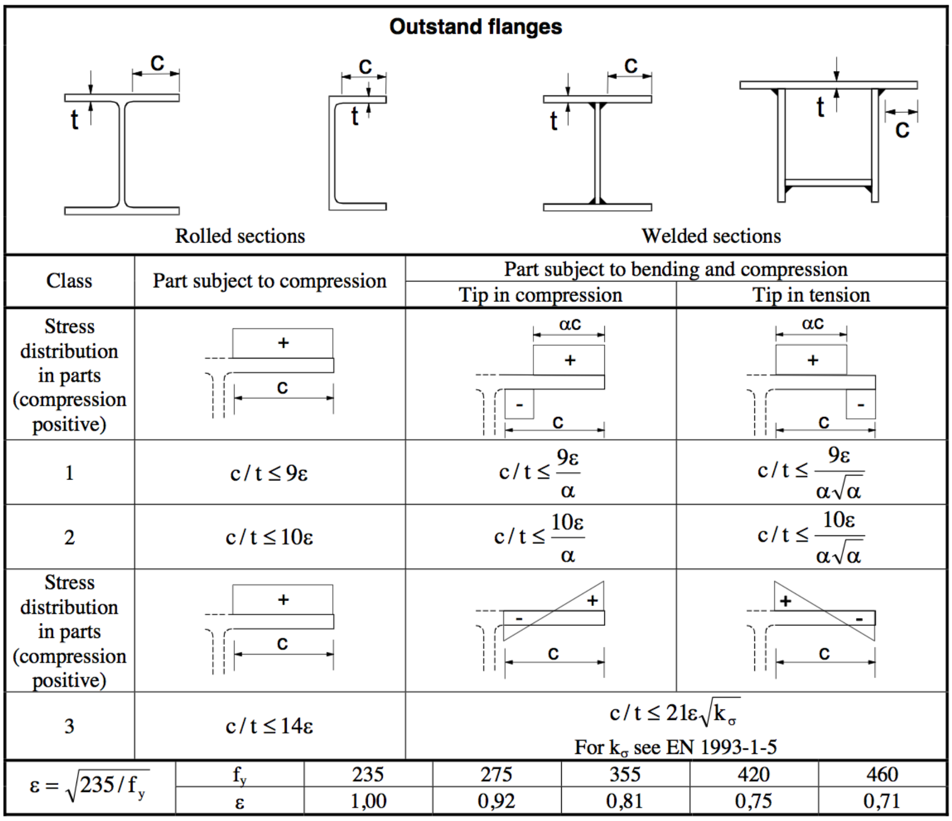

Outstand flanges

Rolled sections | Welded sections

Class	Part subject to compression	Part subject to bending and compression	
		Tip in compression	Tip in tension
Stress distribution in parts (compression positive)	+ c	αc + - c	αc + - c
1	$c/t \le 9\varepsilon$	$c/t \le \frac{9\varepsilon}{\alpha}$	$c/t \le \frac{9\varepsilon}{\alpha\sqrt{\alpha}}$
2	$c/t \le 10\varepsilon$	$c/t \le \frac{10\varepsilon}{\alpha}$	$c/t \le \frac{10\varepsilon}{\alpha\sqrt{\alpha}}$
Stress distribution in parts (compression positive)	+ c	+ - c	+ - c
3	$c/t \le 14\varepsilon$	$c/t \le 21\varepsilon\sqrt{k_\sigma}$ For k_σ see EN 1993-1-5	

$\varepsilon = \sqrt{235/f_y}$	f_y	235	275	355	420	460
	ε	1,00	0,92	0,81	0,75	0,71

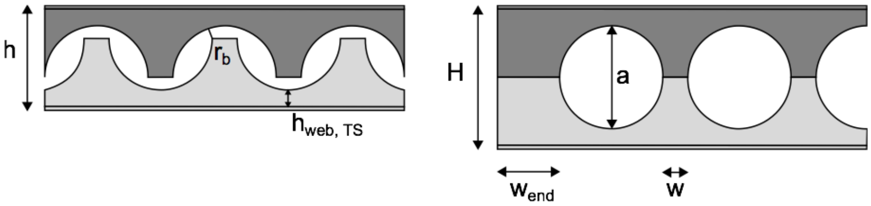

Figure A.1: Dimensions cross-section parent section and cellular member.

$$I_{z,2T} = 2\frac{b^3 t_f}{12} + \frac{(H - t_f - a)t_w^3}{12} \tag{A.4.2}$$

$$I_{y,2T} = \frac{(H - t_f - a)^3 t_w}{12} + 2\left[\frac{bt_f^3}{12} + bt_f\left(\frac{H - t_f - a}{2}\right)^2\right] \tag{A.4.3}$$

$$I_{w,2T} = \frac{h^2}{2}\frac{b^3 t_f}{12} \tag{A.4.4}$$

$$\begin{aligned} I_{t,2T} = \frac{(H - t_f - a)t_w^3}{16}&\left[\frac{16}{3} - 3.36\frac{t_w}{(H - t_f - a)}\left(1 - \frac{t_w^4}{12(H - t_f - a)^4}\right)\right] \\ &+2\frac{bt_f^3}{16}\left[\frac{16}{3} - 3.36\frac{t_f}{b}\left(1 - \frac{t_f^4}{12b^4}\right)\right] \end{aligned} \tag{A.4.5}$$

A.5 Geometrical constraints

Constraints for cellular members according to (CTICM, 2006):

Table A.3: Selection of buckling curves for flexural buckling (CEN, 2005).

Cross section		Limits		Buckling about axis	Buckling curve	
					S 235 S 275 S 355 S 420	S 460
Rolled sections	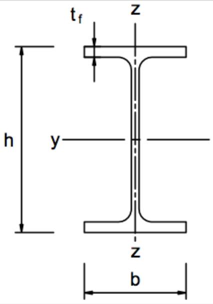	$h/b > 1{,}2$	$t_f \le 40$ mm	y – y z – z	a b	a_0 a_0
			40 mm $< t_f \le 100$	y – y z – z	b c	a a
		$h/b \le 1{,}2$	$t_f \le 100$ mm	y – y z – z	b c	a a
			$t_f > 100$ mm	y – y z – z	d d	c c
Welded I-sections	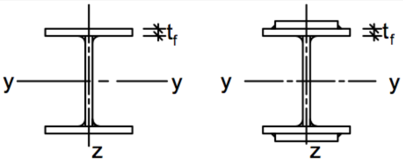	$t_f \le 40$ mm		y – y z – z	b c	b c
		$t_f > 40$ mm		y – y z – z	c d	c d
Hollow sections	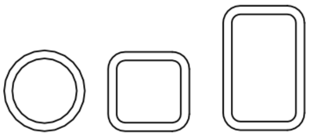	hot finished		any	a	a_0
		cold formed		any	c	c
Welded box sections	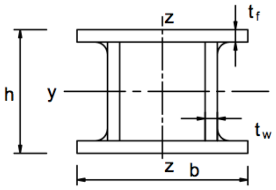	generally (except as below)		any	b	b
		thick welds: $a > 0{,}5t_f$ $b/t_f < 30$ $h/t_w < 30$		any	c	c
U-, T- and solid sections	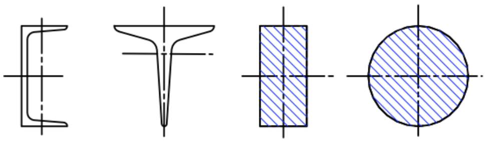			any	c	c
L-sections	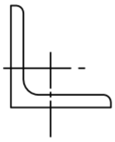			any	b	b

$$(1) \quad \frac{a}{t_w} \leq 90 \tag{A.5.1}$$

$$(2) \quad 0.08 l_0 \leq w \leq 0.75 l_0 \quad (l_0 = a \text{ for cellular beams}) \tag{A.5.2}$$

$$(3) \quad 50\, mm \leq w \tag{A.5.3}$$

$$(4) \quad \frac{H}{a} \geq 1.25 \tag{A.5.4}$$

$$(5) \quad \frac{H}{a} \leq 4 \tag{A.5.5}$$

$$(6) \quad \frac{h_{web}}{t_w} \leq 124\epsilon \quad \text{with} \quad \epsilon = \sqrt{\frac{235}{f_y}} \quad \text{and} \quad h_{web} = H - 2t_f \tag{A.5.6}$$

$$(7) \quad h_{web,TS} - r > 0.01\, m \quad \text{with} \quad h_{web,TS} = \frac{H - 2t_f - a}{2} \tag{A.5.7}$$

$$(8) \quad h_{web,TS} > 0.03\, m \tag{A.5.8}$$

(7) and (8) are practical constraints to ascertain enough room for the nozzle during cutting of the web of the parent section.

Appendix B

Design rules eccentrically loaded members

B.1 Overview stability design rules simply supported members

In this section a summary is given of the applied stability design rules, specifically for simply supported members with fork supports subjected to a strong-axis bending moment M_y and an axial load N.

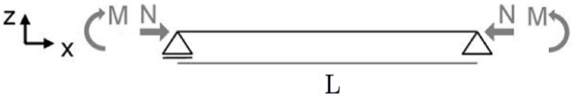

Figure B.1: Members subjected to strong-axis bending moment M_y and axial load N.

B.1.1 ECCS - Vandepitte

1. Buckling in XZ-plane:
$$\frac{N}{A} + \frac{\theta\beta_y|M_{1y}| + N\overline{w_0}}{\left(1-\frac{N}{N_{cr,y}}\right)W_y} \leq f_y \tag{B.1.1}$$

2. Buckling in XY-plane:
$$\frac{N}{A} + \frac{\theta\beta_y|M_{1y}|}{\left(1-\frac{N}{N_{cr,y}}\right)W_y} + \frac{N\overline{v_0}}{\left(1-\frac{N}{N_{cr,z}}\right)W_z} \leq f_y \tag{B.1.2}$$

$$\theta = \left[1 + \left(\frac{\alpha f_y}{\sigma_{cr}}\right)^{2.5}\right]^{\frac{1}{2.5}} \qquad \sigma_{cr} = \frac{M_{cr}}{W_{el,y}} \text{ and } \alpha = \frac{W_{pl,y}}{W_{el,y}} \tag{B.1.3}$$

$$\overline{w}_0 = \left(1 - \frac{N_{b,y,Rd}}{N_{cr,y}}\right)\left(\frac{N_{pl}}{N_{b,y,Rd}} - 1\right)\frac{W_y}{A} \tag{B.1.4}$$

$$\overline{v}_0 = \left(1 - \frac{N_{b,z,Rd}}{N_{cr,z}}\right)\left(\frac{N_{pl}}{N_{b,z,Rd}} - 1\right)\frac{W_z}{A} \tag{B.1.5}$$

3. $N \leq N_{b,y,Rd} = \nu A f_y \omega$ (B.1.6)

4. $N \leq N_{b,z,Rd} = \nu A f_y \omega$ (B.1.7)

where for **3.** and **4.**:
$$\nu = \frac{1}{2\overline{\lambda}^2}\left[1 + \alpha\left(\overline{\lambda} - 0.2\right) + \overline{\lambda}^2 - \sqrt{\left[1 + \alpha\left(\overline{\lambda} - 0.2\right) + \overline{\lambda}^2\right]^2 - 4\overline{\lambda}^2}\right] \tag{B.1.8}$$

In Eq. B.1.8, $\overline{\lambda} = \overline{\lambda}_y$ in $N_{b,y,Rd}$ and $\overline{\lambda} = \overline{\lambda}_z$ in $N_{b,z,Rd}$. Imperfection factor α is given in Table 2.2.

5. $\theta|M_{1y}| \leq M_{y,Rd} = W_y f_y$ (θ according to Eq. B.1.3) (B.1.9)

6. Cross-section resistance of end sections

$\underline{\text{CS} \leq 3}$

6.a. Most outward fibre $\quad \text{M} \leq M_{N,y,Rd}$ (B.1.10)

IPE profiles:

$$\frac{M_{N,y,Rd}}{M_{pl,y}} = 1 \text{ if } \frac{N_{Ed}}{N_{pl}} \geq 0.18; \quad \frac{M_{N,y,Rd}}{M_{pl,y}} = 1.22\left(1 - \frac{N_{Ed}}{N_{pl}}\right) \text{ if } \frac{N_{Ed}}{N_{pl}} \geq 0.18 \tag{B.1.11}$$

HE profiles:

$$\frac{M_{N,y,Rd}}{M_{pl,y}} = 1 \text{ if } \frac{N_{Ed}}{N_{pl}} \leq 0.1; \quad \frac{M_{N,y,Rd}}{M_{pl,y}} = 1.11\left(1 - \frac{N_{Ed}}{N_{pl}}\right) \text{ if } \frac{N_{Ed}}{N_{pl}} \geq 0.1 \tag{B.1.12}$$

$$\text{where } N_{pl} = Af_y \quad \text{and } M_{pl,y} = W_{pl,y}f_y \tag{B.1.13}$$

$\underline{CS > 3} : max(\mathbf{6b.}, \mathbf{6c.}, \mathbf{6d.})$ (B.1.14)

6b. Most outward fibre $\quad \dfrac{N}{N_{pl}} + \dfrac{M_{1y}}{W_{el,y}f_y} \leq 1.$ (B.1.15)

6c. Fibre located at the web-to-flange transition (B.1.16)

$$\sqrt{\sigma_2^2 + 3\tau_2^2} \leq f_y \tag{B.1.17}$$

$$\text{where } \sigma_2 = \frac{N}{A} + \frac{M_{1y}(h/2 - t_f)}{I_y}; \quad S_2 = t_f b\frac{h - t_f}{2}; \quad \tau_2 = \frac{V_{Ed}S_2}{t_w I_y} \tag{B.1.18}$$

6d. Central fibre (B.1.19)

$$\sqrt{\sigma_3^2 + 3\tau_3^2} \leq f_y \tag{B.1.20}$$

$$\text{where } \sigma_3 = \frac{N}{A} + \frac{M_{1y}(h/2 - t_f)}{I_y}; \quad S_3 = t_f b\frac{(h - t_f)}{2} + \frac{(h - t_f)}{2}\frac{t_w(h - t_f)}{4}; \quad \tau_3 = \frac{V_{Ed}S_3}{t_w I_y} \tag{B.1.21}$$

B.1.2 ECCS - Van Impe

1. Buckling y-y: $\quad \dfrac{N}{A} + \dfrac{\beta_y|M_{1y}| + N|\overline{w_0}|}{\left(1 - \frac{N}{N_{cr,y}}\right)W_y} \leq f_y$ (B.1.22)

2. Buckling z-z: $\quad \dfrac{N}{A} + \dfrac{|M_{1y}|}{\left(1 - \frac{N}{N_{cr,y}}\right)W_y} + \dfrac{|M_{1y}|\phi_0 + N|\overline{v_0}|}{\left(1 - \frac{N}{N_{cr,z}} - \frac{M_{1y}^2}{M_{cr}^2}\right)W_z} \leq f_y$ (B.1.23)

$$\text{where } \phi_0 = \left(1 - \frac{M_{b,Rd}^2}{M_{cr}^2}\right)\left(f_y - \frac{M_{b,Rd}}{W_y}\right)\frac{W_z}{M_{b,Rd}} \tag{B.1.24}$$

$M_{b,Rd}$ is calculated according to Eq. 2.4.8 and for M_{cr} (Eq. 2.4.2) $I_t = I_{t,avg}$ (Eq. 5.1.12) is used.

3. $N \leq N_{b,y,Rd} = \dfrac{\chi_y A f_y}{\gamma_{M1}}$ Eq. 2.3.4 (B.1.25)

4. $N \leq N_{b,z,Rd} = \dfrac{\chi_z A f_y}{\gamma_{M1}}$ Eq. 2.3.4 (B.1.26)

5. Cross-section resistance of end sections: max (**5a.**,**5b.**, **5c.**)

5a. Most outward fibre

CS < 3

N $> 0.25\ N_{pl}$ or N $> 0.5ht_wf_y/\gamma_{M0}$

$$(i)\quad \frac{1-N/N_{pl}}{1-0.5a} \leq 1 \rightarrow M_{N,y,Rd} = W_y f_{y,red}\frac{1-N/N_{pl}}{1-0.5a} \quad \text{where } a = \min\left(\frac{A-2bt_f}{A};0.5\right) \tag{B.1.27}$$

$$(ii)\quad \frac{1-N/N_{pl}}{1-0.5a} \geq 1 \rightarrow M_{N,y,Rd} = W_y f_{y,red} \tag{B.1.28}$$

$N \leq 0.25N_{pl}$ or $N \leq 0.5ht_wf_y/\gamma_{M0}$

$$M_{N,y,Rd} = W_y f_{y,red} \tag{B.1.29}$$

$$\text{Condition: } M_{1y} \leq M_{N,y,Rd} \tag{B.1.30}$$

CS < 3

$$\frac{N}{N_{pl}} + \frac{M_{1y}}{W_{el,y}f_y} \leq 1. \tag{B.1.31}$$

5b. Fibre located at the web-to-flange transition

$$\text{CS} < 3: \quad N \leq N_{pl,Rd} \tag{B.1.32}$$

$$\text{CS} \geq 3: \quad \sqrt{\sigma_2^2 + 3\tau_2^2} \leq f_y \tag{B.1.33}$$

$$\text{where } \sigma_2 = \frac{N}{A} + \frac{M_{1y}(h/2-t_f)}{I_y}; \quad S_2 = t_f b(h/2 - t_f/2); \quad \tau_2 = \frac{V_{Ed}S_2}{t_w I_y} \tag{B.1.34}$$

5c. Central fibre

$$\text{CS} \leq 3{:}V \leq V_{pl,Rd} \tag{B.1.35}$$

$$\text{CS} > 3: \quad \sqrt{\sigma_3^2 + 3\tau_3^2} \leq f_y \tag{B.1.36}$$

$$\text{where } \sigma_3 = \frac{N}{A} + \frac{M_{1y}(h/2-t_f)}{I_y}; \quad S_3 = t_f b\frac{(h-t_f)}{2} + \frac{(h-t_f)}{2}\frac{t_w(h-t_f)}{4}; \quad \tau_3 = \frac{V_{Ed}S_3}{t_w I_y} \tag{B.1.37}$$

B.1.3 EC3 - Method 1

1. Buckling y-y:

$$\frac{N_{Ed}}{\chi_y N_{pl,Rd}} + \mu_y \left[\frac{C_{mLT}}{\chi_{LT}} \frac{C_{my} M_{y,Ed}}{\left(1 - \frac{N_{Ed}}{N_{cr,y}}\right) C_{yy} W_y f_y} \right] \leq 1 \tag{B.1.38}$$

2. Buckling z-z

$$\frac{N_{Ed}}{\chi_z N_{pl,Rd}} + \mu_z \left[0.6 \sqrt{\frac{w_y}{w_z}} \frac{C_{mLT}}{\chi_{LT}} \frac{C_{my} M_{y,Ed}}{\left(1 - \frac{N_{Ed}}{N_{cr,y}}\right) C_{zy} W_y f_y} \right] \leq 1 \tag{B.1.39}$$

$$\mu_y = \frac{1 - N_{Ed}/N_{cr,y}}{1 - \chi_y N_{Ed}/N_{cr,y}}; \quad \mu_z = \frac{1 - N_{Ed}/N_{cr,z}}{1 - \chi_z N_{Ed}/N_{cr,z}} \tag{B.1.40}$$

$$\underline{\text{CS} < 3}: \quad w_y = \min(W_{pl,y}/W_{el,y}; 1.5); \quad w_y = \min(W_{pl,z}/W_{el,z}; 1.5) \tag{B.1.41}$$

$$\underline{\text{CS} > 3}: \quad w_y = w_z = 1 \tag{B.1.42}$$

$$C_{mLT} = \frac{C_{my}^2 a_{LT}}{\sqrt{\left(1 - \frac{N_{Ed}}{N_{cr,z}}\right)\left(1 - \frac{N_{Ed}}{N_{cr,T}}\right)}} \geq 1 \tag{B.1.43}$$

$$C_{mz} = C_{mz,0} = 0.79 + 0.21\psi + 0.36(\psi - 0.33)\frac{N}{N_{cr,z}} \tag{B.1.44}$$

$$C_{my,0} = 0.79 + 0.21\psi + 0.36(\psi - 0.33)\frac{N}{N_{cr,y}} \tag{B.1.45}$$

$$C_{my} = C_{my,0} + (1 - C_{my,0})\frac{\sqrt{\epsilon_y} a_{LT}}{1 + \sqrt{\epsilon_y} a_{LT}} \tag{B.1.46}$$

$$\text{where} \quad \epsilon_y = \frac{M_{y,Ed}}{N_{Ed}} \frac{A}{W_{el,y}} \quad (\text{CS 1-3}); \quad a_{LT} = 1 - \frac{I_T}{I_y} \geq 0 \tag{B.1.47}$$

$$C_{yy} = 1 + (w_y - 1)\left[2 - \frac{1.6}{w_y} C_{my}^2 \left(\overline{\lambda}_{max} + \overline{\lambda}_{max}^2\right) \frac{N}{N_{pl}} - b_{LT}\right] \geq \frac{1}{w_y} \tag{B.1.48}$$

$$C_{zy} = 1 + (w_y - 1)\left[\left(2 - 14\frac{C_{my}^2 \overline{\lambda}_{max}^2}{w_y^5}\right) \frac{N}{N_{pl}} - d_{LT}\right] \geq \frac{0.6}{\sqrt{w_y w_z}} \tag{B.1.49}$$

$$b_{LT} = d_{LT} = 0 \quad (M_{z,Ed} = 0) \tag{B.1.50}$$

3. $$N \leq N_{b,y,Rd} = \frac{\chi_y A f_y}{\gamma_{M1}} \quad \text{Eq. 2.3.4} \tag{B.1.51}$$

4. $$N \leq N_{b,z,Rd} = \frac{\chi_z A f_y}{\gamma_{M1}} \quad \text{Eq. 2.3.4} \tag{B.1.52}$$

5. Cross-section resistance of end sections: Idem Van Impe (Condition 5)

B.1.4 EC3 - Method 2

1. Buckling y-y:

$$\frac{N_{Ed}}{\chi_y N_{pl,Rd}} + k_y \frac{C_{my} M_{y,Ed}}{\chi_{LT} M_{pl,y,Rd}} \leq 1 \tag{B.1.53}$$

2. Buckling z-z:

$$\frac{N_{Ed}}{\chi_z N_{pl,Rd}} + k_{LT} \frac{M_{y,Ed}}{\chi_{LT} M_{pl,y,Rd}} \leq 1 \tag{B.1.54}$$

$$k_{LT} = 1 - \frac{0.1\overline{\lambda}_z n_z}{C_{mLT} - 0.25} \geq 1 - \frac{0.1 n_z}{C_{mLT} - 0.25} \tag{B.1.55}$$

$$k_{LT} = 0.6 + \overline{\lambda}_z \leq 1 - \frac{0.1\overline{\lambda}_z}{C_{mLT} - 0.25} n_z \qquad \left[\overline{\lambda}_z < 0.4\right] \tag{B.1.56}$$

$$C_{mLT} = 0.6 + 0.4\psi \geq 0.4 \tag{B.1.57}$$

$$n_z = \frac{N_{Ed}}{\chi_z N_{pl,Rd}} \tag{B.1.58}$$

3. Cross-section resistance of end sections: idem Van Impe (Condition 5)

B.2 Safety of the design rules

Table B.1: Overview μ values for which design rule ECCS-Vandepitte is unsafe. Values of μ for which no maximum was reached in the load-displacement diagram are given in brackets after *.

	Length [m]	$\psi = 1$	$\psi = 0$	$\psi = -1$
IPE120	1.2	$0 - 1 - 5 - 10 - \infty$	$0 - 0.5 - 1 - 5 - 10 - \infty$	$0 - 0.5 - 1 - 5 - 10 - \infty$
	3.6	$0.5 - 1 - 5 - 10 - \infty$	$0.5 - 1 - 5 - 10 - \infty$	$1 - 5 - 10 - \infty$
	6.0	$0.5 - 1 - 5$* (∞)	$0.5 - 1 - 5 - 10$	1
	8.4	$0.5 - 1$* (5,10,∞)	$0.5 - 1$* (5,10,∞)	1
HEA180	1.71	$0 - \infty$	$0 - 5$	0
	5.13	$1 - 5 - 10 - \infty$	$0.5 - 1 - 5 - 10 - \infty$	$0.5 - 1 - 5 - 10 - \infty$
	8.55	$1 - 5 - 10$	$0.5 - 1 - 5 - 10 - \infty$	$1 - 5 - 10 - \infty$
	11.97	1*(∞)	$0.5 - 1 - 5 - 10$	$1 - 5 - 10 - \infty$
IPE240	2.4	$1 - 5 - 10 - \infty$	$0.5 - 1 - 5 - 10 - \infty$	$0.5 - 1 - 5 - 10 - \infty$
	7.2	$0.5 - 1 - 5 - 10$	$0.5 - 1 - 5 - 10$	1
	12.0	$0.5 - 1$* (∞)	$0.5 - 1$* (∞)	1
	16.8	* (5,10,∞)	$0.5 - 1$* (10,∞)	1
HE300A	2.9	$10 - \infty$	$0 - 5$	0
	8.7	$0.5 - 1 - 5 - 10 - \infty$	$0.5 - 1 - 5 - 10 - \infty$	$0.5 - 1 - 5 - 10 - \infty$
	14.5	$0.5 - 1 - 5 - 10 - \infty$	$0.5 - 1 - 5 - 10 - \infty$	$1 - 5 - 10 - \infty$
	20.3	1*(∞)	$0.5 - 1 - 5 - 10$	1
IPEO360	3.64	$0 - 0.5 - 1 - 5 - 10 - \infty$	$0 - 0.5 - 1 - 5 - 10 - \infty$	$0 - 0.5 - 1 - 5 - 10 - \infty$
	10.92	$0.5 - 1 - 5 - 10 - \infty$	$0.5 - 1 - 5 - 10 - \infty$	1
	18.2	$0.5 - 1$	$0.5 - 1 - 5$	1
	25.48	0.5* (5,10,∞)	$0.5 - 1$	1
HE400A	3.9	$0 - 5 - 10 - \infty$	$0 - 5 - 10 - \infty$	$0 - 5$
	10.93	$0.5 - 1 - 5 - 10 - \infty$	$0.5 - 1 - 5 - 10 - \infty$	$0.5 - 1 - 5 - 10 - \infty$
	17.97	$0.5 - 1 - 5$	$0.5 - 1 - 5 - 10$	1-5-10-∞
	25.0	$0.5 - 1$* (∞)	$0.5 - 1 - 5$	1
IPEO450	4.56	$0 - 0.5 - 1 - 5 - 10 - \infty$	$0 - 0.5 - 1 - 5 - 10 - \infty$	$0 - 0.5 - 1 - 5 - 10 - \infty$
	11.37	$0.5 - 1 - 5 - 10 - \infty$	$0.5 - 1 - 5 - 10 - \infty$	1
	18.19	$0.5 - 1 - 5$	$0.5 - 1 - 5$	1
	25.0	$0.5 - 1$* (10,∞)	$0.5 - 1$	1
HE500A	4.9	$0 - 1 - 5 - 10 - \infty$	$0 - 0.5 - 1 - 5 - 10 - \infty$	$0 - 1 - 5 - 10 - \infty$
	11.6	$0.5 - 1 - 5 - 10 - \infty$	$0.5 - 1 - 5 - 10 - \infty$	$0.5 - 1 - 5 - 10 - \infty$
	18.3	$0.5 - 1 - 5 - 10 - \infty$	$0.5 - 1 - 5 - 10 - \infty$	1
	25	$0.5 - 1 - 5$	$0.5 - 1 - 5 - 10$	1
IPEO600	6.1	$0.5 - 1 - 5 - 10 - \infty$	$0.5 - 1 - 5 - 10 - \infty$	$0.5 - 1 - 5 - 10 - \infty$
	12.4	$0.5 - 1 - 5 - 10 - \infty$	$0.5 - 1 - 5 - 10 - \infty$	1
	18.7	$0.5 - 1 - 5 - 10$	$0.5 - 1 - 5 - 10$	1
	25	$0.5 - 1$	$0.5 - 1 - 5$	1
HEM700	7.16	$0.5 - 1 - 5 - 10 - \infty$	$0.5 - 1 - 5 - 10 - \infty$	$0.5 - 1 - 5 - 10 - \infty$
	13.11	$0.5 - 1 - 5 - 10 - \infty$	$0.5 - 1 - 5 - 10 - \infty$	$0.5 - 1 - 5 - 10 - \infty$
	19.05	$0.5 - 1 - 5 - 10 - \infty$	$0.5 - 1 - 5 - 10 - \infty$	$1 - 5 - 10 - \infty$
	25	$0.5 - 1 - 5 - 10$	$0.5 - 1 - 5 - 10 - \infty$	1

B.3 Deviation between $M_{cr,Abq}$ and $M_{cr,2T,avg}$ for cellular members.

Table B.2: Combinations with large deviations between $M_{cr,Abq}$ and $M_{cr,2T,avg}$ due to web-post buckling.

	ψ [-]	k [-]	L [m]	f_a [-]	f_w [-]	a [m]	w [m]	H [m]	$M_{cr,Abq}$ [kNm]	$M_{cr,2T,avg}$ [kNm]	ΔM_{cr} [%]
IPE300	0	1	2.18	0.80	0.10	0.24	0.024	0.41	443.19	976.94	-54.63
	0	1	2.48	1.20	0.10	0.36	0.036	0.47	304.12	865.62	-64.87
	0	1	2.14	0.80	0.70	0.24	0.168	0.37	773.84	936.07	-17.33
	0	1	2.28	1.10	0.65	0.33	0.215	0.41	709.76	911.62	-22.14
	-1	1	2.18	0.80	0.10	0.24	0.024	0.41	223.71	1435.06	-84.41
	-1	1	2.48	1.20	0.10	0.36	0.036	0.47	152.39	1271.54	-88.02
	-1	1	2.14	0.80	0.70	0.24	0.168	0.37	442.62	1375.02	-67.81
	-1	1	2.28	1.10	0.65	0.33	0.215	0.41	374.06	1339.10	-72.07
IPE600	0	1	4.37	0.80	0.10	0.48	0.048	0.83	2066.5	2836.21	-27.14
	0	1	4.97	1.20	0.10	0.72	0.072	0.95	1444.7	2506.12	-42.35
	-1	1	4.37	0.80	0.10	0.48	0.048	0.83	1069.3	4166.19	-74.33
	-1	1	4.97	1.20	0.10	0.72	0.072	0.95	727.8	3681.31	-80.23
	-1	1	4.27	0.80	0.70	0.48	0.336	0.76	1972.6	4032.86	-51.09
	-1	1	4.55	1.15	0.60	0.69	0.414	0.87	1586.4	4014.58	-60.48
HE320A	0	1	4.44	0.80	0.10	0.248	0.025	0.43	1709.0	2917.31	-41.42
	0	1	5.02	1.20	0.10	0.372	0.037	0.49	1191.4	2612.77	-54.40
	0	1	3.89	0.80	0.70	0.248	0.174	0.39	2373.6	3422.65	-30.65
	0	1	4.19	1.00	0.65	0.31	0.202	0.42	2441.5	3199.56	-23.69
	0	1	4.44	0.80	0.10	0.248	0.025	0.43	867.0	2917.31	-70.28
	-1	1	5.02	1.20	0.10	0.372	0.037	0.49	598.1	3837.97	-84.42
	-1	1	3.89	0.80	0.70	0.248	0.174	0.39	1683.3	5027.63	-66.52
	-1	1	4.19	1.00	0.65	0.31	0.202	0.42	1514.3	4699.92	-67.78
HE320M	-1	1	5.14	0.80	0.10	0.287	0.029	0.49	9602.8	13797.70	-30.40
	-1	1	5.50	1.05	0.10	0.377	0.038	0.54	7597.5	13011.55	-41.61
HE650A	0	1	4.66	0.80	0.10	0.512	0.051	0.89	3212.9	9103.81	-64.71
	0	1	5.30	1.20	0.10	0.768	0.077	1.01	2196.2	8061.10	-72.76
	0	1	4.56	0.80	0.70	0.512	0.358	0.81	6202.9	8782.83	-29.37
	0	1	4.86	1.15	0.60	0.736	0.442	0.92	5010.1	8756.43	-42.78
	-1	1	4.66	0.80	0.10	0.512	0.051	0.89	1615.4	13372.82	-87.92
	-1	1	5.30	1.20	0.10	0.768	0.077	1.01	1099.5	11841.17	-90.71
	-1	1	4.56	0.80	0.70	0.512	0.358	0.81	3240.9	12901.33	-74.88
	-1	1	4.86	1.15	0.60	0.736	0.442	0.92	2538.6	12862.56	-80.26
	-1	2	9.73	0.80	0.10	0.512	0.051	0.89	2801.3	3658.23	-23.42
	-1	2	10.37	1.20	0.10	0.768	0.077	1.01	1967.9	3586.48	-45.13
HE650M	0	1	4.86	0.80	0.10	0.534	0.053	0.93	11183.0	15003.74	-25.47
	0	1	5.53	1.20	0.10	0.802	0.080	1.06	7898.4	13271.91	-40.49
	-1	1	4.86	0.80	0.10	0.534	0.053	0.93	5801.6	22039.39	-73.68
	-1	1	5.53	1.20	0.10	0.802	0.080	1.06	3999.1	19495.46	-79.49
	-1	1	4.76	0.80	0.70	0.534	0.374	0.85	11444.0	21477.86	-46.72
	-1	1	5.07	1.15	0.60	0.768	0.461	0.97	9213.1	21249.48	-56.64

B.4 Flexural buckling: additional results for N_{Rd}

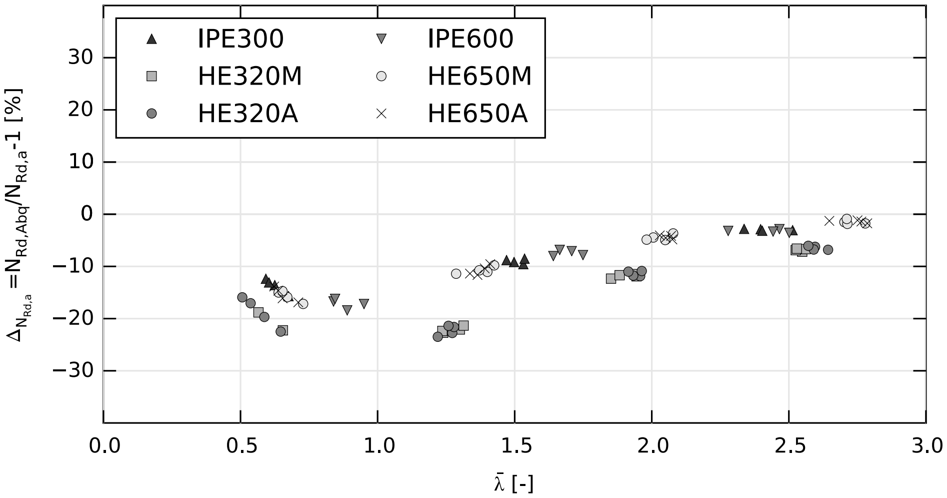

Figure B.2: FB curves: Deviations $N_{Rd,Abq}$ with buckling curve a.

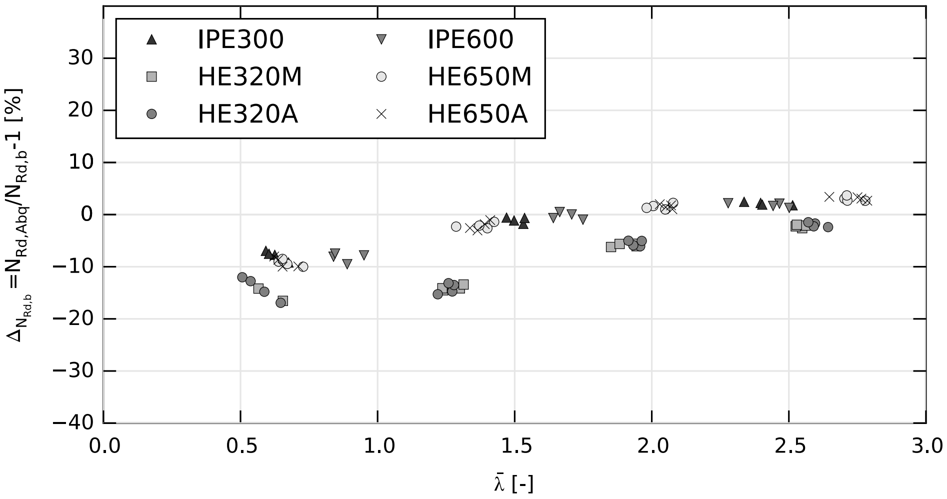

Figure B.3: FB curves: Deviations $N_{Rd,Abq}$ with buckling curve b.

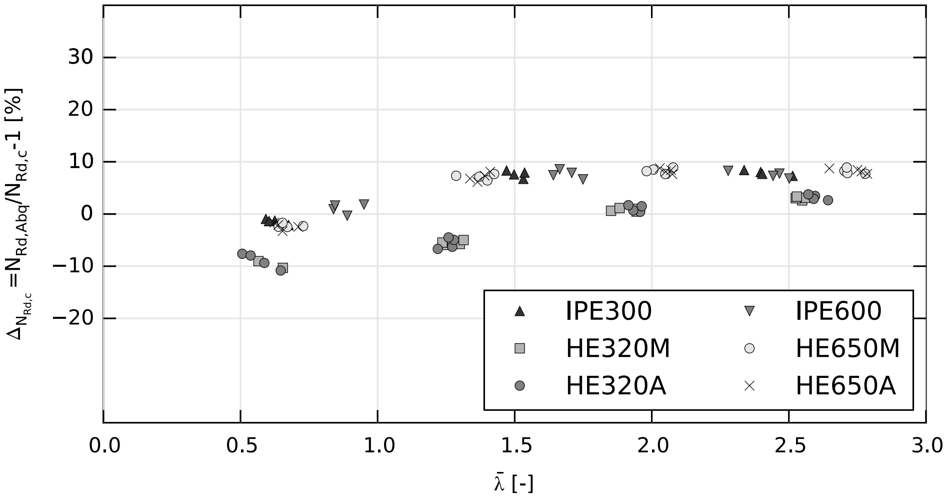

Figure B.4: FB curves: Deviations $N_{Rd,Abq}$ with buckling curve c.

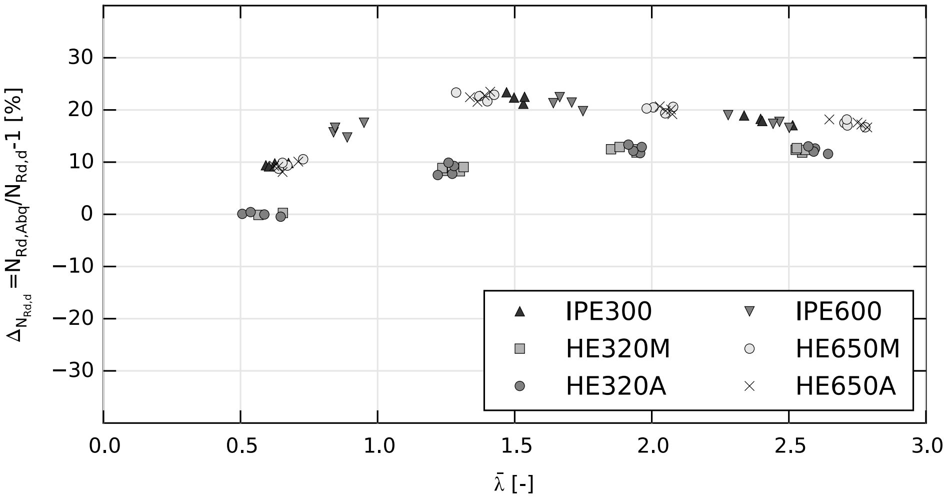

Figure B.5: FB curves: Deviations $N_{Rd,Abq}$ with buckling curve d.

Table B.3: Deviation of $N_{Rd,2T}$ for cellular members under pure compression. The underlined values indicate the best fitting EC3 buckling curves.

IPE300	$\Delta_{min}[\%]$	$\Delta_{max}[\%]$	$\Delta_{mean}[\%]$	$\Delta_{med}[\%]$	$\sum(\chi_{Abq} - \chi_{an})^2[-]$
$\Delta_{N_{Rd,a}}$	-15.7	4.0	-4.3	-3.0	0.06
$\Delta_{N_{Rd,b}}$	-9.2	7.2	0.9	2.1	0.017
$\Delta_{N_{Rd,c}}$	-2.1	10.8	6.6	8.1	$\underline{0.004}$
$\Delta_{N_{Rd,d}}$	9.2	23.4	16.6	17.0	0.036
IPE600	$\Delta_{min}[\%]$	$\Delta_{max}[\%]$	$\Delta_{mean}[\%]$	$\Delta_{med}[\%]$	$\sum(\chi_{Abq} - \chi_{an})^2[-]$
$\Delta_{N_{Rd,a}}$	-18.4	2.7	-5.1	-3.3	0.068
$\Delta_{N_{Rd,b}}$	-9.5	6.0	0.5	1.9	0.012
$\Delta_{N_{Rd,c}}$	-0.3	9.9	6.8	7.8	$\underline{0.003}$
$\Delta_{N_{Rd,d}}$	14.7	22.5	17.4	16.7	0.042
HE320A	$\Delta_{min}[\%]$	$\Delta_{max}[\%]$	$\Delta_{mean}[\%]$	$\Delta_{med}[\%]$	$\sum(\chi_{Abq} - \chi_{an})^2[-]$
$\Delta_{N_{Rd,a}}$	-23.5	-3.0	-12.4	-11.4	0.17
$\Delta_{N_{Rd,b}}$	-16.9	0.8	-7.1	-5.5	0.08
$\Delta_{N_{Rd,c}}$	-10.8	5.1	-1.1	1.1	0.02
$\Delta_{N_{Rd,d}}$	-0.5	13.4	9.1	11.7	$\underline{0.007}$
HE650A	$\Delta_{min}[\%]$	$\Delta_{max}[\%]$	$\Delta_{mean}[\%]$	$\Delta_{med}[\%]$	$\sum(\chi_{Abq} - \chi_{an})^2[-]$
$\Delta_{N_{Rd,a}}$	-16.9	1.9	-6.1	-4.4	0.080
$\Delta_{N_{Rd,b}}$	-10.0	5.6	-0.3	1.6	0.022
$\Delta_{N_{Rd,c}}$	-3.3	9.9	6.1	8.1	$\underline{0.005}$
$\Delta_{N_{Rd,d}}$	8.1	23.5	17.2	17.5	0.042
HE320M	$\Delta_{min}[\%]$	$\Delta_{max}[\%]$	$\Delta_{mean}[\%]$	$\Delta_{med}[\%]$	$\sum(\chi_{Abq} - \chi_{an})^2[-]$
$\Delta_{N_{Rd,a}}$	-22.7	-3.4	-12.2	-11.6	0.117
$\Delta_{N_{Rd,b}}$	-16.5	0.4	-6.6	-5.6	0.049
$\Delta_{N_{Rd,c}}$	-10.3	4.7	-0.5	1.1	0.013
$\Delta_{N_{Rd,d}}$	-0.1	12.9	10.1	12.0	$\underline{0.007}$
HE650M	$\Delta_{min}[\%]$	$\Delta_{max}[\%]$	$\Delta_{mean}[\%]$	$\Delta_{med}[\%]$	$\sum(\chi_{Abq} - \chi_{an})^2[-]$
$\Delta_{N_{Rd,a}}$	-17.2	1.7	-6.2	-4.7	0.082
$\Delta_{N_{Rd,b}}$	-10.0	5.5	-0.3	1.5	0.022
$\Delta_{N_{Rd,c}}$	-2.5	9.8	6.2	7.8	$\underline{0.005}$
$\Delta_{N_{Rd,d}}$	8.7	23.3	17.3	17.54	0.043

B.5 Lateral-torsional buckling: additional results for $M_{b,Rd}$

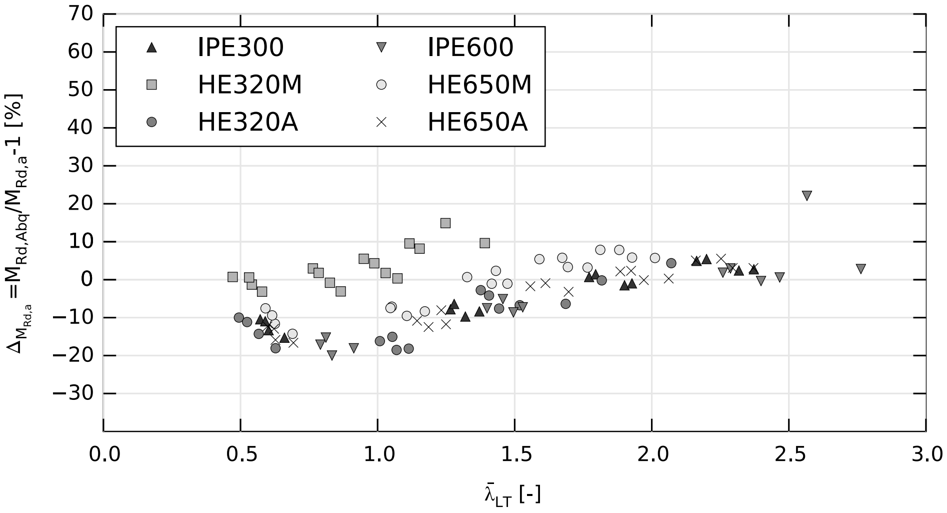

Figure B.6: LTB curves: Deviations $M_{Rd,Abq}$ with buckling curve a.

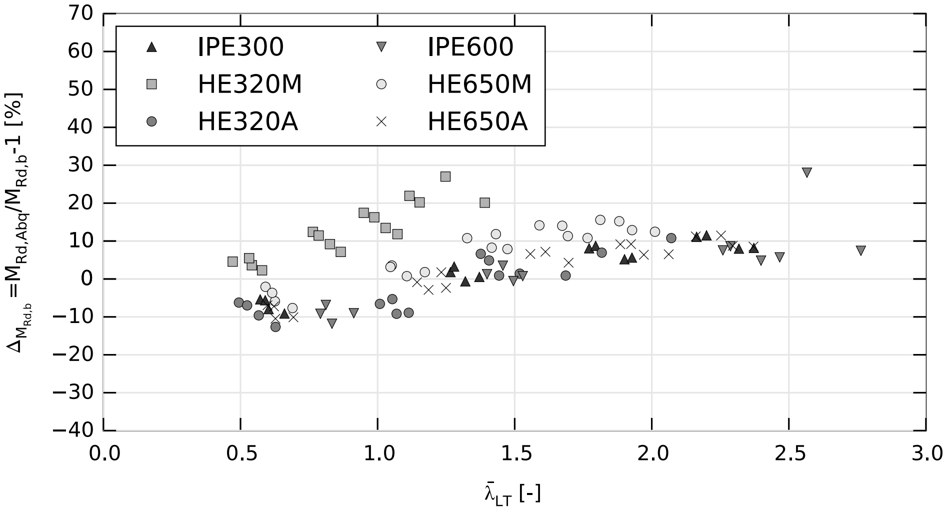

Figure B.7: LTB curves: Deviations $M_{Rd,Abq}$ with buckling curve b.

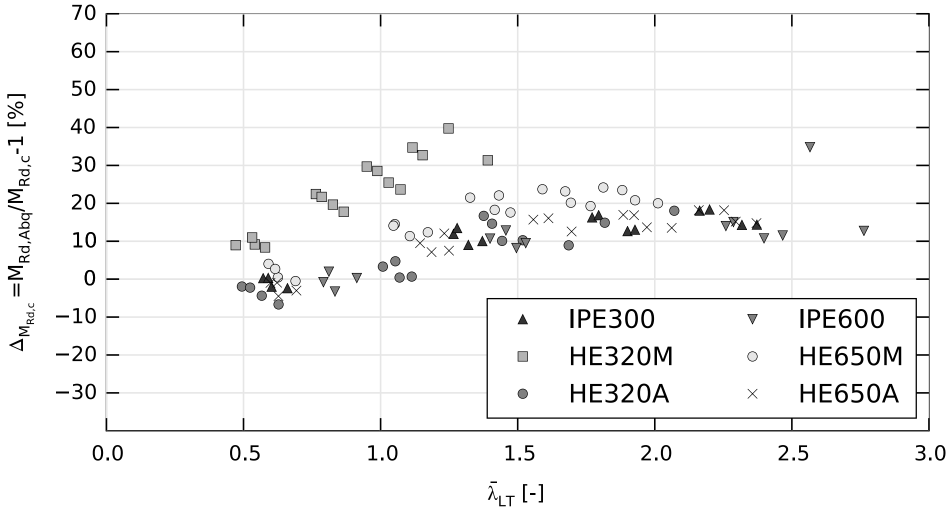

Figure B.8: LTB curves: Deviations $M_{Rd,Abq}$ with buckling curve c.

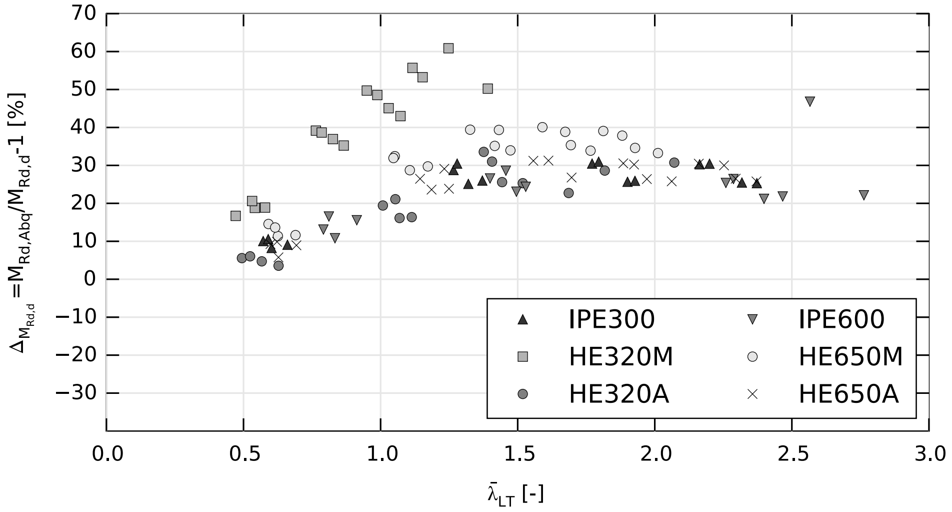

Figure B.9: LTB curves: Deviations $M_{Rd,Abq}$ with buckling curve d.

Table B.4: Deviation of $M_{b,Rd}$ for cellular members under pure bending ($\psi = 1$). The underlined values indicate the best fitting EC3 buckling curves.

IPE300	$\Delta_{min}[\%]$	$\Delta_{max}[\%]$	$\Delta_{mean}[\%]$	$\Delta_{med}[\%]$	$\sum(\chi_{Abq} - \chi_{an})^2[-]$
$\Delta_{M_{Rd,a}}$	-15.3	5.4	-4.2	-3.9	0.056
$\Delta_{M_{Rd,b}}$	-9.1	11.5	2.7	4.2	0.017
$\Delta_{M_{Rd,c}}$	-2.4	18.4	10.3	12.9	$\underline{0.016}$
$\Delta_{M_{Rd,d}}$	8.2	31.0	23.3	25.8	0.074

IPE600	$\Delta_{min}[\%]$	$\Delta_{max}[\%]$	$\Delta_{mean}[\%]$	$\Delta_{med}[\%]$	$\sum(\chi_{Abq} - \chi_{an})^2[-]$
$\Delta_{M_{Rd,a}}$	-20.0	22.1	-4.3	-2.9	0.076
$\Delta_{M_{Rd,b}}$	-11.8	28.0	2.7	3.7	0.019
$\Delta_{M_{Rd,c}}$	-3.3	34.8	10.4	10.7	$\underline{0.012}$
$\Delta_{M_{Rd,d}}$	10.8	46.8	23.4	22.9	0.067

HE320A	$\Delta_{min}[\%]$	$\Delta_{max}[\%]$	$\Delta_{mean}[\%]$	$\Delta_{med}[\%]$	$\sum(\chi_{Abq} - \chi_{an})^2[-]$
$\Delta_{M_{Rd,a}}$	-18.5	4.3	-9.7	-10.0	0.109
$\Delta_{M_{Rd,b}}$	-12.6	10.8	-2.2	-5.3	0.034
$\Delta_{M_{Rd,c}}$	-6.7	18.0	5.8	4.7	$\underline{0.017}$
$\Delta_{M_{Rd,d}}$	3.6	33.6	19.4	21.1	0.072

HE650A	$\Delta_{min}[\%]$	$\Delta_{max}[\%]$	$\Delta_{mean}[\%]$	$\Delta_{med}[\%]$	$\sum(\chi_{Abq} - \chi_{an})^2[-]$
$\Delta_{M_{Rd,a}}$	-16.6	5.5	-4.5	-1.7	0.075
$\Delta_{M_{Rd,b}}$	-10.5	11.5	2.6	6.4	0.023
$\Delta_{M_{Rd,c}}$	-4.5	18.2	10.4	13.5	$\underline{0.021}$
$\Delta_{M_{Rd,d}}$	5.8	31.3	23.8	26.5	0.091

HE320M	$\Delta_{min}[\%]$	$\Delta_{max}[\%]$	$\Delta_{mean}[\%]$	$\Delta_{med}[\%]$	$\sum(\chi_{Abq} - \chi_{an})^2[-]$
$\Delta_{M_{Rd,a}}$	-3.2	14.9	3.2	1.8	$\underline{0.017}$
$\Delta_{M_{Rd,b}}$	2.3	27.0	12.8	12.1	0.105
$\Delta_{M_{Rd,c}}$	8.4	39.8	22.8	23.1	0.273
$\Delta_{M_{Rd,d}}$	16.7	60.9	39.5	41.1	0.633

HE650M	$\Delta_{min}[\%]$	$\Delta_{max}[\%]$	$\Delta_{mean}[\%]$	$\Delta_{med}[\%]$	$\sum(\chi_{Abq} - \chi_{an})^2[-]$
$\Delta_{M_{Rd,a}}$	-14.3	7.9	-1.5	-0.2	0.048
$\Delta_{M_{Rd,b}}$	-7.7	15.6	6.8	9.5	$\underline{0.024}$
$\Delta_{M_{Rd,c}}$	-0.5	24.2	15.7	18.8	0.062
$\Delta_{M_{Rd,d}}$	11.4	40.1	30.7	33.9	0.206

Table B.5: Deviation of $M_{b,Rd}$ for cellular members under pure bending ($\psi = 0$). The underlined values indicate the best fitting EC3 buckling curves.

IPE300	$\Delta_{min}[\%]$	$\Delta_{max}[\%]$	$\Delta_{mean}[\%]$	$\Delta_{med}[\%]$	$\sum(\chi_{Abq} - \chi_{an})^2[-]$
$\Delta_{M_{Rd,a}}$	-4.7	12.6	6.1	7.4	$\underline{0.049}$
$\Delta_{M_{Rd,b}}$	-1.4	22.0	15.1	15.9	0.130
$\Delta_{M_{Rd,c}}$	2.4	34.8	24.7	25.6	0.251
$\Delta_{M_{Rd,d}}$	9.0	55.7	40.9	43.2	0.484

IPE600	$\Delta_{min}[\%]$	$\Delta_{max}[\%]$	$\Delta_{mean}[\%]$	$\Delta_{med}[\%]$	$\sum(\chi_{Abq} - \chi_{an})^2[-]$
$\Delta_{M_{Rd,a}}$	-3.2	13.5	4.3	4.2	$\underline{0.041}$
$\Delta_{M_{Rd,b}}$	7.8	20.2	13.1	12.4	0.121
$\Delta_{M_{Rd,c}}$	15.1	31.9	22.5	21.8	0.241
$\Delta_{M_{Rd,d}}$	27.8	52.5	38.4	38.0	0.474

HE320A	$\Delta_{min}[\%]$	$\Delta_{max}[\%]$	$\Delta_{mean}[\%]$	$\Delta_{med}[\%]$	$\sum(\chi_{Abq} - \chi_{an})^2[-]$
$\Delta_{M_{Rd,a}}$	-20.5	13.6	4.9	7.3	$\underline{0.051}$
$\Delta_{M_{Rd,b}}$	-12.4	24.0	14.5	18.1	0.118
$\Delta_{M_{Rd,c}}$	-3.9	35.3	24.6	28.8	0.237
$\Delta_{M_{Rd,d}}$	10.1	54.3	41.3	47.0	0.483

HE650A	$\Delta_{min}[\%]$	$\Delta_{max}[\%]$	$\Delta_{mean}[\%]$	$\Delta_{med}[\%]$	$\sum(\chi_{Abq} - \chi_{an})^2[-]$
$\Delta_{M_{Rd,a}}$	-29.2	11.2	4.0	7.5	$\underline{0.099}$
$\Delta_{M_{Rd,b}}$	-21.3	21.1	13.2	16.5	0.160
$\Delta_{M_{Rd,c}}$	-13.1	33.4	23.1	27.1	0.269
$\Delta_{M_{Rd,d}}$	0.2	53.9	39.6	45.0	0.497

HE320M	$\Delta_{min}[\%]$	$\Delta_{max}[\%]$	$\Delta_{mean}[\%]$	$\Delta_{med}[\%]$	$\sum(\chi_{Abq} - \chi_{an})^2[-]$
$\Delta_{M_{Rd,a}}$	9.2	25.1	18.6	19.5	$\underline{0.254}$
$\Delta_{M_{Rd,b}}$	11.9	39.2	29.1	31.9	0.517
$\Delta_{M_{Rd,c}}$	14.5	53.7	40.2	45.5	0.824
$\Delta_{M_{Rd,d}}$	19.1	77.3	58.5	67.9	1.342

HE650M	$\Delta_{min}[\%]$	$\Delta_{max}[\%]$	$\Delta_{mean}[\%]$	$\Delta_{med}[\%]$	$\sum(\chi_{Abq} - \chi_{an})^2[-]$
$\Delta_{M_{Rd,a}}$	-6.9	15.1	11.4	12.9	$\underline{0.100}$
$\Delta_{M_{Rd,b}}$	-3.4	27.6	21.9	23.5	0.259
$\Delta_{M_{Rd,c}}$	0.5	41.1	33.1	35.3	0.467
$\Delta_{M_{Rd,d}}$	7.5	63.1	51.7	55.6	0.842

Table B.6: Deviation of $M_{b,Rd}$ for cellular members under pure bending ($\psi = -1$). The underlined values indicate the best fitting EC3 buckling curves.

IPE300	$\Delta_{min}[\%]$	$\Delta_{max}[\%]$	$\Delta_{mean}[\%]$	$\Delta_{med}[\%]$	$\sum(\chi_{Abq} - \chi_{an})^2[-]$
$\Delta_{M_{Rd,a}}$	-84.5	83.2	28.0	54.8	2.286
$\Delta_{M_{Rd,b}}$	-84.1	97.4	39.2	72.4	2.480
$\Delta_{M_{Rd,c}}$	-83.7	113.3	51.2	90.6	2.675
$\Delta_{M_{Rd,d}}$	-83.0	144.3	71.3	120.3	2.969
IPE600	$\Delta_{min}[\%]$	$\Delta_{max}[\%]$	$\Delta_{mean}[\%]$	$\Delta_{med}[\%]$	$\sum(\chi_{Abq} - \chi_{an})^2[-]$
$\Delta_{M_{Rd,a}}$	-35.9	87.7	42.8	57.7	1.022
$\Delta_{M_{Rd,b}}$	-33.0	103.3	55.7	73.4	1.291
$\Delta_{M_{Rd,c}}$	-29.8	120.4	69.5	90.0	1.571
$\Delta_{M_{Rd,d}}$	-24.1	151.7	92.7	117.7	2.010
HE320A	$\Delta_{min}[\%]$	$\Delta_{max}[\%]$	$\Delta_{mean}[\%]$	$\Delta_{med}[\%]$	$\sum(\chi_{Abq} - \chi_{an})^2[-]$
$\Delta_{M_{Rd,a}}$	-26.7	48.6	17.6	28.2	0.396
$\Delta_{M_{Rd,b}}$	-25.5	64.0	27.9	41.7	0.586
$\Delta_{M_{Rd,c}}$	-24.2	80.2	38.6	55.8	0.795
$\Delta_{M_{Rd,d}}$	-21.7	107.1	56.4	78.8	1.135
HE650A	$\Delta_{min}[\%]$	$\Delta_{max}[\%]$	$\Delta_{mean}[\%]$	$\Delta_{med}[\%]$	$\sum(\chi_{Abq} - \chi_{an})^2[-]$
$\Delta_{M_{Rd,a}}$	-67.9	75.0	21.8	28.1	0.790
$\Delta_{M_{Rd,b}}$	-64.9	91.7	33.4	40.3	0.917
$\Delta_{M_{Rd,c}}$	-61.8	109.6	45.6	53.2	1.074
$\Delta_{M_{Rd,d}}$	-56.5	139.7	65.9	74.8	1.348
HE320M	$\Delta_{min}[\%]$	$\Delta_{max}[\%]$	$\Delta_{mean}[\%]$	$\Delta_{med}[\%]$	$\sum(\chi_{Abq} - \chi_{an})^2[-]$
$\Delta_{M_{Rd,a}}$	-17.2	28.6	15.8	17.3	0.271
$\Delta_{M_{Rd,b}}$	-16.3	41.3	23.5	24.9	0.454
$\Delta_{M_{Rd,c}}$	-15.1	54.7	31.9	33.4	0.672
$\Delta_{M_{Rd,d}}$	-13.1	76.8	46.2	47.8	1.053
HE650M	$\Delta_{min}[\%]$	$\Delta_{max}[\%]$	$\Delta_{mean}[\%]$	$\Delta_{med}[\%]$	$\sum(\chi_{Abq} - \chi_{an})^2[-]$
$\Delta_{M_{Rd,a}}$	-43.8	55.4	18.8	32.3	0.597
$\Delta_{M_{Rd,b}}$	-42.4	72.6	29.7	45.7	0.794
$\Delta_{M_{Rd,c}}$	-40.8	90.5	41.1	59.7	1.005
$\Delta_{M_{Rd,d}}$	-38.0	119.9	59.9	82.7	1.343

B.6 Members subjected to bending and compression

Table B.7: Deviation of $M_{N,b,Rd}$ for cellular members under bending and compression ($\psi = 1$). The underlined values indicate the best fitting EC3 buckling curves.

IPE300	$\Delta_{min}[\%]$	$\Delta_{max}[\%]$	$\Delta_{mean}[\%]$	$\Delta_{med}[\%]$	$\sum(\chi_{Abq} - \chi_{an})^2[-]$
$\Delta_{M_{N,Rd,a}}$	-15.3	5.4	-4.2	-3.9	0.056
$\Delta_{M_{N,Rd,b}}$	-9.1	11.5	2.7	4.2	0.017
$\Delta_{M_{N,Rd,c}}$	-2.4	18.4	10.3	12.9	$\underline{0.016}$
$\Delta_{M_{N,Rd,d}}$	8.2	31.0	23.3	25.8	0.074

IPE600	$\Delta_{min}[\%]$	$\Delta_{max}[\%]$	$\Delta_{mean}[\%]$	$\Delta_{med}[\%]$	$\sum(\chi_{Abq} - \chi_{an})^2[-]$
$\Delta_{M_{N,Rd,a}}$	-20.0	22.1	-4.3	-2.9	0.076
$\Delta_{M_{N,Rd,b}}$	-11.8	28.0	2.7	3.7	0.019
$\Delta_{M_{N,Rd,c}}$	-3.3	34.8	10.4	10.7	$\underline{0.012}$
$\Delta_{M_{N,Rd,d}}$	10.8	46.8	23.4	22.9	0.067

HE320A	$\Delta_{min}[\%]$	$\Delta_{max}[\%]$	$\Delta_{mean}[\%]$	$\Delta_{med}[\%]$	$\sum(\chi_{Abq} - \chi_{an})^2[-]$
$\Delta_{M_{N,Rd,a}}$	-18.5	4.3	-9.7	-10.0	0.109
$\Delta_{M_{N,Rd,b}}$	-12.6	10.8	-2.2	-5.3	0.034
$\Delta_{M_{N,Rd,c}}$	-6.7	18.0	5.8	4.7	$\underline{0.017}$
$\Delta_{M_{N,Rd,d}}$	3.6	33.6	19.4	21.1	0.072

HE650A	$\Delta_{min}[\%]$	$\Delta_{max}[\%]$	$\Delta_{mean}[\%]$	$\Delta_{med}[\%]$	$\sum(\chi_{Abq} - \chi_{an})^2[-]$
$\Delta_{M_{N,Rd,a}}$	-16.6	5.5	-4.5	-1.7	0.075
$\Delta_{M_{N,Rd,b}}$	-10.5	11.5	2.6	6.4	0.023
$\Delta_{M_{N,Rd,c}}$	-4.5	18.2	10.4	13.5	$\underline{0.021}$
$\Delta_{M_{N,Rd,d}}$	5.8	31.3	23.8	26.5	0.091

HE320M	$\Delta_{min}[\%]$	$\Delta_{max}[\%]$	$\Delta_{mean}[\%]$	$\Delta_{med}[\%]$	$\sum(\chi_{Abq} - \chi_{an})^2[-]$
$\Delta_{M_{N,Rd,a}}$	-3.2	14.9	3.2	1.8	$\underline{0.017}$
$\Delta_{M_{N,Rd,b}}$	2.3	27.0	12.8	12.1	0.105
$\Delta_{M_{N,Rd,c}}$	8.4	39.8	22.8	23.1	0.273
$\Delta_{M_{N,Rd,d}}$	16.7	60.9	39.5	41.1	0.633

HE650M	$\Delta_{min}[\%]$	$\Delta_{max}[\%]$	$\Delta_{mean}[\%]$	$\Delta_{med}[\%]$	$\sum(\chi_{Abq} - \chi_{an})^2[-]$
$\Delta_{M_{N,Rd,a}}$	-14.3	7.9	-1.5	-0.2	0.048
$\Delta_{M_{N,Rd,b}}$	-7.7	15.6	6.8	9.5	$\underline{0.024}$
$\Delta_{M_{N,Rd,c}}$	-0.5	24.2	15.7	18.8	0.062
$\Delta_{M_{N,Rd,d}}$	11.4	40.1	30.7	33.9	0.206

Table B.8: Deviation of $M_{N,b,Rd}$ for cellular members under bending and compression ($\psi = 0$). The underlined values indicate the best fitting EC3 buckling curves.

IPE300	$\Delta_{min}[\%]$	$\Delta_{max}[\%]$	$\Delta_{mean}[\%]$	$\Delta_{med}[\%]$	$\sum(\chi_{Abq} - \chi_{an})^2[-]$
$\Delta_{M_{N,Rd,a}}$	-4.7	12.6	6.1	7.4	$\underline{0.049}$
$\Delta_{M_{N,Rd,b}}$	-1.4	22.0	15.1	15.9	0.130
$\Delta_{M_{N,Rd,c}}$	2.4	34.8	24.7	25.6	0.251
$\Delta_{M_{N,Rd,d}}$	9.0	55.7	40.9	43.2	0.484

IPE600	$\Delta_{min}[\%]$	$\Delta_{max}[\%]$	$\Delta_{mean}[\%]$	$\Delta_{med}[\%]$	$\sum(\chi_{Abq} - \chi_{an})^2[-]$
$\Delta_{M_{N,Rd,a}}$	-50.9	13.5	1.4	4.2	$\underline{0.224}$
$\Delta_{M_{N,Rd,b}}$	-47.1	20.2	9.9	12.3	0.256
$\Delta_{M_{N,Rd,c}}$	-43.0	31.9	19.0	21.6	0.336
$\Delta_{M_{N,Rd,d}}$	-36.1	52.5	34.5	37.7	0.526

HE320A	$\Delta_{min}[\%]$	$\Delta_{max}[\%]$	$\Delta_{mean}[\%]$	$\Delta_{med}[\%]$	$\sum(\chi_{Abq} - \chi_{an})^2[-]$
$\Delta_{M_{N,Rd,a}}$	9.2	25.1	18.6	19.5	$\underline{0.254}$
$\Delta_{M_{N,Rd,b}}$	11.9	39.2	29.1	31.9	0.517
$\Delta_{M_{N,Rd,c}}$	14.5	53.7	40.2	45.5	0.824
$\Delta_{M_{N,Rd,d}}$	19.1	77.3	58.5	67.9	1.342

HE650A	$\Delta_{min}[\%]$	$\Delta_{max}[\%]$	$\Delta_{mean}[\%]$	$\Delta_{med}[\%]$	$\sum(\chi_{Abq} - \chi_{an})^2[-]$
$\Delta_{M_{N,Rd,a}}$	-20.5	13.6	4.9	7.3	$\underline{0.051}$
$\Delta_{M_{N,Rd,b}}$	-12.4	24.0	14.5	18.1	0.118
$\Delta_{M_{N,Rd,c}}$	-3.9	35.3	24.6	28.8	0.237
$\Delta_{M_{N,Rd,d}}$	10.1	54.3	41.3	47.0	0.483

HE320M	$\Delta_{min}[\%]$	$\Delta_{max}[\%]$	$\Delta_{mean}[\%]$	$\Delta_{med}[\%]$	$\sum(\chi_{Abq} - \chi_{an})^2[-]$
$\Delta_{M_{N,Rd,a}}$	-6.9	15.1	11.4	12.9	$\underline{0.100}$
$\Delta_{M_{N,Rd,b}}$	-3.4	27.6	21.9	23.5	0.259
$\Delta_{M_{N,Rd,c}}$	0.5	41.1	33.1	35.3	0.467
$\Delta_{M_{N,Rd,d}}$	7.5	63.1	51.7	55.6	0.842

HE650M	$\Delta_{min}[\%]$	$\Delta_{max}[\%]$	$\Delta_{mean}[\%]$	$\Delta_{med}[\%]$	$\sum(\chi_{Abq} - \chi_{an})^2[-]$
$\Delta_{M_{N,Rd,a}}$	-29.2	11.2	4.0	7.5	$\underline{0.099}$
$\Delta_{M_{N,Rd,b}}$	-21.3	21.1	13.2	16.5	0.160
$\Delta_{M_{N,Rd,c}}$	-13.1	33.4	23.1	27.1	0.269
$\Delta_{M_{N,Rd,d}}$	0.2	53.9	39.6	45.0	0.497

Table B.9: Deviation of $M_{N,b,Rd}$ for cellular members under bending and compression ($\psi = -1$). The underlined values indicate the best fitting EC3 buckling curves.

IPE300	$\Delta_{min}[\%]$	$\Delta_{max}[\%]$	$\Delta_{mean}[\%]$	$\Delta_{med}[\%]$	$\sum(\chi_{Abq} - \chi_{an})^2[-]$
$\Delta_{M_{N,Rd,a}}$	-84.5	83.2	28.0	54.8	$\underline{2.286}$
$\Delta_{M_{N,Rd,b}}$	-84.1	97.4	39.2	72.4	2.480
$\Delta_{M_{N,Rd,c}}$	-83.7	113.3	51.2	90.6	2.675
$\Delta_{M_{N,Rd,d}}$	-83.0	144.3	71.3	120.3	2.969

IPE600	$\Delta_{min}[\%]$	$\Delta_{max}[\%]$	$\Delta_{mean}[\%]$	$\Delta_{med}[\%]$	$\sum(\chi_{Abq} - \chi_{an})^2[-]$
$\Delta_{M_{N,Rd,a}}$	-81.6	87.7	27.6	44.2	$\underline{2.041}$
$\Delta_{M_{N,Rd,b}}$	-80.7	103.3	39.0	58.0	2.190
$\Delta_{M_{N,Rd,c}}$	-79.8	120.4	51.2	72.6	2.355
$\Delta_{M_{N,Rd,d}}$	-78.1	151.7	71.8	97.0	2.636

HE320A	$\Delta_{min}[\%]$	$\Delta_{max}[\%]$	$\Delta_{mean}[\%]$	$\Delta_{med}[\%]$	$\sum(\chi_{Abq} - \chi_{an})^2[-]$
$\Delta_{M_{N,Rd,a}}$	-26.7	48.6	17.6	28.2	$\underline{0.396}$
$\Delta_{M_{N,Rd,b}}$	-25.5	64.0	27.9	41.7	0.586
$\Delta_{M_{N,Rd,c}}$	-24.2	80.2	38.6	55.8	0.795
$\Delta_{M_{N,Rd,d}}$	-21.7	107.1	56.4	78.8	1.135

HE650A	$\Delta_{min}[\%]$	$\Delta_{max}[\%]$	$\Delta_{mean}[\%]$	$\Delta_{med}[\%]$	$\sum(\chi_{Abq} - \chi_{an})^2[-]$
$\Delta_{M_{N,Rd,a}}$	-67.9	75.0	21.8	28.1	$\underline{0.790}$
$\Delta_{M_{N,Rd,b}}$	-64.9	91.7	33.4	40.3	0.917
$\Delta_{M_{N,Rd,c}}$	-61.8	109.6	45.6	53.2	1.074
$\Delta_{M_{N,Rd,d}}$	-56.5	139.7	65.9	74.8	1.348

HE320M	$\Delta_{min}[\%]$	$\Delta_{max}[\%]$	$\Delta_{mean}[\%]$	$\Delta_{med}[\%]$	$\sum(\chi_{Abq} - \chi_{an})^2[-]$
$\Delta_{M_{N,Rd,a}}$	-17.2	28.6	15.8	17.3	$\underline{0.271}$
$\Delta_{M_{N,Rd,b}}$	-16.3	41.3	23.5	24.9	0.454
$\Delta_{M_{N,Rd,c}}$	-15.1	54.7	31.9	33.4	0.672
$\Delta_{M_{N,Rd,d}}$	-13.1	76.8	46.2	47.8	1.053

HE650M	$\Delta_{min}[\%]$	$\Delta_{max}[\%]$	$\Delta_{mean}[\%]$	$\Delta_{med}[\%]$	$\sum(\chi_{Abq} - \chi_{an})^2[-]$
$\Delta_{M_{N,Rd,a}}$	-43.8	55.4	18.8	32.3	$\underline{0.597}$
$\Delta_{M_{N,Rd,b}}$	-42.4	72.6	29.7	45.7	0.794
$\Delta_{M_{N,Rd,c}}$	-40.8	90.5	41.1	59.7	1.005
$\Delta_{M_{N,Rd,d}}$	-38.0	119.9	59.9	82.7	1.343

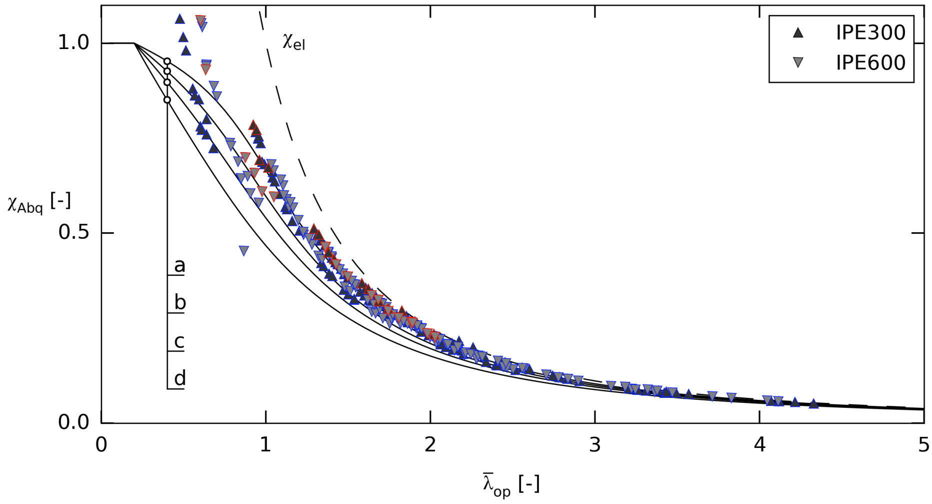

Figure B.10: Comparison numerical results with existing buckling curves for all μ values - IPE sections ($\psi = 0$). Data corresponding to $\mu = \infty$ indicated in red; Blue is used for all other μ values.

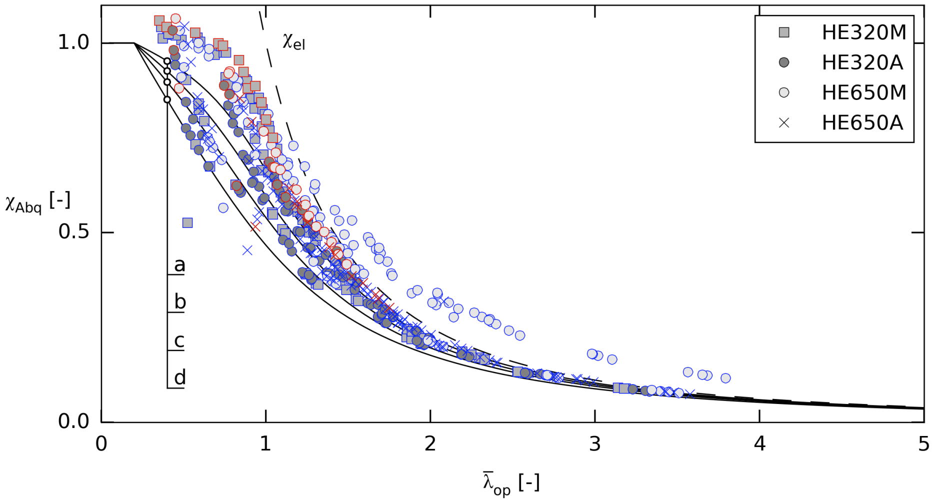

Figure B.11: Comparison numerical results with existing buckling curves for all μ values - HE sections ($\psi = 0$). Data corresponding to $\mu = \infty$ indicated in red; Blue is used for all other μ values.

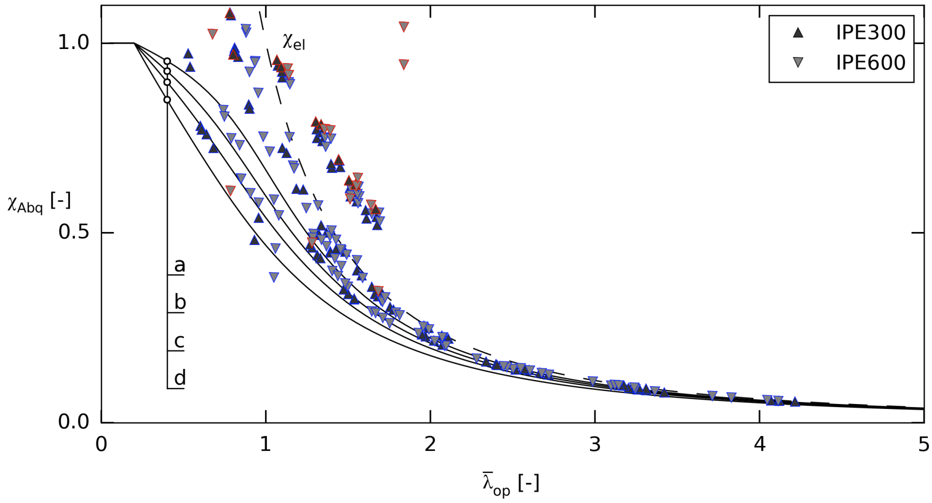

Figure B.12: Comparison numerical results with existing buckling curves for all μ values - IPE sections ($\psi = -1$). Data corresponding to $\mu = \infty$ indicated in red; Blue is used for all other μ values.

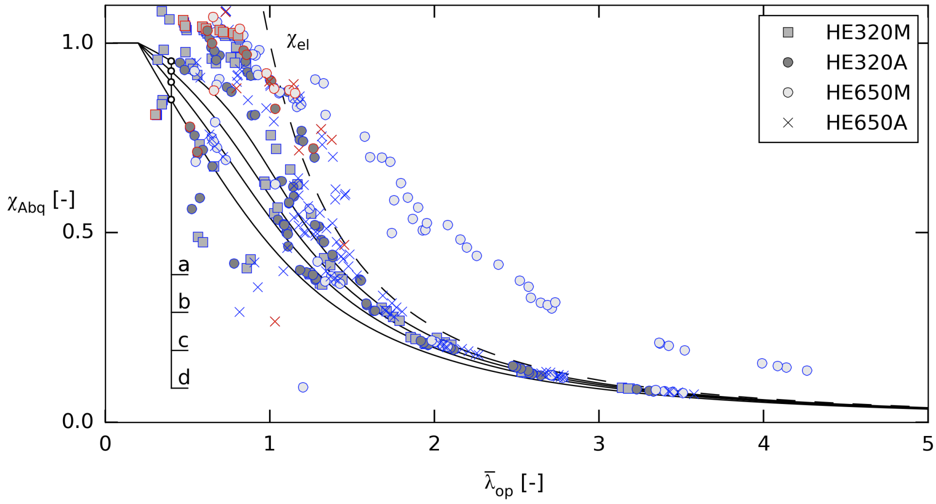

Figure B.13: Comparison numerical results with existing buckling curves for all μ values - HE sections ($\psi = -1$). Data corresponding to $\mu = \infty$ indicated in red; Blue is used for all other μ values.

Table B.10: Deviation of LPF for method ECCS-Vandepitte.

	ψ	Δ_{min} [%]	Δ_{max} [%]	Δ_{mean} [%]	Δ_{med} [%]	σ_{Δ}[%]
IPE300	1	-23.0	11.3	-6.6	-7.4	10.2
	0	-62.3	11.3	-5.6	-5.6	13.4
	-1	-83.8	68.4	10.8	8.5	28.3
IPE600	1	-27.7	12.7	-7.9	-9.8	10.9
	0	-54.5	10.0	-7.0	-6.3	13.0
	-1	-81.8	70.9	9.9	8.2	28.0
HE320A	1	-36.9	46.3	-11.2	-13.0	10.9
	0	-56.6	5.6	-11.1	-9.2	12.1
	-1	-54.2	31.7	-2.4	0.2	14.8
HE650A	1	-24.3	10.4	-7.7	-9.2	10.3
	0	-64.9	39.6	-7.2	-6.9	14.5
	-1	-70.7	56.2	3.2	7.6	22.6
HE320M	1	-15.5	7.0	-4.8	-5.6	5.8
	0	-49.0	10.2	-2.7	-0.1	9.9
	-1	-56.6	14.6	-1.1	2.2	13.2
HE650M	1	-22.0	10.6	-6.0	-7.8	9.5
	0	-66.3	11.2	-4.6	-4.0	12.4
	-1	-90.6	37.8	2.0	7.4	18.7

Table B.11: Deviation of LPF for method ECCS-Van Impe.

	ψ	Δ_{min} [%]	Δ_{max} [%]	Δ_{mean} [%]	Δ_{med} [%]	σ_{Δ}[%]
IPE300	1	-2.1	38.3	16.7	17.9	8.8
	0	-52.1	57.4	28.0	32.7	19.8
	-1	-77.0	155.5	56.4	51.3	54.9
IPE600	1	-0.3	46.8	16.3	16.3	7.1
	0	-34.6	54.8	27.3	31.1	16.8
	-1	-77.0	155.5	56.4	51.3	54.9
HE320A	1	-11.2	118.9	11.6	8.9	14.9
	0	-44.9	55.4	21.9	20.9	21.2
	-1	-29.7	114.1	37.4	17.2	40.8
HE650A	1	-3.3	31.3	17.2	19.1	9.0
	0	-56.6	97.6	27.7	31.3	20.9
	-1	-55.9	142.0	46.4	36.3	49.3
HE320M	1	-10.3	14.9	4.0	4.7	4.3
	0	-36.5	30.7	13.7	17.7	11.1
	-1	-39.4	57.2	14.5	12.4	20.4
HE650M	1	-2.5	24.2	13.3	13.5	7.3
	0	-59.5	41.9	23.8	29.4	16.4
	-1	-85.2	97.7	32.1	19.0	36.6

B.7 Deviation LPF according to four different methods

Table B.12: Deviation of LPF for Method 1.

	ψ	Δ_{min} [%]	Δ_{max} [%]	Δ_{mean} [%]	Δ_{med} [%]	σ_{Δ}[%]
IPE300	1	-2.1	33.0	15.0	16.7	7.4
	0	-60.0	38.5	14.1	14.9	14.1
	-1	-83.8	128.0	32.1	27.2	43.8
IPE600	1	-0.3	39.7	14.8	15.4	5.9
	0	-46.1	33.9	13.5	13.3	11.9
	-1	-81.6	136.0	30.4	23.0	42.2
HE320A	1	-15.6	109.1	7.9	6.7	13.4
	0	-53.0	40.1	4.2	4.2	13.9
	-1	-43.4	72.2	8.4	4.6	21.8
HE650A	1	-3.3	26.0	15.1	18.1	7.5
	0	-63.4	74.5	12.8	14.9	15.7
	-1	-67.3	110.9	20.0	12.2	32.8
HE320M	1	-10.3	48.6	17.4	14.8	14.0
	0	-46.5	44.0	12.2	7.7	15.3
	-1	-49.4	34.7	4.2	4.5	16.3
HE650M	1	-2.5	30.5	16.2	16.2	9.0
	0	-64.0	40.9	14.5	13.1	15.0
	-1	-88.2	74.6	13.3	10.4	25.7

Table B.13: Deviation of LPF for Method 2.

	ψ	Δ_{min} [%]	Δ_{max} [%]	Δ_{mean} [%]	Δ_{med} [%]	σ_{Δ}[%]
IPE300	1	-2.1	43.6	21.4	24.8	12.2
	0	-52.3	63.4	31.7	40.4	21.2
	-1	-82.3	148.1	59.3	65.0	59.3
IPE600	1	-0.3	46.8	21.2	22.8	10.0
	0	-34.6	54.8	31.1	38.0	17.8
	-1	-77.0	155.5	57.5	48.6	55.1
HE320A	1	-10.8	123.9	13.8	12.5	16.7
	0	-46.2	55.9	22.3	18.6	21.7
	-1	-34.6	113.6	30.8	15.3	38.2
HE650A	1	-3.3	40.6	20.8	23.9	11.6
	0	-56.8	116.7	30.6	37.4	22.6
	-1	-55.9	142.0	46.6	34.0	49.7
HE320M	1	-10.3	24.9	7.6	6.6	7.6
	0	-38.9	35.6	16.2	16.2	12.8
	-1	-43.9	49.1	11.1	10.9	18.7
HE650M	1	-2.5	39.8	17.3	19.1	10.9
	0	-59.7	50.0	26.7	34.5	17.9
	-1	-85.3	99.5	30.3	21.8	36.2

Table B.14: Comparison deviations of four methods.

	ψ	Δ_{min} [%]	Δ_{max} [%]	Δ_{mean} [%]	Δ_{med} [%]	σ_{Δ}[%]
ECCS-Vandepitte	1	-36.9	46.3	-7.3	-8.2	9.9
	0	-66.3	39.6	-6.4	-5.6	12.9
	-1	-90.6	70.9	4.2	5.8	22.8
	ψ	Δ_{min} [%]	Δ_{max} [%]	Δ_{mean} [%]	Δ_{med} [%]	σ_{Δ}[%]
ECCS-Van Impe	1	-11.2	118.9	13.3	12.8	10.1
	0	-59.5	97.6	24.2	26.3	18.7
	-1	-85.2	155.5	42.4	22.3	48.6
	ψ	Δ_{min} [%]	Δ_{max} [%]	Δ_{mean} [%]	Δ_{med} [%]	σ_{Δ}[%]
EC3-Method1	1	-15.6	109.1	14.5	14.9	10.3
	0	-64.0	74.5	12.0	12.6	14.7
	-1	-88.2	136.0	19.2	11.0	34.6
	ψ	Δ_{min} [%]	Δ_{max} [%]	Δ_{mean} [%]	Δ_{med} [%]	σ_{Δ}[%]
EC3-Method 2	1	-10.8	123.9	17.1	17.9	12.7
	0	-59.7	116.7	26.9	30.6	20.1
	-1	-85.3	155.5	41.1	24.0	49.0

Appendix C

Method 2

C.1 Members not susceptible to lateral torsional buckling

C.1.1 Buckling under N + M_y

Class 1-2

In-plane buckling about y-axis:

$$\frac{N_{Ed}}{\chi_y N_{pl,Rd}} + k_y \frac{C_{my} M_{y,Ed}}{M_{pl,y,Rd}} \leq 1 \tag{C.1.1}$$

Out-of-plane buckling about z-axis:

$$\frac{N_{Ed}}{\chi_z N_{pl,Rd}} + 0.6 k_y \frac{C_{my} M_{y,Ed}}{M_{pl,y,Rd}} \leq 1 \tag{C.1.2}$$

$$k_y = 1 + (\overline{\lambda}_y - 0.2) n_y \leq 1 + 0.8 n_y \tag{C.1.3}$$

$$C_{my} = 0.6 + 0.4\psi \geq 0.4 \tag{C.1.4}$$

$$n_y = \frac{N_{Ed}}{\chi_y N_{pl,Rd}} \tag{C.1.5}$$

Class 3-4

In-plane buckling about y-axis:

$$\frac{N_{Ed}}{\chi_y N_{pl,Rd}} + k_y \frac{C_{my} M_{y,Ed}}{M_{el,y,Rd}} \leq 1 \tag{C.1.6}$$

Out-of-plane buckling about z-axis:

$$\frac{N_{Ed}}{\chi_z N_{pl,Rd}} + 0.8 k_y \frac{C_{my} M_{y,Ed}}{M_{el,y,Rd}} \leq 1 \tag{C.1.7}$$

$$k_y = 1 + 0.6\overline{\lambda}_y n_y \leq 1 + 0.6 n_y \tag{C.1.8}$$

$$C_{my} = 0.6 + 0.4\psi \geq 0.4 \tag{C.1.9}$$

$$\text{Class 3} \qquad M_{el,y,Rd} = \frac{W_y f_y}{\gamma_{M1}} \tag{C.1.10}$$

$$\text{Class 4} \qquad M_{el,y,Rd} = \frac{W_{y,eff} f_y}{\gamma_{M1}}; \qquad N_{eff,Rd} = \frac{A_{eff} f_y}{\gamma_{M1}} \tag{C.1.11}$$

C.1.2 In plane buckling under N + M_z

The interaction formulae for members in weak-axis bending are comparable to those for strong-axis bending (Eq. C.1.12). Similarly as for the k_y-factor, the expression for the k_z-factor is based on GMNIA-simulations. In contrast to the case of strong-axis bending, the cross-section interaction for $\overline{\lambda}_z \rightarrow 0$ is more pronounced (Greiner & Lindner, 2006). Furthermore, the obtained k_z-values of I-sections for $\overline{\lambda}_z > 1.0$ are considerably larger than the k_y interaction factors due to the higher plastic reserve for weak-axis than for strong axis bending.

$$\frac{N_{Ed}}{\chi_z N_{pl,Rd}} + k_z \frac{C_{my} M_{y,Ed}}{M_{pl,z,Rd}} \leq 1 \tag{C.1.12}$$

$$k_z = 1 + (2\overline{\lambda}_z - 0.6) \cdot n_z \leq 1 + 1.4 n_z \tag{C.1.13}$$

$$C_{mz} = 0.6 + 0.4\psi \geq 0.4 \tag{C.1.14}$$

$$n_z = \frac{N_{Ed}}{\chi_z N_{pl,Rd}} \tag{C.1.15}$$

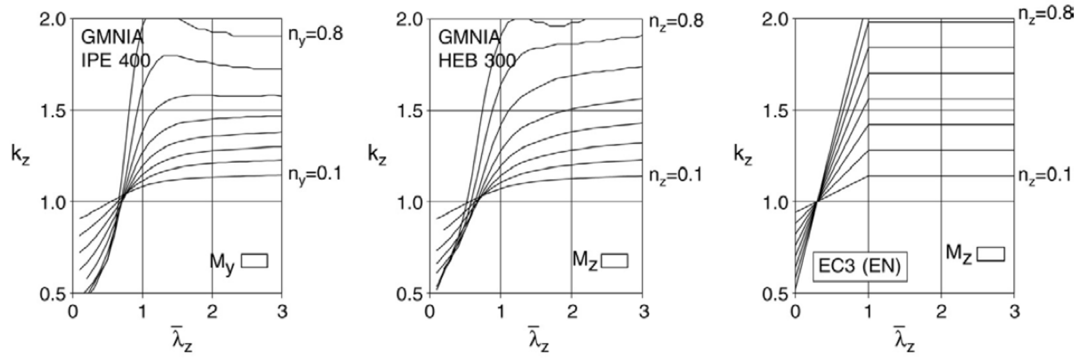

Figure C.1: GMNIA-results interaction factor k_z as function of $\overline{\lambda}_z$. Extracted from (Greiner & Lindner, 2006).

C.1.3 Buckling under biaxial bending and axial compression

$$\text{Buckling mode y-y:} \quad \frac{N_{Ed}}{\chi_y N_{pl,Rd}} + k_y \frac{C_{my} M_{y,Ed}}{M_{pl,y,Rd}} + 0.6 k_z \frac{C_{mz} M_{z,Ed}}{M_{pl,z,Rd}} \leq 1 \tag{C.1.16}$$

$$\text{Buckling mode z-z:} \quad \frac{N_{Ed}}{\chi_y N_{pl,Rd}} + 0.6 k_y \frac{C_{my} M_{y,Ed}}{M_{pl,y,Rd}} + k_z \frac{C_{mz} M_{z,Ed}}{M_{pl,z,Rd}} \leq 1 \tag{C.1.17}$$

$$k_y = 1 + (\overline{\lambda}_y - 0.2) n_y \leq 1 + 0.8 n_y \tag{C.1.18}$$

$$k_z = 1 + (2\overline{\lambda}_z - 0.6) n_z \leq 1 + 1.4 n_z \tag{C.1.19}$$

$$C_{my} = C_{mz} = 0.6 + 0.4\psi \geq 0.4 \tag{C.1.20}$$

The axial compression parameters n_y and n_z are determined similarly as in Eqs.C.1.5-C.1.15 for uniaxial bending.

C.1.4 Class 3 cross-sections

Buckling y-y:

$$\frac{N_{Ed}}{\chi_y N_{pl,Rd}} + k_y \frac{C_{my} M_{y,Ed}}{M_{el,y,Rd}} \leq 1 \tag{C.1.21}$$

Buckling z-z:

$$\frac{N_{Ed}}{\chi_z N_{pl,Rd}} + 0.8 k_y \frac{C_{my} M_{y,Ed}}{M_{el,y,Rd}} \leq 1 \tag{C.1.22}$$

RHS- and I-section:

$$k_y = 1 + 0.6\overline{\lambda}_y n_y \leq 1 + 0.6 n_y \tag{C.1.23}$$

$$C_{my} = 0.6 + 0.4\psi \geq 0.4 \tag{C.1.24}$$

$\boxed{\text{N}+M_y+M_z}$

Buckling y-y:

$$\frac{N_{Ed}}{\chi_y N_{pl,Rd}} + k_y \frac{C_{my} M_{y,Ed}}{M_{el,y,Rd}} + k_z \frac{C_{mz} M_{z,Ed}}{M_{el,z,Rd}} \leq 1 \tag{C.1.25}$$

Buckling z-z:

$$\frac{N_{Ed}}{\chi_z N_{pl,Rd}} + 0.8 k_y \frac{C_{my} M_{y,Ed}}{M_{el,y,Rd}} + k_z \frac{C_{mz} M_{z,Ed}}{M_{el,z,Rd}} \leq 1 \tag{C.1.26}$$

RHS- and I-section:

$$k_z = 1 + 0.6\overline{\lambda}_z n_z \leq 1 + 0.6 n_z \tag{C.1.27}$$

$$C_{mz} = 0.6 + 0.4\psi \geq 0.4 \tag{C.1.28}$$

$$n_z = \frac{N_{Ed}}{\chi_z N_{pl,Rd}} \tag{C.1.29}$$

C.2 Members susceptible to lateral torsional buckling

C.2.1 Buckling under $N + M_y$

The described interaction formulae for torsionally flexible members under $N + M_y$ are listed for completeness.

Class 1-2

In-plane buckling about y-axis:

$$\frac{N_{Ed}}{\chi_y N_{pl,Rd}} + k_y \frac{C_{my} M_{y,Ed}}{\chi_{LT} M_{pl,y,Rd}} \leq 1 \tag{C.2.1}$$

Out-of-plane buckling about z-axis:

$$\frac{N_{Ed}}{\chi_z N_{pl,Rd}} + k_{LT} \frac{M_{y,Ed}}{\chi_{LT} M_{pl,y,Rd}} \leq 1 \tag{C.2.2}$$

$$k_{LT} = 1 - \frac{0.1\overline{\lambda}_z n_z}{C_{mLT} - 0.25} \geq 1 - \frac{0.1 n_z}{C_{mLT} - 0.25} \tag{C.2.3}$$

$$k_{LT} = 0.6 + \overline{\lambda}_z \leq 1 - \frac{0.1\overline{\lambda}_z}{C_{mLT} - 0.25} n_z \qquad \overline{\lambda_z} < 0.4 \tag{C.2.4}$$

Class 3-4

In-plane buckling about y-axis:

$$\frac{N_{Ed}}{\chi_y N_{pl,Rd}} + k_y \frac{C_{my} M_{y,Ed}}{\chi_{LT} M_{el,y,Rd}} \leq 1 \tag{C.2.5}$$

Out-of-plane buckling about z-axis:

$$\frac{N_{Ed}}{\chi_z N_{pl,Rd}} + k_{LT} \frac{C M_{y,Ed}}{\chi_{LT} M_{el,y,Rd}} \leq 1 \tag{C.2.6}$$

$$k_{LT} = 1 - \frac{0.05\overline{\lambda}_z n_z}{C_{mLT} - 0.25} \geq 1 - \frac{0.05 n_z}{C_{mLT} - 0.25} \tag{C.2.7}$$

The applied equivalent moment factor C_{mLT} and the axial compression

$$n_z = \frac{N_{Ed}}{\chi_z N_{pl,Rd}} \tag{C.2.8}$$

N + M_y + M_z

Buckling y-y:

$$\frac{N_{Ed}}{\chi_y N_{pl,Rd}} + k_y \frac{C_{my} M_{y,Ed}}{M_{pl,y,Rd}} + 0.6 k_z \frac{C_{mz} M_{z,Ed}}{M_{pl,z,Rd}} \leq 1 \tag{C.2.9}$$

Buckling z-z:

$$\frac{N_{Ed}}{\chi_z N_{pl,Rd}} + k_{LT} \frac{M_{y,Ed}}{\chi_{LT} M_{pl,y,Rd}} + k_z \frac{C_{mz} M_{z,Ed}}{M_{pl,z,Rd}} \leq 1 \tag{C.2.10}$$

N + M_y + M_z

Buckling y-y:

$$\frac{N_{Ed}}{\chi_y N_{pl,Rd}} + k_y \frac{C_{my} M_{y,Ed}}{M_{el,y,Rd}} + k_z \frac{C_{mz} M_{z,Ed}}{M_{el,z,Rd}} \leq 1 \tag{C.2.11}$$

Buckling z-z:

$$\frac{N_{Ed}}{\chi_z N_{pl,Rd}} + 0.8 k_y \frac{C_{my} M_{y,Ed}}{M_{el,y,Rd}} + k_z \frac{C_{mz} M_{z,Ed}}{M_{el,z,Rd}} \leq 1 \tag{C.2.12}$$

For RHS- and I-section:

$$k_z = 1 + 0.6 \overline{\lambda}_z n_z \leq 1 + 0.6 n_z \tag{C.2.13}$$

$$C_{mz} = 0.6 + 0.4\psi \geq 0.4 \tag{C.2.14}$$

$$n_z = \frac{N_{Ed}}{\chi_z N_{pl,Rd}} \tag{C.2.15}$$

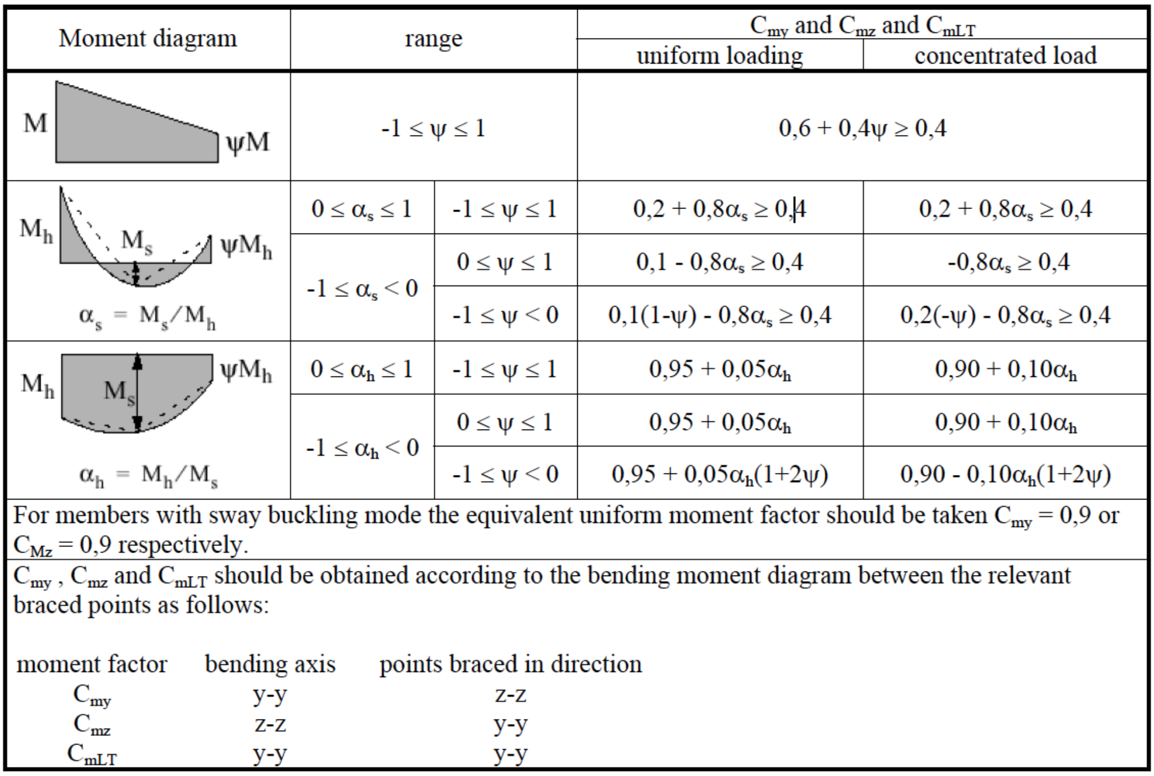

Moment diagram	range		C_{my} and C_{mz} and C_{mLT}	
			uniform loading	concentrated load
M, ψM	$-1 \le \psi \le 1$		$0,6 + 0,4\psi \ge 0,4$	
M_h, M_s, ψM_h $\alpha_s = M_s/M_h$	$0 \le \alpha_s \le 1$	$-1 \le \psi \le 1$	$0,2 + 0,8\alpha_s \ge 0,4$	$0,2 + 0,8\alpha_s \ge 0,4$
	$-1 \le \alpha_s < 0$	$0 \le \psi \le 1$	$0,1 - 0,8\alpha_s \ge 0,4$	$-0,8\alpha_s \ge 0,4$
		$-1 \le \psi < 0$	$0,1(1-\psi) - 0,8\alpha_s \ge 0,4$	$0,2(-\psi) - 0,8\alpha_s \ge 0,4$
M_h, M_s, ψM_h $\alpha_h = M_h/M_s$	$0 \le \alpha_h \le 1$	$-1 \le \psi \le 1$	$0,95 + 0,05\alpha_h$	$0,90 + 0,10\alpha_h$
	$-1 \le \alpha_h < 0$	$0 \le \psi \le 1$	$0,95 + 0,05\alpha_h$	$0,90 + 0,10\alpha_h$
		$-1 \le \psi < 0$	$0,95 + 0,05\alpha_h(1+2\psi)$	$0,90 - 0,10\alpha_h(1+2\psi)$

For members with sway buckling mode the equivalent uniform moment factor should be taken $C_{my} = 0,9$ or $C_{Mz} = 0,9$ respectively.

C_{my}, C_{mz} and C_{mLT} should be obtained according to the bending moment diagram between the relevant braced points as follows:

moment factor	bending axis	points braced in direction
C_{my}	y-y	z-z
C_{mz}	z-z	y-y
C_{mLT}	y-y	y-y

Figure C.2: Equivalent moment factor C_m Method 2.

Appendix D

Additional results parametric study cellular members

D.1 Deviation factor ΔM_{Abq}

By comparison of the numerical results from an GMNIA and LBA analysis, a deviation factor ΔM_{Abq} can be derived indicating whether the bending resistance $M_{Rd,Abq}$ is exceeding the critical LTB bending moment $M_{cr,Abq}$ (Eq. D.1.1). Positive values of the deviation factor correspond with values of M_{Rd} larger than the critical moment.

$$\Delta M_{Abq} = \left(\frac{M_{Rd,Abq}}{M_{cr,Abq}} - 1 \right) \cdot 100\%. \tag{D.1.1}$$

From Figs. D.1-D.3, it can be concluded that the largest positive deviations are obtained for the longest members under a non-uniform bending moment ($\psi = -1$) with maximum values obtained for the most slender sections: IPE300 and IPE600 (Table D.1).

Table D.1: $\Delta M_{Abq,max}$ for different ψ values.

	$\psi = 1$	$\psi = 0$	$\psi = -1$
Profile [-]	IPE300	IPE300	IPE600
$\Delta M_{Abq,max}$ [%]	7.1	2.7	56.6

This exceedance of M_{cr} can also be observed on interaction diagrams where alternatively $M_u/M_{cr,y,avg}$ is represented as function of $N_u/N_{cr,z}$. For the expression of the critical bending moment, an average value of the torsional constant was used as explained in Section 5.1.5. An example is given for profile IPE300 (L=15.19 m; $\psi = 0$), for which the critical LTB moment is slightly exceeded (Fig. D.4). This corresponds with the observations in Fig. D.2, where the considered combination is indicated in red and for which ΔM_{Abq} equals 2.7%. Similarly, the interaction diagram of the combination indicated in Fig. D.3 is given (Fig. D.5). Since for this combination $\psi = -1$, much larger deviations are obtained ($\Delta M_{Abq} = 49.1\%$). It should be noted that although the interaction diagrams are based on a theoretical determination of M_{cr}, a good correspondance can be found with the deviations in Figs. D.1-D.3.

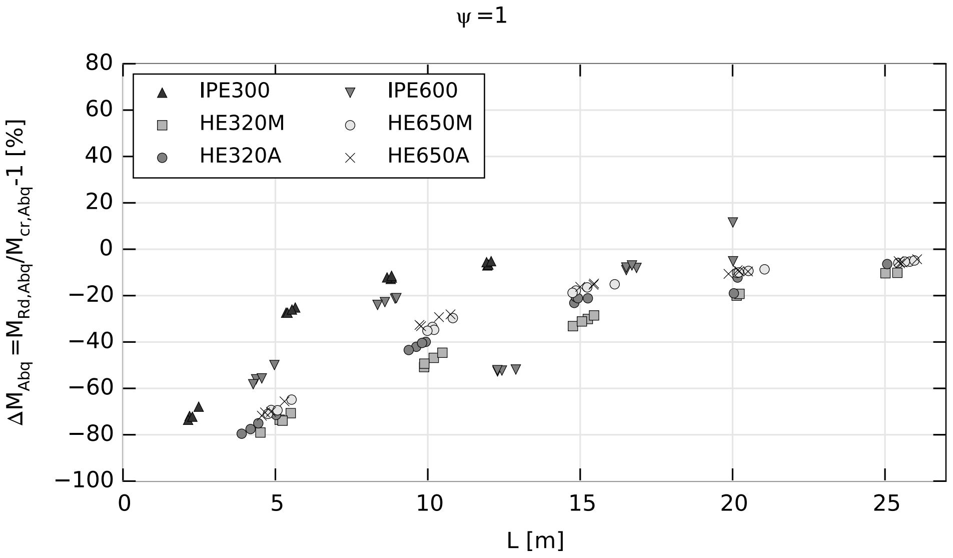

Figure D.1: Comparison GMNIA and LBA results for $\mu = \infty$ and $\psi = 1$.

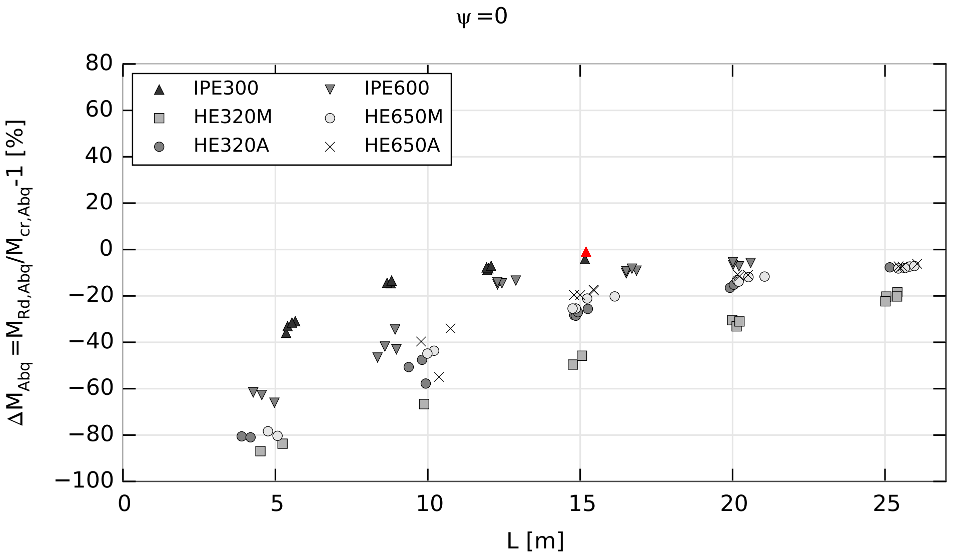

Figure D.2: Comparison GMNIA and LBA results for $\mu = \infty$ and $\psi = 0$.

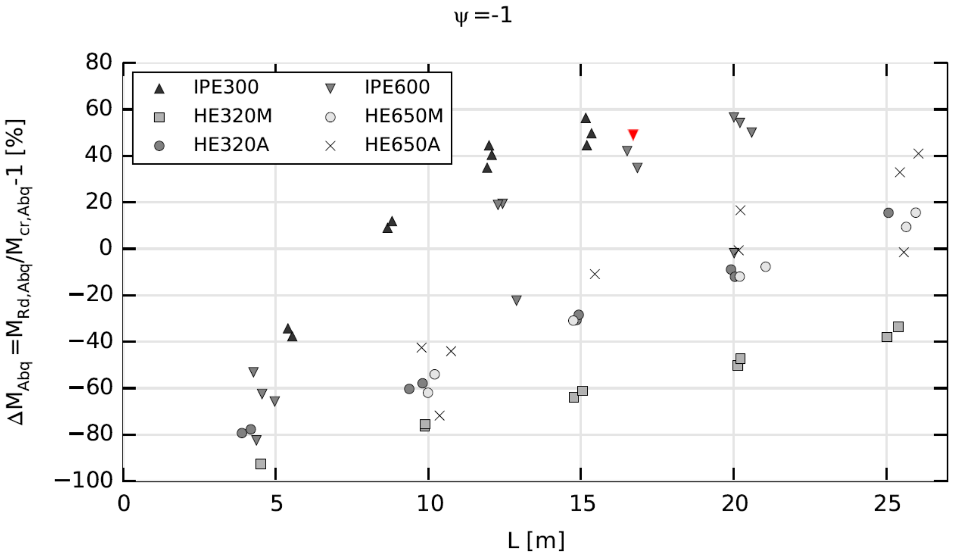

Figure D.3: Comparison GMNIA and LBA results for $\mu = \infty$ and $\psi = -1$.

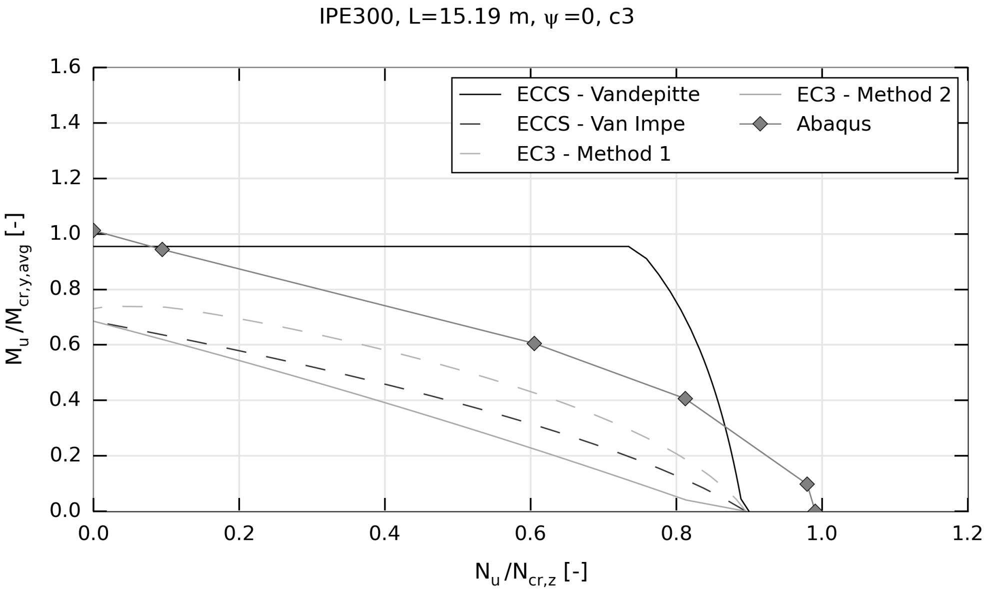

Figure D.4: Interaction diagram $M_u/M_{cr,y}$ - $N_u/N_{cr,z}$ of IPE300 section.

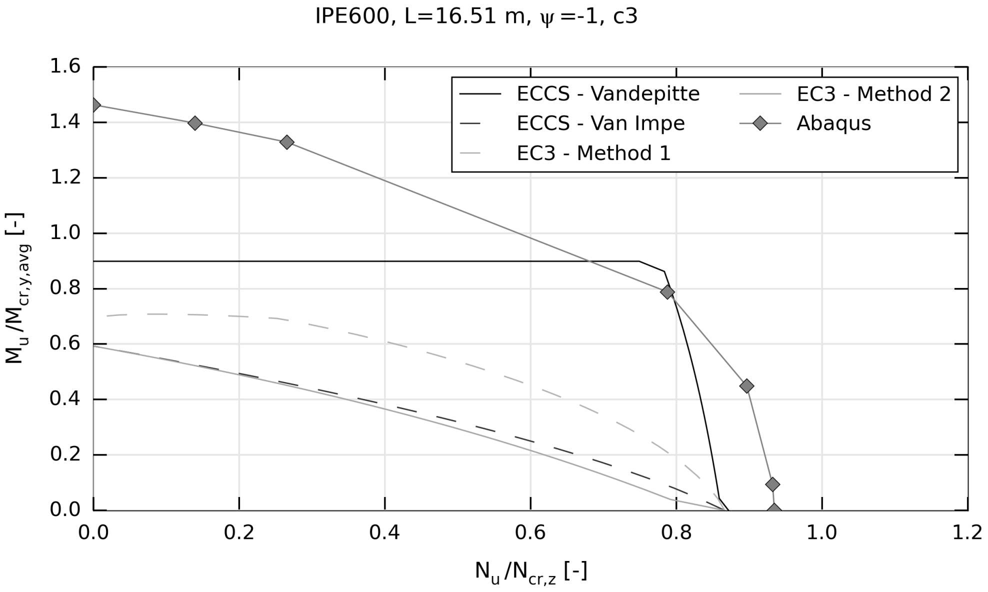

Figure D.5: Interaction diagram $M_u/M_{cr,y}$ - $N_u/N_{cr,z}$ of IPE600 section.

D.2 Deviation of N_{cr}

The deviation factor ΔN_{cr} (Eq. D.2.1) can be derived from an LBA analysis, indicating the deviation of the numerical results N_{cr} from the analytical values $N_{cr,Abq}$. Unsafe deviations were obtained for short length members with a minimum of 4.4% for profile IPE300 (Table D.2). For longer lengths, differences are negligible (Fig. D.6).

$$\Delta N_{cr} = \left(\frac{N_{cr,Abq}}{N_{cr,an}} - 1 \right) \cdot 100\% \tag{D.2.1}$$

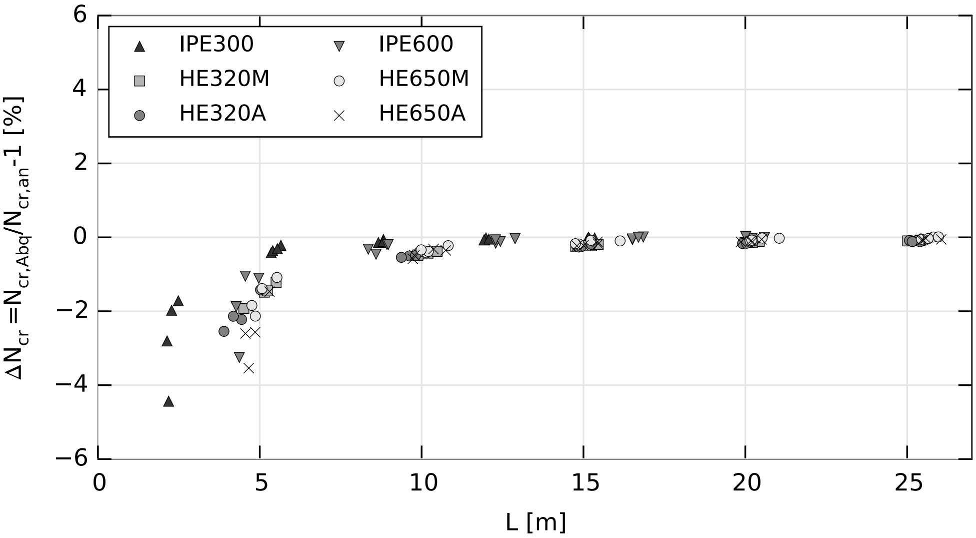

Figure D.6: Deviation of N_{cr} for cellular members.

Table D.2: Minimum deviation of $N_{cr,Abq}$ and $N_{cr,an}$.

	IPE300	IPE600	HE320A	HE650A	HE320M	HE650M
$\Delta N_{cr,min}$[%]	-4.4	-3.3	-2.5	-3.5	-1.9	-2.1

D.3 Yield and buckling phenomena in GMNIA and LBA analysis

As discussed in Section 3.10.1, the cross-section classification will have an influence on the analytical determination of the load proportionality factor. For sections HE320A and HE650M subjected to a constant bending moment ($\psi = 1$), the classification is varying from Class 4 (pure compression, $\mu = 0$) to Class 2 (pure bending, $\mu = \infty$) with increasing μ value (Table 5.6). Observation of a short length HE320A section under pure compression (L=4.2 m; $\psi = 1$; $\mu = 0$) however shows failure by plastic yielding of the flanges, around the web openings and at the web-to-flange transition (Fig. D.7). Also for longer lengths (L=20.0 m), plastic yielding at the upper and lower flange was observed before a maximum in the load displacement diagram was reached. An overview of the results from an GMNIA ($N_{Rd,Abq}$) and LBA analysis ($N_{cr,Abq}$) is given in Table D.3. No local buckling behaviour was observed during the LBA analysis and therefore a good correspondence was obtained with analytical values. For short length members, the critical load $N_{cr,Abq}$ is much larger than N_{pl}. Members behave plastically and calculation of the load proportionality factor according to a plastic theory is possible.

Table D.3: Overview results GMNIA and LBA analysis HE320A for pure compression ($\mu = 0$).

L [m]	N_{pl} [kN]	$N_{Rd,Abq}$ [kN]	$N_{cr,Abq}$ [kN]	$N_{cr,an}$ [kN]	ΔN_{cr}[%]
4.2	2379.1	1800.4	8078.5	8254.8	-2.1
9.8	2379.1	924.3	1494.4	1501.9	-0.5
20.0	2379.1	310.9	359.4	359.9	-0.2

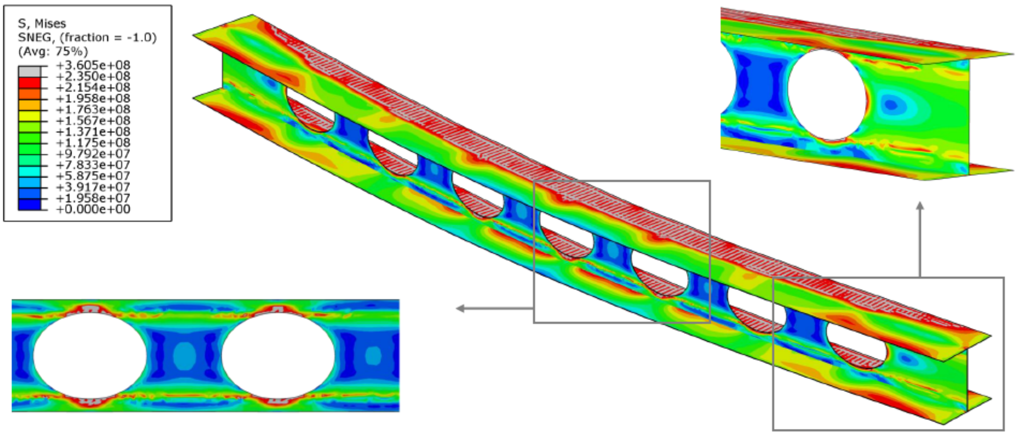
S, Mises
SNEG, (fraction = -1.0)
(Avg: 75%)
+3.605e+08
+2.350e+08
+2.154e+08
+1.958e+08
+1.763e+08
+1.567e+08
+1.371e+08
+1.175e+08
+9.792e+07
+7.833e+07
+5.875e+07
+3.917e+07
+1.958e+07
+0.000e+00

Figure D.7: Yielding of upper flange, lower flange and around web openings of HE320A section (L=4.2 m; $\mu = 0$; $\psi = 1$).

Similarly, for members subjected to pure bending ($\mu = \infty$), the results of an GMNIA and LBA analysis on section HE320A are given in Table D.4. In the GMNIA analysis, local yielding at the corners of the openings was observed for the shortest members (L=4.2 m; $\psi = -1$), as illustrated in Fig. D.8. Furthermore, for this combination a large deviation was obtained between the numerically ($M_{cr,Abq}$) and analytically ($M_{cr,avg}$) determined critical LTB bending moment, which can be explained by the observed web post buckling (Fig. D.9).

Table D.4: Overview results GMNIA and LBA analysis HE320A for pure bending ($\mu = \infty$).

ψ	L [m]	M_{pl} [kNm]	$M_{Rd,Abq}$ [kNm]	$M_{cr,Abq}$ [kNm]	$M_{cr,avg}$ [kNm]	ΔM_{cr}[%]
1	4.2	473.2	387.0	1723.1	1807.7	-4.7
-1	4.2	473.2	337.5	1514.3	4699.9	-67.8
0	25.2	473.2	213.4	231.1	226.9	1.8

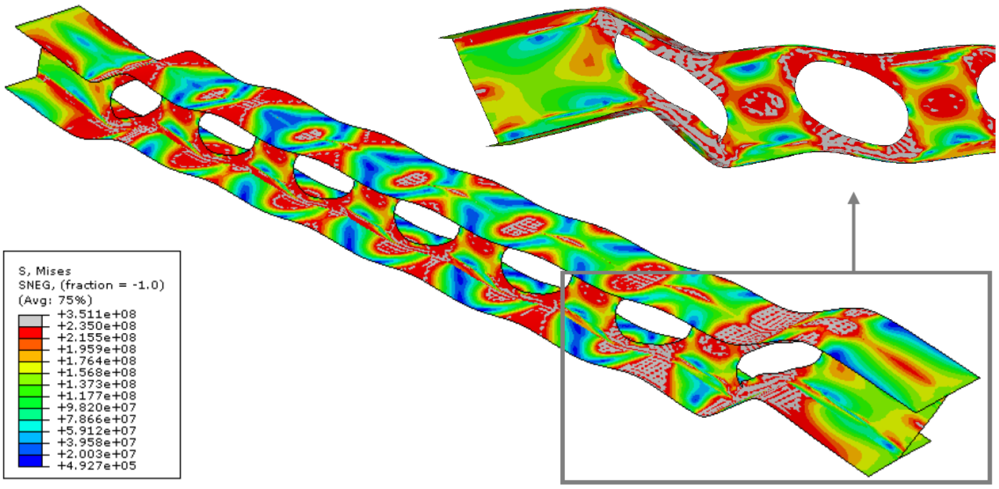
S, Mises
SNEG, (fraction = -1.0)
(Avg: 75%)
+3.511e+08
+2.350e+08
+2.155e+08
+1.959e+08
+1.764e+08
+1.568e+08
+1.373e+08
+1.177e+08
+9.820e+07
+7.866e+07
+5.912e+07
+3.958e+07
+2.003e+07
+4.927e+05

Figure D.8: Plastic yielding at corners of web openings of HE320A section (L=4.2 m; $\mu = \infty$; $\psi = -1$).

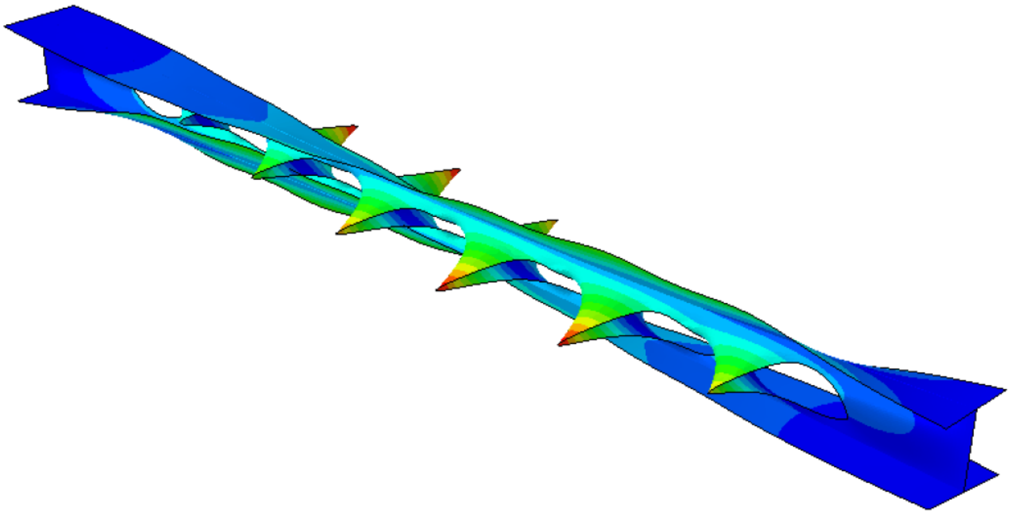

Figure D.9: Web post buckling of HE320A section (L=4.2 m; $\mu = \infty$; $\psi = -1$).

Bibliography

ArcelorMittal. (2008). *Sections and Merchant Bars. Sales catalogue.*

ArcelorMittal. (2008b). Angelina ^{TM} beam. A new generation of castellated beams. Retrieved from `http://sections.arcelormittal.com/library/product-catalogues.html`.

ArcelorMittal. (2008c). ACB (R). Cellular Beams.

Boissonnade, N., Jaspart, J.-P., Muzeau, J.-P., & Villette, M. (2004, March). New interaction formulae for beam-columns in Eurocode 3: The French–Belgian approach. *Journal of Constructional Steel Research*, *60*(3-5), 421–431. doi: 10.1016/S0143-974X(03)00121-4.

CEN. (1998). Eurocode 3 : Design of steel Structures - Part 1-1 : General rules – General rules and rules for buildings. Annex N: Openings in webs. , 83–107.

CEN. (2005). EN 1993-1-1. Eurocode 3. Design of steel structures. Part 1-1: General rules and rules for buildings.

CTICM. (2006). *Arcelor Cellular Beams: Detailed Technical Description.*

Dassault Systèmes. (2012). Abaqus 6.1 2. *Abaqus v.6.12. Interactive Edition*(Using Shell Elements).

Durif, S., Bouchaïr, A., & Vassart, O. (2013). Validation of an analytical model for curved and tapered cellular beams at normal and fire conditions. *Periodica Polytechnica Civil Engineering*(1), 83. doi: 10.3311/PPci.2144.

ECCS. (1984). Ultimate limit state calculation of sway frames with rigid joints.

ECCS. (2006). *Rules for member stability in EN 1993-1-1. Background documentation and design guidelines. (ECCS publication no. 119).*

Gevaert, D. (2010). De sterkte van excentrisch samengedrukte staven.

Greiner, R. (2011). Design guidelines for cross-section and member design according to Eurocode 3 with particular focus on semi-compact sections. (July 2011).

Greiner, R., & Lindner, J. (2006, August). Interaction formulae for members subjected to bending and axial compression in EUROCODE 3—the Method 2 approach. *Journal of Constructional Steel Research*, *62*(8), 757–770. doi: 10.1016/j.jcsr.2005.11.018.

Greiner, R., Taras, A., & Unterweger, H. (2013). Eurocode 3 – Design of Steel Structures. Proposal for amended rules for member buckling and semi-compact cross-section design.

Kerdal, D., & Nethercot, D. A. (1984). Failure Modes for Castellated Beams. , *4*, 295–315.

Lawson, R., & Hicks, S. (2011). *Design of composite beams with large web openings (SCI P355).* SCI (Steel Construction Institute).

Maquoi, R., & Rondal, J. (1978). Mise en Équation des Nouvelles Courbes Européennes de Flambement. , 17–30.

NBN. (2005). *EN 1993-1-1. Eurocode 3. Ontwerp en berekening van staalconstructies. Deel 1-1: Algemene regels en regels voor gebouwen.*

Nethercot, D., & Kerdal, D. (1982). *Lateral-torsional buckling of castellated beams.* The Structural Engineer.

Rebelo, C., Lopes, N., Simões da Silva, L., Nethercot, D., & Vila Real, P. (2009, April). Statistical evaluation of the lateral–torsional buckling resistance of steel I-beams, Part 1: Variability of the Eurocode 3 resistance model. *Journal of Constructional Steel Research*, *65*(4), 818–831.

Salvadory, M. G. (1955). Lateral buckling of i-beams.

Snijder, H. B., & Hoenderkamp, J. H. (2007). Buckling curves for lateral torsional buckling of unrestrained beams.

Sonck, D. (2014). *Global Buckling of Castellated and Cellular Steel Beams and Columns.*

Sonck, D., Belis, J., Lagae, G., Vanlaere, W., & Impe, R. V. (2009). Lateral-torsional and lateral-distortional buckling of I-section members with web openings. , 406–411.

Sonck, D., Impe, S. R. V., & Vanlaere, W. (2012). Lateral-torsional buckling of cellular beams. (Figure 5), 1–2.

Taras, A. (2010). *Contribution to the Development of Consistent Stability Design Rules for Steel Members.* Phd thesis, Graz University of Technology.

Trahair, N. (1993). *Flexural-Torsional buckling of structures.* E & FN Spon.

Trahair, N., Bradford, M., Nethercot, D., & Gardner, L. (2007). *The behaviour and design of steel structures to EC3.*

Tsavdaridis, K. D., Asce, A. M., & Mello, C. D. (2012). Vierendeel Bending Study of Perforated Steel Beams with Various Novel Web Opening Shapes through Nonlinear Finite-Element Analyses. (October), 1214–1230. doi: 10.1061/(ASCE)ST.1943-541X.0000562.

Tsavdaridis, K. D., & D'Mello, C. (2011, October). Web buckling study of the behaviour and strength of perforated steel beams with different novel web opening shapes. *Journal of Constructional Steel Research*, *67*(10), 1605–1620. doi: 10.1016/j.jcsr.2011.04.004

Vandepitte, D. (1979). *Berekening van constructies.* E. Story-Scientia.

Van Impe, R. (2010). *Berekening van constructies III.* Laboratiorium voor ModelOnderzoek.

Verweij, J. G. (2010). Cellular beam-columns in portal frame structures. (November).

Westok. (2013). Applications/Westok. Retrieved from `http://www.asdwestok.co.uk`.

Young, B. (1975). Residual stresses in hot rolled members. , 25–38.